Advanced Discrete-Time Controller Design with Application to Motion Control

Khalid Abidi

A THESIS SUBMITTED

FOR THE DEGREE OF DOCTOR OF PHILOSOPHY

DEPARTMENT OF ELECTRICAL AND COMPUTER ENGINEERING

NATIONAL UNIVERSITY OF SINGAPORE

2009

Acknowledgements

Throughout this four year journey, I counted on the support of many without whom I would not be where I am now. I would like to thank Prof. Xu Jian-Xin for giving me the honor of working under him and for his infinite support and guidance. I would also like to thank my labmates Cai Gouwei and Lin-Feng for their friendship and support. I should not forget my dear friends overseas especially Okan Kurt, Muge Acik, Yildiray Yildiz, and Ozgur Akboga for always being there no matter how much I have annoyed them.

On a personal note, I would like to thank my parents and my brothers and especially my eldest brother Anas.

Contents

Summary

The purpose of this thesis is to create a framework for advanced discrete-time controller analysis and design. We consider three different scenarios: 1) Regulation and Output tracking of Sampled-Data MIMO Systems, 2) Discrete-Time Systems with Periodic Parameters, and 3) Sampled-Data SISO Systems with Iterative Tasks. Each controller design must achieve the best possible performance in comparrison to conventional designs and ensure robustness and ease of implementation.

In the first work we propose a new discrete-time integral sliding mode control (DISMC) scheme for sampled-data systems. The new control scheme is characterized by a discrete-time integral switching surface which inherits the desired properties of the continuous-time integral switching surface, such as full order sliding manifold with eigenvalue assignment, and elimination of the reaching phase. In particular, comparing with existing discrete-time sliding mode control, the new scheme is able to achieve more precise tracking performance. It will be shown in this work that, the new control scheme achieves $O(T^2)$ steady-state error for state regulation and reference tracking while preventing the generation of overlarge control actions.

In the second work a periodic adaptive control approach is proposed for a class of nonlinear discrete-time systems with time-varying parametric uncertainties which are periodic, and the

only prior knowledge is the periodicity. The new adaptive controller updates the parameters and the control signal periodically in a pointwise manner over one entire period, in the sequel achieves the asymptotic tracking convergence. The result is further extended to a scenario with mixed time-varying and time-invariant parameters, and a hybrid classical and periodic adaptation law is proposed to handle the scenario more appropriately. Extension of the periodic adaptation to systems with unknown input gain, higher order dynamics, and tracking problems are also discussed.

Finally the third work aims to present a framework for the stability analysis and design of Iterative Learning Control (ILC) for SISO sampled-data systems. Analysis is presented in both the time-domain and the frequency domain. The insufficient stability conditions in the time-domain are analyzed and the large overshooting phenomenon is explored. Monotonic convergence criteria are derived in both the time-domain and the frequency domain. Four different cases of learning function L are considered namely the P-type, D-type, D^2-type and general filter. Criteria for the selection of each type are presented. In addition a relationship is shown between the sampling time selection and the ILC convergence. Theoretical work concludes with a guideline for the design of the ILC. Simulation results are shown to support the theoretical analysis in the time-domain and the frequency-domain. Further, a successful experimental implementation is shown that is based on the frequency-domain design tools.

List of Figures

List of Tables

Nomenclature

A	state matrix
B	input matrix
C	output matrix
Φ	state matrix of a sampled-data system
Γ	input matrix of a sampled-data system
$O(T^r)$	a scalar or vector function of the order of T^r
DISMC	discrete-time integral sliding mode control
$i.i.c$	identical initial condition
ILC	iterative learning control
PAC	periodic adaptive control
RLC	repetetive learning control

Chapter 1

Introduction

1.1 Background

In recent years there has been a rapid increase in the use of digital controllers in control systems. Digital controls are used for achieving optimal performance, e.g., in the form of maximum productivity, maximum profit, minimum cost, or minimum energy use, [1].

Most recently, the application of computer control has made possible 'intelligent' motion in industrial robots, the optimization of fuel economy in automobiles, and the refinements in the operation of household appliances and machines such as microwaves and sewing machines, among others. Decision-making capability and flexibility in the control program are major advantages of digital control systems, [2].

The current trend toward digital rather than analog control of dynamic systems is mainly due to the availability of low-cost digital computers and the advantages found in working with digital signals rather than continuous-time signals, [2].

It is well known that most, if not all, engineering systems are continuous in nature. Owing

to the capacity of digital computers to process discrete data, the continuous-time systems are controlled using sampled observations taken at discrete-time instants. Thus, the resulting control systems are a hybrid, consisting of interacting discrete and continuous components as depicted in Fig.1.1. These hybrid systems, in which the system to be controlled evolves in continuous-time and the controller evolves in dicrete-time, are called sampled-data systems, [3].

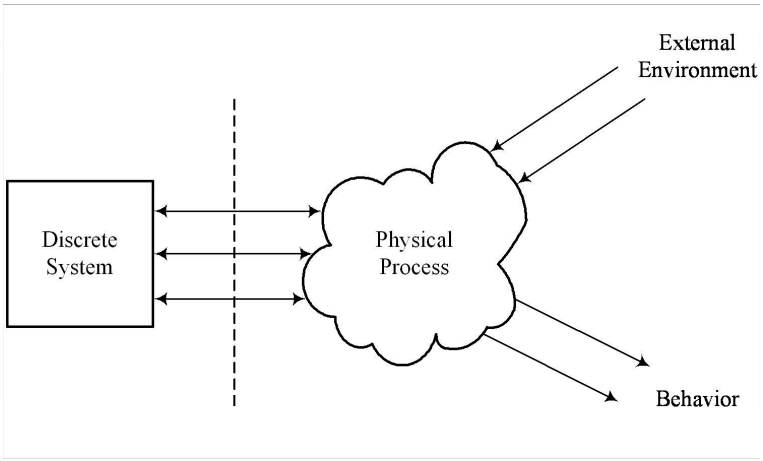

Figure 1.1: General sampled-data arrangement

The significant feature of sampled-data system design that distinguishes it from standard techniques for control system design is that it must contend with plant models and control laws lying in different domains. There are three major methodologies for design and analysis of sampled-data systems which are pictorially represented in Fig.1.2 where G is a continuous-time process and K_d is a discrete-time control law. All three methods begin with begin with the principle continuous-time model G and aim to design the discrete-time controller K_d and analyze its performance, [3].

The two well known approaches follow the paths around the perimeter of the diagram.

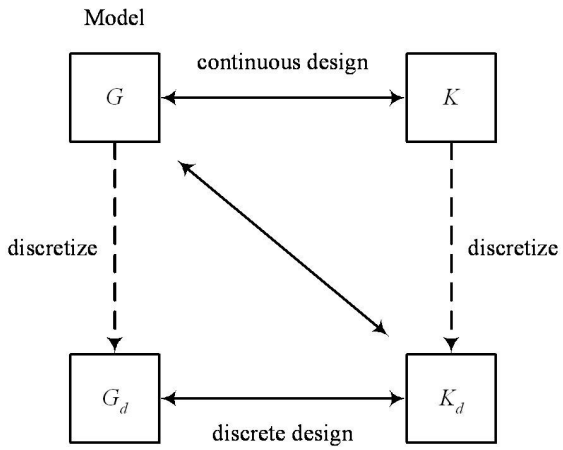

Figure 1.2: Design approaches

The first is to conduct all analysis and design in continuous-time domain using a system that is believed to be a close approximation to the sampled-data system. This is accomplished by associating every continuous-time controller K with a discrete-time approximation K_d via discretization method; synthesis and analysis of the controller are then performed in continuous-time, with the underlying assumption that the closed-loop system behavior obtained controller K closely reflects that achieved with the sampled-data implementation K_d. Thus, this method does not directly address the issue of implementation in the design stage. The second approach starts instead by discretizing the continuous-time systen G, giving a discrete-time approximation G_d, thus, ignoring intersample behavior. Then the controller K_d is designed directly in discrete-time using G_d, with the belief that the performance of this purely discrete-time system approximates that of the sampled-data system. The third approach has attracted conisderable research activity. In this approach the system G and the controller K_d interconnection is treated directly and exaclty. In our work we will as much as possible focus on this approach while in some cases use the second approach in order to more

simply explain our proposed ideas, [3].

In our first work we focus on sliding mode control for sampled-data systems. Sliding mode control is well known in continuous-time control where it is characterized by high frequency switching which gives sliding mode control its very good robustness properties. This, however, is hard to achieve in sampled-data systems due to hardware limitations such as processor speed, A/D and D/A conversion delays, etc. The use of discontinuous control under these circumstances would lead to the well known chattering phenomenon around the sliding manifold (Fig.1.3), leading to a boundary of order $O(T)$, [4]. In order to avoid this problem, in [4] and [5] a discrete-time control equivalent in the prescribed boundary is proposed, whose size is defined by the restriction to the control variables. This approaches results in motion within an $O(T^2)$ boundary around the sliding manifold. In our work we propose a modified sliding manifold that achieves better tracking performance to that in [4] and [5].

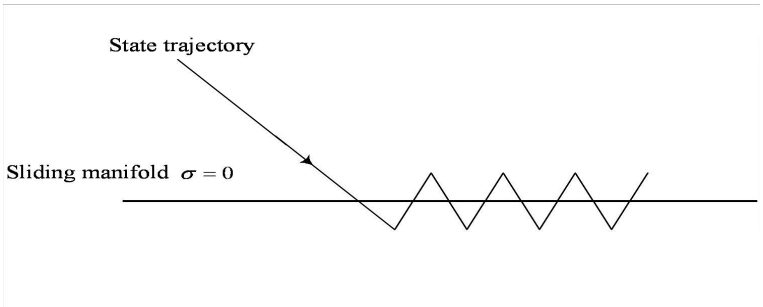

Figure 1.3: Chattering phenomenon with switching sliding mode control

In our second work we propose a new method for discrete-time adaptive control. In [6] the author asks the following question: "Within the current framework of adaptive control, can we deal with time-varying parametric uncertainties?" This is a challenging problem to the control community. Adaptive algorithms have been reported for systems with slow time-varying

parametric uncertainties [7]-[9], etc., with arbitrarily rapid time-varying parameters in a known compact set [10], and with rapid time-varying parameters which converge asymptotically to constants [11]. However, as indicated in [11], no adaptive control algorithms developed hitherto can solve unknown parameters with arbitrarily fast and nonvanishing variations. Considering the fact that, as a function of time, the classes of timevarying parameters are in essence infinite, it would be extremely difficult to find a general solution to such a broad control problem. A more realistic way is first to classify the time-varying parametric uncertainties into subclasses, and then look for an appropriate adaptive control approach for each subclass. Instead of classifying parameters into slow vs rapid time-varying, in this work we classify parameters into periodic vs nonperiodic ones. When the periodicity of system parameters is known a priori, a new adaptive controller with periodic updating can be constructed by means of a pointwise integral mechanism. This method is proposed in [6] for continuous-time systems. As a natural extension to this we propose a similar methodology for discrete-time systems.

Finally in our third work we focus on iterative learning control for sampled-data systems. Iterative learning control (ILC) is based on the idea that the performance of a system that executes the same task multiple times can be improved by learning from previous executions (trials, iterations, passes). When letting a machine do the same task repeatedly it is, at least from an engineering point of view, very sound to use knowledge from previous iterations of the same task to try to reduce the error next time the task is performed. The first academic contribution to what today is called ILC appears to be a paper by Uchiyama [12]. Since it was

published in Japanese only, the ideas did not become widely spread. What is a bit remarkable, however, is that an application for a US patent on 'Learning control of actuators in control systems [13] was already done in 1967 and that it was accepted as a patent in 1971. The idea in the patent is to store a 'command signal in a computer memory and iteratively update this command signal using the error between the actual response and the desired response of the actuator. This is clearly an implementation of ILC, although the actual ILC updating equation was not explicitly formulated in the patent. From an academic perspective it was not until 1984 that ILC started to become an active research area. In this work we present a framework for linear iterative control, which enables several results from linear control theory to be applied.

One may ask the reason why these specific methods are discussed. While the scope of this work is very wide, it was decided to select methods that as much as possible completed a whole picture. For example, the SMC approach is selected for non-parametric systems with known parameters and unknown disturbance while the adaptive control is suitable for parametric systems with unknown parameters while the ILC is an add-on to any controller, either classical or not, provided that the task is repetitive. Thus, all the topics discussed cover as wide an area as possible giving a control engineer as much options as possible for different control problems.

1.2 Contributions

The contributions of this thesis can be summarized as follows:

(1). Discrete-Time Integral Sliding Mode Control

In this work we propose a new discrete-time integral sliding mode control (DISMC) scheme for sampled-data systems. The new control scheme is characterized by a discrete-time integral switching surface which inherits the desired properties of the continuous-time integral switching surface, such as full order sliding manifold with eigenvalue assignment, and elimination of the reaching phase. In particular, comparing with existing discrete-time sliding mode control, the new scheme is able to achieve more precise tracking performance. It will be shown in this work that, the new control scheme achieves $O(T^2)$ steady-state error for state regulation and reference tracking with the widely adopted delay-based disturbance estimation. Another desirable feature is, the proposed DISMC prevents the generation of overlarge control actions, which are usually inevitable due to the deadbeat poles of a reduced order sliding manifold designed for sampled-data systems. Both the theoretical analysis and illustrative example demonstrate the validity of the proposed scheme.

(2). A Discrete-Time Periodic Adaptive Control Approach for Time-Varying Parameters with Known Periodicity

In this work a periodic adaptive control approach is proposed for a class of nonlinear discrete-time systems with time-varying parametric uncertainties which are periodic, and the only prior knowledge is the periodicity. The new adaptive controller updates the parameters and

the control signal periodically in a pointwise manner over one entire period, in the sequel achieves the asymptotic tracking convergence. The result is further extended to a scenario with mixed time-varying and time-invariant parameters, and a hybrid classical and periodic adaptation law is proposed to handle the scenario more appropriately. Extension of the periodic adaptation to systems with unknown input gain, higher order dynamics, and tracking problems are also discussed.

(3). Iterative Learning Control for Sampled-Data Systems

In this work the convergence properties of iterative learning control (ILC) algorithms are considered. The analysis is carried out in a framework using linear iterative systems, which enables several results from the theory of linear systems to be applied. This makes it possible to analyse both first-order and high-order ILC algorithms in both the time and frequency domains. The time and frequency domain results can also be tied together in a clear way. Illustrative examples are presented to support the analytical results.

1.3 Organization of the Thesis

The thesis is organized as follows.

In Chapter 2, we propose Discrete-Time Integral Sliding Mode Control for Sampled-Data systems. Section 2.2 gives the problem formulation and revisits the existing SMC properties in sampled-data systems. Section 2.3 presents the appropriate discrete-time integral sliding manifold designs for state regulation and sections 2.4, 2.5 and 2.6 present appropriate designs

for output tracking. Section 2.7 shows some illustrative examples and section 2.8 gives the conclusions.

In Chapter 3, we present a Discrete-Time Periodic Adaptive Control Approach for Time-Varying Parameters with Known Periodicity. In Section 3.2, we present the new periodic adaptive control approach and give complete analysis. To clearly demonstrate the underlying idea and method, we consided the simplest nonlinear dynamics with a single time-varying parameter. In Section 3.3, we extend the new approach to more general cases. The first extension considers multiple time-varying parameters and time-varying gain of the system input. The second extension consdiers a mixture of time-varying and time-invariant parameters, and a new hybrid adaptive control scheme is developed. The third extension considers a general tracking control problem. The fourth extension considers a higher order system in canonical form. In Section 3.4, an illustrative example is provided.

In Chapter 4, we present Iterative Learning Control for Sampled-Data systems. In Section 4.3, we present the time domain analysis of different ILC. In Section 4.4, we analyze the same ILC laws in the frequency domain and highlight the connection between the time domain and frequency domain results. In sections 4.5 and 4.6, illustrative examples are provided to support the results in each domain.

In Chapter 5, we present a practical application for the discussed control laws. The aim is to design control laws that would achieve high-precision motion of a piezo-motor driven linear stage. In section 5.2 we describe the model of the piezo-motor. In section 5.3 we present the

ISM design and in section 5.4 we show the ILC design.

Finally, conclusions and recommendation for future work will be discussed in Chapter 5.

Throughout this report, $\|\cdot\|$ denotes the Euclidean Norm. For notational convenience, in mathematical expressions f_k represents $f(k)$.

Chapter 2

Sliding Mode Control for Linear MIMO Sampled-Data Systems with Disturbance

2.1 Introduction

Research in discrete-time control has been intensified in recent years. A primary reason is that most control strategies nowadays are implemented in discrete-time. This also necessitated a rework in the sliding mode control strategy for sampled-data systems, [4],[5]. In such systems, the switching frequency in control variables is limited by T^{-1}; where T is the sampling period. This has led researchers to approach discrete-time sliding mode control from two directions. The first is the emulation that focuses on how to map continuous-time sliding mode control to discrete-time, and the switching term can be preserved, [15],[16]. The second is based on the equivalent control design and disturbance observer, [4],[5]. In the former, although high-frequency switching is theoretically desirable from the robustness point of view, it is usually hard to achieve in practice because of physical constraints, such as processor computational

speed, A/D and D/A conversion delays, actuator bandwidth, etc. The use of a discontinuous control law in a sampled-data system will bring about chattering phenomenon in the vicinity of the sliding manifold, hence lead to a boundary layer with thickness $O(T)$, [4].

The effort to eliminate the chattering has been paid over 30 years. In continuous-time SMC, smoothing schemes such as boundary layer (saturator) are widely used, which in fact results in a continuous nonlinear feedback instead of switching control. Nevertheless, it is widely accepted by the community that this class of controllers can still be regarded as SMC. Similarly, in discrete-time SMC, by introducing a continuous control law, chattering can be eliminated. In such circumstance, the central issue is to guarantee the precision bound or the smallness of the error.

In [5] a discrete-time equivalent control was proposed. This approach results in the motion in $O(T^2)$ vicinity of the sliding manifold. The main difficulty in the implementation of this control law is that we need to know the disturbances for calculating the equivalent control. Lack of such information leads to an $O(T)$ error boundary.

The control proposed in [4] drives the sliding mode to $O(T^2)$ in one-step owing to the incorporation of deadbeat poles in the closed-loop system. State regulation was not considered in [4]. In fact, as far as the state regulation is concerned, the same SMC design will produce an accuracy in $O(T)$ instead of $O(T^2)$ boundary. Moreover, the SMC with deadbeat poles requires large control efforts that might be undesirable in practice. Introducing saturation in the control input endangers the global stability or accuracy of the closed-loop system.

In this Chapter, aiming at improving control performance for sampled-data systems, a

discrete-time integral sliding manifold (ISM) is proposed. With the full control of the system closed-loop poles and the elimination of the reaching phase, like the continuous-time integral sliding mode control [17]-[19], the closed-loop system can achieve the desired control performance while avoiding the generation of overly large control inputs. It is worth highlighting that the discrete-time ISM control does not only drive the sliding mode into the $O(T^2)$ boundary, but also achieve the $O(T^2)$ boundary for state regulation.

After focusing on state feedback based regulation, we consider the situation where output tracking and output feedback is required. Based on output feedback two approaches arose – design based on obervers to construct the missing states, [21, 22], or design based on the output measurement only [23, 24]. Recently integral sliding-mode control has been developed to improve controller design and consequently the control performance, [17]-[19], which use full state information. The first objective of this work is to extend ISMC to output-tracking problems. We present three ISMC design approaches associated with state feedback, output feedback, and output feedback with state estimation, respectively.

In the presence of exo-disturbances, we introduce disturbance observers which can effectively reduce the final tracking error by one digital scale. While an one-step delayed observer can be directly constructed for state based ISMC, a dynamic observer is needed for output based ISMC due to the absence of full state information. The second objective of this work is to develop an integral sliding-mode observer (ISMO), which can quickly and effectively estimate the disturbance and avoid the undesirable deadbeat response inherent in conventional sliding-mode based designs for sampled-data systems; in the sequel, avoid the generation of

overly large esitmation signals in the controller.

Most of the existing works on SMC focused on regulation problems or set-point control problems instead of arbitrary reference tracking, [17]-[27]. Arbitrary reference tracking remains a difficult issue in SMC, and becomes more challenging when only outputs are accessible. On the other hand, arbitrary trajectory-tracking problems are widely encountered in control practice, for example servo in motion control systems, temperature profile tracking in process control systems, target tracking in missile control, etc. The third objective of this work is to disclose the relations among minimum-phase conditions, altenative reference models, ISMC approaches, and tracking error bounds. As a result, a guideline is provided to aid in the selection of ISMC designs in terms of the control performance specifications and plant model.

When the system states are accessible, the disturbance can be directly esitmated using state and control signals delayed by one sampling period. The resulting output ISMC can perform arbitrary trajectory tracking with $O(T^2)$ accuracy. When only outputs are accessible, the delayed disturbance estimation cannot be performed. in this Chapter we adopt a dynamic disturbance observer designed with the integral sliding-mode for the second and third output ISMC approaches. With the second ISMC approach that uses output feedback only, arbitrary trajecory tracking is difficult to perform. Two reference models associated with the arbitrary reference are introduced so as to provide the state information of reference models that is required in the integal sliding-mode. We demonstrate that two reference models can be selected according different minimum-phase conditions associated with the plant, in the sequel

an extra degree of freedom in ISMC design is acquired. The second output ISMC approach achieves $O(T)$ accuracy.

The third ISMC approach uses state observer, hence the integral sliding surface can be constructed using estimated states in a way analogous to the state feedback based ISMC. As a result, arbitrary trajectory tracking can be directly performed. This ISMC approach achieves $O(T)$ accuracy in general, and $O(T^2)$ when the original contiuous-time plant has a relative degree above 1.

In this Chapter, eigenvalue assignment of the full-order sliding mode, as well as the closed-loop dynamics in the sliding motion, will be discussed.

2.2 Problem Formulation

2.2.1 Sampled-Data System

Consider the following continuous-time system with a nominal linear time invariant model and matched disturbance

$$\begin{aligned} \dot{\mathbf{x}}(t) &= A\mathbf{x}(t) + B(\mathbf{u}(t) + \mathbf{f}(t)) \\ \mathbf{y}(t) &= C\mathbf{x}(t) \end{aligned} \tag{2.1}$$

where the state $\mathbf{x} \in \Re^n$, the ouput $\mathbf{y} \in \Re^m$, the control $\mathbf{u} \in \Re^m$, and the disturbance $\mathbf{f} \in \Re^m$ is assumed smooth and bounded. The state matrix is $A \in \Re^{n\times n}$ and the control matrix is $B \in \Re^{n\times m}$ and the output matrix is $C \in \Re^{m\times n}$. The discretized counterpart of (5.1) can be given by

$$\begin{aligned} \mathbf{x}_{k+1} &= \Phi\mathbf{x}_k + \Gamma\mathbf{u}_k + \mathbf{d}_k, \quad \mathbf{x}_0 = \mathbf{x}(0) \\ \mathbf{y}_k &= C\mathbf{x}_k \end{aligned} \tag{2.2}$$

where

$$\begin{aligned}\Phi &= e^{AT}, \quad \Gamma = \int_0^T e^{A\tau} d\tau B \\ \mathbf{d}_k &= \int_0^T e^{A\tau} B\mathbf{f}((k+1)T - \tau) d\tau,\end{aligned}$$

and T is the sampling period. Here the disturbance $\mathbf{d}_k$ represents the influence accumulated from kT to $(k+1)T$, in the sequel it shall directly link to $\mathbf{x}_{k+1} = \mathbf{x}((k+1)T)$. From the definition of Γ it can be shown that

$$\Gamma = BT + \frac{1}{2!}ABT^2 + \cdots = BT + MT^2 + O(T^3) \Rightarrow BT = \Gamma - MT^2 + O(T^3) \tag{2.3}$$

where M is a constant matrix because T is fixed.

The control objective is to design a discrete-time integral sliding manifold and a discrete-time SMC law for the sampled-data system (2.2), hence acheive as precisely as possible state regulation. Meanwhile the closed-loop dynamics of the sampled-data system has all its closed-loop poles assigned to desired locations.

Remark 1 *The smoothness assumption made on the disturbance is to ensure that the disturbance bandwidth is sufficiently lower than the controller bandwidth, or the ignorance of high frequency components does not significantly affect the control performance. Indeed, if a disturbance has frequencies nearby or higher than the Nyquist frequency, for instance a non-smooth disturbance, a discrete-time SMC will not be able to handle it.*

In order to proceed further, the following definition is necessary:

Definition: *The magnitude of a variable v is said to be $O(T^r)$ if and only if*

There is a $C > 0$, such that for any sufficiently small T the following inequality holds

$$|v| \leq CT^r$$

where r is an integer. Denote $O(T^0) = O(1)$.

Remark 2 *Note that $O(T^r)$ can be a scalar function or a vector valued function.*

Associated with the above definition if there exists two variables v_1 and v_2 such that $v_1 \in O(T^r)$ and $v_2 \in O(T^{r+1})$ then $v_1 \gg v_2$ and, therefore, the following relations hold

$$O(T^{r+1}) + O(T^r) = O(T^r) \quad \forall r \in Z$$

$$O(T^r) \cdot O(1) = O(T^r) \quad \forall r \in Z$$

$$O(T^r) \cdot O(T^{-s}) = O(T^{r-s}) \quad \forall r, s \in Z$$

where Z is the set of integers.

Based on (2.3) and the Definition, the magnitude of Γ is $O(T)$.

Note that, as a consequence of sampling, the disturbance originally matched in continuous-time will contain mismatched components in the sampled-data system. This is summarized in the following lemma.

Lemma 1 *If the disturbance $\mathbf{f}(t)$ in (5.1) is bounded and smooth, then*

$$\mathbf{d}_k = \int_0^T e^{A\tau} B\mathbf{f}((k+1)T - \tau)d\tau = \Gamma \mathbf{f}_k + \frac{1}{2}\Gamma \mathbf{v}_k T + O(T^3) \tag{2.4}$$

where $\mathbf{v}_k = \mathbf{v}(kT)$, $\mathbf{v}(t) = \frac{d}{dt}\mathbf{f}(t)$, $\mathbf{d}_k - \mathbf{d}_{k-1} \in O(T^2)$, and $\mathbf{d}_k - 2\mathbf{d}_{k-1} + \mathbf{d}_{k-2} \in O(T^3)$.

Proof: See appendix.

Note that the magnitude of the mismatched part in the disturbance $\mathbf{d}_k$ is of the order $O(T^3)$

2.2.2 Discrete-Time Sliding Mode Control Revisited

Consider the well established discrete-time sliding-surface [4]-[5] shown below

$$\boldsymbol{\sigma}_k = D\mathbf{x}_k \tag{2.5}$$

where $\boldsymbol{\sigma} \in \Re^m$ and D is a constant matrix of rank m. The objective is to steer the states towards and force them to stay on the sliding manifold $\boldsymbol{\sigma}_k = 0$ at every sampling instant. The control accuracy of this class of sampled-data SMC is given by the following lemma.

Lemma 2 *With $\boldsymbol{\sigma}_k = D\mathbf{x}_k$ and equivalent control based on a disturbance estimate*

$$\hat{\mathbf{d}}_k = \mathbf{x}_k - \Phi\mathbf{x}_{k-1} - \Gamma\mathbf{u}_{k-1},$$

then there exists a matrix D such that the control accuracy of the closed-loop system is

$$\lim_{k\to\infty} \|\mathbf{x}_k\| \leq O(T).$$

Proof: Discrete-time equivalent control is defined by solving $\boldsymbol{\sigma}_{k+1} = 0$, [4]. This leads to

$$\mathbf{u}_k^{eq} = -(D\Gamma)^{-1}D(\Phi\mathbf{x}_k + \mathbf{d}_k) \tag{2.6}$$

with D selected such that the closed-loop system achieves desired performance and $D\Gamma$ is invertible, [20]. Under practical considerations, the control cannot be implemented in the same

form as in (2.22) because of the lack of prior knowledge regarding the discretized disturbance $\mathbf{d}_k$. However, with some continuity assumptions on the disturbance, $\mathbf{d}_k$ can be estimated by its previous value $\mathbf{d}_{k-1}$, [4]. The substitution of $\mathbf{d}_k$ by $\mathbf{d}_{k-1}$ will at most result in an error of $O(T^2)$. With reasonably small sampling interval as in motion control or mechatronics, such a substitution will be effective. Let

$$\hat{\mathbf{d}}_k = \mathbf{d}_{k-1} = \mathbf{x}_k - \Phi\mathbf{x}_{k-1} - \Gamma\mathbf{u}_{k-1} \tag{2.7}$$

where $\hat{\mathbf{d}}_k$ is the estimate of $\mathbf{d}_k$. Thus, analogous to the equivalent control law (2.22), the practical control law is

$$\mathbf{u}_k = -(D\Gamma)^{-1}D(\Phi\mathbf{x}_k + \mathbf{d}_{k-1}). \tag{2.8}$$

Substituting the sampled-data dynamics (2.2), applying the above control law, and using the conclusions in *Lemma* 1, yield

$$\boldsymbol{\sigma}_{k+1} = D(\Phi\mathbf{x}_k + \Gamma\mathbf{u}_k + \mathbf{d}_k) = D(\mathbf{d}_k - \mathbf{d}_{k-1}) = O(T^2) \tag{2.9}$$

which is the result shown in [4]. The closed-loop dynamics is

$$\mathbf{x}_{k+1} = \left(\Phi - \Gamma(D\Gamma)^{-1}D\Phi\right)\mathbf{x}_k + \left(I - \Gamma(D\Gamma)^{-1}D\right)\mathbf{d}_{k-1} + \mathbf{d}_k - \mathbf{d}_{k-1} \tag{2.10}$$

where the matrix $(\Phi - \Gamma(D\Gamma)^{-1}D\Phi)$ has m zero eigenvalues and $n-m$ eigenvalues to be assigned inside the unit disk in the complex *z-plane*. It is possible to simplify (2.10) further to

$$\mathbf{x}_{k+1} = \left(\Phi - \Gamma(D\Gamma)^{-1}D\Phi\right)\mathbf{x}_k + \boldsymbol{\delta}_k \tag{2.11}$$

where $\boldsymbol{\delta}_k = (I - \Gamma(D\Gamma)^{-1}D)\,\mathbf{d}_{k-1} + \mathbf{d}_k - \mathbf{d}_{k-1}$. From *Lemma* 1,

$$\begin{aligned}\boldsymbol{\delta}_k &= \mathbf{d}_k - \mathbf{d}_{k-1} + (I - \Gamma(D\Gamma)^{-1}D)\left(\Gamma\mathbf{f}_{k-1} + \frac{1}{2}\Gamma\mathbf{v}_{k-1}T + O(T^3)\right) \\ &= O(T^2) + (I - \Gamma(D\Gamma)^{-1}D)O(T^3) = O(T^2). \end{aligned} \tag{2.12}$$

In the above derivation, we use the relations $(I - \Gamma(D\Gamma)^{-1}D)\Gamma = 0$, $\|I - \Gamma(D\Gamma)^{-1}D\| \leq 1$ and $O(1)\cdot O(T^3) = O(T^3)$. Note that since m eigenvalues of $(\Phi - \Gamma(D\Gamma)^{-1}D\Phi)$ are deadbeat, it can be written as

$$(\Phi - \Gamma(D\Gamma)^{-1}D\Phi) = PJP^{-1} \tag{2.13}$$

where P is a transformation matrix and J is the Jordan matrix of the eigenvalues of $(\Phi - \Gamma(D\Gamma)^{-1}D\Phi)$. The matrix J can be written as

$$J = \begin{bmatrix} J_1 & \mathbf{0} \\ \mathbf{0} & J_2 \end{bmatrix} \tag{2.14}$$

where $J_1 \in \Re^{m\times m}$ and $J_2 \in \Re^{(n-m)\times(n-m)}$ are given by

$$J_1 = \begin{bmatrix} \mathbf{0} & I_{m-1} \\ 0 & \mathbf{0} \end{bmatrix}, \quad J_2 = \begin{bmatrix} \lambda_{m+1} & 0 & \cdots & 0 \\ 0 & \ddots & \ddots & \vdots \\ \vdots & \ddots & \ddots & 0 \\ 0 & \cdots & 0 & \lambda_n \end{bmatrix}$$

where λ_j are the eigenvalues of $(\Phi - \Gamma(D\Gamma)^{-1}D\Phi)$. For simplicity it is assumed that the non-zero eigenvalues are designed to be distinct and that their continuous time counterparts are of order $O(1)$. Then the solution of (2.11) is

$$\mathbf{x}_k = PJ^kP^{-1}\mathbf{x}(0) + P\left(\sum_{i=0}^{k-1} J^iP^{-1}\boldsymbol{\delta}_{k-i-1}\right). \tag{2.15}$$

Rewritting (2.15) as

$$\mathbf{x}_k = PJ^kP^{-1}\mathbf{x}(0) + P\left(\sum_{i=0}^{k-1}\begin{bmatrix} J_1^i & \mathbf{0} \\ \mathbf{0} & \mathbf{0} \end{bmatrix} P^{-1}\boldsymbol{\delta}_{k-i-1}\right) + P\left(\sum_{i=0}^{k-1}\begin{bmatrix} \mathbf{0} & \mathbf{0} \\ \mathbf{0} & J_2^i \end{bmatrix} P^{-1}\boldsymbol{\delta}_{k-i-1}\right), \quad (2.16)$$

it is easy to verify that $J_1^i = \mathbf{0}$ for $i \geq m$. Thus, (2.16) becomes (for $k \geq m$)

$$\mathbf{x}_k = PJ^kP^{-1}\mathbf{x}(0) + P\left(\sum_{i=0}^{m}\begin{bmatrix} J_1^i & \mathbf{0} \\ \mathbf{0} & \mathbf{0} \end{bmatrix} P^{-1}\boldsymbol{\delta}_{k-i-1}\right) + P\left(\sum_{i=0}^{k-1}\begin{bmatrix} \mathbf{0} & \mathbf{0} \\ \mathbf{0} & J_2^i \end{bmatrix} P^{-1}\boldsymbol{\delta}_{k-i-1}\right). \quad (2.17)$$

Notice $\|J_1\| = 1$ and $\|J_2\| = \lambda_{max} = max\{\lambda_{m+1}, \cdots, \lambda_n\}$ ($\|\cdot\|$ indicates $\|\cdot\|_2$). Hence, from (2.17), we have

$$\lim_{k\to\infty}\|\mathbf{x}_k\| \leq \|P\|\left(\sum_{i=0}^{m}\left\|\begin{bmatrix} J_1 & \mathbf{0} \\ \mathbf{0} & \mathbf{0} \end{bmatrix}\right\|^i \|P^{-1}\|\|\boldsymbol{\delta}_{k-i-1}\| + \sum_{i=0}^{k-1}\left\|\begin{bmatrix} \mathbf{0} & \mathbf{0} \\ \mathbf{0} & J_2 \end{bmatrix}\right\|^i \|P^{-1}\|\|\boldsymbol{\delta}_{k-i-1}\|\right) \quad (2.18)$$

Since $\lambda_{max} < 1$ for a stable system, we obtain

$$\sum_{i=0}^{\infty}\|J_2\|^i = \frac{1}{1-\lambda_{max}}, \quad \sum_{i=0}^{m}\|J_1\|^i = m.$$

Using Tustin's approximation

$$\lambda_{max} = \frac{2+Tp}{2-Tp} \Rightarrow \frac{1}{1-\lambda_{max}} = \frac{1}{1-\frac{2+Tp}{2-Tp}} = \frac{2-Tp}{-2Tp} \leq O(T^{-1}) \quad (2.19)$$

where $p \geq O(1)$ is the corresponding pole in continuous-time. Assuming $m \in O(1)$, and using the fact $\|P^{-1}\| = \|P\|^{-1}$, it can be derived from (2.18) that

$$\lim_{k\to\infty}\|\mathbf{x}_k\| \leq O(1)\cdot O(T^2) + O(T^{-1})\cdot O(T^2) = O(T). \quad (2.20)$$

■

Remark 3 *Under practical considerations, it is generally advisable to select the pole p large enough such that the system has a fast enough response. With the selection of a small sampling*

time T, a pole of order $O(T)$ would lead to an undesirably slow repsonse. Thus, it makes sense to select a pole of order $O(1)$ or larger.

Remark 4 *The SMC in [4] guarantees that the sliding variable σ is of order $O(T^2)$, but cannot guarantee the same order of magnitude of steady-state errors for the system state variables. In the next section, we show that an integral sliding mode design can achieve a more precise state regulation.*

2.2.3 Output Tracking

Consider the discrete-time sliding manifold given below [4]-[5]

$$\boldsymbol{\sigma}_k = D_o(\mathbf{r}_k - \mathbf{y}_k) \tag{2.21}$$

where D_o is a constant matrix of rank m and $\mathbf{r} \in \Re^m$. The objective is to force the output $\mathbf{y}$ to track the reference $\mathbf{r}$. The property for this class of sampled-data SMC is given by the following lemma.

Lemma 3 *For $\boldsymbol{\sigma}_k = D_o(\mathbf{r}_k - \mathbf{y}_k)$ and control based on a disturbance estimate*

$$\hat{\mathbf{d}}_k = \mathbf{x}_k - \Phi\mathbf{x}_{k-1} - \Gamma\mathbf{u}_{k-1},$$

the closed-loop system has the following properties

$$\boldsymbol{\sigma}_{k+1} \in O(T^2)$$

$$\mathbf{r}_{k+1} - \mathbf{y}_{k+1} \in O(T^2)$$

Proof: Similar to the regulation problem the discrete-time equivalent control is defined by solving $\boldsymbol{\sigma}_{k+1} = 0$, [4]. This leads to

$$\mathbf{u}_k^{eq} = (D_o C\Gamma)^{-1} D_o(\mathbf{r}_{k+1} - C\Phi\mathbf{x}_k - C\mathbf{d}_k) \tag{2.22}$$

with D_o selected such that $D_o C\Gamma$ is invertible. As in the regulation case, the control cannot be implemented in the same form as in (2.22) because of the lack of knowledge of $\mathbf{d}_k$ which requires *a priori* knowledge of the disturbance $\mathbf{f}(t)$. Thus, the delayed disturbance $\mathbf{d}_{k-1}$ will be used

$$\hat{\mathbf{d}}_k = \mathbf{d}_{k-1} = \mathbf{x}_k - \Phi\mathbf{x}_{k-1} - \Gamma\mathbf{u}_{k-1} \tag{2.23}$$

Thus, the control becomes

$$\mathbf{u}_k = (D_o C\Gamma)^{-1} D_o(\mathbf{r}_{k+1} - C\Phi\mathbf{x}_k - C\mathbf{d}_{k-1}) \tag{2.24}$$

The closed-loop system under the control given by (2.24) is

$$\mathbf{x}_{k+1} = \left[\Phi - \Gamma\left(D_o C\Gamma\right)^{-1} D_o C\Phi\right]\mathbf{x}_k + \Gamma(D_o C\Gamma)^{-1} D_o\mathbf{r}_{k+1} + \mathbf{d}_k - \Gamma\left(D_o C\Gamma\right)^{-1} D_o C\mathbf{d}_{k-1} \tag{2.25}$$

Note that $(D_o C\Gamma)^{-1} D_o = (C\Gamma)^{-1}$. Simplifying (2.25) further gives

$$\mathbf{x}_{k+1} = \left[\Phi - \Gamma\left(C\Gamma\right)^{-1} C\Phi\right]\mathbf{x}_k + \Gamma(C\Gamma)^{-1}\mathbf{r}_{k+1} + \mathbf{d}_k - \Gamma\left(C\Gamma\right)^{-1} C\mathbf{d}_{k-1}. \tag{2.26}$$

where the eigenvalues of the matrix $[\Phi - \Gamma(C\Gamma)^{-1}C\Phi]$ are the transmission zeros of the system, [14]. Postmultiplication of (2.26) with C results in,

$$\mathbf{y}_{k+1} = Cx_{k+1} = \mathbf{r}_{k+1} + C(\mathbf{d}_k - \mathbf{d}_{k-1}) = \mathbf{r}_{k+1} + O(T^2). \tag{2.27}$$

Substitution of (2.27) into the forward expression of (2.21) results in

$$\boldsymbol{\sigma}_{k+1} = D_o(\mathbf{r}_{k+1} - \mathbf{y}_{k+1}) \in O(T^2). \tag{2.28}$$

■

The above result shows that with the control given by (2.24) the output is stable and that the tracking error converges to a bound of order $O(T^2)$. However, the stability of the whole system is gauranteed only if the transmission zeros are stable. Looking back at (2.26), it is very simple to show that $[\Phi - \Gamma(C\Gamma)^{-1}C\Phi]$ has m eigenvalues in the origin. Note that those m deadbeat eigenvalues correspond to the output deadbeat response. If the matrices are partitioned as shown

$$\Phi = \begin{bmatrix} \Phi_{11} & \Phi_{12} \\ \Phi_{21} & \Phi_{22} \end{bmatrix}$$

$$C = \begin{bmatrix} C_1 & C_2 \end{bmatrix}$$

$$\Gamma = \begin{bmatrix} \Gamma_1 \\ \Gamma_2 \end{bmatrix}$$

where $(\Phi_{11}, C_1, \Gamma_1) \in \Re^{m\times m}$, $(\Phi_{12}, C_2) \in \Re^{m\times n-m}$, $(\Phi_{21}, \Gamma_2) \in \Re^{n-m\times m}$ and $\Phi_{22} \in \Re^{n-m\times n-m}$. The eigenvalues of $[\Phi - \Gamma(C\Gamma)^{-1}C\Phi]$ can be found from

$$\det[\lambda I_n - (\Phi - \Gamma(C\Gamma)^{-1}C\Phi)] =$$

$$\det \begin{bmatrix} \lambda I_m - \Phi_{11} + \Gamma_1(C\Gamma)^{-1}C \begin{bmatrix} \Phi_{11} \\ \Phi_{21} \end{bmatrix} & -\Phi_{12} + \Gamma_1(C\Gamma)^{-1}C \begin{bmatrix} \Phi_{12} \\ \Phi_{22} \end{bmatrix} \\ -\Phi_{21} + \Gamma_2(C\Gamma)^{-1}C \begin{bmatrix} \Phi_{11} \\ \Phi_{21} \end{bmatrix} & \lambda I_{n-m} - \Phi_{22} + \Gamma_2(C\Gamma)^{-1}C \begin{bmatrix} \Phi_{12} \\ \Phi_{22} \end{bmatrix} \end{bmatrix} = 0 \tag{2.29}$$

If the top row is premultiplied with C_1 and the bottom row premultiplied by C_2 and the results summed and used as the new top row, the following is obtained

$$\det \begin{bmatrix} \lambda C_1 & \lambda C_2 \\ -\Phi_{21} + \Gamma_2(C\Gamma)^{-1}C \begin{bmatrix} \Phi_{11} \\ \Phi_{21} \end{bmatrix} & \lambda I_{n-m} - \Phi_{22} + \Gamma_2(C\Gamma)^{-1}C \begin{bmatrix} \Phi_{12} \\ \Phi_{22} \end{bmatrix} \end{bmatrix} = 0 \qquad (2.30)$$

This can be further simplified to

$$\lambda^m \det \begin{bmatrix} C_1 & C_2 \\ -\Phi_{21} + \Gamma_2(C\Gamma)^{-1}C \begin{bmatrix} \Phi_{11} \\ \Phi_{21} \end{bmatrix} & \lambda I_{n-m} - \Phi_{22} + \Gamma_2(C\Gamma)^{-1}C \begin{bmatrix} \Phi_{12} \\ \Phi_{22} \end{bmatrix} \end{bmatrix} = 0 \qquad (2.31)$$

The above result shows that there are m eigenvalues at the origin.

Remark 5 *The conventional method guarantees that the sliding surface is of order $O(T^2)$ and deadbeat tracking error of order $O(T^2)$. However, deadbeat response is not practical as it requires large control effort and the addition of input saturation would sacrifice global stability.*

2.3 State Regulation with ISM

Consider the new discrete-time integral sliding manifold defined below

$$\begin{aligned} \boldsymbol{\sigma}_k &= D\mathbf{x}_k - D\mathbf{x}_0 + \boldsymbol{\varepsilon}_k \\ \boldsymbol{\varepsilon}_k &= \boldsymbol{\varepsilon}_{k-1} + E\mathbf{x}_{k-1} \end{aligned} \qquad (2.32)$$

where $\boldsymbol{\sigma} \in \Re^m$, $\boldsymbol{\varepsilon} \in \Re^m$, and matrices D and E are constant and of rank m. The term $D\mathbf{x}_0$ is used to eliminate the reaching phase. (2.32) is the discrete-time counterpart of the following sliding manifold, [18]

$$\boldsymbol{\sigma}(t) = D\mathbf{x}(t) - D\mathbf{x}(0) + \int_0^t E\mathbf{x}(\tau)d\tau = 0. \qquad (2.33)$$

Theorem 1 *Assume the pair* (Φ, Γ) *in (2.2) is controllable. There exists a matrix* K *such that the eigenvalues of* $\Phi - \Gamma K$ *are distinct and within the unit circle. Choose the control law*

$$\mathbf{u}_k = (D\Gamma)^{-1} D\mathbf{x}(0) - (D\Gamma)^{-1} \left((D\Phi + E)\mathbf{x}_k + D\hat{\mathbf{d}}_k + \boldsymbol{\varepsilon}_k \right) \tag{2.34}$$

where $D\Gamma$ *is invertible,*

$$E = -D\left(\Phi - I - \Gamma K\right) \tag{2.35}$$

and $\hat{\mathbf{d}}_k$ *is the disturbance compensation (2.57). Then the closed-loop dynamics is*

$$\mathbf{x}_{k+1} = \left(\Phi - \Gamma K\right) \mathbf{x}_k + \boldsymbol{\zeta}_k \tag{2.36}$$

with $\boldsymbol{\zeta}_k \in \Re^n$ *is* $O(T^3)$*, and*

$$\lim_{k \to \infty} \|\mathbf{x}_k\| \leq O(T^2).$$

Proof: Consider a forward expression of (2.32)

$$\begin{aligned} \boldsymbol{\sigma}_{k+1} &= D\mathbf{x}_{k+1} - D\mathbf{x}(0) + \boldsymbol{\varepsilon}_{k+1} \\ \boldsymbol{\varepsilon}_{k+1} &= \boldsymbol{\varepsilon}_k + E\mathbf{x}_k \end{aligned} \tag{2.37}$$

Substituting $\boldsymbol{\varepsilon}_{k+1}$ and (2.2) into the expression of the sliding manifold in (2.37) leads to

$$\boldsymbol{\sigma}_{k+1} = \left(D\Phi + E\right) \mathbf{x}_k + D\left(\Gamma \mathbf{u}_k + \mathbf{d}_k\right) + \boldsymbol{\varepsilon}_k - D\mathbf{x}(0). \tag{2.38}$$

The equivalent control is found by solving for $\boldsymbol{\sigma}_{k+1} = 0$

$$\mathbf{u}_k^{eq} = (D\Gamma)^{-1} D\mathbf{x}(0) - (D\Gamma)^{-1} \left((D\Phi + E)\mathbf{x}_k + D\mathbf{d}_k + \boldsymbol{\varepsilon}_k \right). \tag{2.39}$$

Similar to the classical case with control given by (2.22), implementation of (2.39) would require *a priori* knowledge of the disturbance $\mathbf{d}_k$. By replacing the disturbance in (2.39) with

its estimate $\hat{\mathbf{d}}_k$, which is defined in (2.57), the practical control law is

$$\mathbf{u}_k = (D\Gamma)^{-1} D\mathbf{x}(0) - (D\Gamma)^{-1} \left((D\Phi + E)\mathbf{x}_k + D\hat{\mathbf{d}}_k + \boldsymbol{\varepsilon}_k \right) \tag{2.40}$$

Substitution of $\mathbf{u}_k$ defined by (2.40) into (2.2) leads to the closed-loop equation in the sliding mode

$$\mathbf{x}_{k+1} = [\Phi - \Gamma(D\Gamma)^{-1}(D\Phi + E)]\mathbf{x}_k - \Gamma(D\Gamma)^{-1}\boldsymbol{\varepsilon}_k + \Gamma(D\Gamma)^{-1} D\mathbf{x}(0) + \mathbf{d}_k - \Gamma(D\Gamma)^{-1} D\hat{\mathbf{d}}_k. \tag{2.41}$$

Let us derive the sliding dynamics. Rewriting (2.37)

$$\boldsymbol{\sigma}_{k+1} = D\mathbf{x}_{k+1} + E\mathbf{x}_k - D\mathbf{x}(0) + \boldsymbol{\varepsilon}_k. \tag{2.42}$$

Substituting (2.41) into (2.42) leads to

$$\boldsymbol{\sigma}_{k+1} = D\mathbf{d}_k - D\hat{\mathbf{d}}_k = D\mathbf{d}_k - D\mathbf{d}_{k-1} \in O(T^2), \tag{2.43}$$

that is, the introduction of ISMC leads to the same sliding dynamics as in [4].

Next, solving $\boldsymbol{\varepsilon}_k$ in (2.32) in terms of $\mathbf{x}_k$ and $\boldsymbol{\sigma}_k$

$$\boldsymbol{\varepsilon}_k = \boldsymbol{\sigma}_k - D\mathbf{x}_k + D\mathbf{x}(0), \tag{2.44}$$

and substituting it into (2.41), the closed-loop dynamics becomes

$$\mathbf{x}_{k+1} = \left[\Phi - \Gamma(D\Gamma)^{-1}(D(\Phi - I) + E) \right] \mathbf{x}_k - \Gamma(D\Gamma)^{-1}\boldsymbol{\sigma}_k + \mathbf{d}_k - \Gamma(D\Gamma)^{-1} D\hat{\mathbf{d}}_k. \tag{2.45}$$

In (2.45), $\boldsymbol{\sigma}_k$ can be substituted by $\boldsymbol{\sigma}_k = D\mathbf{d}_{k-1} - D\mathbf{d}_{k-2}$ as can be inferred from (2.43). Also, under (2.35), $D(\Phi - I) + E = D\Gamma K$. Therefore, $\Phi - \Gamma(D\Gamma)^{-1}(D(\Phi - I) + E) = \Phi - \Gamma K$. Since the pair (Φ, Γ) is controllable, there exists a matrix K such that eigenvalues of $\Phi - \Gamma K$ can be

placed anywhere inside the unit disk. Note that, the selection of matrix D is arbitrary as long as it guarantees the invertibility of $D\Gamma$ while matrix E, computed using (2.35), guarantees the desired closed-loop performance. Thus, we have

$$\mathbf{x}_{k+1} = (\Phi - \Gamma K)\,\mathbf{x}_k + \mathbf{d}_k - \Gamma(D\Gamma)^{-1} D\mathbf{d}_{k-1} - \Gamma(D\Gamma)^{-1} D(\mathbf{d}_{k-1} - \mathbf{d}_{k-2}). \tag{2.46}$$

Note that in (2.46), the disturbance estimate $\hat{\mathbf{d}}_k$ has been replaced by $\mathbf{d}_{k-1}$. Further simplification of (2.46) leads to

$$\mathbf{x}_{k+1} = (\Phi - \Gamma K)\,\mathbf{x}_k + \boldsymbol{\zeta}_k \tag{2.47}$$

where

$$\boldsymbol{\zeta}_k = \mathbf{d}_k - 2\Gamma(D\Gamma)^{-1} D\mathbf{d}_{k-1} + \Gamma(D\Gamma)^{-1} D\mathbf{d}_{k-2}. \tag{2.48}$$

The magnitude of $\boldsymbol{\zeta}_k$ can be evaluated as below. Adding and substracting $2\mathbf{d}_{k-1}$ and $\mathbf{d}_{k-2}$ from the right hand side of (2.48) yield

$$\boldsymbol{\zeta}_k = (\mathbf{d}_k - 2\mathbf{d}_{k-1} + \mathbf{d}_{k-2}) + (I - \Gamma(D\Gamma)^{-1} D)(2\mathbf{d}_{k-1} - \mathbf{d}_{k-2}). \tag{2.49}$$

In *Lemma* 1, it has been shown that $(\mathbf{d}_k - 2\mathbf{d}_{k-1} + \mathbf{d}_{k-2}) \in O(T^3)$. On the other hand, from (2.4) we have

$$\begin{aligned}
&(I - \Gamma(D\Gamma)^{-1} D)(2\mathbf{d}_{k-1} - \mathbf{d}_{k-2}) \\
&= (I - \Gamma(D\Gamma)^{-1} D)\left(\Gamma(2\mathbf{f}_{k-1} - \mathbf{f}_{k-2}) + \frac{T}{2}\Gamma(2\mathbf{v}_{k-1} - \mathbf{v}_{k-2}) + O(T^3)\right)
\end{aligned}$$

Note that $(I - \Gamma(D\Gamma)^{-1} D)\Gamma = 0$, thus

$$(I - \Gamma(D\Gamma)^{-1} D)\left(\Gamma(2\mathbf{f}_{k-1} - \mathbf{f}_{k-2}) + \frac{T}{2}\Gamma(2\mathbf{v}_{k-1} - \mathbf{v}_{k-2})\right) = 0.$$

Furthermore, $\|(I - \Gamma(D\Gamma)^{-1}D)\| \leq 1$, thus $(I - \Gamma(D\Gamma)^{-1}D)O(T^3)$ remains $O(T^3)$. This concludes that

$$\boldsymbol{\zeta}_k \in O(T^3).$$

Comparing (2.47) with (2.11), the difference is that $\boldsymbol{\delta}_k \in O(T^2)$ whereas $\boldsymbol{\zeta}_k \in O(T^3)$. Further, by doing a similarity decomposition for dynamics of (2.47), only the J_2 matrix of dimension n exists. Thus the derivation procedure shown in (2.11)-(2.20) holds for (2.47), and the solution is

$$\mathbf{x}_k = (\Phi - \Gamma K)^k \mathbf{x}(0) + \sum_{i=0}^{k-1} (\Phi - \Gamma K)^i \boldsymbol{\zeta}_{k-i-1}. \tag{2.50}$$

Assuming distinct eigenvalues of $\Phi - \Gamma K$ and following the procedure that resulted in (2.20), it can be shown that

$$\lim_{k\to\infty} \left\| \sum_{i=0}^{k-1} (\Phi - \Gamma K)^i \boldsymbol{\zeta}_{k-i-1} \right\| \in O(T^2). \tag{2.51}$$

Finally, it is concluded that

$$\lim_{k\to\infty} \|\mathbf{x}_k\| \leq O(T^2). \tag{2.52}$$

■

Remark 6 *From the foregoing derivations, it can be seen that the state errors are always one order higher than the disturbance term $\boldsymbol{\zeta}$ in the worst case due to convolution as shown by (2.51). After incorporating the intergral sliding manifold, the off-set from the disturbance can be better compensated, in the sequel leading to a smaller steady state error boundary.*

Remark 7 *It is evident from the above analysis that, for the class of systems considered in this Chapter and in [1,2], the equivalent control based SMC with disturbance observer guartantees the motion of the states within an $O(T^2)$ bound, which is smaller than $O(T)$ for T sufficiently small, and is lower than what can be achieved by SMC using switching control [3,4]. In such circumstance, without the loss of precision we can relax the necessity of incorporating a switching term, in the sequel avoid exciting chattering.*

2.4 Output-Tracking ISMC: State Feedback Approach

In this section we discuss the state-feedback-based output ISMC. We first present the controller design using an appropriate integral sliding-surface and a delay-based disturbance estimation. Next the stability condition of the closed-loop system and the error dynnamics under output ISMC are derived. The ultimate tracking error bound is analyzed.

2.4.1 Controller Design

Consider the discrete-time integral sliding surface defined below,

$$\begin{aligned} \boldsymbol{\sigma}_k &= \mathbf{e}_k - \mathbf{e}_0 + \boldsymbol{\varepsilon}_k \\ \boldsymbol{\varepsilon}_k &= \boldsymbol{\varepsilon}_{k-1} + E\mathbf{e}_{k-1} \end{aligned} \tag{2.53}$$

where $\mathbf{e}_k = \mathbf{r}_k - \mathbf{y}_k$ is the tracking error, $\boldsymbol{\sigma}_k$, $\boldsymbol{\varepsilon}_k \in \Re^m$ are the sliding function and integral vectors, and $E \in \Re^{m\times m}$ is an integral gain matrix.

By virtue of the concept of equivalent control, a SMC law can be derived by letting $\boldsymbol{\sigma}_{k+1} = 0$. From (2.53), $-\mathbf{e}_0 + \boldsymbol{\varepsilon}_k = \boldsymbol{\sigma}_k - \mathbf{e}_k$, we have

$$\boldsymbol{\sigma}_{k+1} \;=\; \mathbf{e}_{k+1} - \mathbf{e}_0 + \boldsymbol{\varepsilon}_{k+1} = \mathbf{e}_{k+1} - \mathbf{e}_0 + \boldsymbol{\varepsilon}_k + E\mathbf{e}_k$$

$$= \quad \mathbf{e}_{k+1} - (I_m - E)\mathbf{e}_k + \boldsymbol{\sigma}_k. \tag{2.54}$$

From the system dynamics (2.2), the output error $\mathbf{e}_{k+1}$ is

$$\mathbf{e}_{k+1} = \mathbf{r}_{k+1} - [C\Phi\mathbf{x}_k + C\Gamma\mathbf{u}_k + C\mathbf{d}_k],$$

and

$$\begin{aligned} \boldsymbol{\sigma}_{k+1} &= \mathbf{r}_{k+1} - [C\Phi\mathbf{x}_k + C\Gamma\mathbf{u}_k + C\mathbf{d}_k] - (I_m - E)\mathbf{e} + \boldsymbol{\sigma}_k. \\ &= \mathbf{a}_k - C\Gamma\mathbf{u}_k - C\mathbf{d}_k \end{aligned} \tag{2.55}$$

where $\mathbf{a}_k = \mathbf{r}_{k+1} - \Lambda\mathbf{e}_k - C\Phi\mathbf{x}_k + \boldsymbol{\sigma}_k$, and $\Lambda = I_m - E$. Assuming $\boldsymbol{\sigma}_{k+1} = 0$, we can derive the equivalent control

$$\mathbf{u}_k^{eq} = (C\Gamma)^{-1}(\mathbf{a}_k - C\mathbf{d}_k). \tag{2.56}$$

Note that the control (2.56) is based on the current value of the disturbance $\mathbf{d}_k$ which is unknown and therefore cannot be implemented in the current form. To overcome this, the disturbance estimate will be used. When the system states are accessible, a delay based disturbance estimate can be easily derived from the plant (2.2)

$$\hat{\mathbf{d}}_k = \mathbf{d}_{k-1} = \mathbf{x}_k - \Phi\mathbf{x}_{k-1} - \Gamma\mathbf{u}_{k-1}. \tag{2.57}$$

Note that $\mathbf{d}_{k-1}$ is the exogenous disturbance and bounded, therefore $\hat{\mathbf{d}}_k$ is bounded for all k. Using the disturbance estimation (2.57), the actual ISMC law is given by

$$\mathbf{u}_k = (C\Gamma)^{-1}(\mathbf{a}_k - C\hat{\mathbf{d}}_k). \tag{2.58}$$

2.4.2 Stability Analysis

Since the integral switching surface (2.53) consists of outputs only, it is necessary to examine the closed-loop stability in state space when the ISMC (2.58) and disturbance esitmation (2.57) are used.

Expressing $\mathbf{e}_k = \mathbf{r}_k - C\mathbf{x}_k$, the ISMC law (2.58) can be rewritten as

$$\begin{aligned} \mathbf{u}_k &= (C\Gamma)^{-1}(\mathbf{r}_{k+1} - \Lambda\mathbf{e}_k - C\Phi\mathbf{x}_k + \boldsymbol{\sigma}_k - C\hat{\mathbf{d}}_k) \\ &= -(C\Gamma)^{-1}(C\Phi - \Lambda C)\mathbf{x}_k - (C\Gamma)^{-1}C\hat{\mathbf{d}}_k + (C\Gamma)^{-1}(\mathbf{r}_{k+1} - \Lambda\mathbf{r}_k) \\ &\quad +(C\Gamma)^{-1}\boldsymbol{\sigma}_k. \end{aligned} \tag{2.59}$$

Substituting the above control law (2.60) into the plant (2.2) yields the closed-loop state dynamics

$$\begin{aligned} \mathbf{x}_{k+1} &= [\Phi - \Gamma(C\Gamma)^{-1}(C\Phi - \Lambda C)]\mathbf{x}_k + \mathbf{d}_k - \Gamma(C\Gamma)^{-1}C\hat{\mathbf{d}}_k \\ &\quad +\Gamma(C\Gamma)^{-1}(\mathbf{r}_{k+1} - \Lambda\mathbf{r}_k) + \Gamma(C\Gamma)^{-1}\boldsymbol{\sigma}_k. \end{aligned} \tag{2.60}$$

It can be seen from (2.60) that the stability of $\mathbf{x}_k$ is determined by the matrix $[\Phi - \Gamma(C\Gamma)^{-1}(C\Phi - \Lambda C)]$ and the boundedness of $\boldsymbol{\sigma}_k$.

Lemma 4 *The eignvalues of* $[\Phi - \Gamma(C\Gamma)^{-1}(C\Phi - \Lambda C)]$ *are the eigenvalues of* Λ *and the non-zero eigenvalues of* $[\Phi - \Gamma(C\Gamma)^{-1}C\Phi]$.

Proof See Appendix.

According to Lemma 1, the matrix $[\Phi - \Gamma(C\Gamma)^{-1}(C\Phi - \Lambda C)]$ has m poles to be placed at desired locations while the remaining $n-m$ poles are the open-loop zeros of the plant (Φ, Γ, C). Since, the plant (2.2) is assumed to be minimum-phase, the $n-m$ poles are stable. Therefore,

stability of the closed-loop state dynamics is guaranteed. Note that if Λ is a zero matrix then m poles are zero and the performance will be the same as the conventional deadbeat sliding-mode controller design.

Since we use disturbance estimate, $\boldsymbol{\sigma}_k \neq 0$. To show the boundedness and facilitate later analysis on the tracking performance, we derive the relationship between the switching surface and the distrubance estimate, as well as the relationship between the output tracking error and the disturbance estimate.

Theorem 2 *Assume that the system (2.2) is minimum-phase and the eigenvalues of the matrix Λ are within the unit circle. Then by the control law (2.58) we have*

$$\boldsymbol{\sigma}_{k+1} = C(\hat{\mathbf{d}}_k - \mathbf{d}_k) \tag{2.61}$$

and the error dynamics

$$\mathbf{e}_{k+1} = \Lambda \mathbf{e}_k + \boldsymbol{\delta}_k \tag{2.62}$$

where $\boldsymbol{\delta}_k = C(\hat{\mathbf{d}}_k - \mathbf{d}_k + \mathbf{d}_{k-1} - \hat{\mathbf{d}}_{k-1})$.

Proof: In order to verify the first part of Theorem 2, rewrite (5.11) as

$$\begin{aligned} \boldsymbol{\sigma}_{k+1} &= \mathbf{a}_k - C\Gamma\mathbf{u}_k - C\mathbf{d}_k = \mathbf{a}_k - C\Gamma\mathbf{u}_k^{eq} - C\mathbf{d}_k + C\Gamma(\mathbf{u}_k^{eq} - \mathbf{u}_k) \\ &= C\Gamma(\mathbf{u}_k^{eq} - \mathbf{u}_k), \end{aligned}$$

where we use the property of equivalent control $\boldsymbol{\sigma}_{k+1} = \mathbf{a}_k - C\Gamma\mathbf{u}_k^{eq} - C\mathbf{d}_k = 0$. Comparing two control laws (2.56) and (2.58), we obtain

$$\boldsymbol{\sigma}_{k+1} = C(\hat{\mathbf{d}}_k - \mathbf{d}_k).$$

Note that the switching surface $\boldsymbol{\sigma}_{k+1}$ is no longer zero as desired but a function of the difference $\mathbf{d}_k - \hat{\mathbf{d}}_k$. This, however, is acceptable since the difference is $\mathbf{d}_k - \hat{\mathbf{d}}_k = \mathbf{d}_k - \mathbf{d}_{k-1}$ by the delay based disturbance estimation; thus, according to property P1 the difference is $O(T^2)$ which is quite small in practical applications.

To derive the second part of Theorem 2 regarding the error dynamics, rewritting (2.54) as

$$\mathbf{e}_{k+1} = \Lambda \mathbf{e}_k + \boldsymbol{\sigma}_{k+1} - \boldsymbol{\sigma}_k,$$

and substituting the relationship (2.61), lead to

$$\begin{aligned} \mathbf{e}_{k+1} &= \Lambda \mathbf{e}_k + C(\hat{\mathbf{d}}_k - \mathbf{d}_k) - C(\hat{\mathbf{d}}_{k-1} - \mathbf{d}_{k-1}) \\ &= \Lambda \mathbf{e}_k + C(\hat{\mathbf{d}}_k - \mathbf{d}_k + \mathbf{d}_{k-1} - \hat{\mathbf{d}}_{k-1}) = \Lambda \mathbf{e}_k + \boldsymbol{\delta}_k. \end{aligned}$$

Since $\hat{\mathbf{d}}_k = \mathbf{d}_{k-1}$, $\boldsymbol{\delta}_k$ is bounded, from *Property 2* we can conclude the boundedness of $\mathbf{e}_k$. ■

2.4.3 Tracking Error Bound

The tracking performance of the ISMC can be evaluated in terms of the error dynamics (2.62).

Theorem 3 *Using the delay-based disturbance estimation (2.57), the ultimate tracking error bound with ISM control is given by*

$$\|\mathbf{e}_k\| = O(T^2)$$

where $\|\cdot\|$ *represents the Euclidean norm.*

Proof: In order to calculate the tracking error bound we must find the bound of $\boldsymbol{\delta}_k$. From Theorem 2

$$\boldsymbol{\delta}_k = C(\hat{\mathbf{d}}_k - \mathbf{d}_k + \mathbf{d}_{k-1} - \hat{\mathbf{d}}_{k-1}).$$

Substituting $\hat{\mathbf{d}}_k = \mathbf{d}_{k-1}$ from (2.57)

$$\boldsymbol{\delta}_k = C(\mathbf{d}_{k-1} - \mathbf{d}_k + \mathbf{d}_{k-1} - \mathbf{d}_{k-2})$$

which simplifies to

$$\boldsymbol{\delta}_k = -C(\mathbf{d}_k - 2\mathbf{d}_{k-1} + \mathbf{d}_{k-2}). \tag{2.63}$$

According to property P1, $\mathbf{d}_k - 2\mathbf{d}_{k-1} + \mathbf{d}_{k-2} = O(T^3)$, therefore $\boldsymbol{\delta}_k = O(T^3)$. According to *Property 2*, the ultimate error bound on $\|\mathbf{e}_k\|$ in the expression $\mathbf{e}_{k+1} = \Lambda\mathbf{e}_k + \boldsymbol{\delta}_k$ will be one order higher than the bound on $\boldsymbol{\delta}_k$ due to convolution. Since the bound on $\boldsymbol{\delta}_k$ is $O(T^3)$, the ultimate bound on $\|\mathbf{e}_k\|$ is $O(T^2)$. ■

Remark 8 *In practical control a disturbance could be piece-wise smooth. The delay based estimation (2.57) can quickly capture the varying disturbance after one sampling interval. Assume that the disturbance* $\mathbf{f}$ *undergoes an abrupt change at the time interval* $[(k-1)T, kT]$*, then Property 1 does not hold for the time instance* k *because* $\mathbf{v}(t)$ *becomes extremely big. Novertheless, properties P1 and P2 will be achieved immediately after the time instance* k *if the disturbance becomes smooth again. Analogously property P3 will be achieved after the time instance* $k+1$ *and P4 after* $k+2$*. From this point of view, the delay-based estimation has a very small time delay or equivalently a large bandwidth.*

Remark 9 *Although the state-feedback approach may seem to be not very practical for a number of output tracking tasks, this section serves as a precursor to the output-feedback-based and state-observer-based approaches to be explored in subsequent sections.*

2.5 Output Tracking ISM: Output Feedback Approach

In this section we derive ISMC that only uses the output tracking error. The new design will require a reference model and a dynamic disturbance observer due to the lack of the state information. The reference model will be constructed such that its output is the reference trajectory $\mathbf{r}_k$.

2.5.1 Controller Design

In order to proceed we will first define a reference model

$$\begin{aligned} \mathbf{x}_{r,k+1} &= (\Phi - K_1)\mathbf{x}_{r,k} + K_2\mathbf{r}_k \\ \mathbf{y}_{r,k} &= C\mathbf{x}_{r,k} \end{aligned} \tag{2.64}$$

where $\mathbf{x}_{r,k} \in \Re^m$ is the state vector, $\mathbf{y}_{r,k} \in \Re^m$ is the output vector, and $\mathbf{r}_k \in \Re^m$ is a bounded reference trajectory. K_1 is selected such that $(\Phi - K_1)$ is stable. The selection criteria for the matrices K_1 and K_2 will be discussed in detail in §4.4.

Now consider a new sliding surface

$$\begin{aligned} \boldsymbol{\sigma}_k &= D(\mathbf{x}_{r,k} - \mathbf{x}_k) + \boldsymbol{\varepsilon}_k \\ \boldsymbol{\varepsilon}_k &= \boldsymbol{\varepsilon}_{k-1} + ED(\mathbf{x}_{r,k-1} - \mathbf{x}_{k-1}) \end{aligned} \tag{2.65}$$

where $D = C\Phi^{-1}$, $\boldsymbol{\sigma}_k, \boldsymbol{\varepsilon}_k \in \Re^m$ are the switching function and integral vectors, $E \in \Re^{m\times m}$ is an integral gain matrix. Note that $D\mathbf{x}_k = C\Phi^{-1}(\Phi\mathbf{x}_{k-1}+\Gamma\mathbf{u}_{k-1}+\mathbf{d}_{k-1}) = \mathbf{y}_{k-1}+D(\Gamma\mathbf{u}_{k-1}+\mathbf{d}_{k-1})$ is independent of the states, such a simplification was first proposed in [25].

The equivalent control law can be derived from $\boldsymbol{\sigma}_{k+1} = 0$. From (2.65) $\boldsymbol{\varepsilon}_k = \boldsymbol{\sigma}_k - D(\mathbf{x}_{r,k} - \mathbf{x}_k)$, we have

$$\boldsymbol{\sigma}_{k+1} = D(\mathbf{x}_{r,k+1} - \mathbf{x}_{k+1}) + \boldsymbol{\varepsilon}_{k+1}$$

$$
\begin{aligned}
&= D(\mathbf{x}_{r,k+1} - \mathbf{x}_{k+1}) + \boldsymbol{\varepsilon}_k + ED(\mathbf{x}_{r,k} - \mathbf{x}_k) \\
&= D(\mathbf{x}_{r,k+1} - \mathbf{x}_{k+1}) + \boldsymbol{\sigma}_k - D(\mathbf{x}_{r,k} - \mathbf{x}_k) + ED(\mathbf{x}_{r,k} - \mathbf{x}_k) \\
&= D\mathbf{x}_{r,k+1} - D\mathbf{x}_{k+1} + \boldsymbol{\sigma}_k - \Lambda D(\mathbf{x}_{r,k} - \mathbf{x}_k) \qquad (2.66)
\end{aligned}
$$

where $\Lambda = I - E$. Substituting the system dynamics (2.2) into (2.66) yields

$$
\begin{aligned}
\boldsymbol{\sigma}_{k+1} &= D\mathbf{x}_{r,k+1} - D(\Phi\mathbf{x}_k + \Gamma\mathbf{u}_k + \mathbf{d}_k) + \boldsymbol{\sigma}_k - \Lambda D(\mathbf{x}_{r,k} - \mathbf{x}_k) \\
&= \mathbf{a}_k - D\Gamma\mathbf{u}_k - D\mathbf{d}_k \qquad (2.67)
\end{aligned}
$$

where $\mathbf{a}_k = -(D\Phi - \Lambda D)\mathbf{x}_k + (D\mathbf{x}_{r,k+1} - \Lambda D\mathbf{x}_{r,k}) + \boldsymbol{\sigma}_k$.

Letting $\boldsymbol{\sigma}_{k+1} = 0$, solving for the equivalent control $\mathbf{u}_k^{eq}$, we have

$$
\begin{aligned}
\mathbf{u}_k^{eq} &= (D\Gamma)^{-1}(\mathbf{a}_k - D\mathbf{d}_k) \\
&= -(D\Gamma)^{-1}(D\Phi - \Lambda D)\mathbf{x}_k + (D\Gamma)^{-1}(D\mathbf{x}_{r,k+1} - \Lambda D\mathbf{x}_{r,k}) - (D\Gamma)^{-1}D\mathbf{d}_k.
\end{aligned}
\qquad (2.68)
$$

Controller (2.68) is not implementable as it requires *a priori* knowledge of the disturbance. Thus, the estimation of the disturbance should be used

$$
\mathbf{u}_k = (D\Gamma)^{-1}(\mathbf{a}_k - D\hat{\mathbf{d}}_k) \qquad (2.69)
$$

where $\hat{\mathbf{d}}_k$ is the disturbance estimation.

However, note that the disturbance estimate used in the state feedback controller desgined in §3 requires full state information which is not available in this case. Therefore, an observer that is based on output feedback is proposed and will be detailed in §4.2.

2.5.2 Disturbance Observer Design

Note that according to *Property 1*, the disturbance can be written as

$$\mathbf{d}_k = \Gamma \mathbf{f}_k + \frac{1}{2}\Gamma \mathbf{v}_k T + O(T^3) = \Gamma \boldsymbol{\eta}_k + O(T^3) \tag{2.70}$$

where $\boldsymbol{\eta}_k = \mathbf{f}_k + \frac{1}{2}\mathbf{v}_k T$. If $\boldsymbol{\eta}_k$ can be estimated, then the estimation error of $\mathbf{d}_k$ would be $O(T^3)$ which is acceptable in practical applications.

Define the observer

$$\begin{aligned} \mathbf{x}_{d,k} &= \Phi \mathbf{x}_{d,k-1} + \Gamma \mathbf{u}_{k-1} + \Gamma \hat{\boldsymbol{\eta}}_{k-1} \\ \mathbf{y}_{d,k-1} &= C\mathbf{x}_{d,k-1} \end{aligned} \tag{2.71}$$

where $\mathbf{x}_{d,k-1} \in \Re^n$ is the observer state vector, $\mathbf{y}_{d,k-1} \in \Re^m$ is the observer output vector, $\hat{\boldsymbol{\eta}}_{k-1} \in \Re^m$ is the disturbance estimate and will act as the 'control input' to the observer, therefore we can write $\hat{\mathbf{d}}_{k-1} = \Gamma \hat{\boldsymbol{\eta}}_{k-1}$. Since the disturbance estimate will be used in the final control signal, it must not be overly large. Therefore, it is wise to avoid a deadbeat design. For this reason we design the disturbance observer based on an integral sliding surface

$$\begin{aligned} \boldsymbol{\sigma}_{d,k} &= \mathbf{e}_{d,k} - \mathbf{e}_{d,0} + \boldsymbol{\varepsilon}_{d,k} \\ \boldsymbol{\varepsilon}_{d,k} &= \boldsymbol{\varepsilon}_{d,k-1} + E_d \mathbf{e}_{d,k-1} \end{aligned} \tag{2.72}$$

where $\mathbf{e}_{d,k} = \mathbf{y}_k - \mathbf{y}_{d,k}$ is the output estimation error, $\boldsymbol{\sigma}_{d,k}, \boldsymbol{\varepsilon}_{d,k} \in \Re^m$ are the sliding function and integral vectors, and E_d is an integral gain matrix.

Note that the sliding surface (2.72) is analogous to (2.53), that is, the set $(\mathbf{y}_k, \mathbf{x}_{d,k}, \mathbf{u}_k + \hat{\boldsymbol{\eta}}_k, \mathbf{y}_{d,k}, \boldsymbol{\sigma}_{d,k})$ has duality with the set $(\mathbf{r}_k, \mathbf{x}_k, \mathbf{u}_k, \mathbf{y}_k, \boldsymbol{\sigma}_k)$, except for an one-step delay in the observer dynamics (2.71). Therefore, let $\boldsymbol{\sigma}_{d,k} = 0$ we can derive the virtual equivalent control

$\mathbf{u}_{k-1} + \hat{\boldsymbol{\eta}}_{k-1}$, thus, analogous to (2.60),

$$\hat{\boldsymbol{\eta}}_{k-1} = (C\Gamma)^{-1} \left[\mathbf{y}_k - \Lambda_d \mathbf{e}_{d,k-1} - C\Phi \mathbf{x}_{d,k-1} + \boldsymbol{\sigma}_{d,k-1}\right] - \mathbf{u}_{k-1} \tag{2.73}$$

where $\Lambda_d = I_m - E_d$.

In practice, the quantity $\mathbf{y}_{k+1}$ is not available at the time instance k when computing $\hat{\boldsymbol{\eta}}_k$. Therefore we can only compute $\hat{\boldsymbol{\eta}}_{k-1}$, and in the control law (2.69) we use the delayed estimate $\hat{\mathbf{d}}_k = \Gamma \hat{\boldsymbol{\eta}}_{k-1}$.

The stability and convergence properties of the observer (2.71) and the disturbance estimation (2.73) are analyzed in the following theorem.

Theorem 4 *The observer output $\mathbf{y}_{d,k}$ converges asymptotically to the true outputs $\mathbf{y}_k$, and the disturbance estimate $\hat{\mathbf{d}}_k$ converges to the actual disturbance $\mathbf{d}_{k-1}$ with the precision order $O(T^2)$.*

Proof: Substituting (2.73) into (2.71), and using the relation $\mathbf{e}_{d,k-1} = C(\mathbf{y}_{k-1} - \mathbf{y}_{d,k-1})$, yield

$$\begin{aligned} \mathbf{x}_{d,k} &= \left[\Phi - \Gamma(C\Gamma)^{-1}(C\Phi - \Lambda_d C)\right] \mathbf{x}_{d,k-1} + \Gamma(C\Gamma)^{-1}[\mathbf{y}_k - \Lambda_d \mathbf{y}_{k-1}] \\ &\quad + \Gamma(C\Gamma)^{-1} \boldsymbol{\sigma}_{d,k-1}. \end{aligned} \tag{2.74}$$

Since the control and estimate $\mathbf{u}_{k-1} + \hat{\boldsymbol{\eta}}_{k-1}$ are chosen such that $\boldsymbol{\sigma}_{d,k} = 0$ for any $k > 0$, (2.74) renders to

$$\mathbf{x}_{d,k} = \left[\Phi - \Gamma(C\Gamma)^{-1}(C\Phi - \Lambda_d C)\right] \mathbf{x}_{d,k-1} + \Gamma(C\Gamma)^{-1}[\mathbf{y}_k - \Lambda_d \mathbf{y}_{k-1}]. \tag{2.75}$$

The second term on the right hand side of (2.75) can be expressed as

$$\Gamma(C\Gamma)^{-1}[\mathbf{y}_k - \Lambda_d \mathbf{y}_{k-1}] \;=\; \Gamma(C\Gamma)^{-1}(C\Phi - \Lambda_d C)\mathbf{x}_{k-1} + \Gamma\mathbf{u}_{k-1} + \Gamma(C\Gamma)^{-1}C\mathbf{d}_{k-1}$$

by using the relations $\mathbf{y}_k = C\Phi\mathbf{x}_{k-1} + C\Gamma\mathbf{u}_{k-1} + C\mathbf{d}_{k-1}$ and $\mathbf{y}_{k-1} = C\mathbf{x}_{k-1}$. Therefore (5.26) can be rewritten as

$$\mathbf{x}_{d,k} \;=\; \Phi\mathbf{x}_{d,k-1} + \Gamma(C\Gamma)^{-1}(C\Phi - \Lambda_d C)\Delta\mathbf{x}_{d,k-1} + \Gamma\mathbf{u}_k + \Gamma(C\Gamma)^{-1}C\mathbf{d}_{k-1} \tag{2.76}$$

where $\Delta\mathbf{x}_{d,k-1} = \mathbf{x}_{k-1} - \mathbf{x}_{d,k-1}$.

Further subtracting (2.76) from the system (2.2) we obtain

$$\Delta\mathbf{x}_{d,k} \;=\; \left[\Phi - \Gamma(C\Gamma)^{-1}(C\Phi - \Lambda_d C)\right]\Delta\mathbf{x}_{d,k-1} + [I - \Gamma(C\Gamma)^{-1}C]\mathbf{d}_{k-1} \tag{2.77}$$

where $[I - \Gamma(C\Gamma)^{-1}C]\mathbf{d}_{k-1}$ is $O(T^3)$ because

$$[I - \Gamma(C\Gamma)^{-1}C][\Gamma\boldsymbol{\eta}_{k-1} + O(T^3)] = [I - \Gamma(C\Gamma)^{-1}C]O(T^3) = O(T^3).$$

Applying the *Property 2*, $\Delta\mathbf{x}_{d,k-1} = O(T^2)$.

From (2.77) we can see that the stability of the disturbance observer depends only on the matrix $[\Phi - \Gamma(C\Gamma)^{-1}(C\Phi - \Lambda_d C)]$ and is guaranteed by the selection of the matrix Λ_d and the fact that system (Φ, Γ, C) is minimum phase. It should also be noted that the residue term $[I - \Gamma(C\Gamma)^{-1}C]\mathbf{d}_{k-1}$ in the state space is orthogonal to the output space, as $C[I - \Gamma(C\Gamma)^{-1}C]\mathbf{d}_{k-1} = 0$. Therefore premultliplication of (2.77) with C yields the output tracking error dynamics

$$\mathbf{e}_{d,k} \;=\; \Lambda_d \mathbf{e}_{d,k-1} \tag{2.78}$$

which is asymptotically stable through choosing a stable matrix Λ_d.

Finally we discuss the convergence property of the estimate $\hat{\mathbf{d}}_{k-1}$. Subtracting (2.71) from (2.2) with one-step delay, we obtain

$$\Delta \mathbf{x}_{d,k} = \Phi \Delta \mathbf{x}_{d,k-1} + \Gamma(\boldsymbol{\eta}_{k-1} - \hat{\boldsymbol{\eta}}_{k-1}) + O(T^3). \tag{2.79}$$

Premultiplying (2.79) with C, and substituting (2.78) that describes $C\Delta \mathbf{x}_{d,k}$, yield

$$\hat{\boldsymbol{\eta}}_{k-1} \;=\; \boldsymbol{\eta}_{k-1} + (C\Gamma)^{-1}(C\Phi - \Lambda_d C)\Delta \mathbf{x}_{d,k-1} + (C\Gamma)^{-1} O(T^3). \tag{2.80}$$

The second term on the right hand side of (2.80) is $O(T)$ because $\Delta \mathbf{x}_{d,k-1} = O(T^2)$ but $(C\Gamma)^{-1} = O(T^{-1})$. As a result, from (2.80) we can conclude that $\hat{\boldsymbol{\eta}}_{k-1}$ approaches $\boldsymbol{\eta}_{k-1}$ with the precision $O(T)$. In terms of the relationship

$$\mathbf{d}_{k-1} - \hat{\mathbf{d}}_k = \Gamma(\boldsymbol{\eta}_{k-1} - \hat{\boldsymbol{\eta}}_{k-1}) + O(T^3)$$

and $\Gamma = O(T)$, we conclude $\hat{\mathbf{d}}_k$ converges to $\mathbf{d}_{k-1}$ with the precision of $O(T^2)$. ∎

Remark 10 *At the time k, we can guarantee the convergence of $\hat{\boldsymbol{\eta}}_{k-1}$ to $\boldsymbol{\eta}_{k-1}$ with the precision $O(T)$. In other words, we can guarantee the convergence of the disturbance estimate at the time k, $\hat{\mathbf{d}}_k$, to the actual disturbance at time $k-1$, $\mathbf{d}_{k-1}$, with the precision $O(T^2)$. This result is consistent with the state-based estimation presented in §3 in which $\hat{\mathbf{d}}_k$ is made equal to $\mathbf{d}_{k-1}$. Comparing differences between the state-based and output-based disturbance estimation, the former has only one-step delay with perfect precision, whereas the latter is asymptotic with $O(T^2)$ precision.*

2.5.3 Stability Analysis

To analyze the stability of the closed-loop system, substitute $\mathbf{u}_k$ in (2.69) into the plant (2.2) leading to the closed-loop equation in the sliding mode

$$\begin{aligned}\mathbf{x}_{k+1} &= \left[\Phi - \Gamma(D\Gamma)^{-1}(D\Phi - \Lambda D)\right]\mathbf{x}_k + \mathbf{d}_k - \Gamma(D\Gamma)^{-1}D\hat{\mathbf{d}}_k \\ &\quad + \Gamma(D\Gamma)^{-1}[D\mathbf{x}_{r,k+1} - \Lambda D\mathbf{x}_{r,k} + \boldsymbol{\sigma}_k]. \end{aligned} \tag{2.81}$$

The stability of the above sliding equation is summarized in the following theorem.

Theorem 5 *Using the control law (2.69) the sliding mode is*

$$\boldsymbol{\sigma}_{k+1} = D(\hat{\mathbf{d}}_k - \mathbf{d}_k).$$

Further, the state tracking error $\Delta\mathbf{x}_k = \mathbf{x}_{r,k} - \mathbf{x}_k$ is bounded if system (Φ, Γ, D) is minimum-phase and the eigenvalues of the matrix Λ are within the unit circle.

Proof: In order to verify the first part of Theorem 5, rewrite the dynamics of the slidng mode (2.67)

$$\begin{aligned}\boldsymbol{\sigma}_{k+1} &= \mathbf{a}_k - D\Gamma\mathbf{u}_k - D\mathbf{d}_k = \mathbf{a}_k - D\Gamma\mathbf{u}_k^{eq} - D\mathbf{d}_k + D\Gamma(\mathbf{u}_k^{eq} - \mathbf{u}_k) \\ &= D\Gamma(\mathbf{u}_k^{eq} - \mathbf{u}_k),\end{aligned}$$

where we use the property of equivalent control $\boldsymbol{\sigma}_{k+1} = \mathbf{a}_k - D\Gamma\mathbf{u}_k^{eq} - D\mathbf{d}_k = 0$. Comparing two control laws (2.68) and (2.69), we obtain

$$\boldsymbol{\sigma}_{k+1} = D(\hat{\mathbf{d}}_k - \mathbf{d}_k).$$

Note that if there is no disturbance or we have perfect estimation of the disturbance, then $\boldsymbol{\sigma}_{k+1} = 0$ as desired. From the results of Theorem 3 and *Property 1*

$$\hat{\mathbf{d}}_k - \mathbf{d}_k = \hat{\mathbf{d}}_k - \mathbf{d}_{k-1} - (\mathbf{d}_k - \mathbf{d}_{k-1}) = O(T^2)$$

as $k \to \infty$. Thus $\boldsymbol{\sigma}_{k+1} \to O(T^2)$ which is acceptable in practice.

To prove the boundedness of the state tracking error $\Delta\mathbf{x}_k$, first derive the state error dynamics. Subtracting both sides of (2.81) from the refernece model (2.64), and substituting $\boldsymbol{\sigma}_k = D(\hat{\mathbf{d}}_{k-1} - \mathbf{d}_{k-1})$, yields

$$\begin{aligned} \Delta\mathbf{x}_{k+1} &= \left[\Phi - \Gamma(D\Gamma)^{-1}(D\Phi - \Lambda D)\right]\Delta\mathbf{x}_k \\ &\quad + [I - \Gamma(D\Gamma)^{-1}D](K_2\mathbf{r}_{k+1} - K_1\mathbf{x}_{r,k}) - \boldsymbol{\zeta}_k \end{aligned} \tag{2.82}$$

where

$$\boldsymbol{\zeta}_k = \mathbf{d}_k - \Gamma(D\Gamma)^{-1}D(\hat{\mathbf{d}}_k - \hat{\mathbf{d}}_{k-1} + \mathbf{d}_{k-1}). \tag{2.83}$$

The stability of (2.82) is dependent on $[\Phi - \Gamma(D\Gamma)^{-1}(D\Phi - \Lambda D)]$. From Lemma 1 the closed-loop poles of (2.82) are the eigenvalues of Λ and the open-loop zeros of the system (Φ, Γ, D). Thus, m poles of the closed-loop system can be selected by the proper choice of the matrix Λ while the remaining poles are stable only if the system (Φ, Γ, D) is minimum-phase. Note that both $\mathbf{r}_{k+1}$ and $\mathbf{x}_{r,k}$ are reference signals and are bounded. Therefore we need only to show the boundedness of $\boldsymbol{\zeta}_k$ which is

$$\begin{aligned} \boldsymbol{\zeta}_k &= \left(I - \Gamma(D\Gamma)^{-1}D\right)\mathbf{d}_k + \Gamma(D\Gamma)^{-1}D(\mathbf{d}_k - \hat{\mathbf{d}}_k) \\ &\quad - \Gamma(D\Gamma)^{-1}D(\mathbf{d}_{k-1} - \hat{\mathbf{d}}_{k-1}). \end{aligned} \tag{2.84}$$

From Theorem 3, the second and third terms on the right hand side of (2.84) are $O(T^2)$. From *Property 1*, the first term on the right hand side of (2.84) can be written as

$$\left(I - \Gamma(D\Gamma)^{-1}D\right)\mathbf{d}_k = \left(I - \Gamma(D\Gamma)^{-1}D\right)\left(\Gamma\boldsymbol{\eta}_k + O(T^3)\right) = O(T^3).$$

Therefore $\boldsymbol{\zeta}_k = O(T^2)$ which is bounded. ∎

2.5.4 Reference Model Selection and Tracking Error Bound

We have established the stability condition for the closed-loop system, but, have yet to establish the ultimate tracking error bound. From (2.82) it can be seen that the tracking error bound is dependent on the disturbance estimate $\hat{\mathbf{d}}_k$ as well as the selection of K_1 and K_2. Up to this point, not much was discussed in terms of the selection of the reference model (2.64). As it can be seen from (2.82) the selection of the reference model can effect the overall tracking error bound. Since we consider an arbitrary reference $\mathbf{r}_k$, the reference model must be selected such that its output is the reference signal $\mathbf{r}_k$. To achieve this requirement, we explore two possible selections of the reference model.

Reference model based on (Φ, Γ, C) being minimum-phase

For this reference model select the matrices $K_1 = \Gamma(C\Gamma)^{-1}C\Phi$ and $K_2 = \Gamma(C\Gamma)^{-1}$ and the reference model (2.64) can be written as

$$\begin{aligned} \mathbf{x}_{r,k+1} &= [\Phi - \Gamma(C\Gamma)^{-1}C\Phi]\,\mathbf{x}_{r,k} + \Gamma(C\Gamma)^{-1}\mathbf{r}_{k+1} \\ \mathbf{y}_{r,k} &= C\mathbf{x}_{r,k} = \mathbf{r}_k. \end{aligned} \tag{2.85}$$

It can be easily seen from (2.85) that it is stable only if the matrix $[\Phi - \Gamma(C\Gamma)^{-1}C\Phi]$ is stable, i.e., the system (Φ, Γ, C) is minimum-phase. Substituting the selected matrices K_1 and K_2

into (2.82) and using the fact that $[I - \Gamma(D\Gamma)^{-1}D]\,\Gamma = 0$, we obtain

$$\Delta\mathbf{x}_{k+1} = \left[\Phi - \Gamma(D\Gamma)^{-1}(D\Phi - \Lambda_d D)\right]\Delta\mathbf{x}_k - \boldsymbol{\zeta}_k. \tag{2.86}$$

where $\boldsymbol{\zeta}_k = O(T^2)$ according to Theorem 4.

According to *Property 2*, the ultimate error bound on $\|\Delta\mathbf{x}_k\|$ will be one order higher than the bound on $\boldsymbol{\zeta}_k$. Thus, the ultimate bound on the output tracking error is

$$\|\mathbf{e}_k\| \;\leq\; \|C\|\|\Delta\mathbf{x}_k\| \;=\; O(T). \tag{2.87}$$

Reference model based on (Φ, Γ, D) being minimum-phase

In the case that it is only possible to satisfy (Φ, Γ, D) to be minimum-phase, a different reference model needs to be selected. For this new reference model, select the matrices $K_1 = \Gamma(D\Gamma)^{-1}D\Phi$ and $K_2 = \Gamma(D\Gamma)^{-1}$. Then the reference model (2.64) can be written as

$$\begin{aligned} \mathbf{x}_{r,k+1} &= [\Phi - \Gamma(D\Gamma)^{-1}D\Phi]\,\mathbf{x}_{r,k} + \Gamma(D\Gamma)^{-1}\mathbf{r}_{k+1} \\ \mathbf{y}_{r,k} &= D\mathbf{x}_{r,k} = \mathbf{r}_k. \end{aligned} \tag{2.88}$$

The matrix $[\Phi - \Gamma(D\Gamma)^{-1}C\Phi]$ is stable only if (Φ, Γ, D) is minimum-phase. Substituting the selected matrices K_1 and K_2 into (2.82), and using the property $[I - \Gamma(D\Gamma)^{-1}D]\Gamma = 0$, we have

$$\Delta\mathbf{x}_{k+1} \;=\; \left[\Phi - \Gamma(D\Gamma)^{-1}(D\Phi - \Lambda D)\right]\Delta\mathbf{x}_k - \boldsymbol{\zeta}_k. \tag{2.89}$$

We can see from (2.89) that the tracking error bound is only dependent on the disturbance estimtation $\boldsymbol{\zeta}_k$.

On the other hand, the disturbance observer requires (Φ, Γ, C) to be minimum-phase, hence is not implementable in this case. Without the disturbance estimator, noticing *Property 1*,

(2.83) becomes

$$\begin{aligned}\boldsymbol{\zeta}_k &= \mathbf{d}_k - \Gamma(D\Gamma)^{-1}\mathbf{d}_{k-1} \\ &= \mathbf{d}_k - \mathbf{d}_{k-1} + [I - \Gamma(D\Gamma)^{-1}D](\Gamma\boldsymbol{\eta}_{k-1} + O(T^3)) \\ &= O(T^2) + O(T^3) = O(T^2). \end{aligned} \tag{2.90}$$

As the result, the closed-loop system is

$$\Delta\mathbf{x}_{k+1} = \left[\Phi - \Gamma(D\Gamma)^{-1}(D\Phi - \Lambda D)\right]\Delta\mathbf{x}_k + O(T^2). \tag{2.91}$$

By *Property 2*, the ultimate bound on $\|\Delta\mathbf{x}_k\| = O(T)$, and therefore, the ultimate bound on the tracking error is

$$\|\mathbf{e}_k\| \leq \|D\|\|\Delta\mathbf{x}_k\| = O(T). \tag{2.92}$$

While this approach gives a similar precision in output tracking performance, it only requires (Φ, Γ, D) to be minimum-phase and can be used in the cases (Φ, Γ, C) is not minimum-phase.

2.6 Output Tracking ISM: State Observer Approach

In this section we explore the observer-based approach for the unknown states when only output measurement is available. By virtue of state estimation, it is required that (Φ, Γ, C) to be minimum-phase, thus, the observer based disturnance estimation approach in §2.5.2 is applicable. From the derivation procedure in §2.5.2, we can see that the error dynamics (2.78) of the disturbance observer (2.71) is independent of the control inputs $\mathbf{u}_k$. Therefore the same disturbance observer (2.71) - (2.73) can be incorporated in the state-observer approach

directly without any modification. In this section we focus on the design and analysis of the controller and state observer.

2.6.1 Controller Structure and Closed-Loop System

With the state estimation, the ISMC can be constructed according to the preceding state-feedback based ISMC design (2.60) by substituting $C\Phi\mathbf{x}_k$ with $C\Phi\mathbf{x}_k - C\Phi\tilde{\mathbf{x}}_k$ where $\tilde{\mathbf{x}}_k = \mathbf{x}_k - \hat{\mathbf{x}}_k$ is the state estimation error,

$$\begin{aligned}\mathbf{u}_k &= -(C\Gamma)^{-1}(C\Phi - \Lambda C)\mathbf{x}_k - (C\Gamma)^{-1}C\hat{\mathbf{d}}_k + (C\Gamma)^{-1}(\mathbf{r}_{k+1} - \Lambda\mathbf{r}_k) \\ &\quad +(C\Gamma)^{-1}\boldsymbol{\sigma}_k + (C\Gamma)^{-1}C\Phi\tilde{\mathbf{x}}_k. \end{aligned} \tag{2.93}$$

Comparing the controller (2.60), the controller (2.93) has an extra term $(C\Gamma)^{-1}C\Phi\tilde{\mathbf{x}}_k$ due to the state estimation error. Substituting $\mathbf{u}_k$ (2.93) into (2.2) yields the closed-loop dynamics

$$\begin{aligned}\mathbf{x}_{k+1} &= [\Phi - \Gamma(C\Gamma)^{-1}(C\Phi - \Lambda C)]\mathbf{x}_k + \mathbf{d}_k - \Gamma(C\Gamma)^{-1}C\hat{\mathbf{d}}_k \\ &\quad +\Gamma(C\Gamma)^{-1}(\mathbf{r}_{k+1} - \Lambda\mathbf{r}_k) + \Gamma(C\Gamma)^{-1}\boldsymbol{\sigma}_k + \Gamma(C\Gamma)^{-1}C\Phi\tilde{\mathbf{x}}_k, \end{aligned} \tag{2.94}$$

which, comapring with the state-feedback (2.60), is aolmost the same except for an extra term $\Gamma(C\Gamma)^{-1}C\Phi\tilde{\mathbf{x}}_k$. Hence, following the Theorem 1 proof, the properties of the closed-loop system (2.94) can be derived.

Theorem 6 *Assume that the system (2.2) is minimum-phase and the eigenvalues of the matrix Λ are within the unit circle. Then by the control law (2.93) we have*

$$\boldsymbol{\sigma}_{k+1} = C(\hat{\mathbf{d}}_k - \mathbf{d}_k) - C\Phi\tilde{\mathbf{x}}_k \tag{2.95}$$

and the error dynamics

$$\mathbf{e}_{k+1} = \Lambda\mathbf{e}_k + \boldsymbol{\delta}_k \tag{2.96}$$

where $\boldsymbol{\delta}_k = C(\hat{\mathbf{d}}_k - \mathbf{d}_k + \mathbf{d}_{k-1} - \hat{\mathbf{d}}_{k-1}) - C\Phi(\tilde{\mathbf{x}}_k - \tilde{\mathbf{x}}_{k-1})$.

Proof: In order to prove (2.95), notice that (2.54) can be written as

$$\boldsymbol{\sigma}_{k+1} = \mathbf{r}_{k+1} - C\mathbf{x}_{k+1} - \Lambda\mathbf{r}_k + \Lambda C\mathbf{x}_k + \boldsymbol{\sigma}_k. \tag{2.97}$$

Substituting the closed-loop dynamics (2.94) into (2.97) and simplifying we obtain

$$\boldsymbol{\sigma}_{k+1} = C(\hat{\mathbf{d}}_k - \mathbf{d}_k) - C\Phi\tilde{\mathbf{x}}_k$$

which proves the first part of the theorem.

In order to prove the second part, premultiply (2.94) with C and simplify to obtain the following result

$$\mathbf{y}_{k+1} = \Lambda\mathbf{y}_k + C\mathbf{d}_k - C\hat{\mathbf{d}}_k + \mathbf{r}_{k+1} - \Lambda\mathbf{r}_k + C\Phi\tilde{\mathbf{x}}_k + \boldsymbol{\sigma}_k \tag{2.98}$$

From the result (2.95) it can be obtained that $\boldsymbol{\sigma}_k = C(\hat{\mathbf{d}}_{k-1} - \mathbf{d}_{k-1}) - C\Phi\tilde{\mathbf{x}}_{k-1}$. Substituting in (2.98) and using the fact that $\mathbf{e}_k = \mathbf{r}_k - \mathbf{y}_k$ we obtain

$$\begin{aligned} \mathbf{e}_{k+1} &= \Lambda\mathbf{e}_k + C(\hat{\mathbf{d}}_k - \mathbf{d}_k + \mathbf{d}_{k-1} - \hat{\mathbf{d}}_{k-1}) - C\Phi(\tilde{\mathbf{x}}_k - \tilde{\mathbf{x}}_{k-1}) \\ &= \Lambda\mathbf{e}_k + \boldsymbol{\delta}_k \end{aligned} \tag{2.99}$$

where $\boldsymbol{\delta}_k = C(\hat{\mathbf{d}}_k - \mathbf{d}_k + \mathbf{d}_{k-1} - \hat{\mathbf{d}}_{k-1}) - C\Phi(\tilde{\mathbf{x}}_k - \tilde{\mathbf{x}}_{k-1})$. ■

As in the state-feedback approach, the output tracking error depends on the proper selection of the eigenvalues of Λ, as well as the disturbance estimation and state estimation precision. The influence of the disturbance estimation has been discussed in Theorem 4. The effect of $\tilde{\mathbf{x}}_k$ on the tracking error bound will be evaluated, we will discuss the state observer in the next subsection.

2.6.2 State Observer

State estimation will be accomplished with the following state-observer

$$\hat{\mathbf{x}}_{k+1} = \Phi\hat{\mathbf{x}}_k + \Gamma\mathbf{u}_k + L(\mathbf{y}_k - \hat{\mathbf{y}}_k) + \hat{\mathbf{d}}_k \tag{2.100}$$

where $\hat{\mathbf{x}}_k$, $\hat{\mathbf{y}}_k$ are the state and output estimates and L is a design matrix. Observer (5.33) is well-known, however, the term $\hat{\mathbf{d}}_k$ has been added to compensate for the disturbance. It is necessary to investigate the effect of the disturbance estimation on the state estimation. Subtracting (2.100) from (2.2) we get

$$\tilde{\mathbf{x}}_{k+1} \quad = \quad [\Phi - LC]\tilde{\mathbf{x}}_k + \mathbf{d}_k - \hat{\mathbf{d}}_k. \tag{2.101}$$

It can be seen that the state estimation is indepdendent of the control inputs. Under the assumption that (Φ, Γ, C) is controllable and observable, we can choose L such that $\Phi - LC$ is asymptotically stable. From Theorem 4, $\mathbf{d}_k - \hat{\mathbf{d}}_k = O(T^2)$, thus, from *Property 2* the ultimate bound of $\tilde{\mathbf{x}}_k$ is $O(T)$. Later we will show that, for systems of relative degree greater than 1, by virtue of the integral action in the ISM control, the state estimation error will be reduced to $O(T^2)$ in the closed-loop system.

2.6.3 Tracking Error Bound

In order to calculate the tracking error bound we need first calculate the bound of $\boldsymbol{\zeta}_k$ in Theorem 5. From the error dynamics of the state estimation (2.101), the solution trajectory is

$$\tilde{\mathbf{x}}_k = [\Phi - LC]^k\tilde{\mathbf{x}}_0 + \sum_{i=0}^{k-1}\left([\Phi - LC]^{k-1-i}(\mathbf{d}_i - \hat{\mathbf{d}}_i)\right). \tag{2.102}$$

The difference $\tilde{\mathbf{x}}_k - \tilde{\mathbf{x}}_{k-1}$ can be calculated

$$\begin{aligned}\tilde{\mathbf{x}}_k - \tilde{\mathbf{x}}_{k-1} &= [(\Phi - LC) - I_n](\Phi - LC)^{k-1}\tilde{\mathbf{x}}_0 \\ &\quad + \sum_{i=0}^{k-1}\Big([\Phi - LC]^{k-1-i}(\mathbf{d}_i - \hat{\mathbf{d}}_i)\Big) \\ &\quad - \sum_{i=0}^{k-2}\Big([\Phi - LC]^{k-1-i}(\mathbf{d}_i - \hat{\mathbf{d}}_i)\Big)\end{aligned}$$

which can be simplified to

$$\tilde{\mathbf{x}}_k - \tilde{\mathbf{x}}_{k-1} = [(\Phi - LC) - I_n](\Phi - LC)^{k-1}\tilde{\mathbf{x}}_0 + (\mathbf{d}_k - \hat{\mathbf{d}}_k).$$

Since $(\Phi - LC)$ is asymptotically stable, the ultimate bound is

$$\tilde{\mathbf{x}}_k - \tilde{\mathbf{x}}_{k-1} = \mathbf{d}_k - \hat{\mathbf{d}}_k, \tag{2.103}$$

and $\boldsymbol{\delta}_k$ can be expressed ultimately as

$$\begin{aligned}\boldsymbol{\delta}_k &= C(\hat{\mathbf{d}}_k - \mathbf{d}_k + \mathbf{d}_{k-1} - \hat{\mathbf{d}}_{k-1}) - C\Phi(\tilde{\mathbf{x}}_k - \tilde{\mathbf{x}}_{k-1}) \\ &= C(\hat{\mathbf{d}}_k - \mathbf{d}_k + \mathbf{d}_{k-1} - \hat{\mathbf{d}}_{k-1}) - C\Phi(\mathbf{d}_k - \hat{\mathbf{d}}_k). \end{aligned}\tag{2.104}$$

From Theorem 4, the disturbance estimation error $\mathbf{d}_k - \hat{\mathbf{d}}_k$ is $O(T^2)$. Therefore we have

$$\boldsymbol{\delta}_k = C \cdot \Big(O(T^2) + O(T^2)\Big) - C\Phi \cdot O(T^2) = O(T^2).$$

The ultimate bound on $\boldsymbol{\sigma}_k$ is $O(T^2)$ according to (2.95), and, from (2.99) the ultimate bound on $\|\mathbf{e}_k\|$ is $O(T)$.

Remark 11 *Note that the guaranteed tracking precision is $O(T)$ because the control problem becomes highly challenging in the presence of state estimation and disturbance estimation errors, and meanwhile aiming at arbitrary reference tracking.*

In many motion control tasks the system relative degree is 2, for instance from the torque or force to position tracking in motion control. Now we derive an interesting property by the following corollary.

Corollary 1 *For a continuous system of relative degree greater than 1, the ultimate bound of* $\|\mathbf{e}_k\|$ *is* $O(T^2)$.

Proof: From Theorem 5 (2.62) and *Property 2*, $\|\mathbf{e}_k\|$ is $O(T^2)$ if $\boldsymbol{\delta}_k = O(T^3)$. When the system relative degree is 2, $CB = 0$, and

$$\begin{aligned} C\Gamma &= C\left(BT + \frac{1}{2!}ABT^2 + \frac{1}{3!}A^2BT^3 + \cdots\right) \\ &= \frac{1}{2!}CABT^2 + \frac{1}{3!}CA^2BT^3 + \cdots = O(T^2). \end{aligned}$$

Similarly

$$\begin{aligned} C\Phi\Gamma &= C(I + AT + \frac{1}{2!}A^2T^2 + \cdots)\Gamma \\ &= C\left(I + O(T)\right)\Gamma = C\Gamma + O(T^2) = O(T^2). \end{aligned}$$

Now rewrite

$$\begin{aligned} \boldsymbol{\delta}_k &= C(\hat{\mathbf{d}}_k - \mathbf{d}_k + \mathbf{d}_{k-1} - \hat{\mathbf{d}}_{k-1}) - C\Phi(\mathbf{d}_k - \hat{\mathbf{d}}_k) \\ &= C\Gamma(\hat{\boldsymbol{\eta}}_k - \boldsymbol{\eta}_k + \boldsymbol{\eta}_{k-1} - \hat{\boldsymbol{\eta}}_{k-1}) - C\Phi\Gamma(\boldsymbol{\eta}_k - \hat{\boldsymbol{\eta}}_k) + O(T^3). \end{aligned} \tag{2.105}$$

Note that the ultimate bound of $\boldsymbol{\eta}_k - \hat{\boldsymbol{\eta}}_k$, derived in Theorem 3, is $O(T)$. Thus we conclude from (2.105)

$$\boldsymbol{\delta}_k = O(T^2) \cdot (O(T) + O(T)) - O(T^2) \cdot O(T) + O(T^3) = O(T^3)$$

and consequently $\|\mathbf{e}_k\|$ is ultimately $O(T^2)$. ∎

Remark 12 *From the result we see that even though the state estimation error is $O(T)$ we can still obtain $O(T^2)$ output tracking by virtue of the integral action in the controller design for relative degree greater than 1.*

2.6.4 Systems with a Piece-Wise Smooth Disturbance

In practice, the disturbance of a motion system, $\mathbf{f}$, may become discontinuous at certain circumstances. For example, due to the static friction force, a discontinuity occurs when the motion speed drops to zero. It is thus vital to examine the system performance around the time the dicontinuity occurs.

Suppose the the discontinuity of $\mathbf{f}$ occurs at the jth sampling instance. The immediate consequence of the discontinuity in $\mathbf{f}$ is the loss of the property $P2$: $\mathbf{d}_j - \mathbf{d}_{j-1} = O(T)$ instead of $O(T^2)$, and the loss of the property $P3$: $\mathbf{d}_j - 2\mathbf{d}_{j-1} + \mathbf{d}_{j-2} = O(T)$ instead of $O(T^3)$.

Since we focus on tracking tasks in this Chapter, it can be reasonably assumed that the discontinuity occurs only occasionally. As such, property $P1$ will be restored one step after the occurence of the discontinuity, and property $P2$ will be restored two step after the occurence of the discontinuity. The discontinuity presents an impulse-like impact to the system behavior at the instance $k = j$. It is worth to investigate the *Property 2*. Write

$$\mathbf{e}_k = \Lambda^k \mathbf{e}_0 + \sum_{i=0}^{k-1} \Lambda^i \boldsymbol{\delta}_{k-i-1}.$$

For simplicity assume $\Lambda^k \mathbf{e}_0$ can be ignored and $\mathbf{e}_k = O(T^2)$ at $k = j$. Then $\boldsymbol{\delta}_j$ will give $\mathbf{e}_k$

an offset with the magnitude $O(T)$, which can be viewed as a new initial error at the time instance j and will disppear exponentially with the rate Λ^k.

Note that Λ is a design matrix, thus can be chosen to be sufficiently small such that the impact from $\boldsymbol{\delta}_j$, which is $O(T)$, can be quickly attenuated. As a result, the analysis of the preceding sections still holds for discontinuous disturbances.

In the worst case the non-smooth disturbance presents for a long interval, we can consider a nonlinear switching control action. Denote $\mathbf{u}_k$ the ISMC designed in preceding sections, a new nonlinear controller is

$$\mathbf{u}_k^n = \mathbf{u}_k + \mu \ \mathrm{sat}(\boldsymbol{\sigma}_k) \tag{2.106}$$

where $\mathrm{sat}(\boldsymbol{\sigma}_k)$ is a vector with each of the elements given by

$$\mathrm{sat}(x) = \begin{cases} 1 & x \geq \epsilon \\ \frac{x}{\epsilon} & -\epsilon < x < \epsilon \\ -1 & x \leq -\epsilon \end{cases}$$

and ϵ is the required bound on the sliding function $\boldsymbol{\sigma}_k$.

Remark 13 *Let $\epsilon \to 0$, it is known that sat$(\cdot)$ renders to a signum function and improves the control system bandwidth, hence supress the discontiuous disturbance. In digital implementation, however, the actual bandwidth, being limited by the sampling frequency, is $\pi/2T$ where T is the sampling period.*

2.7 Illustrative Example

2.7.1 State Regulation

Consider the system (2.1) with the following parameters

$$A = \begin{bmatrix} 1 & -2 & 3 \\ -4 & 5 & -6 \\ 7 & -8 & 9 \end{bmatrix}, \quad B = \begin{bmatrix} 1 & -2 \\ -3 & 4 \\ 5 & 6 \end{bmatrix},$$
$$C = \begin{bmatrix} 0 & 1 & 2 \\ 4 & -1 & 2 \end{bmatrix}, \quad \text{and} \quad \mathbf{f}(t) = \begin{bmatrix} 0.3\sin(4\pi t) \\ 0.3\cos(4\pi t) \end{bmatrix}$$

The initial states are $\mathbf{x}(0) = [1 \quad 1 \quad -1]^T$. The system will be simulated for a sample interval of 1ms. For the classical SMC, the D matrix is chosen such that the non-zero pole of the sliding dynamics is $p = -5$ in continuous-time, or $z = 0.9950$ in discrete-time. Hence, the poles of the system with SM are $[0 \quad 0.9950 \quad 0]^T$ respectively. Accordingly the D matrix is

$$D = \begin{bmatrix} 0.2621 & -0.3108 & -0.0385 \\ 3.4268 & 2.4432 & 1.1787 \end{bmatrix}.$$

Using the same D matrix given above, the system with ISM is designed such that the dominant (non-zero) pole remains the same, but, the remaining poles are not deadbeat. The poles are selected as $z = [0.9048 \quad 0.9950 \quad 0.8958]^T$ respectively.

Using the pole placement command of Matlab, the gain matrices can be obtained

$$K = \begin{bmatrix} 66.6705 & 9.4041 & 15.8872 \\ 18.2422 & 21.3569 & 8.5793 \end{bmatrix}.$$

According to (2.35)

$$E = \begin{bmatrix} 0.0297 & -0.0313 & -0.0034 \\ 0.3147 & 0.2366 & 0.1115 \end{bmatrix}.$$

The delayed disturbance compensation is used. Fig.2.1a shows that the system state $x_1(t)$ is asymptotically stable for both discrete-time SMC and ISMC, which show almost the same behavior globally. On the other hand, the difference in the steady-state response between discrete-time SMC and ISMC can be seen from Fig.2.1b. The control inputs are shown in Fig.2.2. Note that the control inputs of the SMC has much larger values at the initial phase in comparison with ISMC, due to the existence of deadbeat poles. Another reason for the lower value of the control inputs in the ISMC is the elimination of the reaching phase by compensating for the non-zero intial condition in (2.40).

To demonstrate the quality of both designs, the open-loop transfer function matrices, $G_{i,j}^{OL}$, for the systems with SM and ISM are computed and Bode plots of some elements are shown in Fig.2.3 In addition, the sensitivity function of state x_1 with respect to the disturbance components $f_1(t)$ and $f_2(t)$ is plotted in Fig.2.4. It can be seen from Fig.2.3 and Fig.2.4 that ISMC greatly reduces the effect of the disturbance as compared to SMC. Moreover ISM presents a larger open-loop gain at the lower frequency band by virtue of the integral action in the sliding manifold, which ensures a more accurate closed-loop response to possible reference inputs.

2.7.2 State Feedback Approach

Consider the system (2.1) with the parameters

$$A = \begin{bmatrix} 10 & 1 \\ -10 & -10 \end{bmatrix}, \quad B = \begin{bmatrix} 4 \\ 4.2 \end{bmatrix}, \quad C = \begin{bmatrix} 1 & 0 \end{bmatrix}.$$

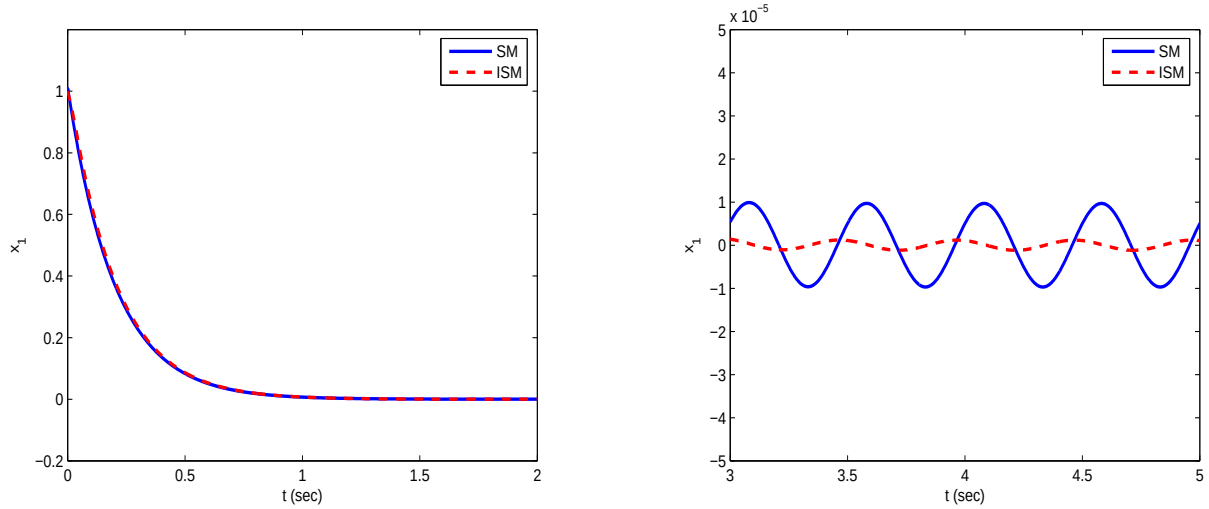

(a) (b)

Figure 2.1: System state x_1

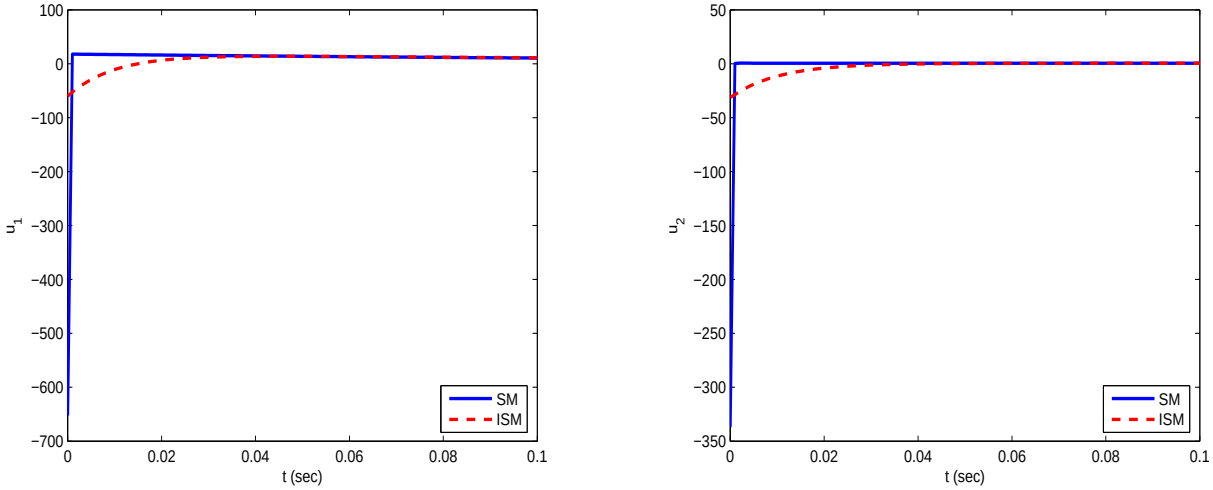

(a) (b)

Figure 2.2: System control inputs u_1 and u_2

The sampled-data system obtained with a sampling period $T = 1$ms is

$$\Phi = \begin{bmatrix} 1.01 & -0.001 \\ -0.01 & 0.99 \end{bmatrix}, \quad \Gamma = \begin{bmatrix} 0.0040 \\ 0.0042 \end{bmatrix}, \quad C = \begin{bmatrix} 1 & 0 \end{bmatrix}.$$

The zero of (Φ, Γ, C) is $z = 0.989$ and, therefore, the system is minimum-phase. Let the desired pole, the remaining pole of the closed-loop system to be designed, be $z = 0.75$, then

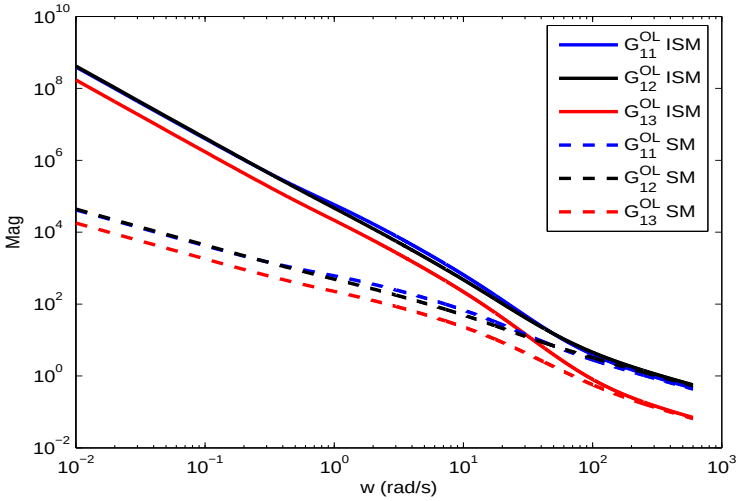

Figure 2.3: Bode plot of some of the elements of the open-loop transfer matrix

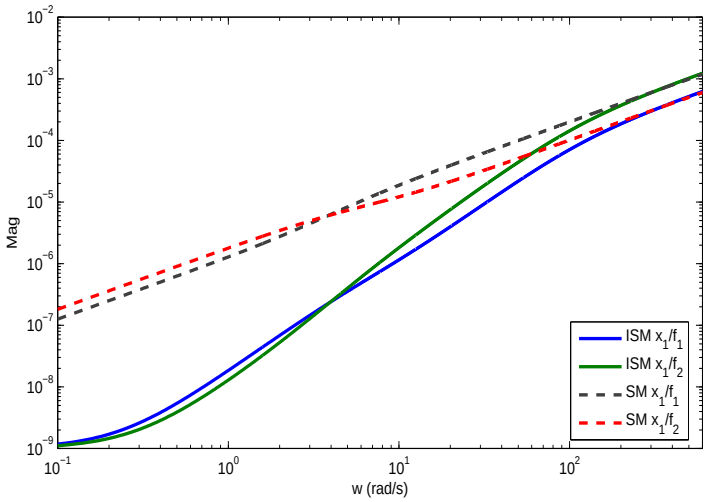

Figure 2.4: Sensitivity function of x_1 with respect to f_1 and f_2

the design parameter is given by $E = 0.25$. The system is simulated with an ouput reference $r_k = 1 + sin(8\pi kT - \pi/2)$, shown in Fig.2.5. The disturbance acting on the system will be non-smooth when speed crosses zero and given by

$$f = \begin{cases} 10 & if \quad x_2 < 0 \\ 0 & if \quad x_2 = 0 \\ -10 & if \quad x_2 > 0. \end{cases} \tag{2.107}$$

The system is simulated using controller (2.58). The controller performance is compared with that of a PI controller having a proportional gain of $k_p = 240$ and integral gain of $k_i = 8$. In Fig.2.6 the tracking error is 4×10^{-6} which corresponds to $O(T^2)$ and is almost invisible as compared with the PI controller performance. Note worthy is the fact that the control signal for the PI control is much larger initially as compared to the ISMC control. A smaller control signal is more desirable in practice as it would not create a heavy burden on actuators.

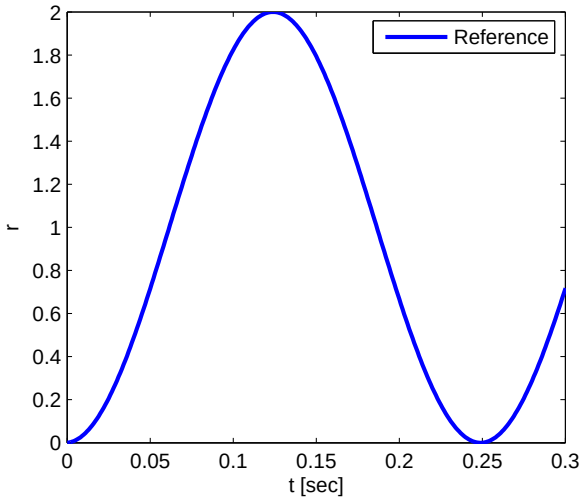

Figure 2.5: The output reference trajectory

2.7.3 Output Feedback Approach

Consider the system (2.1) with the parameters

$$A = \begin{bmatrix} -60 & -10 \\ 10 & -10 \end{bmatrix}, \quad B = \begin{bmatrix} 4 \\ 4.2 \end{bmatrix}, \quad C = \begin{bmatrix} 1 & 0 \end{bmatrix}.$$

After sampling the system at $T = 1$ms, the discretized system is

$$\Phi = \begin{bmatrix} 0.9417 & -0.0097 \\ 0.0097 & 0.9900 \end{bmatrix}, \quad \Gamma = \begin{bmatrix} 0.0039 \\ 0.0042 \end{bmatrix}, \quad C = \begin{bmatrix} 1 & 0 \end{bmatrix}.$$

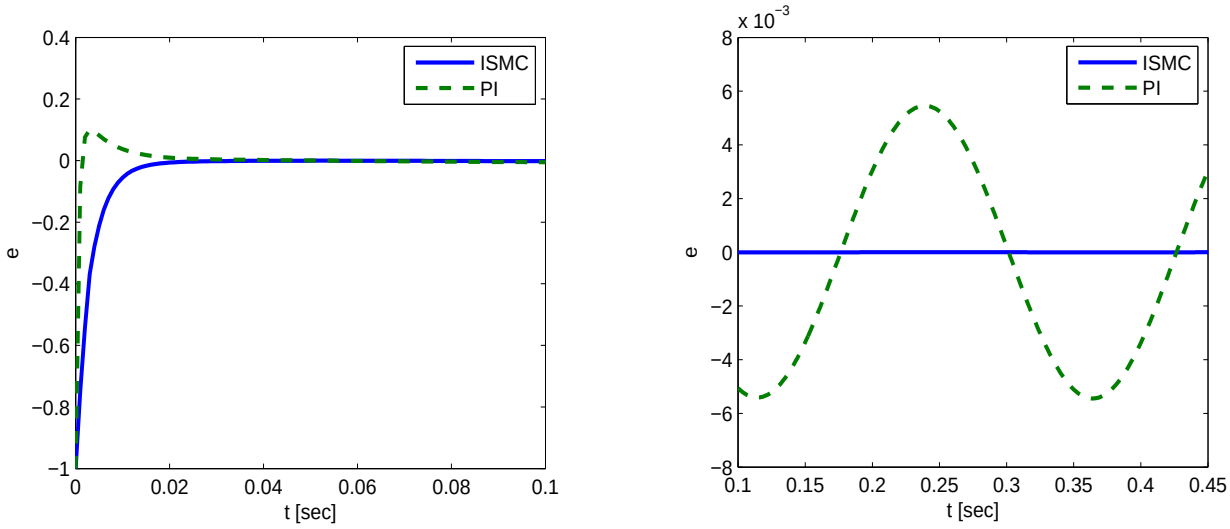

(a) (b)

Figure 2.6: Tracking error of ISMC and PI controllers

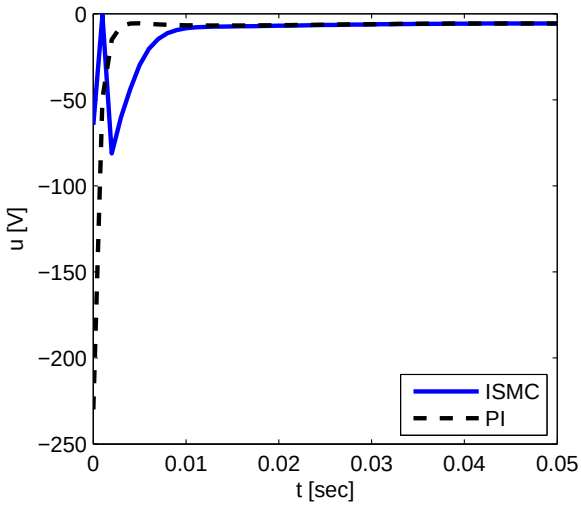

Figure 2.7: Control inputs of ISMC with state feedback and PI

For this system the zero of (Φ, Γ, C) is $z = 1.001$ whereas the zero of (Φ, Γ, D) is $z = 0.998$. Therefore, the output-feedback approach with the reference model in §2.5.4 is the only option. Using the same disturbance f and reference trajectory r_k, the system is simulated. The controller performance is compared with that of a PI controller having a proportional gain of $k_p = 200$ and integral gain of $k_i = 30$. As it can be seen from Fig.2.8, the performance is

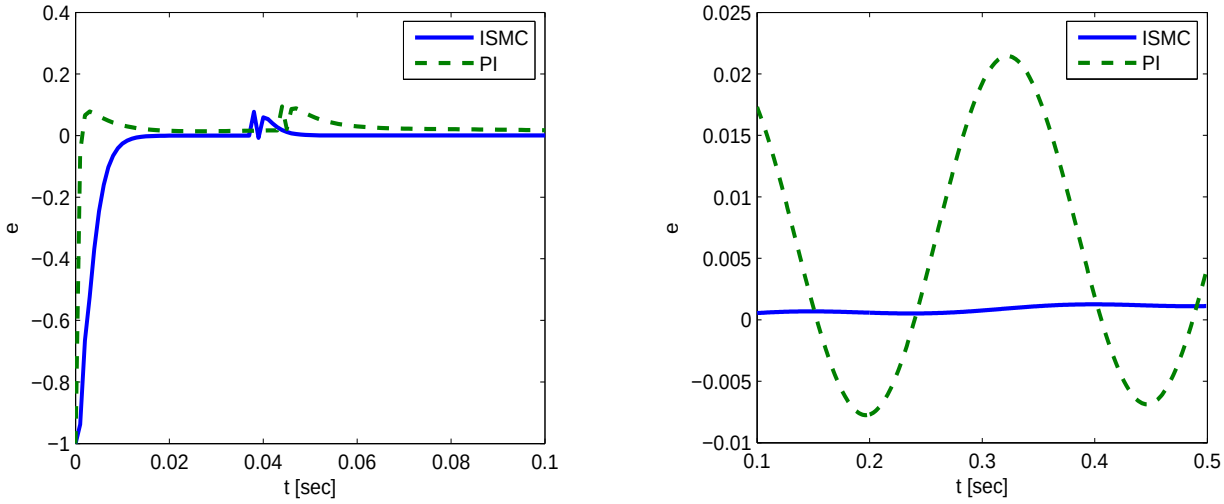

(a) (b)

Figure 2.8: Tracking error of ISMC and PI controllers

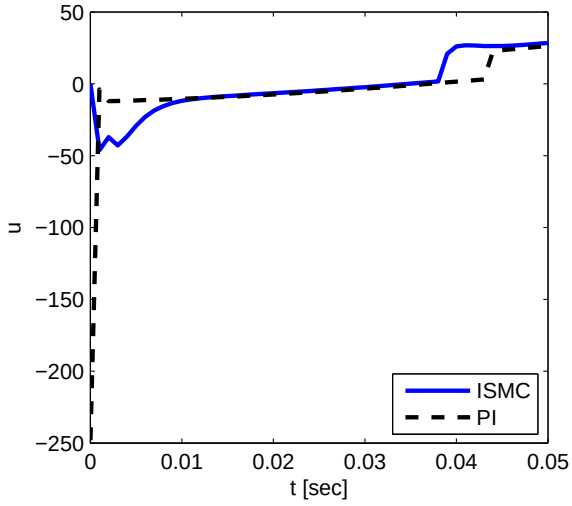

Figure 2.9: Control inputs of ISMC and PI output feedback

quite good and better than that of a PI controller. The tracking error for the ISMC is about 17×10^{-6} which corresponds to $O(T^2)$ at steady state. Note that even though the worst case scenario of $O(T)$ was predicted for this approach it was possible to achieve $O(T^2)$ at steady state. Also, similar to the state feedback approach the control signal of the ISMC controller is much smaller than that of the PI controller at the onset of motion.

2.7.4 State Observer Approach

For this approach we will go back to the system in §2.7.2, and estimate x_2 using the observer (2.100). The observer has a gain of $L = \begin{bmatrix} 1.19 & 342.23 \end{bmatrix}$ and is designed such that two poles are at $z = 0.4$ allowing a fast enough convergence. From Fig.2.10 the estimation of error $\tilde{x}_2$ is plotted. As we can see the estimation is quite good and deviating only when the discontinuities occur but attenuates very quickly. The disturbance estimation is seen in Fig.2.11 and the estimation converges quickly to the actual disturbance. From Fig.2.12 we can see the tracking error performance. The tracking error is about 6×10^{-6} which matches the theoretical results of $O(T^2)$ bound. Again like the previous two approaches, the control signal of the ISMC is smaller than that of the PI controller at the initial phase. Finally

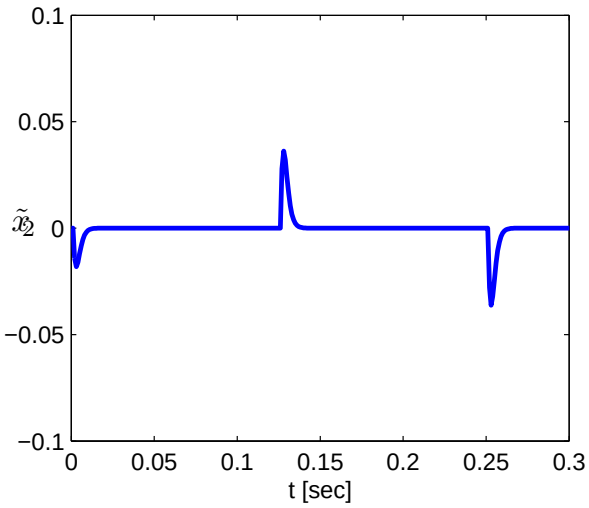

Figure 2.10: Observer state estimation error $\tilde{x}_2$

we need to show the effects of a more frequently occuring discontinuous disturbance and how adding a nonlinear term, (2.106), would improve the performance. The disturbance is shown in Fig.2.16. As it can be seen from Fig.2.14 the rapid disturbance degrades the performance of

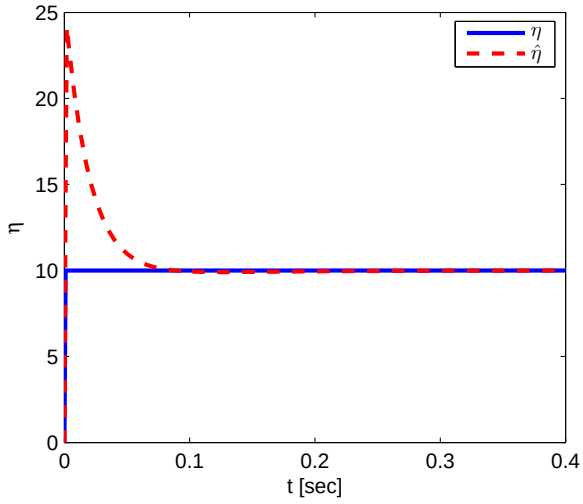

Figure 2.11: Disturbance η and estimate $\hat{\eta}$

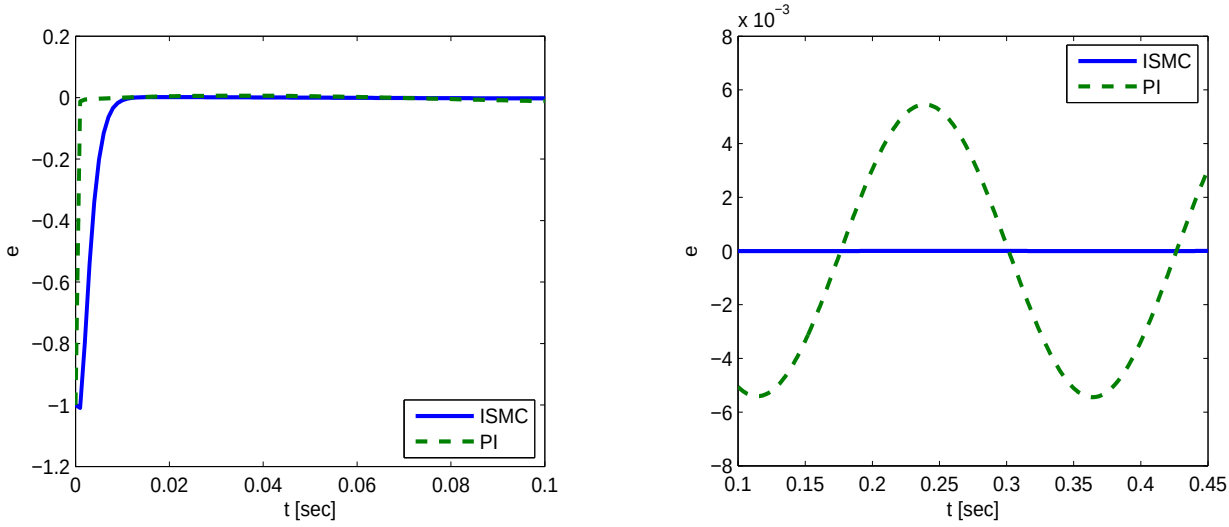

(a) (b)

Figure 2.12: Tracking error of ISMC and PI controllers

the ISMC and PI controllers, however, addition of a switching term with $\mu = 10$ and $\epsilon = 0.01$ improves the tracking performance. In Fig.2.15, we can see that the control inputs for both the ISMC and the ISMC with switching is considerably less than the PI controller at the onset of motion. Note also from Fig.2.16 that the disturbance estimate $\hat{\eta}$ converges quickly to the disturbance.

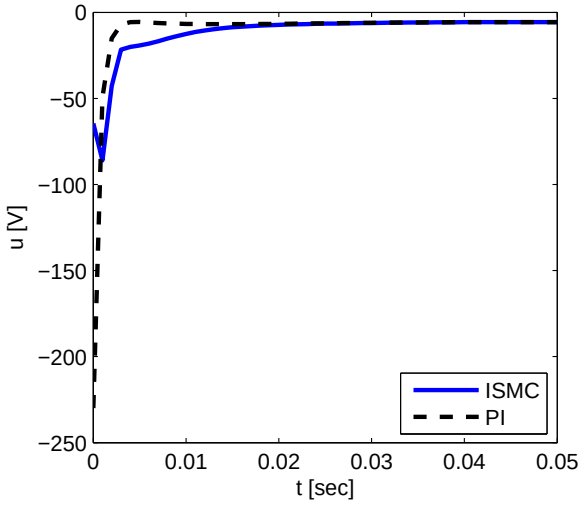

Figure 2.13: Control inputs of ISMC with state observer and PI

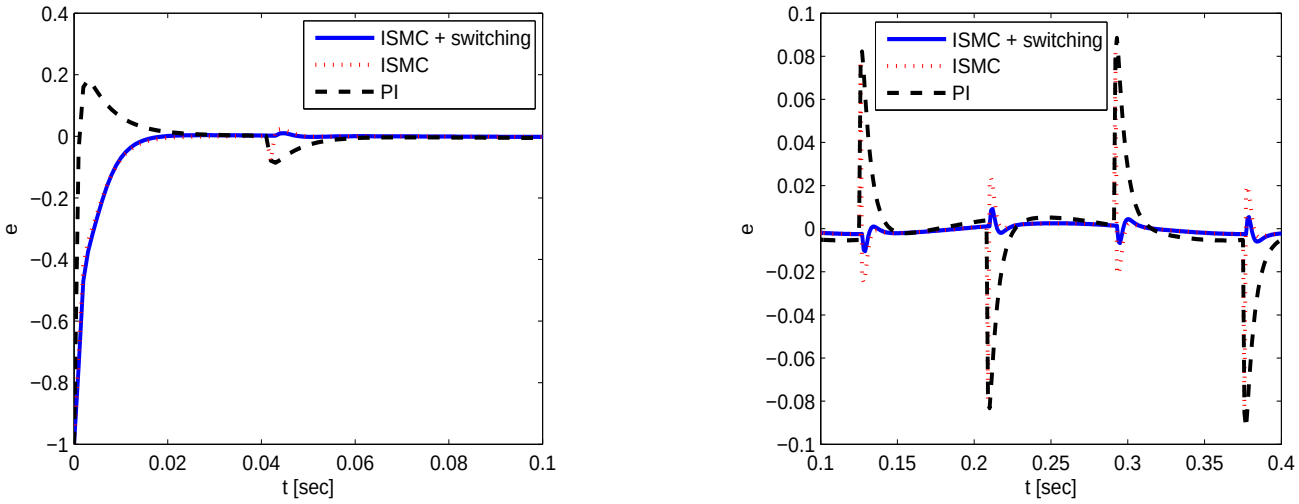

(a) (b)

Figure 2.14: Tracking errors of ISMC, PI and ISMC with switching under a more frequent discontinuous disturbance

2.8 Conclusion

This Chapter presents a new discrete-time integral sliding control design for sampled-date systems under state regulation and output tracking. Using the new discrete-time integral type sliding manifold, the SMC design retains the deadbeat structure of the discrete-time

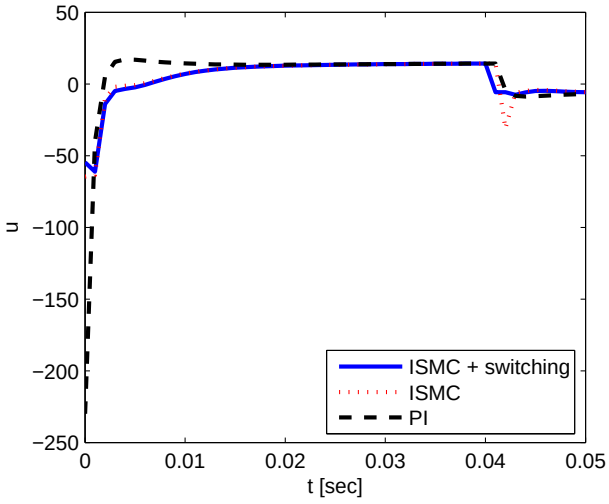

Figure 2.15: Control inputs of ISMC, PI and ISMC with switching under a more frequent discontinuous disturbance

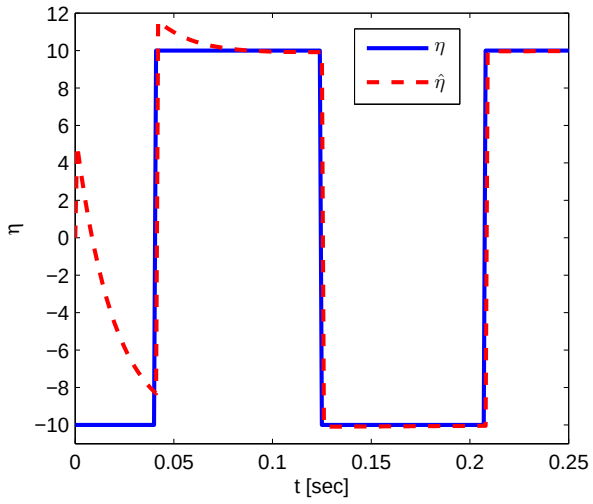

Figure 2.16: Disturbance η and estimate $\hat{\eta}$

sliding mode, and at the same time allocates the closed-loop eigenvalues for the full-order multi-input system. The discrete-time ISMC achieves accurate control performance for the sliding mode, state regulation and output tracking, meanwhile eliminates the reaching phase and avoids overlarge control efforts. The theoretical results were confirmed through both theoretical analysis and a numerical example.

Chapter 3

Discrete-Time Periodic Adaptive Control Approach for Time-Varying Parameters with Known Periodicity

3.1 Introduction

Adaptive control theory for continuous-time systems is one of the most well established control theories, and numerous results have been reported, e.g., [32]-[36]. In the classical adaptive control, the parametric adaptation mechanism essentially consists of a number of integrators, thus the adaptive control system is able to achieve asymptotic tracking convergence in the presence of constant parametric uncertainties. In [6], a method for dealing with a class of time-varying periodic unknown paramters is introduced that is based on pointwise integration relying on the *a priori* knowledge of the periodicity of the parameters.

Considering the fact that, as a function of time, the classes of time-varying parameters are in essence infinite, it would be extremely difficult to find a general solution to such a broad control problem. A more realistic way is first to classify the time-varying parametric

uncertainties into subclasses, and then look for an appropriate adaptive control approach for each subclass. Instead of classifying parameters into slow vs rapid time-varying, in this Chapter we classify parameters into periodic vs nonperiodic ones. When the periodicity of system parameters is known *a priori*, an adaptive controller with periodic updating can be constructed by means of a pointwise update mechanism.

Periodic variations are encountered in many real systems. These variations can exist in the system parameters, [37],[38], or as a disturbance to the system, [39]-[41]. This necessitates the effort in formulating an adaptive control scheme that can handle a class of systems with time-varying periodic unknown parameters or disturbances by taking into account the periodicity of the variations.

In this Chapter, we apply the concept of periodic adaptation, originally proposed for continuous-time systems, to discrete-time systems. In particular, we will show that the new periodic adaptive controller can work effectively to nullify the influence from the time-varying parametric uncertainties to the control error, in the sequel achieve the asymptotic convergence. Comparing with the continuous-time adaptive control, the discrete-time periodic adaptation is a more natural extension of the classical adaptive control: from the updating in two consecutive intances to the updating in the same instance of two consecutive periods. This is owing to the fact that the value of a periodic parameter will be invariant if shifting the time by one period. This feature necissitates the need to explore a new parametric estimation law and a new convergence property analysis tool. In the periodic adaptive control, the parametric values of the preceding period, instead of the preceding time instance, are used to update

the current parameter estimate. Analogously, the boundedness of the parametric estimate and convergence analysis are conducted by deriving the difference between two consecutive periods, that is, the convergence is asymptotic with respect to the number of periods, instead of the time instances. When there exist both time-invariant and time-varying periodic parameters, the classical adaptation and the new periodic adaptation laws can be employed simultaneously, whereas the convergence analysis will be based on the number of periods.

3.2 Discrete-Time Periodic Adaptive Control

In order to clearly demonstrate the idea, first consider a scalar discrete-time system with only one unknown parameter

$$x_{k+1} = \theta_k \xi_k + u_k, \qquad x_0 = x(0) \tag{3.1}$$

where θ_k is periodic, i.e. $\theta(k) = \theta(k-N)$ with a known period $N > 1$, and $\xi_k = \xi(x_k)$ is a known nonlinear function. For simplicity we will consider the regulation problem only and leave the extension to tracking tasks to the next section.

3.2.1 Discrete-Time Adaptive Control Revisited

If θ_k is time invariant, i.e. $\theta(k) = \theta(k-1)$, then the standard approach would be to combine a certainty equivalence controller with a least-squares estimator

$$u_k = -\hat{\theta}_k \xi_k \tag{3.2}$$

$$\hat{\theta}_k = \hat{\theta}_{k-1} + P_k \xi_{k-1} x_k, \tag{3.3}$$

$$P_k = P_{k-1} - \frac{P_{k-1}^2 \xi_{k-1}^2}{1 + P_{k-1} \xi_{k-1}^2}, \quad P_0 > 0 \tag{3.4}$$

where P_k is a scalar for this case. Defining $\tilde{\theta} = \theta - \hat{\theta}$, and substituting the adaptive law (3.2) into the dynamical relation (3.1), the closed-loop system can be expressed as

$$\begin{aligned} x_{k+1} &= \tilde{\theta}_k \xi_k, \\ \tilde{\theta}_{k+1} &= \tilde{\theta}_k - P_{k+1}\xi_k x_{k+1} \\ P_{k+1} &= P_k - \frac{P_k^2 \xi_k^2}{1 + P_k \xi_k^2}. \end{aligned} \tag{3.5}$$

The least-squares estimator has several desirable properties [43], for instance the boundedness and positivity of P_k which can be found by rewritting (3.4) as

$$P_{k+1}^{-1} = P_k^{-1} + \xi_k^2, \tag{3.6}$$

implying $P_k^{-1} \geq P_0^{-1} > 0$ or $P_0 \geq P_k > 0$ for all $k \geq 0$. Now, consider a nonnegative function $V_k = P_k^{-1}\tilde{\theta}_k^2$, its difference over one step is

$$\begin{aligned} V_{k+1} - V_k &= P_{k+1}^{-1}\tilde{\theta}_{k+1}^2 - P_k^{-1}\tilde{\theta}_k^2 \\ &= P_{k+1}^{-1}\left(\tilde{\theta}_k - P_{k+1}\xi_k x_{k+1}\right)^2 - P_k^{-1}\tilde{\theta}_k^2 \\ &= -\frac{x_{k+1}^2}{1 + P_k \xi_k^2} \leq 0. \end{aligned} \tag{3.7}$$

From (3.7), the term $x_{k+1}/(1 + P_k\xi_k^2)^{1/2}$ converges to zero as $k \to \infty$. Further, if the nonlinear function $\xi(x)$ is sector-bounded

$$|\xi(x)| \leq c_1 + c_2|x| \tag{3.8}$$

with c_1 and c_2 arbitary positive constants, then it is possible to establish the condition, [42],

$$|\xi(x_k)| \leq c_1^0 + c_2^0 \max_{j \in [0,k]} |x_{j+1}| \tag{3.9}$$

where c_1^0 and c_2^0 are constants, then the Key Technical Lemma ensures that $x_k \to 0$ as $k \to \infty$.

3.2.2 Periodic Adaptation

Can the concept of adaptation control still be applied to periodic but arbitrarily time-varying $\theta(k)$? Note that, the dynamics $\tilde{\theta}_{k+1}$ in the closed-loop system (3.5) is derived by subtracting the parameter adaptation law (3.3) from the time invariance relationship $\theta_k = \theta_{k-1}$, which however does not hold for a time-varying $\theta(k)$. On the other hand, for the periodic parameter we have $\theta_k = \theta_{k-N}$. Note that $N = 1$ renders a periodic θ_k to a constant. Hence a periodic parameter, with the periodicity $N > 1$, can be viewed as a "constant" with respect to the interval N. As such, we can modify the standard adaptation law (3.3), originally designed to update the parameter estimate between two consecutive intstances, namely from $k-1$ to k, into a new periodic adaptation law that updates the parameter estimate after a fixed interval N, namely from $k-N$ to k. In the following we will verify and demonstrate this simple idea.

Revise the adaptive control mechanism (3.2-3.4) into the following periodic one

$$u_k = -\hat{\theta}_k \xi_k \tag{3.10}$$

$$\hat{\theta}_k = \begin{cases} \hat{\theta}_{k-N} + P_k \xi_{k-N} x_{k-N+1}, & k \in [N, \infty) \\ \hat{\theta}_0, & k = [0, N) \end{cases} \tag{3.11}$$

$$P_k = \begin{cases} P_{k-N} - \dfrac{P_{k-N}^2 \xi_{k-N}^2}{1 + P_{k-N} \xi_{k-N}^2}, & k \in [N, \infty) \\ P_0 > 0 & k \in [0, N) \end{cases} \tag{3.12}$$

where $k = k_0 + nN$ and n is the total number of periods in the interval $[0, k)$. From (3.12) we can derive a result similar to (3.6)

$$P_k^{-1} = P_{k-N}^{-1} + \xi_{k-N}^2 \tag{3.13}$$

which implies that $P_k^{-1} \geq P_0^{-1} > 0$ and $P_0 \geq P_k > 0$ for all $k \geq N$.

Remark 14 *Note that the adaptation process starts only after the first cycle is completed or* $k \geq N$. *The estimate* $\hat{\theta}_k$ *for* $k < N$ *is set to* $\hat{\theta}_0$, *which can be chosen according to some prior knowledge, or simply zero if no prior knowledge is available. Similarly, we can choose* P_0 *to be a sufficiently large constant over the interval* $[0, N)$.

3.2.3 Convergence Analysis

Define the parameter estimation error $\tilde{\theta}_k = \theta_k - \hat{\theta}_k$. Substituting the adaptive control (3.10) into the dynamical relation (3.1), and subtracting the adaptive law (3.11) from $\theta_k = \theta_{k-N}$, the closed-loop system, for any $k \geq N$, can be expressed as

$$\begin{aligned} x_{k+1} &= \tilde{\theta}_k \xi_k \\ \tilde{\theta}_k &= \tilde{\theta}_{k-N} - P_k \xi_{k-N} x_{k-N+1} \\ P_k &= P_{k-N} - \frac{P_{k-N}^2 \xi_{k-N}^2}{1 + P_{k-N} \xi_{k-N}^2}. \end{aligned} \tag{3.14}$$

The convergence property of the periodic adaptive control system (3.14) is summarized in the following theorem.

Theorem 7 *For the closed-loop system (3.14), the parameter estimation error* $\tilde{\theta}$ *is bounded and the regulation error* x_k *converges to zero asymptotically.*

Proof: Similar to the time-invariant case, select a nonnegative function $V_k = P_k^{-1} \tilde{\theta}_k^2$, its difference with respect to the interval N for any $k \geq N$ is

$$\begin{aligned} \Delta V_k &= V_k - V_{k-N} \\ &= P_k^{-1} \tilde{\theta}_k^2 - P_{k-N}^{-1} \tilde{\theta}_{k-N}^2 \end{aligned}$$

$$
\begin{aligned}
&= P_k^{-1}\left(\tilde{\theta}_{k-N} - P_k\xi_{k-N}x_{k-N+1}\right)^2 - P_{k-N}^{-1}\tilde{\theta}_{k-N}^2 \\
&= (P_k^{-1} - P_{k-N}^{-1})\tilde{\theta}_{k-N}^2 - 2\tilde{\theta}_{k-N}\xi_{k-N}x_{k-N+1} + P_k\xi_{k-N}^2 x_{k-N+1}^2 \\
&= -\frac{x_{k-N+1}^2}{1 + P_{k-N}\xi_{k-N}^2} \leq 0. \qquad (3.15)
\end{aligned}
$$

Thus V_k is nonincreasing, implying that $\tilde{\theta}_k$ is bounded. Applying (3.15) repeatedly for any $k \in [pN, (p+1)N]$, and noticing $k_0 = k - pN$, we have

$$
V(k) = V(k_0) + \sum_{i=1}^{p} \Delta V(k_0 + iN) \qquad (3.16)
$$

Since $k_0 \in [0, N)$, and

$$
p = \frac{k - k_0}{N} \to \infty
$$

when $k \to \infty$, according to (3.15)

$$
\lim_{p\to\infty} V(k) < \max_{k_0\in[0,N)} V(k_0) - \lim_{p\to\infty} \sum_{i=1}^{p} \frac{x(k_0 + (i-1)N + 1)^2}{1 + P(k_0 + (i-1)N)\xi(k_0 + (i-1)N)^2}. \qquad (3.17)
$$

Consider that $V(k)$ is nonnegative, $V(k_0)$ is finite in the interval $[0, N)$, thus according to the convergence theorem of the sum of series, we have

$$
\lim_{k\to\infty} \frac{x_{k-N+1}^2}{1 + P_{k-N}\xi_{k-N}^2} \to 0. \qquad (3.18)
$$

Using (3.18) and the sector condition (3.9), the Key Technical Lemma guarantees that ξ_k is bounded and consequently the regulation error $x_k \to 0$ as $k \to \infty$. ■

Remark 15 *Since difference equations do not have a finite escape time, the finiteness of $V(k_0)$ is obvious. From the viewpoint of achieving asymptotic convergence, the initial phase control performance in $[0, N)$ is not as cruitial as that of the continuous-time periodic adaptive*

control. One can choose any controller, not necessarily the same as (3.10), for the initial phase $[0, N)$*, so long as a better performance can be obtained.*

3.3 Extension to More General Cases

In this section we consider four extensions to multiple periodic parameters, mixed periodic and time-invariant parameters, the trajectory tracking problem, and the higher order systems, respectively.

3.3.1 Extension to Multiple Parameters and Time-Varying Input Gain

For simplicity, we will still consider a scalar system

$$x_{k+1} = \left(\boldsymbol{\theta}_k^0\right)^T \boldsymbol{\xi}_k^0 + b_k u_k, \qquad x(0) = x_0 \tag{3.19}$$

where $\boldsymbol{\theta}^0 = [\theta_1^0, \cdots, \theta_m^0]^T$ are unknown periodic parameters, $\boldsymbol{\xi}^0 = [\xi_1^0, \cdots, \xi_m^0]^T$ is a known vector valued function. $b_k \in C[0, \infty)$ is a time-varying and uncertain gain of the system input. The prior information with regards to b_k is that the control direction is known and invariant, that is, b_k is either positive or negative and nonsingular for all k. Without loss of generality, assume that $b_k > 0$. Note that each unknown parameter, $\theta_i^0(k)$ or b_k, may have its own period N_i or N_b. The periodic adaptive control will still be applicable if there exists a common period N, such that each N_i and N_b can divide N with an integer quotient. In such a case, N can be used as the updating period. The presence of the uncertain system input gain makes the controller design more complex. To derive the periodic adaptive control law, define

$\hat{b}_k$ to be the estimation of b_k and $\tilde{b}_k = b_k - \hat{b}_k$, the system dynamics (3.19) can be rewritten as

$$x_{k+1} = \left(\boldsymbol{\theta}_k^0\right)^T \boldsymbol{\xi}_k^0 + b_k u_k - \hat{b}_k u_k + \hat{b}_k u_k = \left(\boldsymbol{\theta}_k^0\right)^T \boldsymbol{\xi}_k^0 + \hat{b}_k u_k + \tilde{b}_k u_k. \tag{3.20}$$

By observation, we can choose the control law

$$u_k = -\hat{b}_k^{-1} \left(\hat{\boldsymbol{\theta}}_k^0\right)^T \boldsymbol{\xi}_k^0 \tag{3.21}$$

where $\hat{\boldsymbol{\theta}} = [\hat{\theta}_1, \cdots, \hat{\theta}_m]$. Substituting (3.21) into (3.20) yields the closed-loop system

$$x_{k+1} = \tilde{\boldsymbol{\theta}}_k^T \boldsymbol{\xi}_k \tag{3.22}$$

where $\tilde{\boldsymbol{\theta}}_k = \left[\left(\tilde{\boldsymbol{\theta}}_k^0\right)^T, \tilde{b}_k\right]^T$, and $\boldsymbol{\xi}_k = \left[\left(\boldsymbol{\xi}_k^0\right)^T, -\hat{b}_k^{-1}\left(\hat{\boldsymbol{\theta}}_k^0\right)^T \boldsymbol{\xi}_k^0\right]^T$. Based on (3.22), the adaptation law is

$$\hat{\boldsymbol{\theta}}_k = \begin{cases} \hat{\boldsymbol{\theta}}_{k-N} - P_k \boldsymbol{\xi}_{k-N} x_{k-N+1}, & k \in [N, \infty) \\ \hat{\boldsymbol{\theta}}_0, & k \in [0, N) \end{cases} \tag{3.23}$$

$$P_k = \begin{cases} P_{k-N} - \dfrac{P_{k-N}\boldsymbol{\xi}_{k-N}^T \boldsymbol{\xi}_{k-N} P_{k-N}}{1 + \boldsymbol{\xi}_{k-N}^T P_{k-N} \boldsymbol{\xi}_{k-N}}, & k \in [N, \infty) \\ P_0 > 0 & k \in [0, N) \end{cases} \tag{3.24}$$

where the covariance P_k is a positive definite matrix of dimension $m+1$ and derived from the relationship $P_k^{-1} = P_{k-N}^{-1} + \boldsymbol{\xi}_{k-N}\boldsymbol{\xi}_{k-N}^T$ by means of the Matrix Inversion Lemma.

The validity of the above periodic adaption law is verified by the following theorem.

Theorem 8 *Under the periodic adaptation law (3.23) and (3.24), the closed-loop dynamics (3.22) is asymptotically stable.*

Proof: The convergence analysis is analogous to the preceding case. Selecting a nonnegative function $V_k = \tilde{\boldsymbol{\theta}}_k^T P_k^{-1} \tilde{\boldsymbol{\theta}}_k$, its difference with respect to the interval N is

$$\Delta V_k = V_k - V_{k-N}$$

$$
\begin{aligned}
&= \tilde{\boldsymbol{\theta}}_k^T P_k^{-1} \tilde{\boldsymbol{\theta}}_k - \tilde{\boldsymbol{\theta}}_{k-N}^T P_{k-N}^{-1} \tilde{\boldsymbol{\theta}}_{k-N} \\
&= \left(\tilde{\boldsymbol{\theta}}_{k-N} - P_k \boldsymbol{\xi}_{k-N} x_{k-N+1}\right)^T P_k^{-1} \left(\tilde{\boldsymbol{\theta}}_{k-N} - P_k \boldsymbol{\xi}_{k-N} x_{k-N+1}\right) - \tilde{\boldsymbol{\theta}}_{k-N}^T P_{k-N}^{-1} \tilde{\boldsymbol{\theta}}_{k-N} \\
&= \tilde{\boldsymbol{\theta}}_{k-N}^T (P_k^{-1} - P_{k-N}^{-1}) \tilde{\boldsymbol{\theta}}_{k-N} - 2\tilde{\boldsymbol{\theta}}_{k-N}^T \boldsymbol{\xi}_{k-N} x_{k-N+1} + \boldsymbol{\xi}_{k-N}^T P_k \boldsymbol{\xi}_{k-N} x_{k-N+1}^2 \\
&= \tilde{\boldsymbol{\theta}}_{k-N}^T (\boldsymbol{\xi}_{k-N} \boldsymbol{\xi}_{k-N}^T) \tilde{\boldsymbol{\theta}}_{k-N} - 2\tilde{\boldsymbol{\theta}}_{k-N}^T \boldsymbol{\xi}_{k-N} x_{k-N+1} + \boldsymbol{\xi}_{k-N}^T P_k \boldsymbol{\xi}_{k-N} x_{k-N+1}^2 \\
&= -\frac{x_{k-N+1}^2}{1 + \boldsymbol{\xi}_{k-N}^T P_{k-N} \boldsymbol{\xi}_{k-N}} \leq 0. \qquad (3.25)
\end{aligned}
$$

Following the same steps that lead to (3.18) in Theorem 1, we conclude that

$$
\lim_{k \to \infty} \frac{x_{k-N+1}^2}{1 + \boldsymbol{\xi}_{k-N}^T P_{k-N} \boldsymbol{\xi}_{k-N}} \to 0. \qquad (3.26)
$$

The result (3.25) shows that $\hat{\boldsymbol{\theta}}^0$ and $\hat{b}$ are bounded because V_k is non-increasing and, thus the control signal $\|u_k\| \leq \|\hat{b}_k^{-1}\| \|\hat{\boldsymbol{\theta}}_k^0\| \|\boldsymbol{\xi}_k^0\| \leq q \|\boldsymbol{\xi}_k^0\|$ for some constant q. If the nonlinear function is sector-bounded, i.e. $\|\boldsymbol{\xi}_k^0\| \leq c_1^0 + c_2^0 |x_k|$ for some positive constants c_1^0 and c_2^0, then $\|\boldsymbol{\xi}_k\| \leq \|\boldsymbol{\xi}_k^0\| + |u_k| \leq c_1 + c_2 |x_k|$ for some positive constants c_1 and c_2. Thus, establishing the condition for (3.9) required by the Key Technical Lemma guarantees $x_k \to 0$ as $k \to \infty$. ∎

3.3.2 Extension to Mixed Parameters

Often, we have some prior knowledge about the system parametric uncertainties, for instance we may know that some unknown parameters are time invariant, whereas the rest are time-varying. This is a nontrivial case, as the more we know, the better we should be able to improve the control performance. It would be far-fetched if we still apply the periodic adaptation to those constant parameters, and the traditional adaptation is more suitable.

Consider the simplest scalar case

$$x_{k+1} = \theta_1(k)\xi_1(k) + \theta_2\xi_2(k) + u, \qquad x_0 = x(0) \tag{3.27}$$

where $\theta_1(k)$ is a periodic unknown parameter with period N, θ_2 is an unknown constant, ξ_1 and ξ_2 are known sector-bounded nonlinear functions. The control law is chosen to be

$$u_k = -\hat{\theta}_1(k)\xi_1(k) - \hat{\theta}_2(k)\xi_2(k). \tag{3.28}$$

The hybrid periodic adaptation law is chosen to be

$$\hat{\theta}_1(k) = \begin{cases} \hat{\theta}_1(k-N) + q_1\dfrac{\xi_1(k-N)x_{k-N+1}}{1+\boldsymbol{\xi}_{k-N}^T Q\boldsymbol{\xi}_{k-N}}, & k \in [N,\infty) \\ \hat{\theta}_1^0, & k \in [0,N) \end{cases}$$

$$\hat{\theta}_2(k) = \hat{\theta}_2(k-1) + q_2\frac{\xi_2(k-1)x_k}{1+\boldsymbol{\xi}_{k-1}^T Q\boldsymbol{\xi}_{k-1}}$$

where q_1 and q_2 are positive gains, $Q = diag(q_1, q_2)$, $\boldsymbol{\xi}_k = [\xi_1(k), \xi_2(k)]^T$, and the value of $\hat{\theta}_1^0$ can be chosen to be zero for the initial period $[0, N)$ if no prior information is available. Substituting the control law (3.28) into (3.27), the closed-loop system is

$$x_{k+1} = \tilde{\theta}_1(k)\xi_1(k) + \tilde{\theta}_2\xi_2(k). \tag{3.29}$$

Using the periodic property $\theta_1(k) = \theta_1(k-N)$ and time invariant property $\theta_2(k) = \theta_2(k-1)$, subtracting the hybrid adaption law for $k \geq N$ yields

$$\tilde{\theta}_1(k) = \tilde{\theta}_1(k-N) - q_1\frac{\xi_1(k-N)x_{k-N+1}}{1+\boldsymbol{\xi}_{k-N}^T Q\boldsymbol{\xi}_{k-N}} \tag{3.30}$$

$$\tilde{\theta}_2(k) = \tilde{\theta}_2(k-1) - q_2\frac{\xi_2(k-1)x_k}{1+\boldsymbol{\xi}_{k-1}^T Q\boldsymbol{\xi}_{k-1}}. \tag{3.31}$$

Now let us show the asymptoitical stability of the closed-loop system with the hybrid adaptive control.

Theorem 9 *For the closed-loop system defined by (3.29), (3.30) and (3.31), the parameter estimation errors $\tilde{\theta}_1$ and $\tilde{\theta}_2$ are bounded, and the regulation error x_k approaches to zero aymptotically.*

Proof: Choose a nonnegative function below

$$V_k = \sum_{i=k-N}^{k-1} \left(\frac{1}{q_1} \tilde{\theta}_1^2(i) \right) + \frac{1}{q_2} \tilde{\theta}_2^2(k-N), \tag{3.32}$$

its difference with respect to the interval N is

$$\begin{aligned} \Delta V_k &= V_k - V_{k-N} \\ &= \sum_{i=k-N}^{k-1} \frac{1}{q_1} \left(\tilde{\theta}_1^2(i) - \tilde{\theta}_1^2(i-N) \right) + \frac{1}{q_2} \left(\tilde{\theta}_2^2(k-N) - \tilde{\theta}_2^2(k-2N) \right). \end{aligned} \tag{3.33}$$

This can be rewritten as

$$\begin{aligned} \Delta V_k &= \sum_{i=k-N}^{k-1} \left(\frac{1}{q_1} \left(\tilde{\theta}_1^2(i) - \tilde{\theta}_1^2(i-N) \right) + \frac{1}{q_2} \left(\tilde{\theta}_2^2(i-N+1) - \tilde{\theta}_2^2(i-N) \right) \right) \\ &= \sum_{i=k-N}^{k-1} \left(\left[\begin{array}{cc} \tilde{\theta}_1(i) & \tilde{\theta}_2(i-N+1) \end{array} \right] Q^{-1} \left[\begin{array}{c} \tilde{\theta}_1(i) \\ \tilde{\theta}_2(i-N+1) \end{array} \right] - \tilde{\boldsymbol{\theta}}_{i-N}^T Q^{-1} \tilde{\boldsymbol{\theta}}_{i-N} \right) \end{aligned} \tag{3.34}$$

where $\tilde{\boldsymbol{\theta}}_k = [\tilde{\theta}_1(k), \tilde{\theta}_2(k)]^T$. Next shifting the parameter estimate (3.31) back N steps yields

$$\tilde{\theta}_2(k-N+1) = \tilde{\theta}_2(k-N) - q_2 \frac{\xi_2(k-N) x_{k-N+1}}{1 + \boldsymbol{\xi}_{k-N}^T Q \boldsymbol{\xi}_{k-N}}. \tag{3.35}$$

Combining the above expression (3.35) with that of $\tilde{\theta}_1(k)$ in (3.30) results in the following

$$\left[\begin{array}{c} \tilde{\theta}_1(k) \\ \tilde{\theta}_2(k-N+1) \end{array} \right] = \tilde{\boldsymbol{\theta}}_{k-N} - Q \frac{\boldsymbol{\xi}_{k-N} x_{k-N+1}}{1 + \boldsymbol{\xi}_{k-N}^T Q \boldsymbol{\xi}_{k-N}}. \tag{3.36}$$

Substituting (3.36) into (3.34) with calculation leads to

$$\Delta V_k = - \sum_{i=k-N}^{k-1} \left(\frac{2}{1 + \boldsymbol{\xi}_{i-N}^T Q \boldsymbol{\xi}_{i-N}} - \frac{\boldsymbol{\xi}_{i-N}^T Q \boldsymbol{\xi}_{i-N}}{\left(1 + \boldsymbol{\xi}_{i-N}^T Q \boldsymbol{\xi}_{i-N} \right)^2} \right) x_{i-N+1}^2 \tag{3.37}$$

$$\leq - \sum_{i=k-N}^{k-1} \left(\frac{x_{i-N+1}^2}{1 + \boldsymbol{\xi}_{i-N}^T Q \boldsymbol{\xi}_{i-N}} \right) \tag{3.38}$$

which implies that V_k is nonincreasing (w.r.t. N) and, thus, $\tilde{\theta}_1$ and $\tilde{\theta}_2$ are bounded. Similar to previous derivations, applying (3.38) repeatedly for any $k \in [pN, (p+1)N]$, and denoting $k_0 = k - pN$, we have

$$V(k) = V(k_0) + \sum_{i=1}^{p} \Delta V(k_0 + iN) \tag{3.39}$$

Since $k_0 \in [0, N)$, according to (3.38)

$$\lim_{p\to\infty} V(k) < \max_{k_0\in[0,N)} V(k_0) - \lim_{p\to\infty} \sum_{j=1}^{p} \left(\sum_{i=k_0(j-1)N}^{k_0+jN-1} \left(\frac{x_{i-N+1}^2}{1 + \boldsymbol{\xi}_{i-N}^T Q \boldsymbol{\xi}_{i-N}} \right) \right). \tag{3.40}$$

Considering the positiveness of $V(k)$ and the boundedness of $V(k_0)$ in the interval $[0, N)$ then, according to the convergence theorem of the sum of series, we have

$$\lim_{k\to\infty} \sum_{i=k-N}^{k-1} \left(\frac{x_{i-N+1}^2}{1 + \boldsymbol{\xi}_{i-N}^T Q \boldsymbol{\xi}_{i-N}} \right) \to 0. \tag{3.41}$$

Using (3.41) and the sector-bounded condition $\|\boldsymbol{\xi}_k\| \leq c_1 + c_2|x_k|$ for some constants c_1 and c_2, then the Key Technical Lemma guarantees that $x_k \to 0$ as $k \to \infty$. ∎

3.3.3 Extension to Tracking Tasks

Consider the scalar system (3.19) with multiple unknown parameters and the unknown periodic input gain. It is required that the state, x_k, follow a given reference trajectory $r(k)$. Specifying the tracking error as $e_k = x_k - r_k$, we have

$$e_{k+1} = x_{k+1} - r_{k+1} = \left(\boldsymbol{\theta}_k^0\right)^T \boldsymbol{\xi}_k^0 + b_k u_k - r_{k+1}. \tag{3.42}$$

Rewrite (3.42) in the form

$$e_{k+1} = \left(\boldsymbol{\theta}_k^0\right)^T \boldsymbol{\xi}_k^0 + b_k u_k - r_{k+1} - \hat{b}_k u_k + \hat{b}_k u_k = \left(\boldsymbol{\theta}_k^0\right)^T \boldsymbol{\xi}_k^0 + \hat{b}_k u_k + \tilde{b}_k u_k - r_{k+1}. \tag{3.43}$$

To accomodate the tracking task, the periodic adaptive control (3.21)-(3.24) can be revised as below

$$u_k = \hat{b}_k^{-1}\left(r_{k+1} - \left(\hat{\boldsymbol{\theta}}_k^0\right)^T \boldsymbol{\xi}_k^0\right) \tag{3.44}$$

$$\hat{\boldsymbol{\theta}}_k = \begin{cases} \hat{\boldsymbol{\theta}}_{k-N} + P_k \boldsymbol{\xi}_{k-N} e_{k-N+1}, & k \in [N, \infty) \\ \hat{\boldsymbol{\theta}}_0, & k \in [0, N) \end{cases} \tag{3.45}$$

$$P_k = \begin{cases} P_{k-N} - \frac{P_{k-N}\boldsymbol{\xi}_{k-N}^T \boldsymbol{\xi}_{k-N} P_{k-N}}{1+\boldsymbol{\xi}_{k-N}^T P_{k-N} \boldsymbol{\xi}_{k-N}}, & k \in [N, \infty) \\ P_0 > 0 & k \in [0, N) \end{cases} \tag{3.46}$$

where $\hat{\boldsymbol{\theta}}_k = \left[\left(\hat{\boldsymbol{\theta}}_k^0\right)^T, \tilde{b}_k\right]^T$, and $\boldsymbol{\xi}_k = \left[\left(\boldsymbol{\xi}_k^0\right)^T, \hat{b}_k^{-1}\left(r_{k+1} - \left(\hat{\boldsymbol{\theta}}_k^0\right)^T \boldsymbol{\xi}_k^0\right)\right]^T$. The closed-loop system for any $k \geq N$ is given by

$$\begin{aligned} e_{k+1} &= \tilde{\boldsymbol{\theta}}_k^T \boldsymbol{\xi}_k \\ \tilde{\boldsymbol{\theta}}_k &= \tilde{\boldsymbol{\theta}}_{k-N} - P_k \boldsymbol{\xi}_{k-N} e_{k-N+1} \\ P_k &= P_{k-N} - \frac{P_{k-N}\boldsymbol{\xi}_{k-N}^T \boldsymbol{\xi}_{k-N} P_{k-N}}{1 + \boldsymbol{\xi}_{k-N}^T P_{k-N} \boldsymbol{\xi}_{k-N}}. \end{aligned} \tag{3.47}$$

Note that the tracking error dynamics in (3.47) has the same form as (3.22), and the adaption mechanism (3.45)-(3.46) also has the same form as (3.23)-(3.24) with the state x_k replaced by the tracking error e_k. Thus, *Theorem 2* is directly applicable to this case and the asymptotic convergence of the tracking error e_k can easily be verified.

3.3.4 Extension to Higher Order Systems

Finally consider the single input higher order system in canonical form

$$\mathbf{x}_{k+1} = \begin{bmatrix} \mathbf{0} & I_{n-1} \\ 0 & \mathbf{0} \end{bmatrix} \mathbf{x}_k + \begin{bmatrix} \mathbf{0} \\ 1 \end{bmatrix} \left(\boldsymbol{\theta}_k^T \boldsymbol{\xi}_k + u_k\right) \tag{3.48}$$

where $\mathbf{x} \in \Re^n$, $\boldsymbol{\theta} = [\theta_1, \cdots, \theta_m]^T$ are unknown periodic parameters, $\boldsymbol{\xi} = \boldsymbol{\xi}(\mathbf{x}) = [\xi_1, \cdots, \xi_m]^T$ is a known vector valued function which is sector bounded, $\|\boldsymbol{\xi}\| \leq c_1 + c_2\|\mathbf{x}\|$ (c_1 and c_2 being arbitrary positive constants). Similar to the previous case, it is assumed that the unknown parameters have a common period N.

Assuming that all the states are available, the following control is proposed

$$u_k = -\hat{\boldsymbol{\theta}}_k^T \boldsymbol{\xi}_k \tag{3.49}$$

with the following parameter adaptation law

$$\hat{\boldsymbol{\theta}}_k = \begin{cases} \hat{\boldsymbol{\theta}}_{k-N} + P_k \boldsymbol{\xi}_{k-N} x_n(k-N+1), & k \in [N, \infty) \\ \hat{\boldsymbol{\theta}}_0, & k \in [0, N) \end{cases} \tag{3.50}$$

$$P_k = \begin{cases} P_{k-N} - \frac{P_{k-N}\boldsymbol{\xi}_{k-N}^T \boldsymbol{\xi}_{k-N} P_{k-N}}{1+\boldsymbol{\xi}_{k-N}^T P_{k-N} \boldsymbol{\xi}_{k-N}}, & k \in [N, \infty) \\ P_0 > 0 & k \in [0, N) \end{cases} \tag{3.51}$$

where the covariance P_k is a positive definite matrix of dimension m and derived from the relationship $P_k^{-1} = P_{k-N}^{-1} + \boldsymbol{\xi}_{k-N}\boldsymbol{\xi}_{k-N}^T$ by means of the Matrix Inversion Lemma. Note that the perameter estimate (3.50) is dependent on $x_n(k)$ where the subscript n denotes the n-th state variable. Substitute the control (3.49) into (3.48) and rewrite the result into two subsystems

$$\mathbf{x}_a(k+1) = \begin{bmatrix} \mathbf{0} & I_{n-2} \\ 0 & \mathbf{0} \end{bmatrix} \mathbf{x}_a(k) + \begin{bmatrix} \mathbf{0} \\ 1 \end{bmatrix} x_n(k) \tag{3.52}$$

$$x_n(k+1) = \tilde{\boldsymbol{\theta}}_k^T \boldsymbol{\xi}_k \tag{3.53}$$

where $\mathbf{x}_a = [x_1, \cdots, x_{n-1}]^T$. Looking into (3.50), (3.51) and (3.53), it is clear that this problem is transformed to the previous multiple parameter case. Thus the derivations and conclusions in *Theorem 2* hold, as far as the Key Technical Lemma is still valid under the sector condition.

In order to establish the sector condition, note that the solution of (3.52) is given by

$$\mathbf{x}_a(k) = \begin{bmatrix} \mathbf{0} & I_{n-2} \\ 0 & \mathbf{0} \end{bmatrix}^k \mathbf{x}_a(0) + \sum_{i=0}^{k-1} \begin{bmatrix} \mathbf{0} & I_{n-2} \\ 0 & \mathbf{0} \end{bmatrix}^i \begin{bmatrix} \mathbf{0} \\ 1 \end{bmatrix} x_n(k-i-1) \tag{3.54}$$

and for $k \geq n-1$ it can be shown that the solution is reduced to

$$\mathbf{x}_a(k) = \sum_{i=0}^{n-2} \begin{bmatrix} \mathbf{0} & I_{n-2} \\ 0 & \mathbf{0} \end{bmatrix}^i \begin{bmatrix} \mathbf{0} \\ 1 \end{bmatrix} x_n(k-i-1). \tag{3.55}$$

Applying the norm on both sides of (3.55) leads to

$$\max_{j\in[0,k]} \|\mathbf{x}_a(j+1)\| \leq (n-1) \max_{j\in[0,k]} \|x_n(j)\|. \tag{3.56}$$

The above result is then used to simplify the sector condition $\|\boldsymbol{\xi}\| \leq c_1 + c_2\|\mathbf{x}\|$ as follows

$$\begin{aligned} \|\boldsymbol{\xi}_k\| &\leq c_1 + c_2\|\mathbf{x}_k\| \leq c_1 + c_2\left(\|\mathbf{x}_a(k)\| + \|x_n(k)\|\right) \\ &\leq c_1 + c_2\left((n-1)\max_{j\in[0,k]} \|x_n(j-1)\| + \max_{j\in[0,k]} \|x_n(j)\|\right). \end{aligned}$$

Note that $\max_{j\in[0,k]} \|x_n(j-1)\| \leq \max_{j\in[0,k]} \|x_n(j)\|$, thus,

$$\begin{aligned} \|\boldsymbol{\xi}_k\| &\leq c_1 + nc_2 \max_{j\in[0,k]} \|x_n(j)\| \leq c_1 + nc_2\left(\|x_n(0)\| + \max_{j\in[0,k]} \|x_n(j+1)\|\right) \\ &\leq c_1^0 + c_2^0 \max_{j\in[0,k]} \|x_n(j+1)\| \end{aligned} \tag{3.57}$$

where $c_1^0 = c_1 + nc_2\|x_n(0)\|$ and $c_2^0 = nc_2$.

Remark 16 *Extension from the first order to higher order can also be applied to systems with the unknown input gain, mixed parameters, or tracking problems, as discussed in preceding subsections 3.3.1, 3.3.2, and 3.3.3.*

3.4 Illustrative Example

Consider a system

$$x_{k+1} = \theta_k \sin(x_k + 1) + b_k u_k, \qquad x(0) = 1 \tag{3.58}$$

where $\theta_k = \sin(\pi k/25)$. We use $|x_i|_{sup}$ to record the maximum absolute regulation error during the i-th period.

First let $b_k = 3 + 0.5\sin(\pi k/50)$. The minimum common period is $N = 100$. A typical adaptive controller is used with the Least Squares estimator. Fig.3.1 (a) shows the regulation error over each period. By virtue of the rapid time-varying nature, the tracking error does not converge. Applying the proposed periodic adaptation method, Fig.3.1 (b) shows the maximum regulation error over each period. We can clearly see the effectiveness, as the regulation error has been reduced to less than 1% after 50 periods.

Next, let $b_k = 3$ be an unknown constant. Still using the periodic adaptation law, the result is shown in Fig.3.2 (a). Now assume that it is known *a priori* that b_k is an unknown constant, the hybrid adaptation law is adopted and the result is shown in Fig.3.2 (b). The performance improvement is immediately obvious.

Finally, let $b_k = 3 + 0.5\sin(\pi k/50)$ again, and it is required that x_k track a given reference $r_k = sin(\pi k/50)$. Fig.3.3 shows that the tracking error is asymptotically convergent.

3.5 Conclusion

In this Chapter we propose an adaptive control approach characterized by periodic parameter adaptation, which complements the existing adaptive control characterized by instantaneous adaptation. By virtue of the periodic adaptation, the approach is applicable to system with periodic parameters or periodic disturbances which can be rapidly time-varying. The only prior knowledge needed in the periodic adaptation is the periodicity. A hybrid adaptation scheme is also proposed when more of the parameter knowledge is available. Both regulation and tracking problems were discussed. Extension to higher order processes was also exploited The validity of the proposed approach is confirmed through theoretical analysis and numerical simulations.

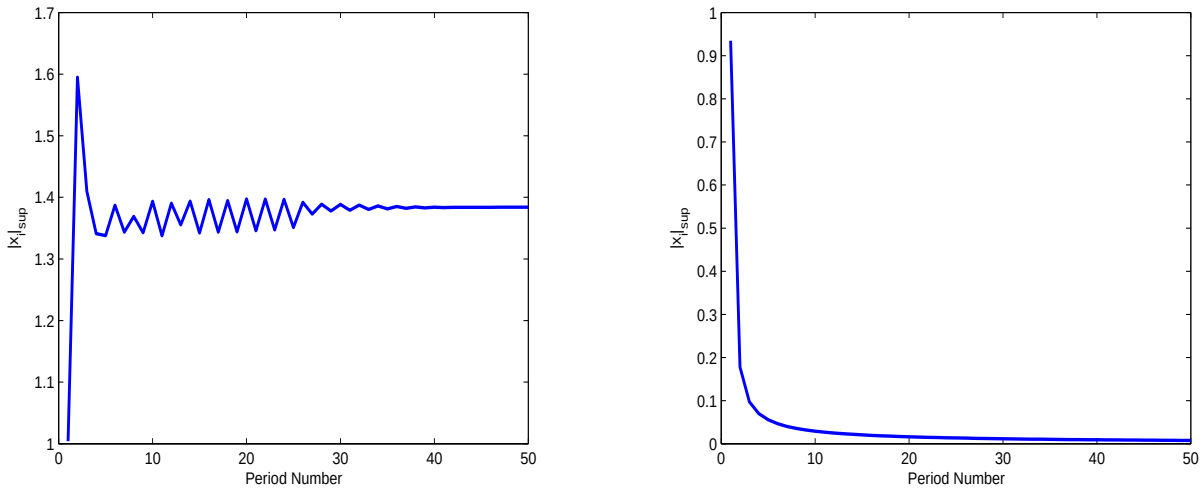

(a) (b)

Figure 3.1: Error convergence using (a) classical adaptation and (b) periodic adaptation

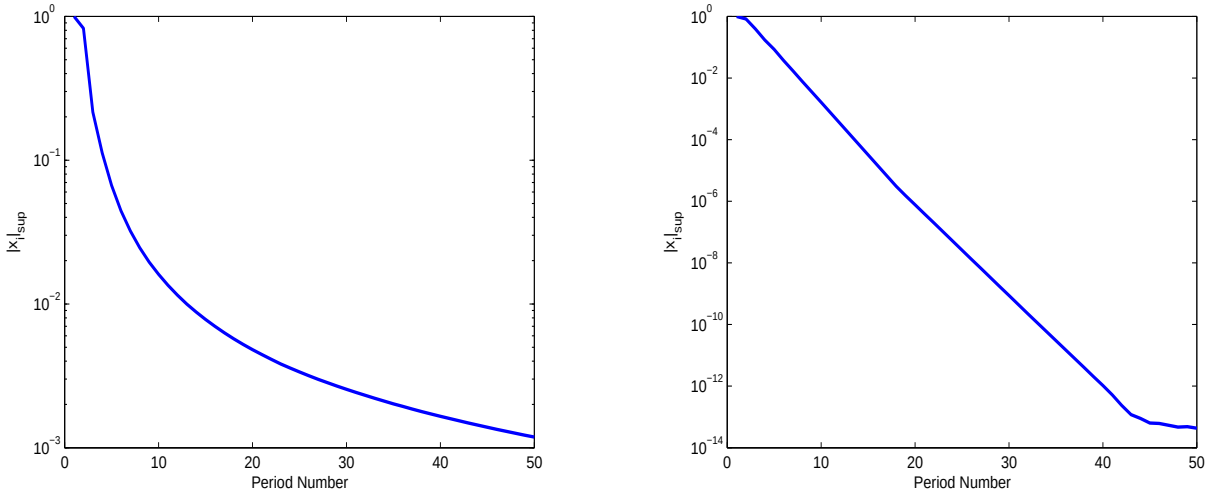

(a) (b)

Figure 3.2: Error convergence with mixed parameters using (a) periodic adaptation and (b) hybrid periodic adaptation

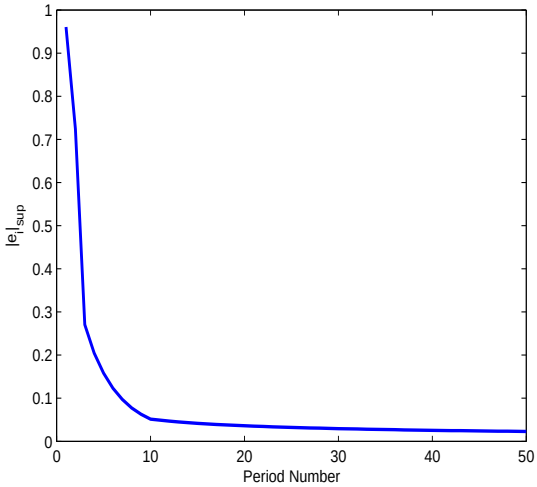

Figure 3.3: Tracking error convergence using periodic adaptation

Chapter 4

Iterative Learning Control for SISO Sampled-Data Systems

4.1 Introduction

The idea of using an iterative method to compensate for a repetitive error is not new. For example, physical feats such as dance routines need to be repeated iteratively to be perfected. During each repitition, a dancers observes how he/she correctly executes the required motions correcting any errors each time. As the dancer continues to practice, the correct motion is learned and becomes ingrained into the muscle memory so that the execution of the routine is iteratively improved. The converged muscle motion profile is an open-loop control generated through repetition and learning. This type of learned open-loop control strategy is the essence of ILC.

We consider learning controllers for systems that perform the same operation repeatedly and under the same operating conditions. For such systems, a nonlearning controller yields the same tracking error on each pass. Although error signals from previous iterations are infor-

mation rich, they are unused by a nonlearning controller. The objective of ILC is to improve performance by incorporating error information into the control for subsequent iterations. In doing so, high performance can be achieved with low transient tracking error despite large model uncertainties and repeating disturbances.

ILC differs from other learning-type control strategies, such as adaptive control, neural networks, and repetitive control (RC). Adaptive control strategies modify the controller, which is a system, whereas ILC modifies the control input, which is a signal [44]. Additionally, adaptive controllers typically do not take advantage of the information contained in repetitive command signals. Similarly, neural network learning involves the modification of controller parameters rather than a control signal; in this case, large networks of nonlinear neurons are modified. These large networks require extensive training data, and fast convergence may be difficult to guarantee [45], whereas ILC usually converges adequately in just a few iterations.

ILC is perhaps most similar to RC [46] except that RC is intended for continuous operation, whereas ILC is intended for discontinuous operation. For example, an ILC application might be to control a robot that performs a task, returns to its home position, and comes to a rest before repeating the task. On the other hand, an RC application might be the control of a conveyer system in a mass-production line moving items at periodic intervals where the next iteration immediately follows the current iteration. The difference between RC and ILC is the setting of the initial conditions for each trial [47]. In ILC, the initial conditions are set to the same value on each trial. In RC, the initial conditions are set to the final conditions of the previous trial. The difference in initial-condition resetting leads to different analysis

techniques and results [47].

Traditionally, the focus of ILC has been on improving the performance of systems that execute a single, repeated operation. This focus includes many practical industrial systems in manufacturing, robotics, and chemical processing, where mass production on an assembly line entails repetition. ILC has been successfully applied to industrial robots [48]-[52], computer numerical control (CNC) machine tools [53], wafer stage motion systems [54], injection-molding machines [55], [56], and many more.

The basic ideas of ILC can be found in a U.S. patent [13] filed in 1967 as well as the 1978 journal publication [12] written in Japanese. However, these ideas lay dormant until a series of articles in 1984 [48], [57]-[59] sparked widespread interests in ILC. Since then, the number of publications on ILC has been growing rapidly, including two special issues [60], [61], several books [44], [62]-[64], and three surveys [65]-[67].

The aim of this Chapter is to present a summary of theoretical analysis and design of ILC algorithms in the time and frequency domain. The analysis is based on the use of linear iterative systems. By incorporating the ILC algorithm and the system to be controlled into this class of systems many useful results from linear systems theory can be applied. As a consequence both first-order and high-order ILC algorithms can be analysed. The work concludes with a real-time application on a high-precision piezo-motor.

4.2 Preliminaries

In this section we shall present the problem description as well as highlight the basic differences between continuous-time ILC and sampled-data ILC.

4.2.1 Problem Description

Considering a tracking task that ends in a finite interval $[0,\ N]$ and repeats. Let the desired trajectory be $y_r(k)$, $k \in [0,\ N]$. Consider the ILC law

$$\begin{aligned} u_{i+1}(k) &= Q(\mathrm{q})[u_i(k) + \beta L(\mathrm{q}) e_i(k+1)] \\ e_i(k) &= y_r(k) - y_i(k) \end{aligned} \tag{4.1}$$

where $Q(\mathrm{q})$ is a filter function, $L(\mathrm{q})$ is a learning function, $\beta > 0$ is a learning gain, i denotes the iteration number, and $y_i(k)$ is the output of the sampled-data system

$$\begin{aligned} \mathbf{x}_i(k+1) &= \Phi \mathbf{x}_i(k) + \Gamma u_i(k) \\ y_i(k) &= C\mathbf{x}_i(k) \end{aligned} \tag{4.2}$$

with the initial states $\mathbf{x}_i(0)$. Define

$$\begin{aligned} \mathbf{x}_r(k+1) &= \Phi \mathbf{x}_r(k) + \Gamma u_r(k) \\ y_r(k) &= C\mathbf{x}_r(k) \end{aligned} \tag{4.3}$$

where $\mathbf{x}_r$, y_r are the desired state and output trajectories and u_r is the required control input to achieve those trajectories. Subtracting (4.2) from (4.3) leads to

$$\begin{aligned} \Delta\mathbf{x}_i(k+1) &= \Phi \Delta\mathbf{x}_i(k) + \Gamma \Delta u_i(k) \\ e_i(k) &= C\Delta\mathbf{x}_i(k). \end{aligned} \tag{4.4}$$

In all the analysis it is assumed that the identical initial condition *i.i.c*, $e(0) = 0$, holds.

The control problem is to design the learning function $L(\mathrm{q})$ and filter $Q(\mathrm{q})$ such that the maximum bound of the tracking error in an iteration converges to zero asymptotically with

respect to iteration, i.e,

$$\sup_{k\in(0,N)} |e_i(k)|_{i\to\infty} \to 0. \tag{4.5}$$

4.2.2 Difference with Continuous-Time Iterative Learning Control

In the derivation of the ILC, the question of the relative degree of the system is very important.

For example, consider the n-order SISO system with a relative degree of n

$$\begin{aligned} \dot{\mathbf{x}}(t) &= A\mathbf{x}(t) + Bu(t) \\ y(t) &= C\mathbf{x}(t). \end{aligned} \tag{4.6}$$

Since the system is of relative degree n, the term $CA^{n-1}B$ is non-zero which is inferred from

$$\frac{d^n}{dt^n}y(t) = CA^n\mathbf{x}(t) + CA^{n-1}Bu(t) \tag{4.7}$$

while CB upto $CA^{n-2}B$ are 0.

Now, consider that (4.6) is sampled with time T resulting in the system

$$\begin{aligned} \mathbf{x}_{k+1} &= \Phi\mathbf{x}_k + \Gamma u_k \\ y_k &= C\mathbf{x}_k. \end{aligned} \tag{4.8}$$

The input gain for the sampled data system (4.8) is given by

$$\Gamma = \int_0^T e^{A\tau}Bd\tau = \int_0^T \left(B + AB\tau\frac{1}{2!}A^2B\tau^2 + \cdots + \frac{1}{(n-1)!}A^{n-1}B\tau^{n-1} + O(T^n)\right)d\tau \tag{4.9}$$

which can be solved to give the expression

$$\Gamma = BT + \frac{1}{2!}ABT^2 + \cdots + \frac{1}{n!}A^{n-1}BT^n + O(T^{n+1}) \tag{4.10}$$

premultiplying (4.10) with C results in

$$C\Gamma = \frac{1}{n!}CA^{n-1}BT^n + O(T^{n+1}). \tag{4.11}$$

This has an important implication, which is that the relative degree of the system has changed from n to 1 upon sampling. This can be seen from

$$y_{k+1} \;=\; C\Phi\mathbf{x}_k + C\Gamma u_k. \tag{4.12}$$

This result shows that in the continuous-time, the ILC would require the *nth* derivative of the output signal while it is not so in the sampled-data ILC. This greatly simplifies the ILC derivation for sampled-data systems irrespective of order and relative degree in continuous-time. However, note that the size of the term $C\Gamma$ depends on the sampling time and order of the system. Based on this result we can proceed to the analysis of the discrete-time ILC.

Remark 17 *The above discussion may also be extended to LTV systems provided that the condition* $C\Gamma \neq 0$ *is satisfied.*

4.3 General Iterative Learning Control: Time Domain

Considering (4.4) and define $\Delta\bar{\mathbf{x}}_i = [\Delta\mathbf{x}_i(1), \cdots, \Delta\mathbf{x}_i(N)]^T$, $\mathbf{e}_i = [e_i(1), \cdots, e_i(N)]^T$, and $\Delta\mathbf{u}_i = [\Delta u_i(0), \cdots, \Delta u_i(N-1)]^T$. Assuming that the *i.i.c is satisfied*, (4.4) can be written as

$$\begin{aligned}
\Delta\bar{\mathbf{x}}_i &= \begin{bmatrix} \Gamma & 0 & \cdots & 0 \\ \Phi\Gamma & \Gamma & \cdots & 0 \\ \vdots & \vdots & \ddots & \vdots \\ \Phi^{N-1}\Gamma & \Phi^{N-2}\Gamma & \cdots & \Gamma \end{bmatrix} \Delta\mathbf{u}_i \\
\mathbf{e}_i &= \underbrace{\begin{bmatrix} C\Gamma & 0 & \cdots & 0 \\ C\Phi\Gamma & C\Gamma & \cdots & 0 \\ \vdots & \vdots & \ddots & \vdots \\ C\Phi^{N-1}\Gamma & C\Phi^{N-2}\Gamma & \cdots & C\Gamma \end{bmatrix}}_{\mathbf{P}} \Delta\mathbf{u}_i.
\end{aligned} \tag{4.13}$$

If the rational functions $Q(\mathrm{q})$ and $L(\mathrm{q})$ are assumed causal and expanded as infinite series by dividing the denominator into its numerator, yielding

$$Q(\mathrm{q}) \;=\; q_0 + q_1\mathrm{q}^{-1} + q_2\mathrm{q}^{-2} + \cdots$$

and

$$L(\mathrm{q}) \;=\; l_0 + l_1\mathrm{q}^{-1} + l_2\mathrm{q}^{-2} + \cdots$$

respectively. In the lifted form the matrices $\mathbf{Q}$ and $\mathbf{L}$ are lower-triangular Toeplitz matrices as shown below

$$\mathbf{Q} \;=\; \begin{bmatrix} q_0 & 0 & \cdots & 0 \\ q_1 & \ddots & \ddots & \vdots \\ \vdots & \ddots & \ddots & 0 \\ q_{N-1} & \cdots & q_1 & q_0 \end{bmatrix}, \;\; \mathbf{L} \;=\; \begin{bmatrix} l_0 & 0 & \cdots & 0 \\ l_1 & \ddots & \ddots & \vdots \\ \vdots & \ddots & \ddots & 0 \\ l_{N-1} & \cdots & l_1 & l_0 \end{bmatrix}. \tag{4.14}$$

Subtracting both sides of (4.1) from $u_r(k)$ and writing the result in lifted form

$$\Delta\mathbf{u}_{i+1} \;=\; \mathbf{Q}\Delta\mathbf{u}_i - \beta\mathbf{Q}\mathbf{L}\mathbf{e}_i + (I - \mathbf{Q})\mathbf{u}_r \tag{4.15}$$

where $\mathbf{u}_r = [u_r(0), \cdots, u_r(N-1)]^T$. Substituting (4.13) into (4.15) gives

$$\Delta\mathbf{u}_{i+1} \;=\; \underbrace{\mathbf{Q}(I - \beta\mathbf{L}\mathbf{P})}_{\mathbf{F}}\Delta\mathbf{u}_i + (I - \mathbf{Q})\mathbf{u}_r. \tag{4.16}$$

It can easily be shown that $\mathbf{F}$ has $q_0(1 - \beta l_0 C\Gamma)$ as a repeated eigenvalue. Stability of (4.16) is guaranteed if

$$|q_0(1 - \beta l_0 C\Gamma)| < 1. \tag{4.17}$$

Remark 18 *Condition (4.17) is possible since $C\Gamma \neq 0$. This is true for sampled-data systems as was shown previously. However, depending on the order and degree of the continuous system, $C\Gamma$ can be quite small requiring a large learning gain.*

Remark 19 *Condition (4.17) is sufficient for BIBO stability, but, does not necessarily guarantee a montonically decreasing* $\|\mathbf{e}_i\|$*, [68].*

4.3.1 Convergence Properties

We can further investigate the convegence properties of the ILC system by looking at the matrix $\mathbf{F}$ in (4.16). Now consider (4.1) with $Q(\mathrm{q}) = L(\mathrm{q}) = I$, (4.16) becomes

$$\Delta \mathbf{u}_{i+1} \;=\; (I - \beta \mathbf{P}) \Delta \mathbf{u}_i \tag{4.18}$$

which can be expanded to the form

$$\Delta \mathbf{u}_{i+1} \;=\; \underbrace{\begin{bmatrix} (1-\beta C\Gamma) & 0 & \cdots & 0 \\ -\beta C\Phi\Gamma & (1-\beta C\Gamma) & \ddots & \vdots \\ \vdots & \vdots & \ddots & 0 \\ -\beta C\Phi^{N-1}\Gamma & -\beta C\Phi^{N-2}\Gamma & \cdots & (1-\beta C\Gamma) \end{bmatrix}}_{\mathbf{F}} \Delta \mathbf{u}_i. \tag{4.19}$$

The stability of (4.19) is now reduced to

$$|(1 - \beta C\Gamma)| < 1. \tag{4.20}$$

Assume that

$$\alpha = \sup_{1 \le k \le N-1} |\beta C\Phi^k\Gamma| \tag{4.21}$$

and let $\gamma = 1 - \beta C\Gamma$. Thus, we approximate the worst case matrix $\mathbf{F}$ as follows

$$\mathbf{F}_{\mathbf{wc}} = \begin{bmatrix} \gamma & 0 & \cdots & 0 \\ -\alpha & \ddots & \ddots & \vdots \\ \vdots & \ddots & \ddots & 0 \\ -\alpha & \cdots & -\alpha & \gamma \end{bmatrix}. \tag{4.22}$$

Note that a general solution of (4.19) is given by

$$\Delta \mathbf{u}_{i+1} \;=\; \mathbf{F}^i \Delta \mathbf{u}_0 \tag{4.23}$$

where $\Delta \mathbf{u}_0$ is the error in control at the zeroth iteration. If we use the approximation of $\mathbf{F}$ to compute $\mathbf{F}^i$ we get

$$\mathbf{F_{wc}}^i = \begin{bmatrix} \gamma & 0 & \cdots & 0 \\ -\alpha & \ddots & \ddots & \vdots \\ \vdots & \ddots & \ddots & 0 \\ -\alpha & \cdots & -\alpha & \gamma \end{bmatrix}^i = \begin{bmatrix} \gamma^i & 0 & \cdots & 0 \\ S(1) & \ddots & \ddots & \vdots \\ \vdots & \ddots & \ddots & 0 \\ S(N-1) & \cdots & S(1) & \gamma^i \end{bmatrix} \tag{4.24}$$

where

$$S(m) \;=\; \sum_{p=1}^{\min(i,m)} (-1)^p \left({}^iC_p\right) \left({}^{m-1}C_{p-1}\right) \gamma^{i-p} \alpha^p. \tag{4.25}$$

The binomial coefficient ${}^mC_p$ is plotted for a constant m as a function of p in Fig.4.1. It can be seen that the coefficient attains a very large value before converging to unity and if the convergence due to α and γ is slower than that of the initial divergence of ${}^mC_p$ then $S(m)$ would also follow the characteristic of ${}^mC_p$. This overshooting phenomenon will be illustrated in later examples. From the above results it is obvious that we need to guarantee monotonic convergence. Two conditions exist that guarantee montonic convergence. The first one is time domain based while the other is frequency domain based and will be investigated later on. According to [65], if $|1 - \beta C\Gamma| < 1$ then the monotonic convergence is guaranteed if the following condition is satisfied

$$\begin{array}{rcll} |C\Gamma| & > & \sum_{j=2}^{N} |C\Phi^{j-1}\Gamma|, & \forall \beta C\Gamma \in (0,1) \\ |C\Gamma| & < & \frac{1}{|\beta|} - \sum_{j=2}^{N} |C\Phi^{j-1}\Gamma|, & \forall \beta C\Gamma \in (1,2). \end{array} \tag{4.26}$$

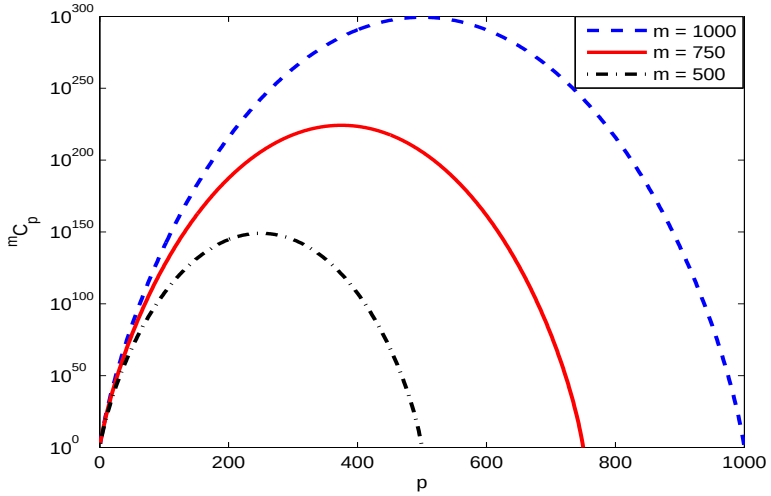

Figure 4.1: Plot of ${}^{m}C_{i}$

Later it will be shown that with the proper selection of the learning function, $L(\mathrm{q})$, likelihood of satisfying the above condition is increased. Based on (4.25) and (4.26) it is worthwhile to ponder the effect of sampling time on the ILC convergence. Note that the parameter N in (4.24) and (4.26) represents the number of samples per iteration and that the lower the value of N (larger the sampling time) the lower the peak of the function ${}^{m}C_{p}$ as can be infered from Fig.4.1. Similarly, a lower value of N makes (4.26) more likely to be satisfied. However, this is true only for the ideal case of a stable LTI system with no disturbance. If the system is subjected to a repeatable disturbance then the sampling-time must be selected such that as much as possible of the disturbance bandwidth is covered. Thus, a trade-off will exist between the selection of the sampling-time and how much of the disturbance bandwidth we will need to cover.

4.3.2 D-Type and D^2-type ILC

In this section, two representative designs of the learning function, $L(\mathrm{q})$ will be considered and later on a detailed guideline will be presented from the frequency-domain perspective for the selection of appropriate learning functions. Consider the ILC

$$u_{i+1}(k) = u_i(k) + \beta L(\mathrm{q}) e_i(k+1). \tag{4.27}$$

If we are to consider the D-type ILC then $L(\mathrm{q})$ represents a first order difference and is given by, $L(\mathrm{q}) = 1 - \mathrm{q}^{-1}$. In the lifted form the learning function $L(\mathrm{q})$ is given by

$$\mathbf{L} = \begin{bmatrix} 1 & 0 & \cdots & \cdots & 0 \\ -1 & \ddots & \ddots & \ddots & \vdots \\ 0 & \ddots & \ddots & \ddots & \vdots \\ \vdots & \ddots & \ddots & \ddots & 0 \\ 0 & \cdots & 0 & -1 & 1 \end{bmatrix}. \tag{4.28}$$

Subtracting both sides of (4.27) from $u_r(k)$ and writing the result into the lifted form

$$\Delta \mathbf{u}_{i+1} = \Delta \mathbf{u}_i - \beta \begin{bmatrix} 1 & 0 & \cdots & \cdots & 0 \\ -1 & \ddots & \ddots & \ddots & \vdots \\ 0 & \ddots & \ddots & \ddots & \vdots \\ \vdots & \ddots & \ddots & \ddots & 0 \\ 0 & \cdots & 0 & -1 & 1 \end{bmatrix} \mathbf{e}_i. \tag{4.29}$$

Substituting (4.13) into (4.29) results in

$$\Delta \mathbf{u}_{i+1} = \begin{bmatrix} \gamma & 0 & \cdots & 0 \\ -\beta C\Phi^0(\Phi - I)\Gamma & \gamma & \ddots & \vdots \\ \vdots & \ddots & \ddots & 0 \\ -\beta C\Phi^{N-2}(\Phi - I)\Gamma & \cdots & -\beta C\Phi^0(\Phi - I)\Gamma & \gamma \end{bmatrix} \Delta \mathbf{u}_i \tag{4.30}$$

where $\gamma = (1 - \beta C\Gamma)$. A closer look at the matrix in (4.30) will reveal that the eigenvalues are similar to that of the matrix in (4.19). Thus, BIBO stability is guaranteed if

$$|(1 - \beta C\Gamma)| < 1. \tag{4.31}$$

Another point to note is that in (4.30) the term $(\Phi - I) \approx AT$ for small T. This indicates that in comparison to the matrix in (4.19) the non-diagonal elements in (4.30) are smaller with an order $O(T)$. If we revisit condition (4.26), for the D-type it is modified to

$$\begin{array}{rcl} |C\Gamma| & > & \sum_{j=2}^{N} |C\Phi^{j-2}(I-\Phi)\Gamma|, \quad \forall \beta C\Gamma \in (0,1) \\ |C\Gamma| & < & \frac{1}{|\beta|} - \sum_{j=2}^{N} |C\Phi^{j-2}(I-\Phi)\Gamma|, \quad \forall \beta C\Gamma \in (1,2). \end{array} \tag{4.32}$$

Since, $(\Phi - I) \approx AT$, the above conditions are more likely to be satisfied for the D-type as opposed to the P-type. If we proceed further and introduce the D^2-type where the learning function $L(\mathrm{q})$ represents a 2^{nd}-order difference given by

$$L(\mathrm{q}) \; = \; 1 - 2\mathrm{q}^{-1} + \mathrm{q}^{-2}. \tag{4.33}$$

In the lifted form the learning function $L(\mathrm{q})$ is given by

$$\mathbf{L} = \begin{bmatrix} 1 & 0 & \cdots & \cdots & \cdots & 0 \\ -2 & 1 & \ddots & \ddots & \ddots & \vdots \\ 1 & -2 & 1 & \ddots & \ddots & \vdots \\ 0 & \ddots & \ddots & \ddots & \ddots & \vdots \\ \vdots & \ddots & \ddots & \ddots & \ddots & 0 \\ 0 & \cdots & 0 & 1 & -2 & 1 \end{bmatrix}. \tag{4.34}$$

Following the same procedure as in the derivation of (4.30) we obtain

$$\Delta \mathbf{u}_{i+1} \; = \; \begin{bmatrix} \gamma & 0 & \cdots & \cdots & 0 \\ -\beta C\Phi^0(2\Phi - I)\Gamma & \gamma & \ddots & \ddots & \vdots \\ -\beta C\Phi^0(\Phi - I)^2\Gamma & \ddots & \ddots & \ddots & \vdots \\ \vdots & \ddots & \ddots & \ddots & 0 \\ -\beta C\Phi^{N-3}(\Phi - I)^2\Gamma & \cdots & -\beta C\Phi^0(\Phi - I)^2\Gamma & -\beta C\Phi^0(2\Phi - I)\Gamma & \gamma \end{bmatrix} \Delta \mathbf{u}_i \tag{4.35}$$

where $\gamma = 1 - \beta C\Gamma$. Note that as in the case of the D-type ILC the eigenvalues are the same as that of the P-type ILC. However, most of the non-diagonal elements contain the term

$(\Phi - I)^2$ which is significant since $(\Phi - I)^2 \approx (AT)^2 \approx O(T^2)$. Condition (4.26) for the D^2-type is modified to

$$\begin{array}{rcl} |C\Gamma| & > & |C(I-2\Phi)\Gamma| + \sum_{j=3}^{N} |C\Phi^{j-3}(I-\Phi)^2\Gamma|, \quad \forall \beta C\Gamma \in (0,1) \\ |C\Gamma| & < & \frac{1}{|\beta|} - |C(I-2\Phi)\Gamma| - \sum_{j=3}^{N} |C\Phi^{j-3}(I-\Phi)^2\Gamma|, \quad \forall \beta C\Gamma \in (1,2). \end{array} \tag{4.36}$$

Note that in condition (4.36) the term $(\Phi - I)^2$ is dominating. Since $(\Phi - I)^2 \approx O(T^2)$ it increases the likelihood of (4.36) being satisfied, thus, guaranteeing asymptotic convergence.

4.3.3 Effect of Time-Delay

Consider the following LTI system with control input delay

$$\begin{array}{rcl} \dot{\mathbf{x}}_i(t) & = & A\mathbf{x}_i(t) + Bu_i(t - T_d) \\ y_i(t) & = & C\mathbf{x}_i(t) \end{array} \tag{4.37}$$

where T_d is the time delay. If system (4.37) is sampled with a sampling time T then it is possible to write

$$T_d = mT + T_f$$

where $m \in Z^+$, Z^+ being the set of positive integers, and $0 \leq T_f < T$ such that

$$\begin{array}{rcl} \mathbf{x}_i(k+1) & = & \Phi\mathbf{x}_i(k) + \Gamma_1 u_i(k-m) + \Gamma_2 u_i(k-m-1) \\ y_i(k) & = & C\mathbf{x}_i(k). \end{array} \tag{4.38}$$

It can be easily shown that

$$\Gamma_1 = \int_{T_f}^{T} e^{A\tau} B d\tau, \quad \Gamma_2 = \int_{0}^{T_f} e^{A\tau} B d\tau. \tag{4.39}$$

Rewrite (4.38)

$$\begin{array}{rcl} \mathbf{x}_i(k+m+1) & = & \Phi\mathbf{x}_i(k+m) + \Gamma_1 u_i(k) + \Gamma_2 u_i(k-1) \\ y_i(k+m) & = & C\mathbf{x}_i(k+m). \end{array} \tag{4.40}$$

Define

$$\begin{aligned} \mathbf{x}_r(k+m+1) &= \Phi \mathbf{x}_r(k+m) + \Gamma_1 u_r(k) + \Gamma_2 u_r(k-1) \\ y_r(k+m) &= C\mathbf{x}_r(k+m) \end{aligned} \tag{4.41}$$

where x_r, y_r are the desired state and output trajectories, and u_r is the control input required to achieve those trajectories. Subtracting (4.40) from (4.41) gives the following error dynamics

$$\begin{aligned} \Delta\mathbf{x}_i(k+m+1) &= \Phi \Delta\mathbf{x}_i(k+m) + \Gamma_1 \Delta u_i(k) + \Gamma_2 \Delta u_i(k-1) \\ e_i(k+m) &= C\Delta\mathbf{x}_i(k+m). \end{aligned} \tag{4.42}$$

Defining $\Delta\bar{\mathbf{x}}_i = [\Delta\mathbf{x}_i(m+1), \cdots, \Delta\mathbf{x}_i(N)]^T$, $\mathbf{e}_i = [e_i(m+1), \cdots, e_i(N)]^T$, and $\Delta\mathbf{u}_i = [\Delta u_i(0), \cdots, \Delta u_i(N-m-1)]^T$. Assuming that the *i.i.c is satisfied* ($\Delta\mathbf{x}_i(m) = e_i(m) = 0$), (4.42) can be written as

$$\begin{aligned} \Delta\bar{\mathbf{x}}_i &= \begin{bmatrix} \Gamma_1 & 0 & \cdots & 0 \\ \Phi\Gamma_1 + \Gamma_2 & \Gamma_1 & \cdots & 0 \\ \vdots & \vdots & \ddots & \vdots \\ \Phi^{N-m-2}(\Phi\Gamma_1 + \Gamma_2) & \Phi^{N-m-3}(\Phi\Gamma_1 + \Gamma_2) & \cdots & \Gamma_1 \end{bmatrix} \Delta\mathbf{u}_i \\ \mathbf{e}_i &= \begin{bmatrix} C\Gamma_1 & 0 & \cdots & 0 \\ C\Phi\Gamma_1 + C\Gamma_2 & C\Gamma_1 & \cdots & 0 \\ \vdots & \vdots & \ddots & \vdots \\ C\Phi^{N-m-2}(\Phi\Gamma_1 + \Gamma_2) & C\Phi^{N-m-3}(\Phi\Gamma_1 + \Gamma_2) & \cdots & C\Gamma_1 \end{bmatrix} \Delta\mathbf{u}_i. \end{aligned} \tag{4.43}$$

Consider the ILC law

$$u_{i+1}(k) = u_i(k) + \beta e_i(k+m+1). \tag{4.44}$$

Note that (4.44) has been modified for the time-delay. If both sides of(4.44) are subtracted from $u_r(k)$ and the result written in the lifted form similar to (4.13), then we get

$$\Delta \mathbf{u}_{i+1} = \Delta \mathbf{u}_i - \beta \mathbf{e}_i. \tag{4.45}$$

Substituting (4.43) into (4.45) leads to

$$\Delta \mathbf{u}_{i+1} = \begin{bmatrix} (1-\beta C\Gamma_1) & 0 & \cdots & 0 \\ -\beta(C\Phi\Gamma_1 + C\Gamma_2) & (1-\beta C\Gamma_1) & \cdots & 0 \\ \vdots & \vdots & \ddots & \vdots \\ -\beta C\Phi^{N-m-2}(\Phi\Gamma_1+\Gamma_2) & -\beta C\Phi^{N-m-3}(\Phi\Gamma_1+\Gamma_2) & \cdots & (1-\beta C\Gamma_1) \end{bmatrix} \Delta \mathbf{u}_i. \tag{4.46}$$

Note that the matrix in (4.46) has $(1-\beta C\Gamma_1)$ as a repeated eigenvalue. BIBO stability of (4.46) requires that

$$|(1-\beta C\Gamma_1)| < 1. \tag{4.47}$$

Remark 20 *From the above results it can be seen that for a special case of fractional time-delay, i.e $m = 0$, (4.1) can still guarantee BIBO stability provided that condition (4.47) is satisfied. Also note that as T_f approaches T then Γ_1 will decrease and, therefore, the learning gain β must increase to satisfy (4.47).*

4.4 General Iterative Learning Control: Frequency Domain

We have seen that based on the time-domain analysis it is only possible to guarantee BIBO stability. Based on this the system may not behave in a desirable manner. Thus, it is necessary to explore the possibility of guaranteeing monotonic convergence.

Consider the one-sided z-transformation of (4.4)

$$\begin{aligned} \Delta \mathbf{X}_i(z) &= (Iz - \Phi)^{-1}\Gamma \Delta U_i(z) \\ E_i(z) &= C\Delta \mathbf{X}_i(z) = \underbrace{C\,(Iz-\Phi)^{-1}\,\Gamma}_{P(z)}\,\Delta U_i(z). \end{aligned} \tag{4.48}$$

Obtain the z-transform of (4.1) and after subtracting both sides from $U_r(z)$ we get

$$\Delta U_{i+1}(z) = Q(z)\left[\Delta U_i(z) - z\beta L(z) E_i(z)\right] + \left[1 - Q(z)\right] U_r(z). \tag{4.49}$$

Substitution of (4.48) into (4.49) leads to

$$\Delta U_{i+1}(z) = \underbrace{Q(z)\left[1 - z\beta L(z) P(z)\right]}_{F(z)}\,\Delta U_i(z) + \left[1 - Q(z)\right] U_r(z). \tag{4.50}$$

An important point to note is that if $F(z)$ is expanded as an infinite series

$$F(z) = f_0 + f_1 z^{-1} + f_2 z^{-2} + f_3 z^{-3} + \cdots$$

then the first N coefficients of the series represent the first column of the Toeplitz matrix $\mathbf{F}$ in (4.16), in other words

$$\mathbf{F} = \begin{bmatrix} f_0 & 0 & \cdots & 0 \\ f_1 & \ddots & \ddots & \vdots \\ \vdots & \ddots & \ddots & 0 \\ f_{N-1} & \cdots & f_1 & f_0 \end{bmatrix}.$$

According to [68], if $F(z)$ in (4.50) is stable and causal then the condition

$$\sup_{\theta\in[-\pi,\pi]} \left|F(e^{j\theta})\right| = \sup_{\theta\in[-\pi,\pi]} \left|Q(e^{j\theta})\left[1 - e^{j\theta}\beta L(e^{j\theta}) P(e^{j\theta})\right]\right| < 1 \tag{4.51}$$

where $\theta = \omega k T$, implies that the matrix norm of $\mathbf{F}$

$$\|\mathbf{F}\| < 1.$$

Remark 21 *Condition (4.51) is more conservative than (4.20) as it implies that the norm* $\|\mathbf{e}_i\|$ *is monotonically decreasing and, thus, guarantees monotonic convergence.*

Remark 22 *Note that in many cases the plant* $P(z)$ *may not be stable, however, a stable* $P(z)$ *is needed as a prerequisite to satisfying condition (4.51). This can be achieved using current-cycle iterative learning control.*

4.4.1 Current-Cycle Iterative Learning

It was seen in the previous sections that along with condition (4.51) the plant $P(z)$ must be stable in order to guarantee monotonic convergence of the ILC system. This can be achieved by including an inner closed-loop feedback to stabalize the plant.

Consider once more the sampled-data system (4.2)

$$\begin{aligned} \mathbf{x}_i(k+1) &= \Phi \mathbf{x}_i(k) + \Gamma u_i(k) \\ y_i(k) &= C\mathbf{x}_i(k) \end{aligned}$$

where it will be assumed that Φ has one or more unstable eigenvalues (or poles). The closed-loop control approach can be based on state feedback or output feedback depending on the availability of measured states. The state feedback approach is rather straight forward and will not be covered in details. Consider the closed-loop state feedback combined ILC law

$$u_i(k) = -K\mathbf{x}_i(k) + v_i(k) \tag{4.52}$$

where v_i can be any of the ILC laws that were discussed up to this point. Note that the

substitution of (4.52) in (4.2) results in

$$\mathbf{x}_i(k+1) \;=\; (\Phi - \Gamma K)\mathbf{x}_i(k) + \Gamma v_i(k). \tag{4.53}$$

Clearly the state feedback gain K can be desigend such that the system has stable eigenvlaues. From here on, all the results shown earlier apply.

Now consider if only the output measurement is available. In this case we will use an output feedback controller and the closed-loop output feedback combined ILC law is

$$u_i(k) \;=\; G(\mathrm{q})e_i(k) + v_i(k) \tag{4.54}$$

where $G(\mathrm{q})$ represents the controller function. For this analysis we will consider a general ILC. Thus, v_i is

$$v_i(k) \;=\; Q(\mathrm{q})\left[v_{i-1}(k) + \beta L(\mathrm{q})e_{i-1}(k+1)\right]. \tag{4.55}$$

The z-transformations of (4.54) and (4.55) are, [67],

$$U_i(z) \;=\; G(z)E_i(z) + V_i(z) \tag{4.56}$$

and

$$V_i(z) \;=\; Q(z)\left[V_{i-1}(z) + \beta z L(z)E_{i-1}(z)\right]. \tag{4.57}$$

The input-output relationship of the plant in z domain is given by

$$Y_i(z) \;=\; \underbrace{C(Iz - \Phi)^{-1}\Gamma}_{P(z)} U_i(z). \tag{4.58}$$

Note that the tracking error is $e_i(k) = y_r(k) - y_i(k)$. Thus,

$$E_i(z) \;=\; Y_r(z) - Y_i(z) \;=\; Y_r(z) - P(z)U_i(z). \tag{4.59}$$

Substitution of (4.56) in (4.59) and simplifying the result we get

$$E_i(z) \;=\; \frac{1}{1+G(z)P(z)}Y_r(z) - \frac{P(z)}{1+G(z)P(z)}V_i(z) \tag{4.60}$$

which can be rewritten as

$$-\frac{P(z)}{1+G(z)P(z)}V_i(z) \;=\; E_i(z) - \frac{1}{1+G(z)P(z)}Y_r(z). \tag{4.61}$$

If both sides of (4.57) are multiplied by $-\frac{P(z)}{1+G(z)P(z)}$ we get

$$-\frac{P(z)}{1+G(z)P(z)}V_i(z) \;=\; -\frac{Q(z)P(z)}{1+G(z)P(z)}V_{i-1}(z) - \beta\frac{zQ(z)L(z)P(z)}{1+G(z)P(z)}E_{i-1}(z). \tag{4.62}$$

Substituting (4.61) and simplifying we get

$$E_i(z) \;=\; Q(z)\left(1-\beta\frac{zL(z)P(z)}{1+G(z)P(z)}\right)E_{i-1}(z) + \frac{1-Q(z)}{1+G(z)P(z)}Y_r(z). \tag{4.63}$$

Define $P'(z)$ as the closed-loop transfer function

$$P'(z) \;=\; \frac{P(z)}{1+G(z)P(z)}, \tag{4.64}$$

(4.63) becomes

$$E_i(z) \;=\; Q(z)\left(1-z\beta L(z)P'(z)\right)E_{i-1}(z) + \frac{1-Q(z)}{1+G(z)P(z)}Y_r(z). \tag{4.65}$$

From (4.65) we see that monotonic convergence requires that $P'(z)$ be stable and the condition

$$\sup_{\theta\in-\pi,\pi}\left|Q(e^{j\theta})\left(1-e^{j\theta}\beta L(e^{j\theta})P'(e^{j\theta})\right)\right| < 1 \tag{4.66}$$

be satisfied. The poles of the transfer function $P'(z)$ can be properly selected by designing $G(z)$ while condition (4.66) can be satisified by the proper designs of $Q(z)$, $L(z)$ and β.

However, note that the tracking error $E(z)$ is effected by $Y_r(z)$ through $\frac{1-Q(z)}{1+G(z)P(z)}$. Thus, the designs of $G(z)$ and $Q(z)$ must also take into account that

$$\sup_{\theta\in-\pi,\pi}\left|\frac{1-Q(e^{j\theta})}{1+G(e^{j\theta})P(e^{j\theta})}\right| \ll 1. \tag{4.67}$$

4.4.2 Considerations for L(q) and Q(q) Selection

In this section we will discuss selection criteria for L(q) and Q(q) to achieve the desired monotone convergence of the ILC system.

Consider the ILC system given by (4.65). Without loss of generality we will assume that the $P(z)$ is stable and $G(z) \equiv 0$. Thus, without a feedback loop (4.65) becomes

$$E_i(z) \;=\; Q(z)\left[1-\beta z L(z)P(z)\right]E_{i-1}(z) + \left[1-Q(z)\right]Y_r(z). \tag{4.68}$$

If it is assumed that $Q(z) = 1$ then, ideally, selecting $L(z) = \frac{1}{z\beta P(z)}$ would lead to the fastest possible convergence in the monotone sense. This, however, is impractical as it is not possible to identify $P(z)$ exactly for real systems. Consider the term $[1-\beta z L(z)P(z)]$. The monotonic convergence requires that $[1-\beta z L(z)P(z)]$ be within a unit circle centered at the origin of the complex plane. This can be restated as a requirement that $\beta z L(z)P(z)$ be within a unit circle centered at $(1,0)$ on the complex plane as shown in Fig.4.2. From this condition we observe that stability requires that

$$\begin{aligned}&\angle(e^{j\theta}L(e^{j\theta})P(e^{j\theta})) = \varphi \in (-\pi/2,\pi/2),\;\; \forall\theta\in[-\pi,\pi]\\ &\sup_{\theta\in[-\pi,\pi]}|\beta e^{j\theta(\varphi)}L(e^{j\theta(\varphi)})P(e^{j\theta(\varphi)})| < 2\cos(\varphi).\end{aligned} \tag{4.69}$$

An important fact to note is that $zL(z)$ should ensure that as $|\angle(e^{j\theta}L(e^{j\theta})P(e^{j\theta}))| \to \pi/2$ then $|\beta e^{j\theta}L(e^{j\theta})P(e^{j\theta})| \to 0$.

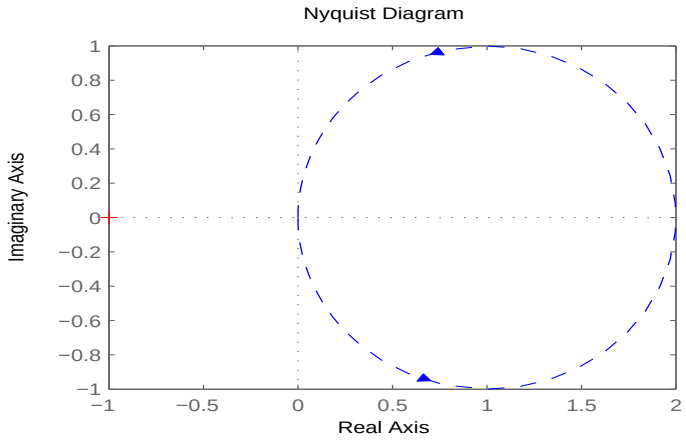

Figure 4.2: Monotonic convergence region for $\beta z L(z)P(z)$

On the other hand, the selection of $Q(z)$ must take into consideration that the term $[1-Q(z)]$ be minimized and be as close as possible to zero at steady-state thereby preventing any steady state errors. Thus, $Q(z)$ is generally selected as a low pass filter. An advantage of using $Q(z)$ is that the stability region for certain frequencies can be increased if $Q(z)$ is a filter with a gain that is less than one. This can be seen from the condition shown below, [69],

$$\left|1-\beta e^{j\theta}L(e^{j\theta})P(e^{j\theta})\right| \;<\; \frac{1}{|Q(e^{j\theta})|}, \quad \theta\in[-\pi,\pi]. \tag{4.70}$$

Later on, some examples will be presented to highlight the above points.

4.4.3 D-Type and D^2-type ILC

Consider the ILC

$$u_{i+1}(k) \;=\; Q(\mathrm{q})\left[u_i(k)+\beta \mathrm{q} L(\mathrm{q})e_i(k)\right] \tag{4.71}$$

substituting $L(\mathrm{q})=1-\mathrm{q}^{-1}$ and performing the z-transform of (4.71) after subtracting both sides from u_r we obtain

$$\Delta U_{i+1}(z) \;=\; Q(z)\left[\Delta U_i(z)-(z-1)\beta E_i(z)\right]+\left[1-Q(z)\right]U_r(z). \tag{4.72}$$

Substitution of (4.48) into (4.72) leads to

$$\Delta U_{i+1}(z) \;=\; Q(z)\left[1-(z-1)\beta P(z)\right]\Delta U_i(z)+\left[1-Q(z)\right]U_r(z). \tag{4.73}$$

According to the results with the P-type ILC, monotonic convergence is guaranteed if

$$\sup_{\theta\in[-\pi,\pi]}\left|Q(e^{j\theta})\left[1-\beta(e^{j\theta}-1)P(e^{j\theta})\right]\right|<1. \tag{4.74}$$

Similarly for $L(\mathrm{q})=1-2\mathrm{q}^{-1}+\mathrm{q}^{-2}$, the stability condition would be

$$\sup_{\theta\in[-\pi,\pi]}\left|Q(e^{j\theta})\left[1-\beta(e^{j\theta}-2+e^{-j\theta})P(e^{j\theta})\right]\right|<1. \tag{4.75}$$

In Fig.4.3 the magnitude and phase diagrams of $zL(z)$ are plotted w.r.t to the frequency normalized by the sampling frequency $w_s=\frac{2\pi}{T}$. The phase diagram indicates that at low frequency the phase response is 90 degrees which would violate the stability condition (4.69) if $P(z)$ has a phase greater than or equal to 0 degrees at low frequencies. This learning function would work well if it is applied to a second order system with a single integrator or a third order system with a single integrator and a cut-off frequency near $\frac{w_s}{2}$. Similarly for the D^2-type, the learning function would work ideally for a double integrator system or a third order system with a double integrator and cutoff frequency near $\frac{w_s}{2}$.

4.5 Numerical Example: Time Domain

4.5.1 P-type ILC

Consider the second order system

$$\begin{aligned}\dot{\mathbf{x}}_i(t) &= A\mathbf{x}_i(t)+Bu_i(t)\\ y_i(t) &= C\mathbf{x}_i(t)\end{aligned} \tag{4.76}$$

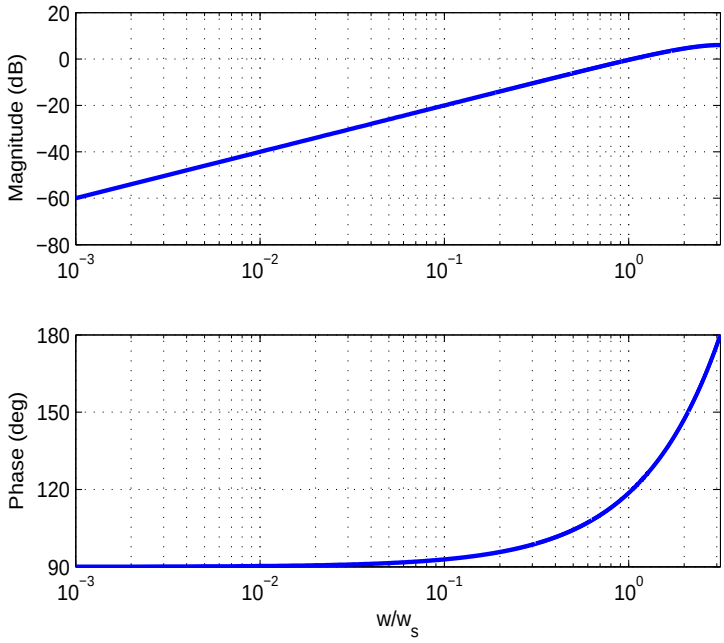

Figure 4.3: Magnitude and Phase of z$L(z)$ for $L(z) = 1 - z^{-1}$

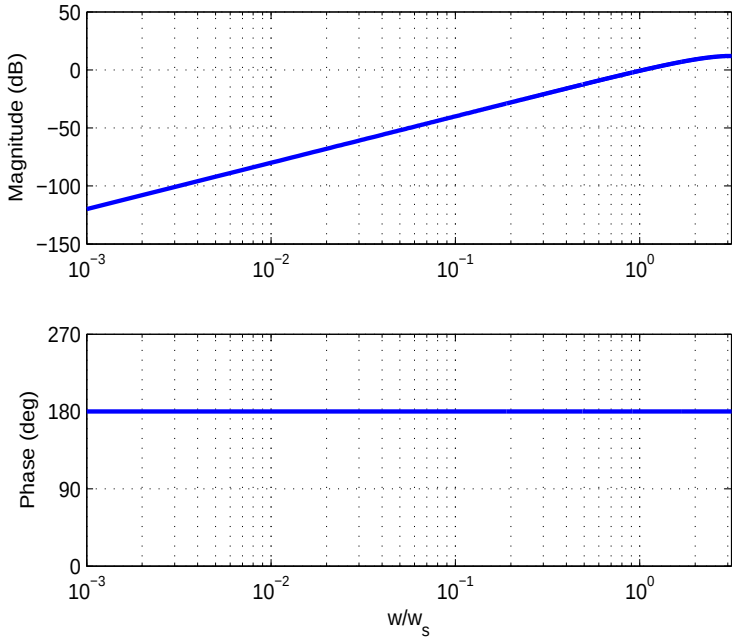

Figure 4.4: Magnitude and Phase of $zL(z)$ for $L(z) = 1 - 2z^{-1} + z^{-2}$

where the system matrices are given by

$$A = \begin{bmatrix} 0 & 1 \\ 0 & -144 \end{bmatrix}, \quad B = \begin{bmatrix} 0 \\ 6 \end{bmatrix}$$

$$C = \begin{bmatrix} 1 & 0 \end{bmatrix}.$$

This is the nominal model of a piezo-motor stage that will be used in the experimental application of the ILC laws. The sampled-data system representation of (4.76) is given by

$$\begin{aligned} \mathbf{x}_i(k+1) &= \Phi \mathbf{x}_i(t) + \Gamma u_i(k) \\ y_i(k) &= C\mathbf{x}_i(k) \end{aligned} \tag{4.77}$$

where the system matrices are given by

$$\Phi = e^{AT}, \quad \Gamma = \int_0^T e^{A\tau} d\tau B \tag{4.78}$$

and T is the sampling period. If the sampling time is set to $1ms$, (4.78) becomes

$$\Phi = \begin{bmatrix} 1 & 9.313 \times 10^{-4} \\ 0 & 0.8659 \end{bmatrix}, \quad \Gamma = \begin{bmatrix} 2.861 \times 10^{-6} \\ 0.0056 \end{bmatrix}.$$

If the following ILC is used

$$\begin{aligned} u_{i+1}(k) &= u_i(k) + \beta e_i(k+1) \\ e_i(k) &= y_r(k) - y_i(k) \end{aligned} \tag{4.79}$$

where the desired output trajectory is selected as $y_r(k) = 0.030 + 0.030\sin(2\pi kT - \frac{\pi}{2})$ and each iteration is $0.5s$ in duration. The learning gain, β, is selected as 2×10^5 such that $1 - \beta C\Gamma = 0.4278$. The maximum error for each iteration is plotted in Fig.A.10.

4.5.2 D-Type and D^2-type ILC

Now consider the D-type ILC

$$u_{i+1}(k) = u_i(k) + \beta(e_i(k+1) - e_i(k)) \tag{4.80}$$

where the learning gain, β, is selected as 2×10^5 similar to the P-type ILC case. This is because the eigenvalues of the system in the iteration domain are the same for both cases. Thus, $1 - \beta C\Gamma = 0.4278$ for this example. The maximum error for each iteration is plotted in Fig.4.7. In Fig.4.8 the time-domain repsonse is plotted. Note that the performance with the D-type ILC is similar to the P-type ILC. However, in the frequency domain analysis it will be shown that it is possible to select proper learning gain to achieve monotonic $\|\mathbf{e}_i\|$. It will also be shown that this is not possible for the P-type ILC.

Finally consider the D^2-type ILC

$$u_{i+1}(k) \;=\; u_i(k) + \beta(e_i(k+1) - 2e_i(k) + e_i(k-1)) \tag{4.81}$$

where the learning gain, β, is selected as 2×10^5 similar to the P-type and D-type ILC cases. The maximum error for each iteration is plotted in Fig.4.10. Note that the performance with the D^2-type ILC is much better than the previous cases. Monotone convergence is achieved in this case as opposed to the P-type and D-type with the same learning gain. This is because in condition (4.36) the term $(\Phi - I)^2$ is rather small and, thus, the condition can be met easily.

4.6 Numerical Example: Frequency Domain

4.6.1 P-type ILC

In order to have more insight into the example considered in the Time domain analysis, again consider the system (4.77), the input-output relationship is given by

$$Y(z) \;=\; P(z)U(z). \tag{4.82}$$

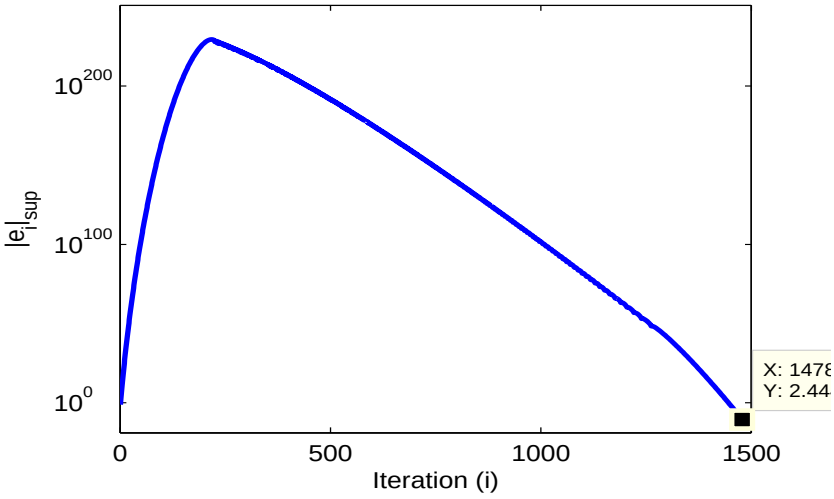

Figure 4.5: Tracking error profile of the system using P-type ILC

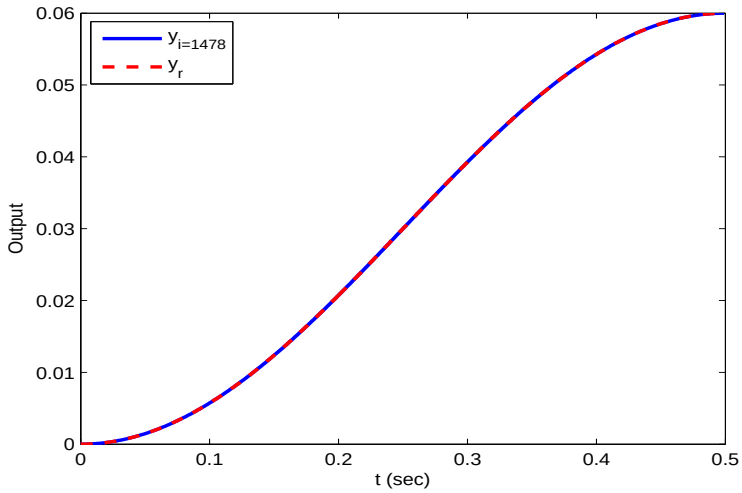

Figure 4.6: Desired and actual ouput of the system using P-type ILC

Using the same parameters as in the time-domain example, the transfer function of the system, $P(z)$, is

$$P(z) \;=\; C(Iz-\Phi)^{-1}\Gamma \;=\; \frac{2.861\times10^{-6}z+2.727\times10^{-6}}{z^2-1.866z+0.866}. \tag{4.83}$$

The filter $Q(z)$ and learning function $L(z)$ are set to unity. Thus, the Nyquist diagram of $F(z)$ is constructed in Fig.4.10. From the figure we see that $|F(e^{j\theta})|$ does not lie inside the

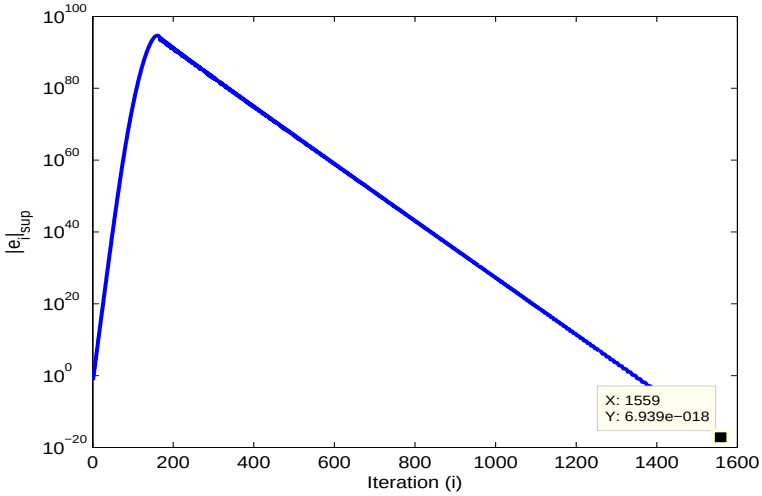

Figure 4.7: Tracking error profile of the system using D-type ILC

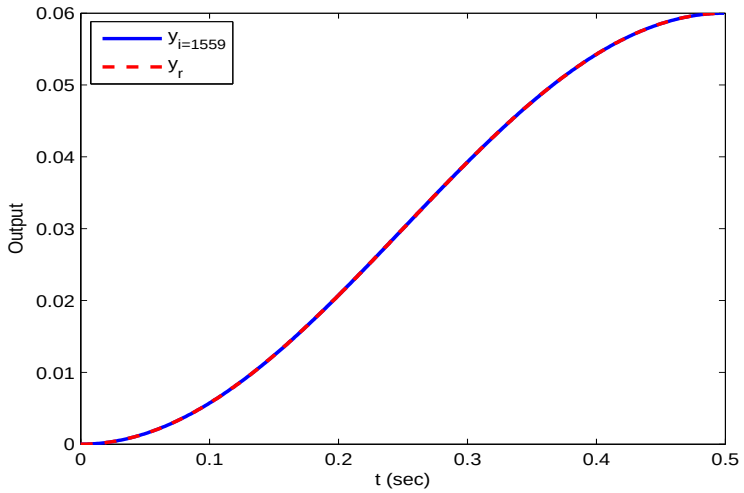

Figure 4.8: Desired and actual ouput of the system using D-type ILC

unit circle for any frequencies and as $\theta \to 0$ then $|F(e^{j\theta})| \to \infty$. Thus, condition (4.51) is not satisfied and monotonically decreasing $\|\mathbf{e}_i\|$ is not guaranteed.

4.6.2 D-type and D^2-type ILC

Consider now if the Nyquist diagram of $Q(z)\left[1 - \beta z L(z) P(z)\right]$ is constructed using the same parameters as the P-type ILC example while using $L(z) = 1 - z^{-1}$. From Fig.4.11 we see that

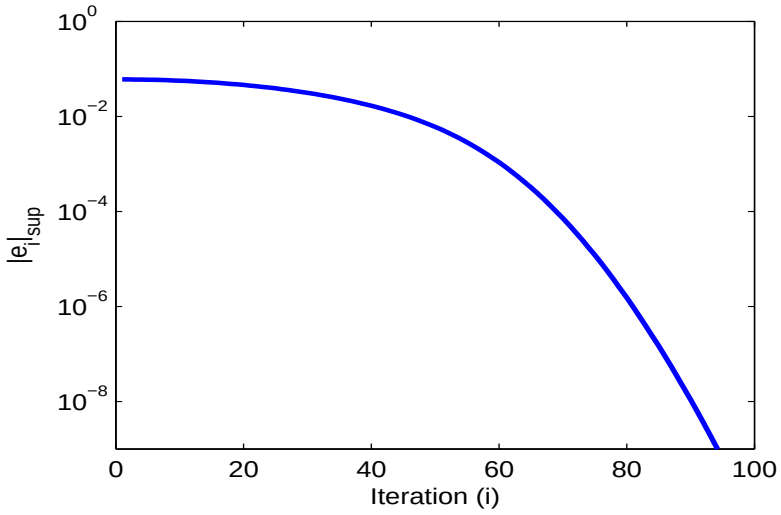

Figure 4.9: Tracking error profile of the system using D^2-type ILC

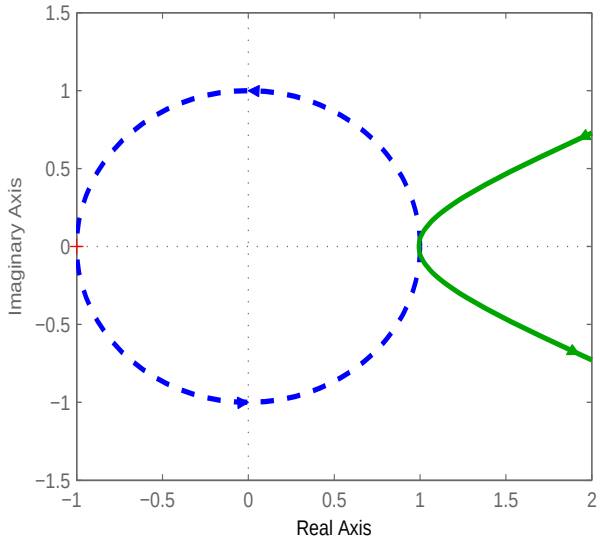

Figure 4.10: Nyquist plot of F(z) for P-type ILC

the Nyquist diagram of $Q(e^{j\theta})\left[1-\beta(e^{j\theta}-1)P(e^{j\theta})\right]$ lies outside the unit disk but there is a possibility of selecting learning gains β that would allow it to stay inside the unit circle. For example choosing the value of β at around 4.75×10^4 or below will lead to a Nyquist plot inside the unit circle as shown in Fig.4.12. Now, if we go back to the time-domain analysis and use $\beta = 4.75\times10^4$ then the repeated eigenvlaue of (4.30) is $1-\beta C\Gamma = 0.8641 < 1$.

The maximum tracking error for each iteration is plotted in Fig.4.13 which shoes a monotonic convergence of the error in the iteration domain.

If instead the D^2-type or $L(z) = 1 - 2z^{-1} + z^{-2}$ is used with the same initial learning gain for the D-type, we see that from Fig.4.14 the Nyquist plot of $Q(z)\left[1 - \beta z L(z)P(z)\right]$ is within the unit disk but takes a value close to 1 at very low frequencies. This is because $(z-1)^2 \to 0$ as $\omega \to 0$. If the plant was a double integrator type then this problem would not exist.

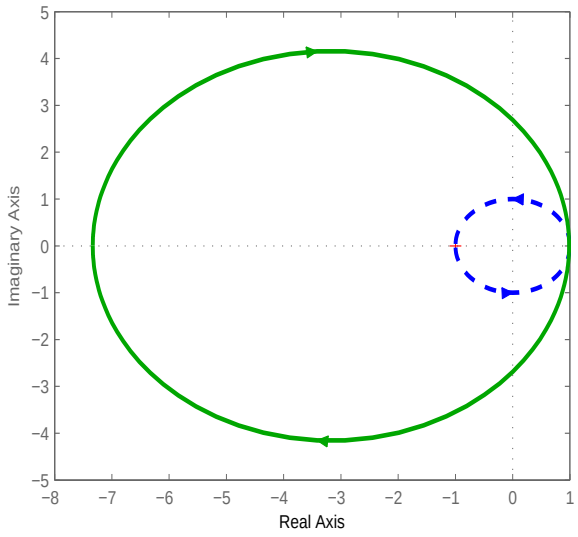

Figure 4.11: Nyquist plot for D-type ILC example with $\beta = 2 \times 10^5$

4.6.3 Current-Cycle Iterative Learning Control

We had seen in the previous P-type ILC example that monotonic converegence was not possible due to the presence of an integrator in $P(z)$ which would lead to $|zP(z)| \to \infty$ as $\omega \to 0$. Thus, we will try to eliminate the undesired pole by employing closed-loop feedback. As a start, we will check the possibility of achieving a stable closed-loop with simple proportional

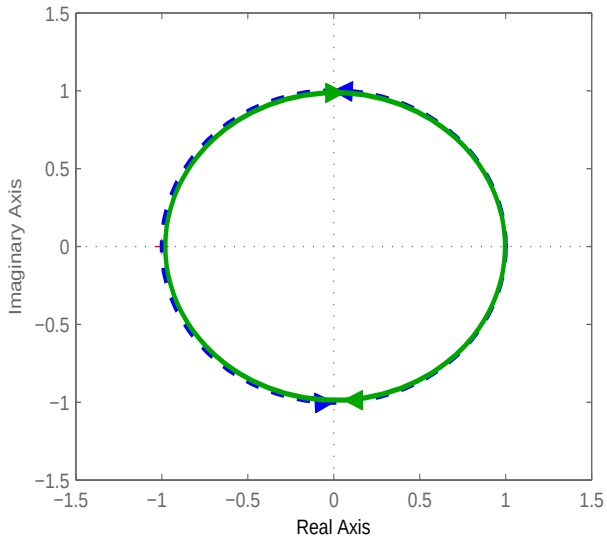

Figure 4.12: Nyquist plot for D-type ILC example with $\beta = 4.75 \times 10^4$

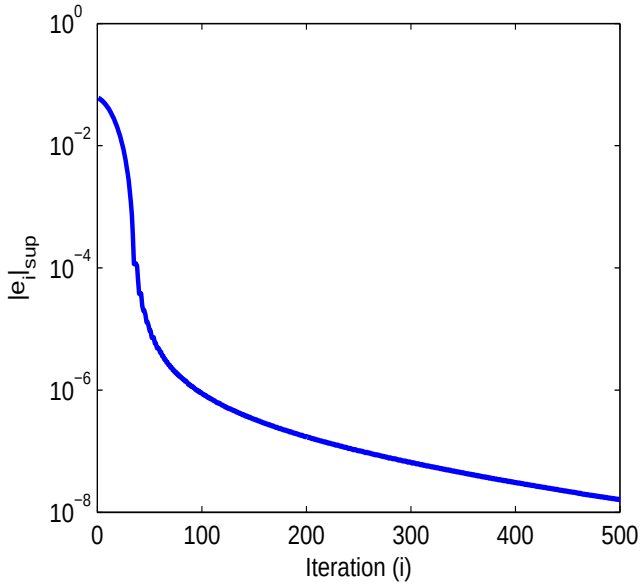

Figure 4.13: Tracking error profile of the system using D-type ILC and $\beta = 4.75 \times 10^4$

feedback. Thus, $G(z)$ is simply

$$G(z) \;=\; K_p$$

where K_p is the proportional gain. For this we plot the root locus of $P(z)$ shown by Fig.4.15 and Fig.4.16. We select the proportional gain as, $K_p = 834$ (no overshoot and damping ratio

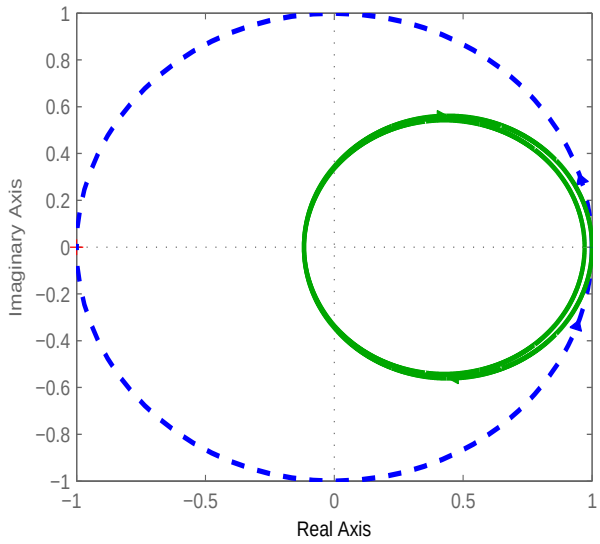

Figure 4.14: Nyquist plot for D^2-type ILC example with $\beta = 2 \times 10^5$

equal to 1), and proceed to plot the Nyquist diagram of $|1 - \beta z P'(z)|$ shown by Fig.4.17. We see that the Nyquist plot is so close to the edge of the unit-circle and escapes it for frequencies larger than 77 rad/s. Thus, we decide to include filtering as well in the ILC and select the learning function $L(z) = 1$ while the filter $Q(z)$ is

$$Q(z) = \frac{0.4337z^2 + 0.8675z + 0.4337}{z^2 + 0.5159z + 0.219}$$

which is a 2^{nd}-order Butterworth with a cut-off frequency of 200 rad/s. The reason for this selection is to have as simple as possible filter design while at the same time achieving a minimum $[1 - Q(z)]$ for as wide as possible range of frequencies. Now we plot the Nyquist diagram for $Q(z)[1 - \beta z L(z) P'(z)]$ shown in Fig.4.18. We see now that the Nyquist diagram is within the unit-circle for all frequencies. The maximum tracking error for the system at every iteration is shown in Fig.4.19. From Fig.4.19 it can be seen that monotonic convergence of the tracking error is achieved. The time responses are shown in Fig.4.20 for the system

at $i = 0$ and $i = 500$ respectively. The ILC achieves better performance than with simple proportional control.

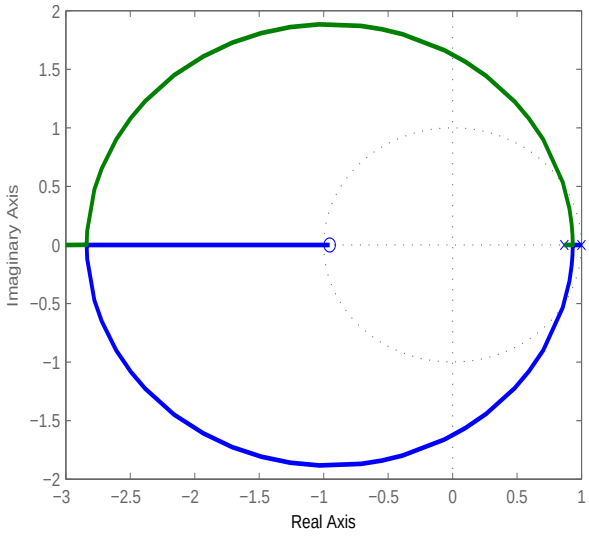

Figure 4.15: Root locus plot for $P(z)$

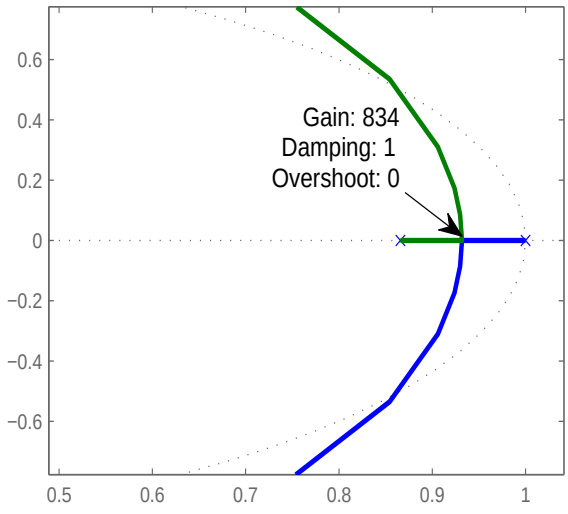

Figure 4.16: Root locus plot for $P(z)$(close-up)

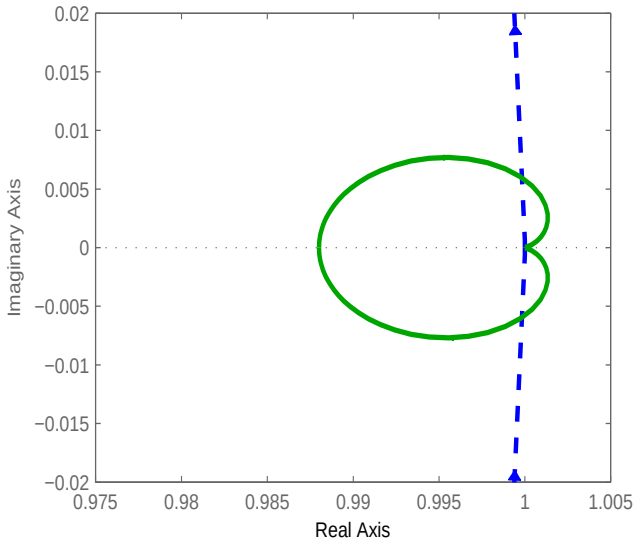

Figure 4.17: Nyquist plot for P-type ILC with closed-loop P-control

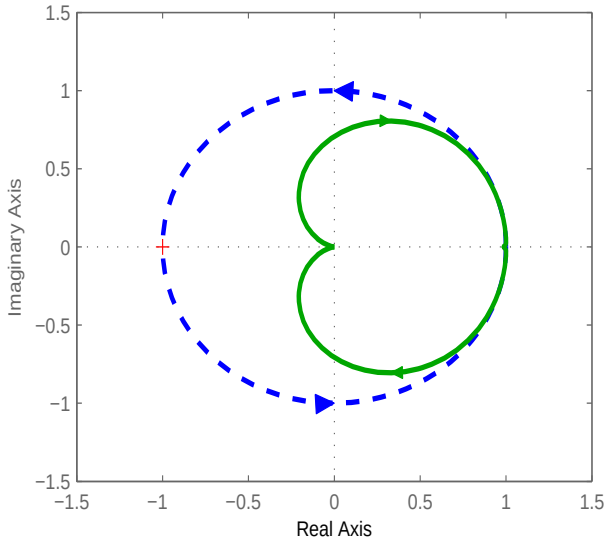

Figure 4.18: Nyquist plot for P-type ILC with closed-loop P-control and Filtering

4.6.4 $L(\mathbf{q})$ Selection

In the previous cases the learning function, $L(\mathrm{q})$, was either selected as unity or the special case of D-type and D^2-type. In this example we will select the learning function, $L(\mathrm{q})$, in order to obtain the best possible performance of the ILC system. Consider the system (4.83)

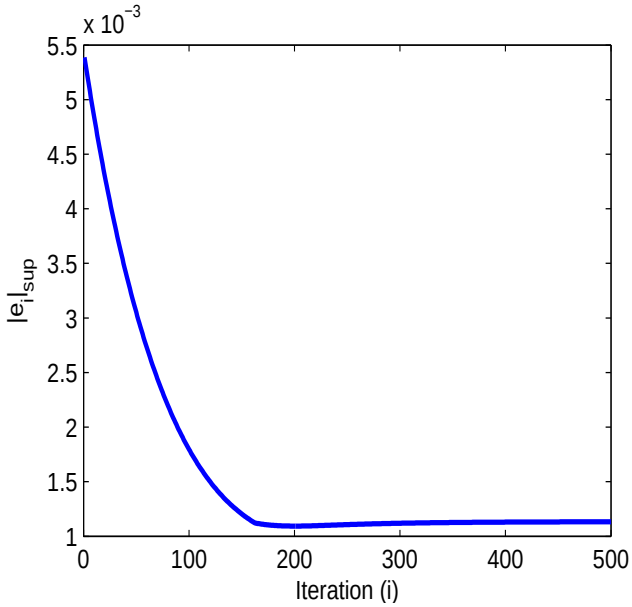

Figure 4.19: Tracking error profile of the system using P-type ILC with closed-loop P-control and filtering

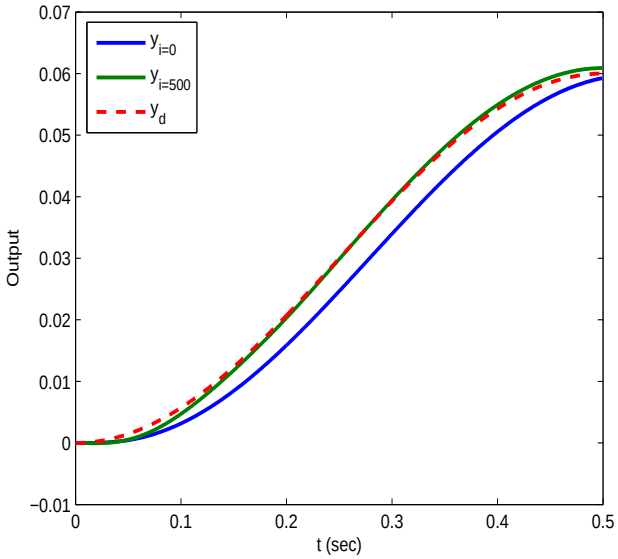

Figure 4.20: Desired and actual ouput of the system using P-type ILC with closed-loop P-control and filtering

which is stable and has the magnitude and phase diagrams shown in Fig.4.21. We see that the phase varies from 0 degrees to -270 degrees. We also note that roughly at 0.1 rad/s the phase

changes to -90 degrees and at 200 rad/s it changes from -90 degrees to -270 degrees. So in order to keep the overall phase between 90 degrees and -90 degrees, we select our learning function as a combination of two lead compensators as follows

$$L(z) \;=\; \left(\frac{5001z + 5000}{z}\right)\left(\frac{14.17z - 12.5}{z + 0.6667}\right). \tag{4.84}$$

The inverse of $L(z)$ has very similar phase characteristics as that of the system $P(z)$ as seen from Fig.4.22. Plotting $zL(z)P(z)$ in Fig.4.23 we see that the combination $zL(z)P(z)$ has a phase within the stability range and magnitude also in the stability range. If we plot the Nyquist plot in Fig.4.24 for $[1 - zL(z)P(z)]$ we see that it is well within the unit disk and, thus, the condition for monotone convergence is satisfied. Fig.4.25 shows the maximum error at each iteration.

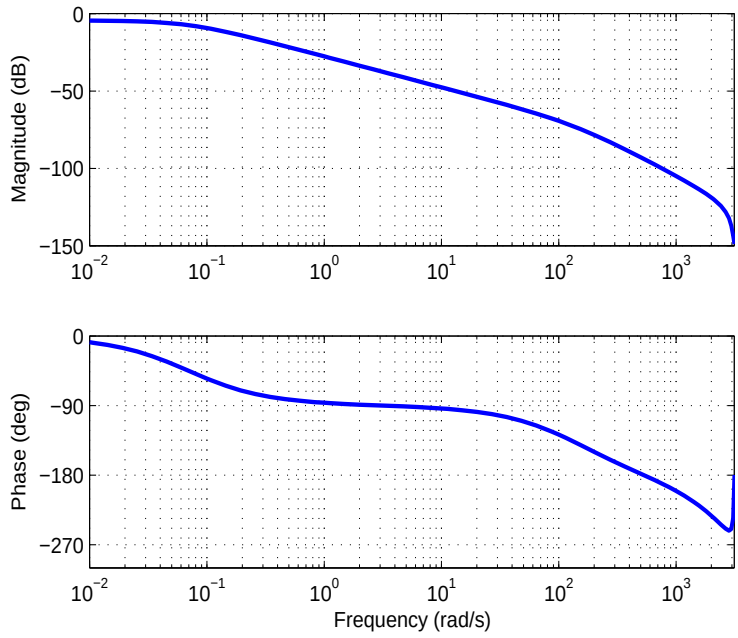

Figure 4.21: Bode plot of $P(z)$ in (4.83)

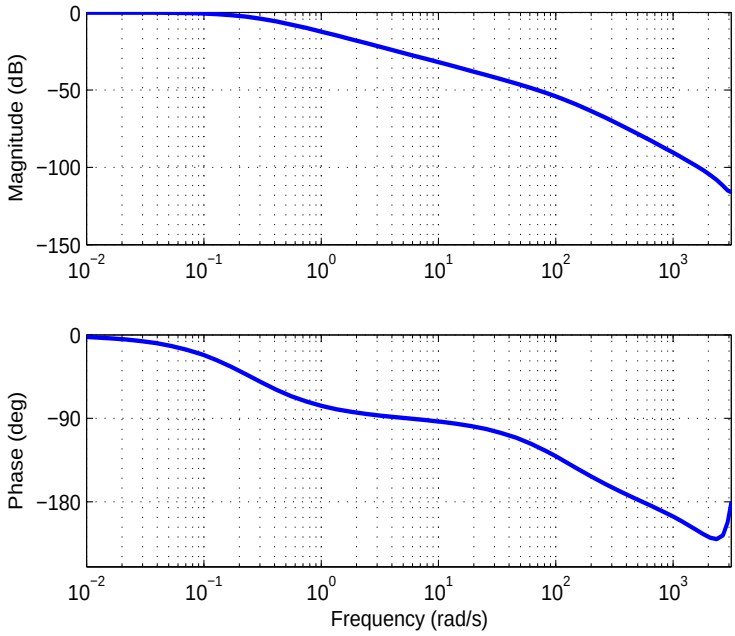

Figure 4.22: Bode plot of $L^{-1}(z)$

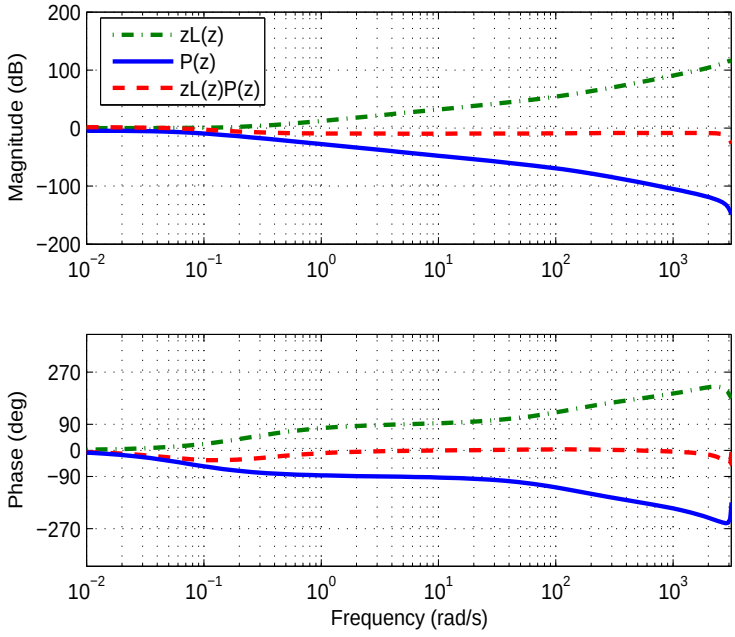

Figure 4.23: Bode plot of $zL(z)P(z)$

4.6.5 Sampling Time selection

Consider the system $P(z)$ defined by (4.83) at sampling time $T = 1$ms. From Fig.4.21 we see that the phase response crosses -90^o degrees at nearly 2π rad/s. If we also look at the

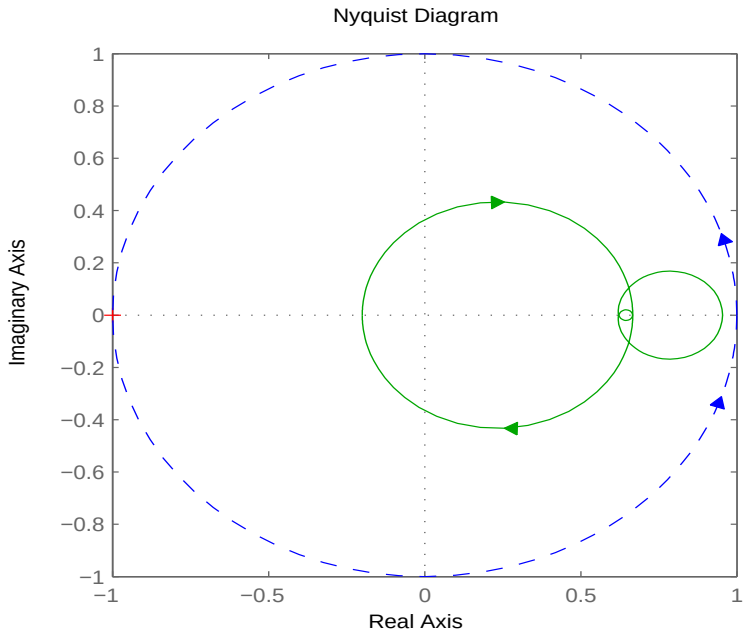

Figure 4.24: Nyquist plot of $1 - zL(z)P(z)$

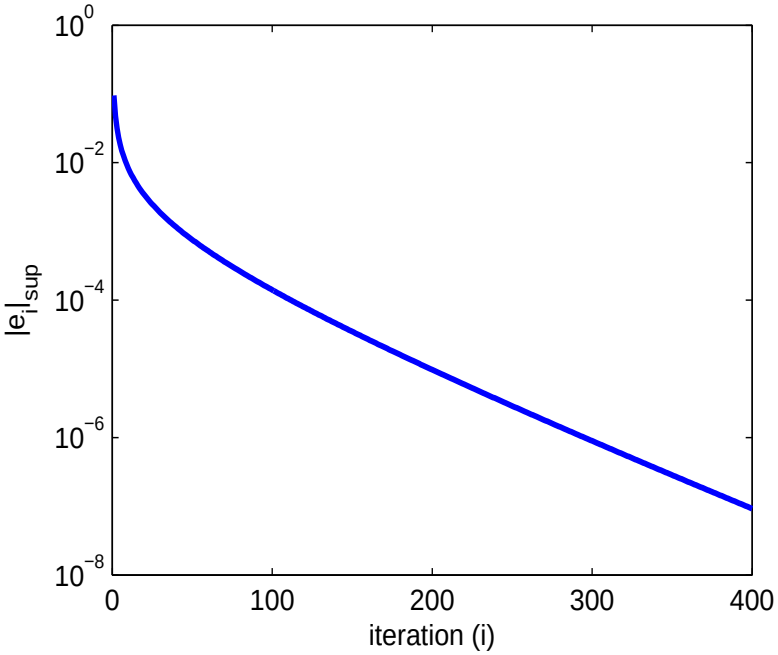

Figure 4.25: Tracking error profile of the system using P-type ILC with closed-loop P-control and filtering

phase diagram of z we see that it is linearly increasing from 0^o to 180^o degrees as a function of frequency. From here it seems obvious that if we select a larger sampling time such that the phase response of $P(z)$ slightly crosses the $(-90^o, 90^o)$ stability bound, then combined with z the overall phase response, φ, would be within $(-90^o, 90^o)$. Thus, we select sampling time $T = 10$ ms and draw the maginitude and phase of $zP(z)$ in Fig.4.27. We see from Fig.4.27 that the overall phase response of $zP(z)$ still crosses the stability bound $(-90^o, 90^o)$, hence, we will increase the sampling time to $T = 15$ms and redraw the maginitude and phase of $zP(z)$ in Fig.4.28. We see from Fig.4.28 that with the new sampling time, the phase response of $zP(z)$ is now within the stability bound $(-90^o, 90^o)$ and since for all the cases the magnitude of $zP(z)$ was within the stability bound, the system can now achieve monotone convergence of the tracking error. To conclude we can tabulate all the results in the form of a guideline

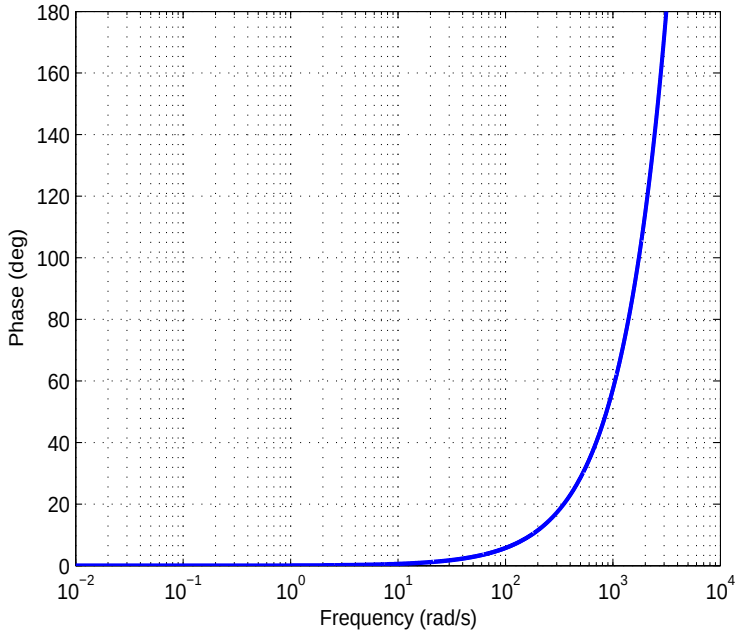

Figure 4.26: Phase diagram of z

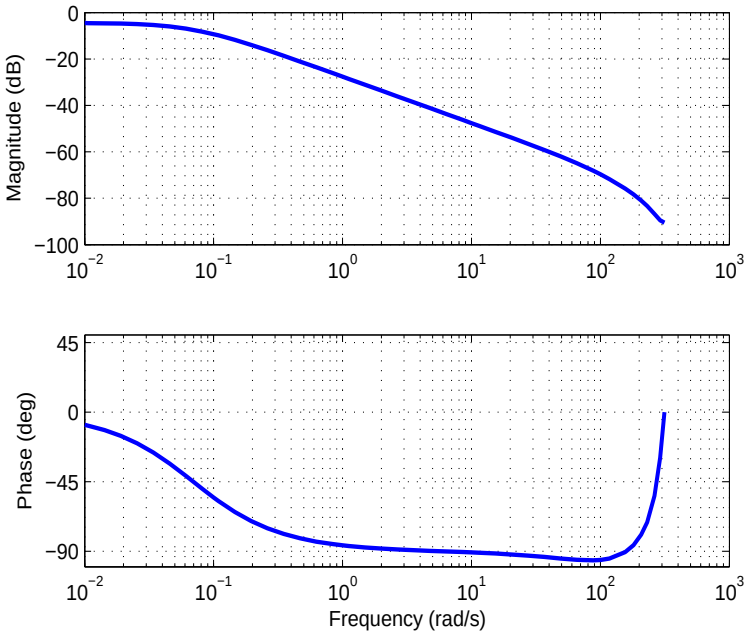

Figure 4.27: Bode plot of $zP(z)$ at $T = 10$ms

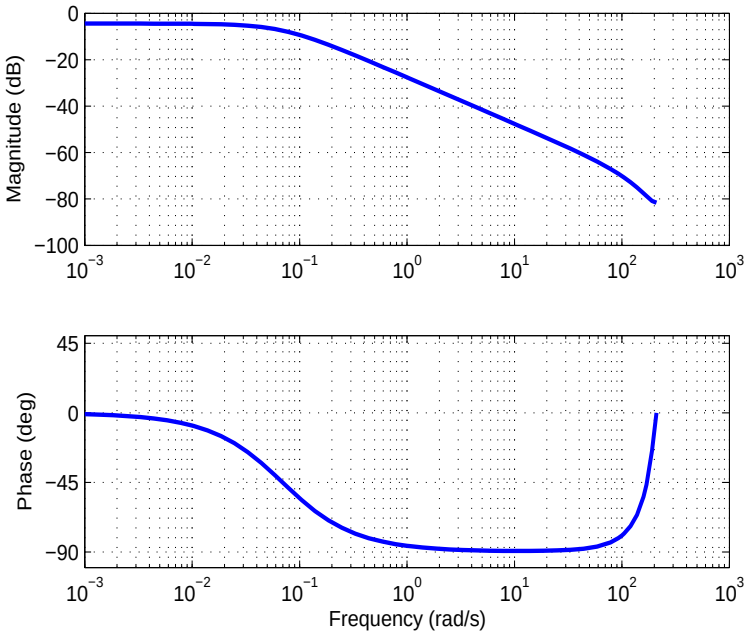

Figure 4.28: Bode plot of $zP(z)$ at $T = 15$ms

to help with the ILC design. This can be seen in Table 4.1.

Table 4.1: Guideline for ILC Design

Design Factor		Design Considerations
Sampling Time T		Selection of a larger sampling-time increases the chances of achieving monotone convergence, however, the trade-off would be that the system bandwidth does not cover the whole range of disturbances and uncertainties that may exist and, therefore, incur large tracking errors.
Q(z)		The filter $Q(z)$ increases the stability bound, however, it would create steady state errors and, therefore, should only be used if stability cannot be achieved by $L(z)$ alone. $Q(z)$ is typically selected as a low-pass filter.
$L(z)$	P-type	P-type is suitable if $P(z)$ has a phase within $(-90^o, 90^o)$ degrees.
	D-type	D-type is suitable if $P(z)$ is 2^{nd}-order with a single integrator.
	D^2-type	D^2-type is suitable for either a 2^{nd}-order or a 3^{rd}-order $P(z)$ with atmost two integrators.
	Filter	For cases where $P(z)$ is of high order or does not satisfy the above conditions then $L(z)$ can be designed as a combination of lead compensators depending on the order of $P(z)$.

4.7 Conclusion

this Chapter summarizes the theoretical results of ILC for sampled-data SISO systems in the time and frequency domain. Stability and convergence criterias are shown as well as design procedures with numerous examples. Finally, the discussed design procedure is applied to a real system with promising results.

Chapter 5

Controller Design for a Piezo-Motor Driven Linear Stage

5.1 Introduction

In this work, the discrete-time integral sliding control is applied to a linear piezo-motor driven stage which has many promising applications in industries. The piezo-motors are characterized by low speed and high torque, which are in contrast to the high speed and low torque properties of the conventional electromagnetic motors. Moreover, piezo-motors are compact, light, operates quietly, and robust to external magnetic or radioactive fields. Piezo-electric motors are mainly applied to high precision control problems as it can easily reach the precision scale of micro-meters or even nano-meters. This gives rise to extra difficulty in establishing an accurate mathematical model for piezo-motors: any tiny factors, nonlinear and unknown, will severely affect their characteristics and control performance.

It is well known that sliding mode control (SMC) is a very popular robust control method owing to its ease of design and robustness to "matched" disturbances, hence was widely

adopted in various industiral applications [15]–[20]. Computer implementation of control algorithms presents a great convenience and has, hence, caused the research in the area of discrete-time control to intensify. This also necessitated a rework in the sliding mode control strategy for sampled-data systems. Most of the discrete-time sliding mode approaches are based on full state information [20]–[27].

On the other hand, this work considers the output tracking of the piezo-motor driven stage. To accomplish the task of arbitrary output reference tracking in the presence of disturbances, an output feedback controller with a state observer and a disturbance observer are designed. The objective is to drive the output tracking error to a certain neighborhood of the origin. For this purpose discrete-time integral sliding surfaces are proposed for the controller and observers.

Delays in the state or disturbance estimation in sampled-data systems is an inevitable phenomenon and must be studied carefully. In [27] it was shown that in the case of delayed disturbance estimation a worst case accuracy of $O(T)$ can be guaranteed for deadbeat sliding mode control design and a worst case accuracy of $O(T^2)$ for integral sliding mode control. While deadbeat control is a desired phenomenon, it is undesirable in practical implementation due to the over large control action required. In [27] the integral sliding mode design avoided the deadbeat response by eliminating the poles at zero. In this Chapter, we extend the integral sliding mode design to output tracking.

The proposed discrete-time SMC can achieve the $O(T^2)$ boundary for output tracking error when the system is moving in a certain direction and a maximum of $O(T)$ tracking error

while a change in direction occurs.

In output feedback based sliding mode control [20]–[24], there are mainly two design approaches: design using only the output measurement [20, 22], and design based on observers to construct the missing states [16, 24]. The purely output based design imposed extra stability requirements that are not practical in most cases. Hence in this Chapter we adopt a discrete-time state observer.

5.2 Model of the Piezo-Motor Driven Linear Motion Stage

In this section we first discuss the continuous-time piezo-motor stage model, then the friction model. Next the discretized model and disturbance properties are presented.

5.2.1 Overall Model in Continuous-Time

A major objective of this Chapter is to design a controller based on the simplest possible model of the piezo-motor stage. Therefore, we consider the following second-order continuous-time model of the piezo-motor stage

$$\begin{aligned} \dot{x}_1(t) &= x_2(t) \\ \dot{x}_2(t) &= -\tfrac{k_{fv}}{m}x_2(t) + \tfrac{k_f}{m}u(t) - \tfrac{1}{m}(f(\mathbf{x},t) + g(t)) \\ y(t) &= x_1(t) \end{aligned} \tag{5.1}$$

where x_1 is the linear displacement which is measurable, x_2 is the linear velocity which is not available, u is the voltage input, $f(\mathbf{x},t)$ represents the friction, $g(t)$ represents the effect of process perturbations and is assumed smooth and bounded. The constants m, k_{fv}, and k_f are the nominal mass, damping, and force constants respectively. This model closely represents

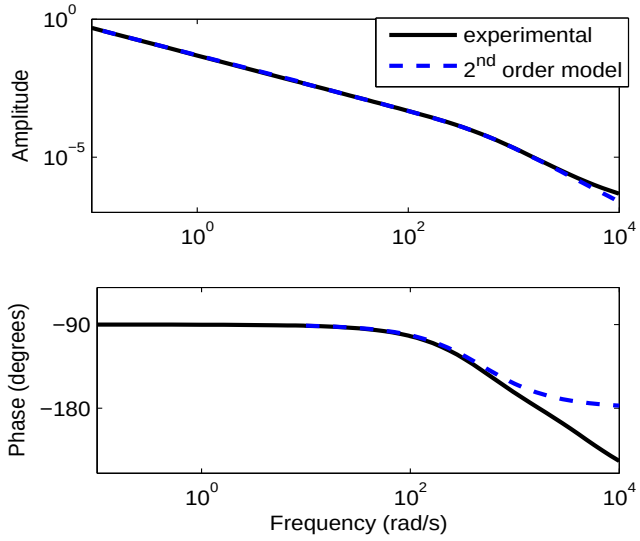

Figure 5.1: Frequency responses of the piezo-motor stage

the dynamics of the system as shown in Fig.5.1. As can be seen for a wide spectrum of frequencies the dyanimcs of the real system is indeed that of a second-order system.

5.2.2 Friction Models

Through experiments, it is found there exists a large friction in the piezo-motor stage, which is discontinuous when the velocity acrosses zero. In this Chapter, we treat the friction as an unknown disturbance and use a disturbance observer to estimate. In order to understand the behavior of the piezo-motor stage under friction $f(\mathbf{x}, t)$, hence facilitate the performance analysis on the controller and disturbance observer, we consider three widely accepted friction models, in the sequel determine the most appropriate model.

Static Friction Model

Here the friction is modelled as a bounded piece-wise continuous function and the discontinuity occurs only when x_2 changes sign. In details $f(\mathbf{x}, t)$ can be represented as follows, [30],

$$f(\mathbf{x}, t) = \begin{cases} k_f a_{max} & x_2(t) > 0 \\ k_f SAT[a(t)] & x_2(t) = 0 \\ k_f a_{min} & x_2(t) < 0 \end{cases} \tag{5.2}$$

where $SAT[a(t)]$ is a saturation function given by

$$SAT[a(t)] = \begin{cases} a_{max} & u(t) \geq a_{max} \\ a(t) & a_{min} < a(t) < a_{max} \\ a_{min} & a(t) \leq a_{min} \end{cases} \tag{5.3}$$

where a_{min} and a_{max} are unknown constant coefficients of the static friction.

Gaussian Friction Model

This model [31] considers three kinds of frictions – the static friction, viscous friction, and kinetic friction

$$f(x, t) = -\frac{1}{m}\left(\left(f_c + (f_s - f_c)e^{-(\frac{x_2}{v_s})^{\delta}}\right) sgn(x_2) + f_v x_2\right) \tag{5.4}$$

where f_c is the minimum level of kinetic friction, f_s is the level of static friction, f_v is the level of viscous friction, $v_s > 0$ and $\delta > 0$ are empirical parameters. The signum function from static friction represents a discontinuity crossing the zero velocity.

Lugre Friction

One motivation behind the LuGre model is to offer a regularised static friction model with stiction. The model captures several friction characteristics, such as increased friction force

at lower velocities, [30]. It is a first order dynamic model and the most commonly used form is

$$\begin{aligned} \dot{z} &= x_2 - \rho_0 \frac{|x_2|}{g(x_2)} z \\ g(x_2) &= \alpha_0 + \alpha_1 e^{-\left(\frac{x_2}{x_{2,s}}\right)^2} \\ f &= \rho_0 z + \rho_1 \dot{z} \end{aligned} \tag{5.5}$$

where α_0, α_1, $x_{2,s}$, ρ_0 and ρ_1 are positive parameters. Since the state z cannot be measured, it is necessary to use an observer to get an estimate of the friction based on this model.

The three models presented allow different degrees of accuracy. The first model is the simplest, the second model is more generic while the third model is dynamic. However, it is in general difficult to detemine the model parameters. A number of experimental tests were conducted and the results of three trials were shown in Fig.5.2. In the experiment, a

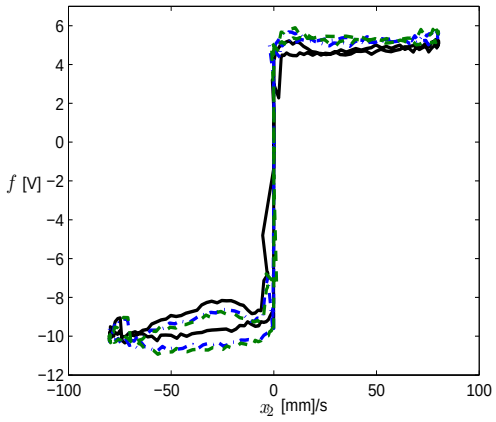

Figure 5.2: Experimentally obtained friction f w.r.t velocity x_2

slow sinusoidal input was injected into the to generate a low speed motion with very low acceleration. In this way the control input injected is solely to overcome the friction of the

piezo-motor stage. Thus the force-velocity relationship in Fig.5.2 can be obtained. It can be seen that none of the three friction models can perfectly capture the behaviors of the piezo-motor stage. Comparatively the static friction model can better fit the experimental results by choosing $k_f a_{max} = 5\text{v}$ and $k_f a_{min} = -10\text{v}$. Thus we can use the static friction model in the performance analysis.

The modeling mismatching can be considered as some unknown disturbance, due to the presence of many unknown factors such as unmodelled electrical dynamics, the hysterisis, measurement errors, system and sensor noise, as well as other random purterbations which cannot be modelled. We will introduce disturbance observer to estimate and compensate it ultimately. Moreover, by virtue of the robustness in sliding mode control, we may not need a perfect plant model.

5.2.3 Overall Model in Discrete-Time

The discretized counterpart of (5.1) can be given by

$$\begin{aligned} \mathbf{x}_{k+1} &= \Phi \mathbf{x}_k + \boldsymbol{\gamma} u_k + \mathbf{d}_k \\ y_k &= \mathbf{c}\mathbf{x}_k = x_{1,k}, \quad y_0 = y(0) \end{aligned} \tag{5.6}$$

where

$$\begin{aligned} \Phi(T) &= \begin{bmatrix} q_{11} & q_{12} \\ q_{21} & q_{22} \end{bmatrix} = exp\left(\begin{bmatrix} 0 & 1 \\ 0 & -\frac{k_{fv}}{m} \end{bmatrix} T \right), \\ \boldsymbol{\gamma} &= \begin{bmatrix} \gamma_1 \\ \gamma_2 \end{bmatrix} = \int_0^T \Phi(\tau) d\tau \begin{bmatrix} 0 \\ \frac{k_f}{m} \end{bmatrix}, \\ \mathbf{c} &= \begin{bmatrix} c_1 & c_2 \end{bmatrix} = \begin{bmatrix} 1 & 0 \end{bmatrix}. \end{aligned}$$

The equivalent disturbance term $\mathbf{d}_k = [d_1,\ d_2]^T$ can be calculated for the three scenarios given in (5.2)

$$\mathbf{d}_k = \mathbf{h}_k - \begin{cases} \boldsymbol{\gamma} a_{max} & x_{2,k} > 0 \\ \boldsymbol{\gamma} SAT[a(t)] & x_{2,k} = 0 \\ \boldsymbol{\gamma} a_{min} & x_{2,k} < 0 \end{cases} \tag{5.7}$$

where $\mathbf{h}_k$ is given by

$$\mathbf{h}_k = -\int_0^T \Phi(\tau) \begin{bmatrix} 0 \\ \frac{k_f}{m} \end{bmatrix} g((k+1)T - \tau) d\tau,$$

and T is the sampling period. Here the disturbance $\mathbf{h}_k$ represents the influence accumulated from kT to $(k+1)T$.

The following useful properties apply for the disturbance $\mathbf{d}_k$ when the motor speed is not zero [27]

Property 1.

$$\mathbf{d}_k = \boldsymbol{\gamma}(g_k + a_m) + \frac{1}{2}\boldsymbol{\gamma} v_k T + O(T^3).$$
$$\mathbf{d}_k = O(T).$$
$$\mathbf{d}_k - \mathbf{d}_{k-1} = O(T^2).$$
$$\mathbf{d}_k - 2\mathbf{d}_{k-1} + \mathbf{d}_{k-2} = O(T^3).$$

where a_m is either a_{min} or a_{max}, $v_k = v(kT)$ and $v(t) = \frac{d}{dt} g(t)$. Note that the magnitude of the mismatched part in the disturbance $\mathbf{d}_k$ is of the order $O(T^3)$.

Property 2. For stable dynamics $x_{k+1} = \lambda x_k + \delta_k$, $|\lambda| < 1$ and $\delta_k = O(T^n)$, then $|x_k| = O(T^{n-1})$ when $k \to \infty$.

5.3 Discrete-Time Output ISM Control

In this section we will discuss the design of the output tracking controller for the piezo-motor stage. The controller will be designed based on an appropriate integral sliding-surface. Further, the stability conditions of the closed-loop system will be analyzed. Appropriate observers for the disturbance and the unknown state x_2 will be derived and this section will conclude with a discussion on the tracking-error bound.

5.3.1 Controller Design and Stability Analysis

Consider the discrete-time integral sliding-surface below,

$$\begin{aligned} \sigma_k &= e_k - e_0 + \varepsilon_k \\ \varepsilon_k &= \varepsilon_{k-1} + \beta e_{k-1} \end{aligned} \tag{5.8}$$

where $e_k = r_k - y_k$ is the output tracking error, e_0 is the initial tracking error, r_k is an arbitrary time-varying reference, σ_k, ε_k are the sliding function and integral of the tracking error, and β is a design constant. The output tracking problem is to force $y_k \to r_k$.

Let us first derive the discrete-time ISMC law by using to the concept of equivalent control.

Theorem 10 *The new ISMC law porposed is*

$$u_k = \gamma_1^{-1}[r_{k+1} - \lambda e_k - \phi_{11} x_{1,k} - \phi_{12}\hat{x}_{2,k} + \sigma_k] - \hat{\eta}_{k-1} \tag{5.9}$$

where $\hat{\eta}_{k-1}$ and $\hat{x}_{2,k}$ are estimates of the disturbance observer and state observer respectively as will be shown later, $\lambda = 1 - \beta$.

Further, the controller (5.9) drives the sliding variable to

$$\sigma_{k+1} = \gamma_1 \hat{\eta}_{k-1} - d_{1,k} - \phi_{12}\tilde{x}_{2,k}$$

and results in the output error dynamics

$$e_{k+1} = \lambda e_k + \delta_k,$$

where $\tilde{x}_{2,k} = x_{2,k} - \hat{x}_{2,k}$ *is state estimation error, and*

$$\delta_k = -(d_{1,k} - \gamma_1 \hat{\eta}_{k-1} - d_{1,k-1} + \gamma_1 \hat{\eta}_{k-2}) + \phi_{12}(\tilde{x}_{2,k} - \tilde{x}_{2,k-1}), \tag{5.10}$$

which consists disturbance and state estimation errors.

Proof: The control law (5.9) can be derived using the design method based on equivalent control. To proceed, consider a forward expression of (5.8)

$$\begin{aligned} \sigma_{k+1} &= e_{k+1} - e_0 + \varepsilon_{k+1} \\ \varepsilon_{k+1} &= \varepsilon_k + \beta e_k. \end{aligned} \tag{5.11}$$

The objective of a sliding mode controller is to achieve $\sigma_{k+1} = 0$, therefore, we need to derive an explicit expression in terms of the sliding surface and system dynamics. For this substitute ε_{k+1} and the expression $\varepsilon_k - e_0 = \sigma_k - e_k$ into the expression of the sliding surface in (5.11) in order to eliminate the term ε_k from the resulting expression. Equating the resulting expression of σ_{k+1} to zero we obtain

$$\sigma_{k+1} = e_{k+1} + \beta e_k - e_0 + \varepsilon_k = e_{k+1} - (1-\beta)e_k + \sigma_k = 0. \tag{5.12}$$

Note that (5.6) can be rewritten as

$$\begin{aligned} x_{1,k+1} &= \phi_{11} x_{1,k} + \phi_{12} x_{2,k} + \gamma_1 u_k + d_{1,k} \\ x_{2,k+1} &= \phi_{21} x_{1,k} + \phi_{22} x_{2,k} + \gamma_2 u_k + d_{2,k}. \end{aligned} \tag{5.13}$$

Using the relation $e_{k+1} = r_{k+1} - y_{k+1} = r_{k+1} - x_{1,k+1}$, and substituting y_{k+1} or $x_{1,k+1}$ dynamics into (5.12) and solve for the equivalent control u_k^{eq}, we have

$$u_k^{eq} = \gamma_1^{-1} \left[r_{k+1} - \lambda e_k - \phi_{11} x_{1,k} - \phi_{12} x_{2,k} - d_{1,k} + \sigma_k. \right] \tag{5.14}$$

Note that the control (5.14) is based on the state $x_{2,k}$ as well as the current value of the disturbance $d_{1,k}$ which are unknown and therefore cannot be implemented in this current form. To overcome this, we will introduce the state estimate and disturbance estimate. Therefore, the final controller structure is given by (5.9) which is to replace $x_{2,k}$ and $d_{1,k}$ in the equivalent control (5.14) by the state estimate $\hat{x}_{2,k}$ and disturbance estimate $\hat{d}_{1,k-1} = \gamma_1 \hat{\eta}_{k-1}$.

In order to verify the second part of Theorem 13 with regard to the losed-loop stability, first derive the closed-loop state dynamics. Substitute u_k in (5.9) and $\hat{x}_{2,k}$ into (5.6), we obtain

$$\begin{aligned} \mathbf{x}_{k+1} &= \left[\Phi - \boldsymbol{\gamma}\gamma_1^{-1}\left([\phi_{11}\ \phi_{12}] - \lambda \mathbf{c}\right)\right]\mathbf{x}_k + \mathbf{d}_k - \boldsymbol{\gamma}\hat{\eta}_{k-1} + \boldsymbol{\gamma}\gamma_1^{-1}\phi_{12}\tilde{x}_{2,k} \\ &\quad + \boldsymbol{\gamma}\gamma_1^{-1}(r_{k+1} - \lambda r_k) + \boldsymbol{\gamma}\gamma_1^{-1}\sigma_k \end{aligned} \tag{5.15}$$

where $\tilde{x}_{2,k} = x_{2,k} - \hat{x}_{2,k}$ is state estimation error.

Now rewrite (5.12) as follows

$$\sigma_{k+1} = r_{k+1} - \mathbf{c}\mathbf{x}_{k+1} - \lambda(r_k - \mathbf{c}\mathbf{x}_k) + \sigma_k = 0 \tag{5.16}$$

and substitute (5.15) into (5.16), which yields the closed-loop sliding dynamics

$$\sigma_{k+1} = \gamma_1 \hat{\eta}_{k-1} - d_{1,k} - \phi_{12}\tilde{x}_{2,k}. \tag{5.17}$$

As expected, due to the fact that the estimates $\hat{x}_2$ and $\hat{d}_1$ are used in the control law, the sliding function σ_k no longer converges to the origin as desired but convergences to a region around the origin. The size of this region depends on the performance of the state and disturbance estimation, and will be shown to be of $O(T^2)$.

Returning to the stability issue of (5.15). Since the system being studied is of 2^{nd} order, it is easy to compute the closed-poles $z_1 = \lambda$ and $z_2 = \frac{k_{fv}Te^{-k_{fv}T} + e^{-k_{fv}T} - 1}{k_{fv}T + e^{-k_{fv}T} - 1}$. The first pole is a

function of the integral constant β while the second pole is the open-loop zero and is stable for $T > 0$. Thus, the system is stable as long as β is properly selected.

Finally, since it is desired to achieve proper performance characteristics for the output tracking error, we will derive the tracking error dynamics in terms of the design parameter λ. Substitution of (5.15) into $y_{k+1} = \mathbf{c}\mathbf{x}_{k+1}$ yields the dynamics

$$y_{k+1} = -\lambda e_k + r_{k+1} + d_{1,k} - \gamma_1 \hat{\eta}_{k-1} + \phi_{12}\tilde{x}_{2,k} + \sigma_k. \tag{5.18}$$

Substituting the result $\sigma_k = \gamma_1 \hat{\eta}_{k-2} - d_{1,k-1} - \phi_{12}\tilde{x}_{2,k-1}$ obtained from (5.17) into (5.18)

$$y_{k+1} = -\lambda e_k + r_{k+1} + d_{1,k} - \gamma_1 \hat{\eta}_{k-1} - d_{1,k-1} + \gamma_1 \hat{\eta}_{k-2} + \phi_{12}(\tilde{x}_{2,k} - \tilde{x}_{2,k-1}) \tag{5.19}$$

which yields the tracking error dynamics

$$e_{k+1} = \lambda e_k + \delta_k \tag{5.20}$$

where δ_k is given by (5.10) as a sum of state and disturbane estimation errors. ■

Remark 23 *It will be shown in subsequenct subsections that under smoothness and boundedness conditions for the disturbance, the disturbance estimate $\hat{\eta}_k$ and the state estimate $\hat{x}_{2,k}$ converge to their actual values.*

5.3.2 Disturbance Observer Design

In order to design the observer we need to first note that according to **Property 1** the disturbance can be written as

$$\mathbf{d}_k = \boldsymbol{\gamma}\eta_k + O(T^3) \tag{5.21}$$

where the magnitude of $O(T^3)$ term is in proportion to T^3. Define the observer

$$\begin{aligned} \mathbf{x}_{d,k} &= \Phi \mathbf{x}_{d,k-1} + \boldsymbol{\gamma} u_{k-1} + \boldsymbol{\gamma} \hat{\eta}_{k-1} \\ y_{d,k-1} &= \mathbf{c}\mathbf{x}_{d,k-1} \end{aligned} \tag{5.22}$$

where $\mathbf{x}_d$ is the observer state vector, y_d is the observer output vector, $\hat{\eta}_k$ is the disturbance estimate and will act as the 'control input' to the observer, therefore the estimate $\hat{\mathbf{d}}_{k-1} = \boldsymbol{\gamma}\hat{\eta}_{k-1}$ and $\hat{d}_{1,k-1} = \gamma_1 \hat{\eta}_{k-1}$. Since the disturbance estimate will be used in the final control signal it must not be overly large, therefore, it is wise to avoid a deadbeat design. For this reason we will use an observer based on an integral sliding surface

$$\begin{aligned} \sigma_{d,k} &= e_{d,k} - e_{d,0} + \varepsilon_{d,k} \\ \varepsilon_{d,k} &= \varepsilon_{d,k-1} + \beta_d e_{d,k-1} \end{aligned} \tag{5.23}$$

where $e_{d,k} = y_k - y_{d,k}$ is the output estimation error, $e_{d,0}$ is the initial estimation error, $\sigma_{d,k}$, $\varepsilon_{d,k}$ are the sliding function and integral vectors, and β_d is an integral gain matrix.

Since the sliding surface (5.23) is the same as (5.8), the set $(y_k, \mathbf{x}_{d,k}, u_k + \hat{\eta}_k, y_{d,k}, \sigma_{d,k})$ has duality with the set $(r_k, \mathbf{x}_k, u_k, y_k, \sigma_k)$, therefore, $\hat{\eta}_k$ is given by

$$\hat{\eta}_{k-1} = \gamma_1^{-1} \left(y_k - \lambda_d e_{d,k-1} - [\phi_{11}\ \phi_{12}]\mathbf{x}_{d,k-1} + \sigma_{d,k-1} \right) - u_{k-1} \tag{5.24}$$

where $\lambda_d = 1 - \beta_d$. Expression (5.24) is the required disturbance estimate and is similar in form to (5.14).

The stability and convergence property of the observer is summarized in the following theorem.

Theorem 11 *The state dynamics (5.22) is stable when closing the loop with the disturbance estimate (5.24). The disturbance estimate $\hat{\eta}_{k-1}$ from (5.24) converges to an $O(T)$ bound around the actual disturbance η_{k-1} asymptotically.*

Proof: To analyze the stability of the observer, substitute (5.24) into (5.22) and follow the same steps of the derivation of (5.15) to obtain

$$\mathbf{x}_{d,k} = \left[\Phi - \boldsymbol{\gamma}\gamma_1^{-1}\left([\phi_{11}\ \phi_{12}] - \lambda_d \mathbf{c}\right)\right]\mathbf{x}_{d,k-1} + \boldsymbol{\gamma}\gamma_1^{-1}[y_k - \lambda_d y_{k-1}] + \boldsymbol{\gamma}\gamma_1^{-1}\sigma_{d,k-1}. \quad (5.25)$$

By substituting (5.25) into $\sigma_{d,k+1}$, the sliding dynamcis becomes $\sigma_{d,k} = 0$. Therefore,

$$\mathbf{x}_{d,k} = \left[\Phi - \boldsymbol{\gamma}\gamma_1^{-1}\left([\phi_{11}\ \phi_{12}] - \lambda_d \mathbf{c}\right)\right]\mathbf{x}_{d,k-1} + \boldsymbol{\gamma}\gamma_1^{-1}[y_k - \lambda_d y_{k-1}]. \quad (5.26)$$

Subtracting (5.26) from a delayed form of the system (5.6) and substituting $\mathbf{d}_{k-1} = \boldsymbol{\gamma}\eta_{k-1} + O(T^3)$ we obtain

$$\Delta\mathbf{x}_{d,k} = \left[\Phi - \boldsymbol{\gamma}\gamma_1^{-1}\left([\phi_{11}\ \phi_{12}] - \lambda_d \mathbf{c}\right)\right]\Delta\mathbf{x}_{d,k-1} + O(T^3) \quad (5.27)$$

where $\Delta\mathbf{x}_{d,k} = \mathbf{x}_k - \mathbf{x}_{d,k}$. From (5.27) we see that the convergence of the disturbance observer states, $\mathbf{x}_{d,k}$, to the actual system states $\mathbf{x}_k$, depends only on the matrix $\left[\Phi - \boldsymbol{\gamma}\gamma_1^{-1}\left([\phi_{11}\ \phi_{12}] - \lambda_d \mathbf{c}\right)\right]$ whose stability is dependent on the selection of the constant λ_d. Also note that premultliplication of (5.27) with $\mathbf{c}$ yields the tracking error dynamics

$$e_{d,k} = \lambda_d e_{d,k-1}. \quad (5.28)$$

To prove the second part of theorem, subtract (5.22) from a delayed (5.6) to obtain

$$\Delta\mathbf{x}_{d,k} = \Phi\Delta\mathbf{x}_{d,k-1} + \boldsymbol{\gamma}(\eta_{k-1} - \hat{\eta}_{k-1}) + O(T^3). \quad (5.29)$$

To obtain the relationship between η_k and $\hat{\eta}_k$, premultiplying both sides of (5.29) with $\mathbf{c}$ and substituting (5.28) yield

$$\hat{\eta}_{k-1} = \gamma_1^{-1}\left([\phi_{11}\ \phi_{12}] - \lambda_d \mathbf{c}\right)\Delta\mathbf{x}_{d,k-1} + \eta_{k-1}. \quad (5.30)$$

Substituting (5.27) recursively we have

$$\Delta \mathbf{x}_{d,k-1} = \left[\Phi - \boldsymbol{\gamma}\gamma_1^{-1}\left([\phi_{11}\ \phi_{12}] - \lambda_d \mathbf{c}\right)\right]^{k-1} \Delta \mathbf{x}_{d,0} + O(T^2). \tag{5.31}$$

Substituting (5.31) into (5.30) we obtain

$$\begin{aligned} \hat{\eta}_{k-1} &= \gamma_1^{-1}\left([\phi_{11}\ \phi_{12}] - \lambda_d \mathbf{c}\right)\left[\Phi - \boldsymbol{\gamma}\gamma_1^{-1}\left([\phi_{11}\ \phi_{12}] - \lambda_d \mathbf{c}\right)\right]^{k-1} \Delta \mathbf{x}_{d,0} \\ &\quad + \gamma_1^{-1}\left([\phi_{11}\ \phi_{12}] - \lambda_d \mathbf{c}\right) O(T^2) + \eta_{k-1}. \end{aligned} \tag{5.32}$$

For this particular system it can be shown that $\phi_{11} = 1$, $\phi_{12} = \frac{1-e^{-k_{fv}T}}{k_{fv}} = O(T)$, $\gamma_1 = O(T^2)$ and that a reasonable choice of the controller pole is $\lambda \approx 1 - O(T)$. From these it can be found that $([\phi_{11}\ \phi_{12}] - \lambda_d \mathbf{c}) = O(T)$. Since, $\left[\Phi - \boldsymbol{\gamma}\gamma_1^{-1}\left([\phi_{11}\ \phi_{12}] - \lambda_d \mathbf{c}\right)\right]$ is stable, when $k \to \infty$

$$\left[\Phi - \boldsymbol{\gamma}\gamma_1^{-1}\left([\phi_{11}\ \phi_{12}] - \lambda_d \mathbf{c}\right)\right]^{k-1} \to 0$$

and the disturbance estimate will converge to a worste case of $O(T)$ around the actual disturbance. ■

Remark 24 *It should be noted that the sliding dynamics (5.26), output error dynamics (5.28), hence the disturbance estimation error, are independent of the control input u_k and the state estimation error. This decoupling property is highly desirable for any control system combined with observers.*

5.3.3 State Observer Design

State estimation is accomplished with the following state observer

$$\hat{\mathbf{x}}_{k+1} = \Phi \hat{\mathbf{x}}_k + \boldsymbol{\gamma} u_k + \mathbf{l}(y_k - \hat{y}_k) + \hat{\mathbf{d}}_{k-1} \tag{5.33}$$

where $\hat{\mathbf{x}}_k$, $\hat{y}_k$ are the state and output estimates and $\mathbf{l}$ is a vector valued observer gain. Notice that in observer (5.33), the term $\hat{\mathbf{d}}_{k-1}$ has been added to compensate for the disturbance. Since only the delayed disturbance is available it is necessary to investigate the effect it may have on the state estimation. Subtracting (5.33) from (5.6) yields

$$\tilde{\mathbf{x}}_{k+1} = [\Phi - \mathbf{lc}]\tilde{\mathbf{x}}_k + \mathbf{d}_k - \hat{\mathbf{d}}_{k-1} \tag{5.34}$$

where $\tilde{\mathbf{x}}_k = \mathbf{x}_k - \hat{\mathbf{x}}_k$ is the state estimation error. The solution of (5.34) is given by

$$\tilde{\mathbf{x}}_k = [\Phi - \mathbf{lc}]^k \tilde{\mathbf{x}}_0 + \sum_{i=0}^{k-1} \left([\Phi - \mathbf{lc}]^{k-1-i} (\mathbf{d}_i - \hat{\mathbf{d}}_{i-1}) \right). \tag{5.35}$$

The state estimation error $\tilde{x}_{2,k} = x_{2,k} - \hat{x}_{2,k}$ is given by

$$\tilde{x}_{2,k} = [0\ 1]\,[\Phi - \mathbf{lc}]^k\,\tilde{\mathbf{x}}_0 + \sum_{i=0}^{k-1} [0\ 1] \left([\Phi - \mathbf{lc}]^{k-1-i} (\mathbf{d}_i - \hat{\mathbf{d}}_{i-1}) \right). \tag{5.36}$$

Using **Property 1**, $\mathbf{d}_k - \hat{\mathbf{d}}_{k-1} = O(T^2)$ when no discontinuity occurs. From (5.34) and **Property 2** we know that the ultimate bound on $\tilde{\mathbf{x}}_k$, hence $\tilde{x}_{2,k}$ is $O(T)$.

5.3.4 Ultimate Tracking Error Bound

Now we are in a position to derive the ultimate tracking error bound of the piezo-motor stage (5.1) when the proposed discrete-time ISMC is applied.

Theorem 12 *Using the discrete-time ISMC law (5.9), the disturbance observer (5.24) and (5.22), the state observer (5.33), the ultimate bound of output tracking error is* $O(T^2)$.

Proof: In order to calculate the output tracking error bound we must find the bound of δ_k in (5.20). From (5.36) we can derive the difference $\tilde{x}_{2,k} - \tilde{x}_{2,k-1}$

$$\tilde{x}_{2,k} - \tilde{x}_{2,k-1} = [0\ 1][I - (\Phi - \mathbf{lc})](\Phi - \mathbf{lc})^{k-1}\tilde{\mathbf{x}}_0 - \sum_{i=0}^{k-1} [0\ 1] \left([\Phi - \mathbf{lc}]^{k-1-i} (\mathbf{d}_i - \hat{\mathbf{d}}_{i-1}) \right)$$

$$+\sum_{i=0}^{k-2}[0\ 1]\left([\Phi-\mathbf{lc}]^{k-1-i}(\mathbf{d}_i-\hat{\mathbf{d}}_{i-1})\right) \tag{5.37}$$

where I is a unity matrix. (5.37) can be simplified to

$$\tilde{x}_{2,k}-\tilde{x}_{2,k-1} \;=\; [0\ 1][I-(\Phi-\mathbf{lc})](\Phi-\mathbf{lc})^{k-1}\tilde{\mathbf{x}}_0-(d_{2,k}-\gamma_2\hat{\eta}_{k-1}). \tag{5.38}$$

Since $(\Phi-\mathbf{lc})^k\to 0$ ultimately, we have

$$\tilde{x}_{2,k}-\tilde{x}_{2,k-1} \;=\; -(d_{2,k}-\gamma_2\hat{\eta}_{k-1}) \tag{5.39}$$

as $k\to\infty$. Substituting (5.39) into (5.10) yields

$$\delta_k \;=\; -(d_{1,k}-\gamma_1\hat{\eta}_{k-1}-d_{1,k-1}+\gamma_1\hat{\eta}_{k-2})-\phi_{12}(d_{2,k}-\gamma_2\hat{\eta}_{k-1}). \tag{5.40}$$

Next by substitution of the relations $d_{1,k}=\gamma_1\eta_k+O(T^3)$, $d_{2,k}=\gamma_2\eta_k+O(T^3)$, and into (5.40), we obtain

$$\delta_k \;=\; -\gamma_1(\eta_k-\hat{\eta}_{k-1}-\eta_{k-1}+\hat{\eta}_{k-2})-\phi_{12}\gamma_2(\eta_k-\hat{\eta}_{k-1})+O(T^3). \tag{5.41}$$

Since we are trying to calculate the steady state error bound, using the fact that at steady state $\hat{\eta}_k=\eta_k+O(T)$ and substituting it in (5.41)

$$\delta_k \;=\; -\gamma_1(\eta_k-2\eta_{k-1}+\eta_{k-2}+O(T))-\phi_{12}\gamma_2(\eta_{k-1}-\eta_{k-2}+O(T))+O(T^3). \tag{5.42}$$

For sampled-data system (5.6), $\boldsymbol{\gamma}=O(T)$ and $\phi_{12}=O(T)$. If η_k is smooth and bounded, then from **Property 1**

$$\delta_k \;=\; O(T^2)\cdot O(T)+O(T)\cdot O(T)\cdot O(T)+O(T^3)=O(T^3). \tag{5.43}$$

In order to derive the output tracking error bound, look into output tracking error dynamics derived in Theorem 1, $e_{k+1} = \lambda e_k + \delta_k$, whose solution is

$$e_k = \lambda^k e_0 + \sum_{i=0}^{k-1} \lambda^i \delta_{k-i-1}. \tag{5.44}$$

According to **Property 2**, the ultimate error bound of e_k will be one order higher than the bound of δ_k, therefore, since the bound of δ_k is $O(T^3)$ the ultimate bound of e_k is $O(T^2)$, i.e.,

$$|e_k| = O(T^2). \tag{5.45}$$

We have computed the tracking error in the case when the disturbance is smooth and bounded. Now, we look at what happens to the tracking error when there is a discontinuity in the disturbance, i.e, when there is a change in the sign of x_2. Consider the disturbance term associated with the closed-loop system (5.40). It can be reasonably assumed that the discontinuity occurs rarely, therefore, if we assume that the discontinuity occurs at the kth sampling point, then $\delta_k = O(T^2)$ rather than $O(T^3)$ as the difference $d_{1,k} - 2d_{1,k-1} + d_{1,k-2}$ will no longer be $O(T^3)$ but of the order of $d_{1,k}$ which is $O(T)$. If the discontinuity occurs at a time instance k', then $\delta_k = O(T)$ at $k = k', k'+1, k'+2$, and return to $\delta_k = O(T^3)$ for subsequent sampling instances. Therefore the solution of (5.44) would lead to the worst case error bound

$$|e_k| = O(T) \tag{5.46}$$

for certain time interval but $O(T^2)$ ultimately. ■

We have computed the tracking error in the case when the disturbance is smooth and bounded. Now, we look at what happens to the tracking error when there is a discontinuity in the disturbance, i.e, when there is a change in the sign of x_2. Consider the disturbance term associated

with the closed-loop system (5.40). It can be reasonably assumed that the discontinuity occurs rarely, therefore, if we assume that the discontinuity occurs at the kth sampling point, then $\delta_k = O(T^2)$ rather than $O(T^3)$ as the difference $d_{1,k} - 2d_{1,k-1} + d_{1,k-2}$ will no longer be $O(T^3)$ but of the order of $d_{1,k}$ which is $O(T)$. If the discontinuity occurs at a time instance k', then $\delta_k = O(T)$ at $k = k', k'+1, k'+2$, and return to $\delta_k = O(T^3)$ for subsequent sampling instances. Therefore the solution of (5.44) would lead to the worst case error bound

$$|e_k| = O(T) \tag{5.47}$$

for certain time interval but $O(T^2)$ ultimately.

5.3.5 Experimental Investigation

The configuration of the whole control system is outlined in Fig.5.4. The nominal parameters of the system are $m = 1kg$, $k_{fv} = 144N$ and $k_f = 6N/Volt$. This simple linear model does

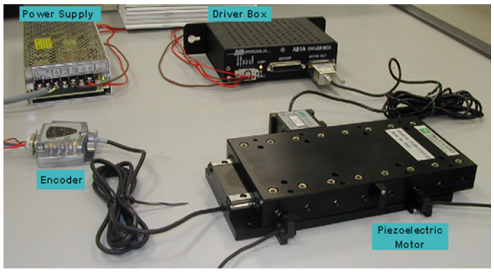

Figure 5.3: The piezo motor driven linear motion stage

not contain any nonlinear and uncertain effects such as the frictional force in the mechanical part, high-order electrical dynamics of the driver, loading condition, etc., which are hard to model in practice. In general, producing a high precision model will require more efforts than

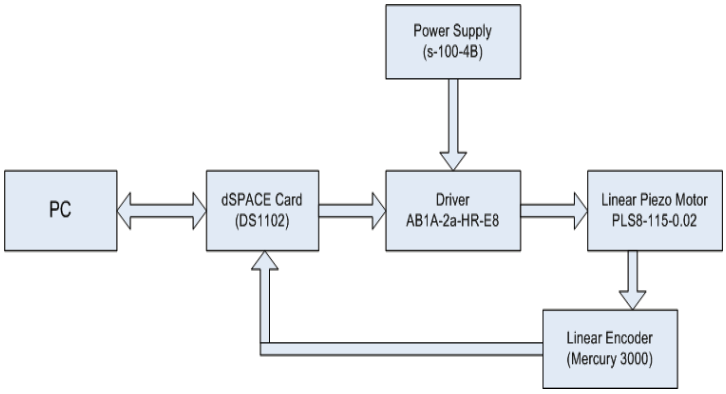

Figure 5.4: The control system block diagram of the piezo-motor driven linear motion stage

performing a control task with the same level of precision.

Determination of Controller Parameters

In order to select an appropriate sampling period T, the open-loop zero of the system is plotted in Fig.5.5 as a function of sampling period. We see from Fig.5.5 that a sampling

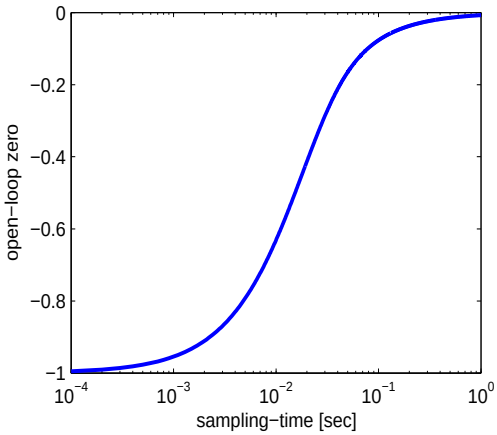

Figure 5.5: Open-loop zero with respect to sampling period

period below 10^{-4} second would produce a less stable open-loop zero. On the other hand, an over large sampling period will degrade the feedback effect. In the experimental tests we

select two sampling periods of $1ms$ and $10ms$ respectively.

To proceed with the implementation, three parameters need to be designed: the state observer gain $\mathbf{l}$, the disturbance observer integral gain matrix β_d, and the controller integral gain β. The state observer gain is selected such that the observer poles are $(0.4, 0.4)$. This selection is arbitrary, but, the poles are selected to ensure quick convergence. Next, the constant β_d is designed. To ensure the quick convergence of the disturbance observer, β_d is selected such that the observer pole at $1ms$ sampling is $\lambda_d = 0.9$ and at $10ms$ sampling is $\lambda_d = 0.6$. Since the remaining pole of the observer is the non-zero open-loop zero (-0.958 at $1ms$ and -0.683 at $10ms$), it is the dominant pole. Finally, the controller pole is selected as $\lambda = 0.958$ at $1ms$ sampling and $\lambda = 0.683$ at $10ms$ sampling which are found to be the best possible after some trials. Thus, the design parameters are as follows

$$
\begin{aligned}
\mathbf{l} &= \begin{bmatrix} 0.4269 & 5.3260 \end{bmatrix}^T, \quad T = 10ms, \\
\mathbf{l} &= \begin{bmatrix} 1.059 & 231.048 \end{bmatrix}^T, \quad T = 1ms, \\
\beta_d &= 1 - \lambda_d = 0.4, \quad T = 10ms, \\
\beta_d &= 1 - \lambda_d = 0.1, \quad T = 1ms, \\
\beta &= 1 - \lambda = 0.317, \quad T = 10ms, \\
\beta &= 1 - \lambda = 0.042, \quad T = 1ms.
\end{aligned}
$$

The reference trajectory r_k is shown in Fig.5.6 and as it can be seen the initial conditions $e_0 = 0$ and $e_{d,0} = 0$. For comparison purpose, a PI control is also applied to piezo-motor and PI gains were optimized through intensive tests. The PI gains are at $k_p = 1.5$ and $k_i = 55$

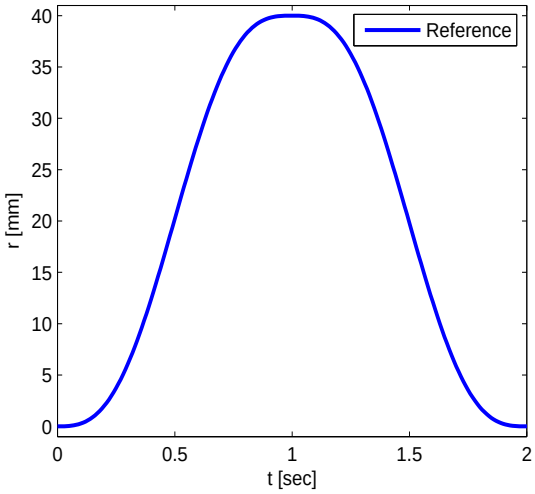

Figure 5.6: The reference trajectory

at the sampling period of 1ms and $k_p = 0.6$ and $k_i = 6$ at the sampling period of 10 ms. To verify that the PI gains used are optimally tuned, PI gains are made to vary from their optimal values by $\pm 20\%$. The optimally tuned PI gains can be determined when other PI values either produce larger tracking errors or lead to oscillatory responses.

Experimental Results and Discussions

DOISMC is applied with both sampling period of $10ms$ and $1ms$. For comparison the PI control is also applied. The tracking errors of both controllers as shown in Fig.5.7. It can be seen that at $10ms$ the performance of DOISMC and PI controller are comparable whereas at $1ms$ the performance of the DOISMC is far better. Fig.5.8 shows the control signals of DOISMC and PI. It can be seen that DOISMC control profile at $1ms$ is smoother comparing with at $10ms$. In Fig.5.9 the reference velocity and the estimated velocity under the state observer is plotted. It is clearly seen that the smaller sampling period of $1ms$ produces a better estimate, $\hat{x}_2$, in comparison with $10ms$ sampling period. Fig.5.10 demonstrates estimation

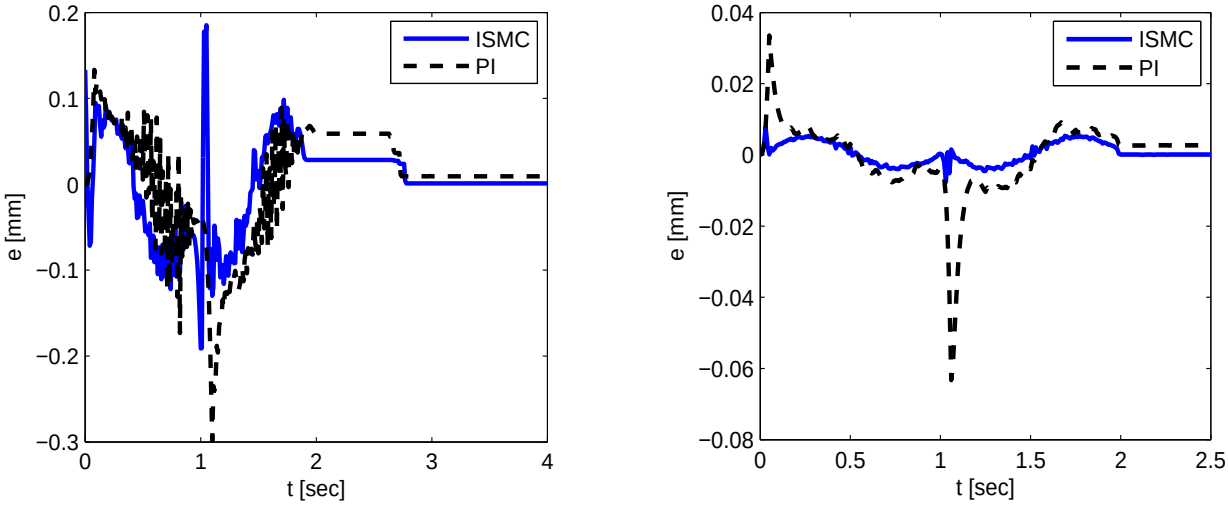

(a) (b)

Figure 5.7: Tracking error of DOISMC and PI control at (a) $10ms$ sampling period and (b) $1ms$ sampling period

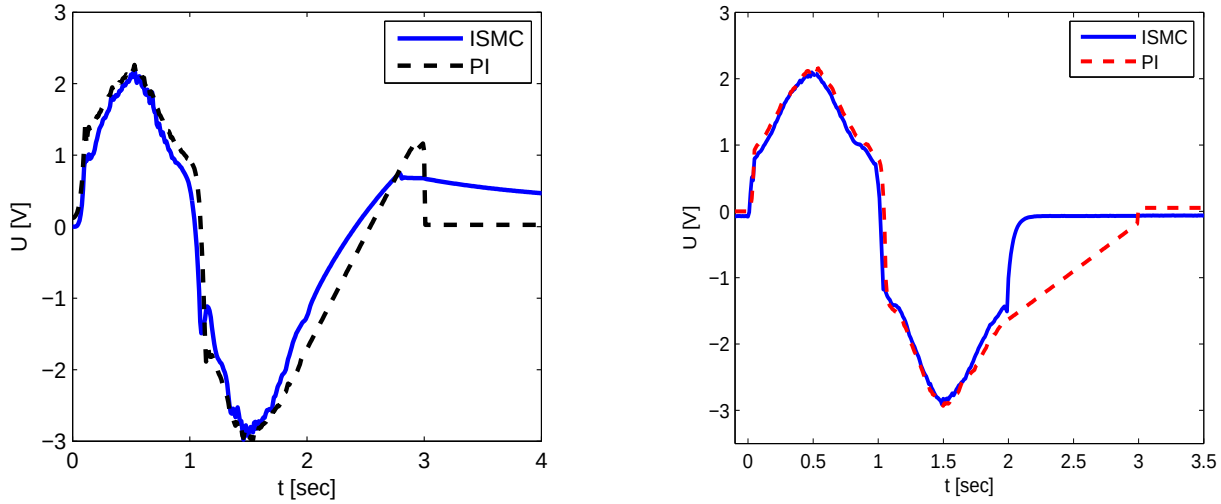

(a) (b)

Figure 5.8: Comparison of the control inputs of DOISMC and PI controllers at (a) $10ms$ sampling period and (b) $1ms$ sampling period

result of the disturbance observer. It can be observed that the sliding mode control will produce some chattering due to the limited sampling frequency. It is well known that sliding mode control requires a fast switching frequency in order to maintain the sliding motion. In

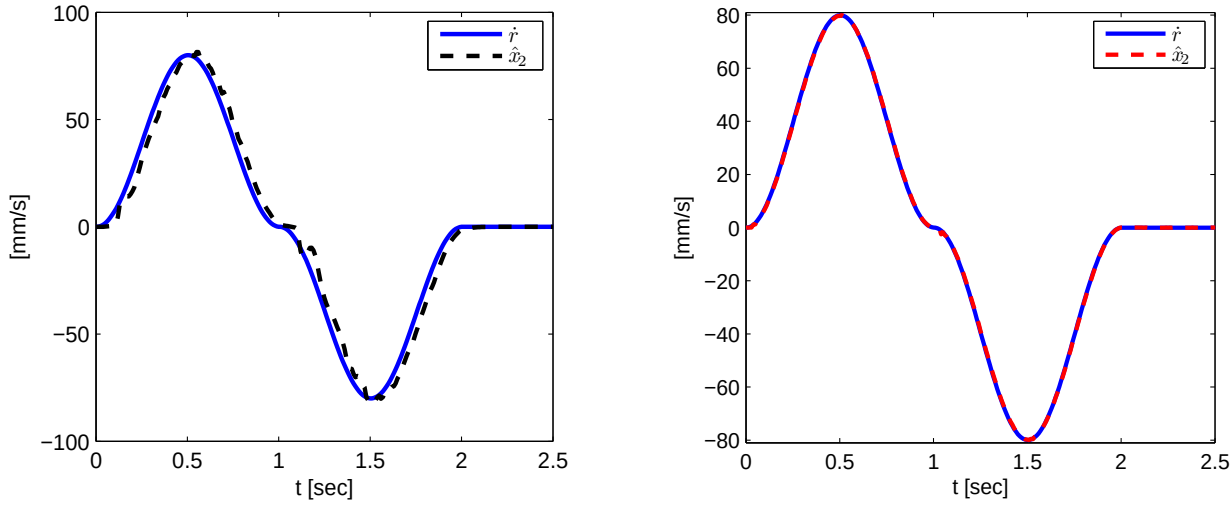

(a) (b)

Figure 5.9: Estimated state $\hat{x}_2$ and reference velocity $\dot{r}$ at (a) $10ms$ sampling period and (b) $1ms$ sampling period

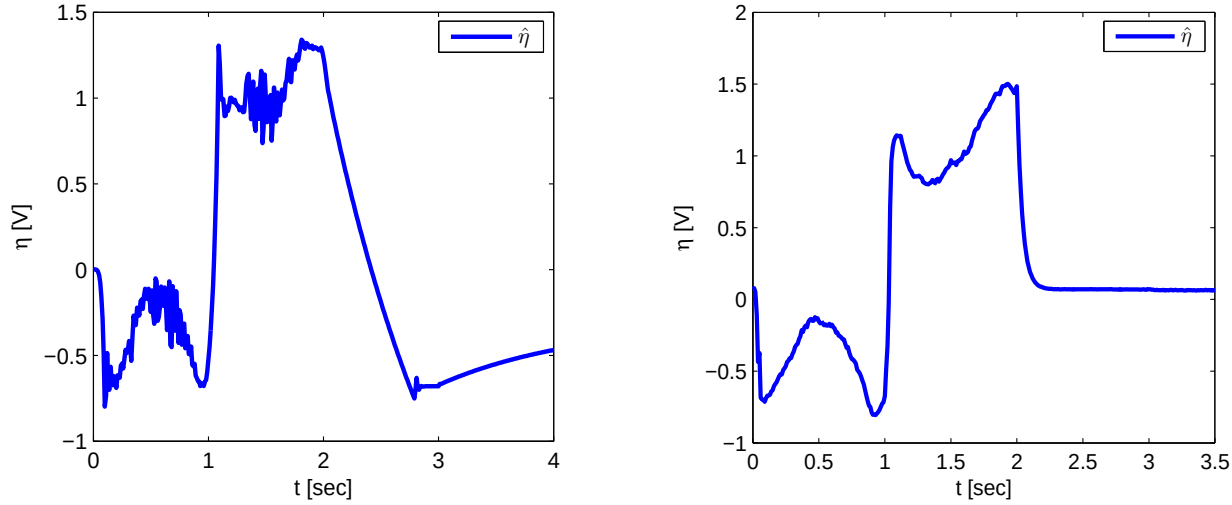

(a) (b)

Figure 5.10: Disturbance observer response at (a) $10ms$ sampling period (b) $1ms$ sampling period

this Chapter, the output ISMC is designed in discrete-time, but the real plant is analog in nature. Moreover, through analysis we have shown the tracking error bound is proportional to the size of the sampling period T. Therefore, we can expect a smoother control response and

lower tracking error when the sampling period is reduced to $1ms$. Nonetheless, the magnitude of the tracking error is at the scale of 5×10^{-4}, confirming the theoretical error bound of $O(T^2) = O(0.01^2) = O(10^{-4})$. It is interesting to note that, when reducing the sampling period by 10 times, the tracking error bound is about 100 times less. This result is consistent the theoretical analysis, because the magnitude of the tracking error is at the scale of 5×10^{-6}, or equivalently $O(T^2) = O(0.001^2) = O(10^{-6})$.

Fig.5.11(a) shows the sliding function σ at $1ms$ sampling period. From Fig.5.10(b) we can

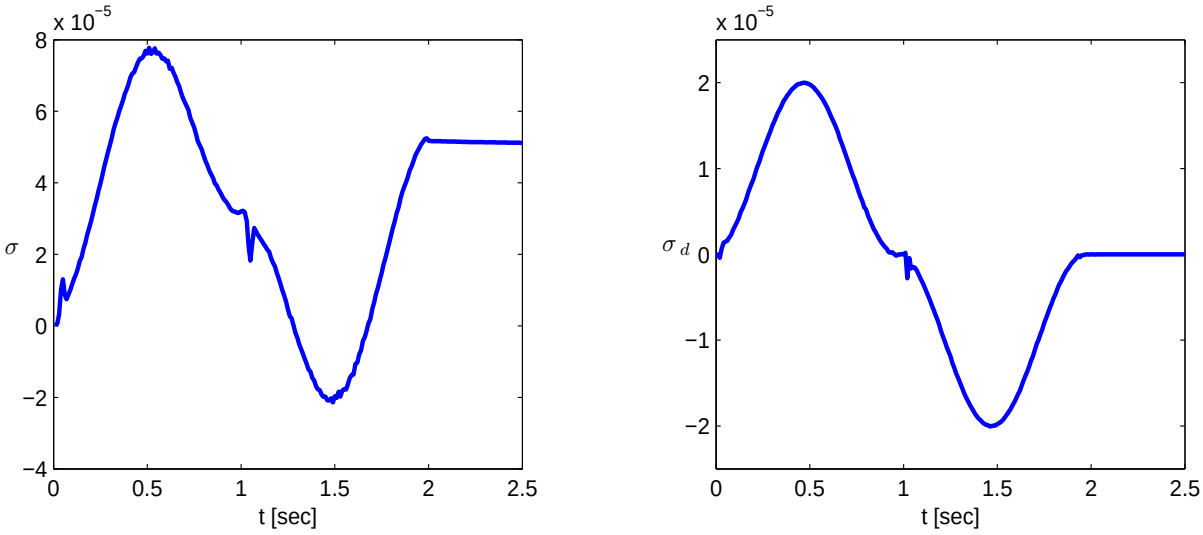

(a) (b)

Figure 5.11: Sliding function (a) σ and (b) σ_d at 1ms sampling period

see that the DOISMC can respond very fast when encountering a discontinuity generated by the static friction at around 1 second. This fast control response is owing to the incorporation of the disturbance observer which can effectively estimate unknown changes. Fig.5.11(b) shows the sliding function σ_d which has a magnitude of 20×10^{-6} which is quite small.

Finally, to illustrae the robustness of DOISMC, an extra load of $2.5kg$ is added to the piezo-motor driven linear motion stage, which is 250% of the original motor mass of $1kg$,

meanwhile the parameters of the controller and observers remain unchanged. Fig.5.12 shows the responses with and without the extra load. It can be seen that the tracking error remains at a low level despite the extra load.

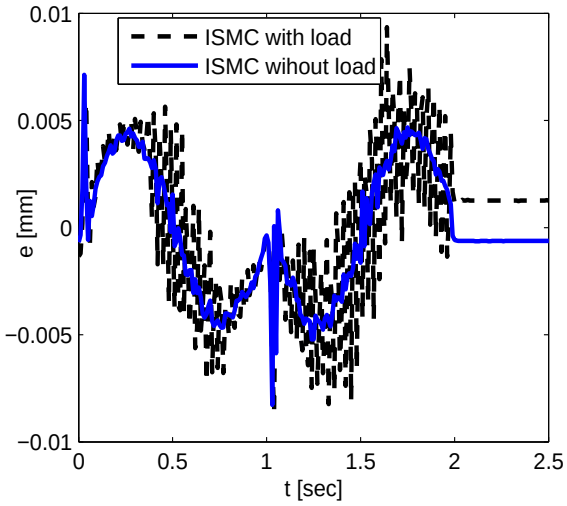

Figure 5.12: Tracking errors of DOISMC with and without the $2.5kg$ load at $1ms$ sampling period

5.4 Sampled-Data ILC Design

In this section we shall show the ILC design for the piezo-motor stage. Unlike the DOISMC controller design where the controller structure is designed from the model, the ILC controller has a standard control structure and the design factors $Q(z)$ and $L(z)$ are determined from the nominal model or from experimentally obtained frequency response data.

5.4.1 Controller Parameter Design and Experimental Results

The objective of the ILC design is to achieve as precisely as possible motion control after the smallest number of iterations. Due to the existence of uncertainties and other unmodelled

disturbances the most suitable selection would be the current-cycle iterative learning control where the iterative controller would act as an add-on to the feedback controller. Experiments conducted on the system have shown that PI control works quite well and, so, it shall be used as the feedback control law. The optimum PI gains found for this system are $K_p = 6$ and $K_i = 10$, [70]. The resulting closed-loop system is given by

$$P'(z) = \frac{2.826 \times 10^{-6} z^2 - 5.124 \times 10^{-8} z - 2.771 \times 10^{-6}}{z^3 - 2.944 z^2 + 2.888 z - 0.944} \tag{5.48}$$

This system is stable and so it will be possible for us to use the frequency domain tools for the design of the ILC controller.

Since, we want to achieve the best possible tracking performance we will not retune the sampling-time according to Table 4.1, instead we will use the other design factors $Q(z)$ and $L(z)$. Before we proceed with the design of the function $Q(z)$ and $L(z)$ we plot the phase and magnitude diagram for $zP'(z)$ in order to decide on what type of functions $Q(z)$ and $L(z)$ should be. According to Table 4.1, $L(z)$ cannot be selected as P-type, D-type, or D^2-type as the order of $P(z)$ is 3 and it has no integrators. Therefore, $L(z)$ will be selected as a lead compensator. From Fig.5.13 we see that the phase falls below $-\frac{\pi}{2}$ and so we need $L(z)$ to have a leading phase of no more than 90 degrees. We select the following simple function $L(s) = 0.1(s + 1)$ which would be $L(z) = \frac{z-0.9996}{0.0004}$ in discrete-time, we can also plot $L(z)$ in Fig.5.14. If we now combine $L(z)$ and $zP'(z)$ we obtain the frequency response in Fig.5.15 which satisfies our requirements. We can also plot the Nyquist diagram for $1 - zL(z)P'(z)$ to confirm if $|1 - zL(z)P'(z)| < 1$. This can be seen from Fig.5.16. Since, stability is achieved

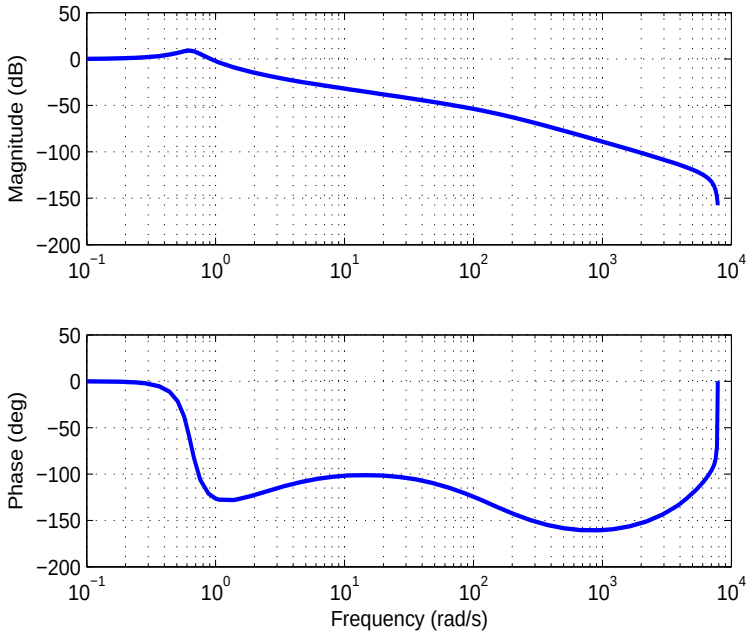

Figure 5.13: Phase and Magnitude for $zP'(z)$

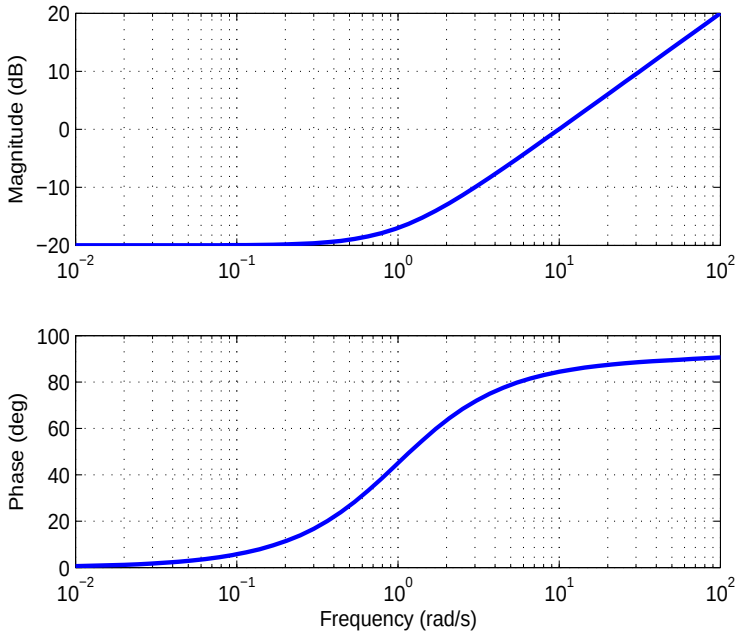

Figure 5.14: Phase and Magnitude for $L(z)$

the function $Q(z)$ is selected as unity.

We are now ready to implement the ILC control law with the designed parameters. The

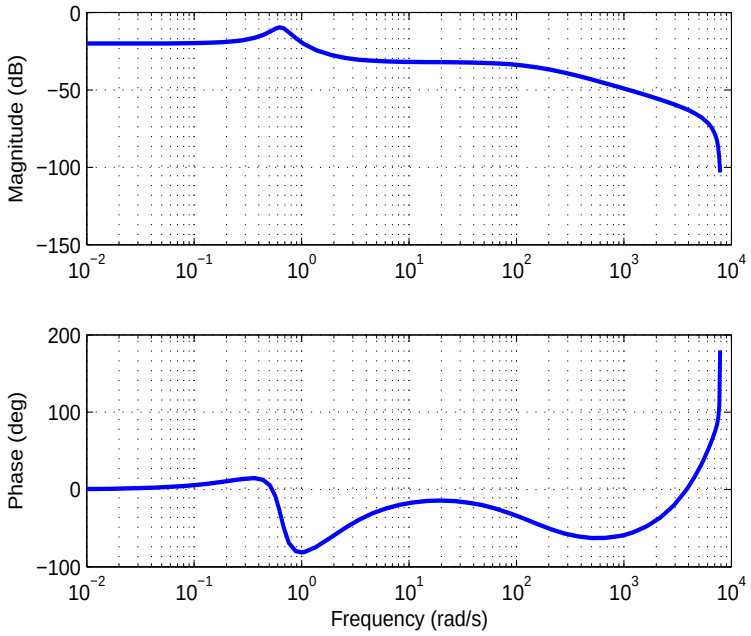

Figure 5.15: Phase and Magnitude for $zL(z)P'(z)$

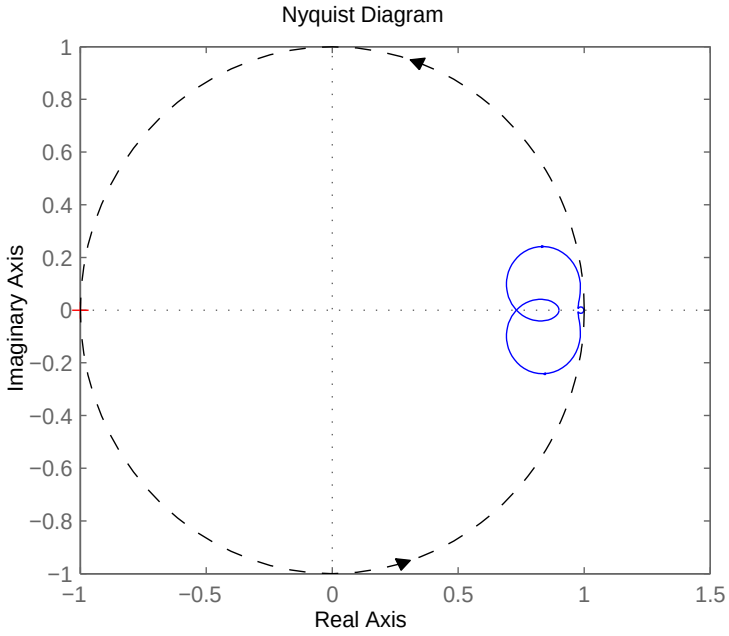

Figure 5.16: Nyquist diagram for $1 - zL(z)P'(z)$

reference trajectory of the system is shown in Fig.5.17. Fig.5.18 shows the output tracking error of the system at the $0th$ and the $15th$ iterations. It is easily seen that the tracking error

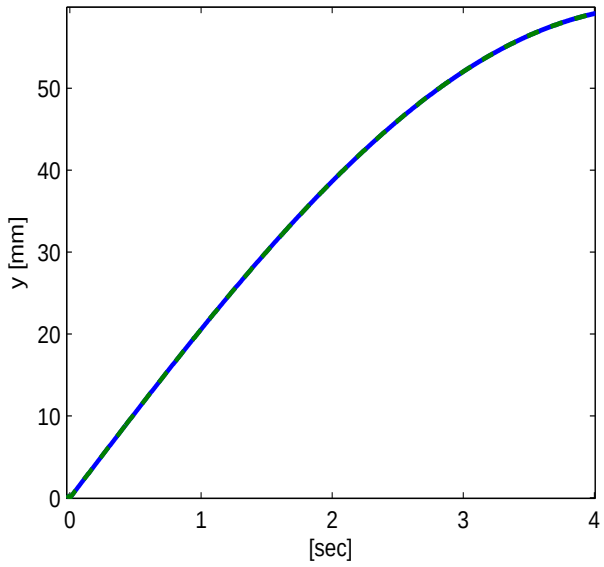

Figure 5.17: Desired and actual output of the system

is greatly reduced by the $15th$ iteration and is of a magnitude of 2 μm at the transient and 0.6 μm at steady state. Finally, Fig.5.19 shows the control effort at the 0^{th} and the 15^{th} iteration.

The above results show the exceptional performance of the ILC laws as add-ons to existed

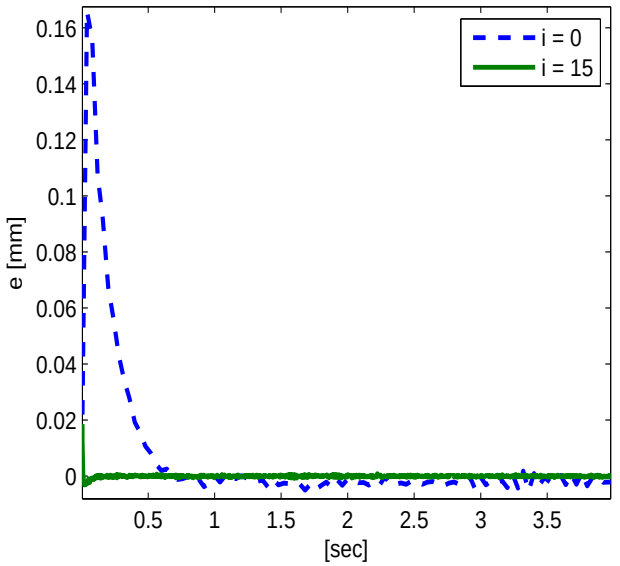

Figure 5.18: Ouput tracking error of the system at the 0^{th} and the 15^{th} iteration

feedback control. The rather straight forward design also shows that the method has a lot of

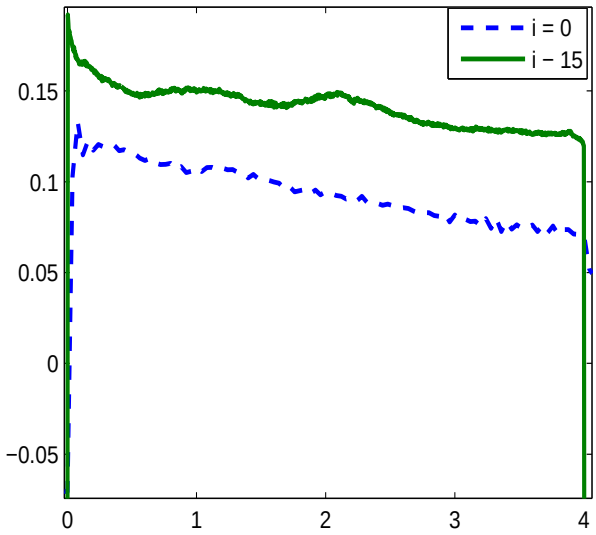

Figure 5.19: Control input of the system at the 0^{th} and the 15^{th} iteration

promise for practical applications.

5.5 Conclusion

This chapter presents a few the various controller designs for sampled-data systems applied to the tracking control of a piezo-motor driven linear motion stage.

For the DOISMC design, proper disturbance and state observers were presented, and in particular the disturbance observer is designed using the idea and method of integral sliding mode to achieve the desired performance. Experimental comparisons with a PI controller evidence the effectiveness of the proposed control method. It is worth to point out that the designs of controller and obervsers are separate, in other words, what we present in this Chapter is a modular design approach. Two observers can be added or removed individually according to practical applications. For instance, state observer can be removed if the ve-

locity is accesssible. The disturbance observer can also be removed when the disturbance is negligible. In either cases, the DOISMC design remain valid and the tracking error bound is guaranted at least to be $O(T^2)$.

For the ILC design, the parameter and filter selection has been shown. The design procedure has been shown to be straight forward and intuitive. With some basic information about the system it was possible to achieve high-precision motion for a repetitive task.

Chapter 6

Conclusions

6.1 Summary of Results

In this Thesis, Chapter 2 deals with sliding mode control for sampled-data systems. The class of system used is LTI with matched disturbance. We show that the introduction of integral action in the sliding manifold improves the state regulation as well as the output tracking as opposed to the classical sliding mode control. We also show that the integral action eliminates the presence of deadbeat poles by allowing full poleplacement thereby eliminating the risk of overlarge control action. Simulation results are shown for both state regulation and output tracking to verify the analytical results. The proposed controllers are shown to outperform classical SMC in the simulation trials confirming the theoretical results.

In Chapter 3 we deal with a class of nonlinear discrete-time systems with uncertainties. The uncertainties assumed in an unknown compact set, periodic, nonvanishing, rapid timevarying, and the only prior knowledge is the periodicity. The proposed method is shown to deal with such uncertainties and in the sequel lead to asymptotic stability. Some more variations in the

unknowns are presented and methods are proposed and shown to deal with them.

In Chapter 4 we show an analysis of ILC for sampled-data LTI systems. Problems in stability, performance, learning transient behavior, and robustness were discussed along in both the time domain and frequency domain. The work is done as means to provide a clearer picture about the potential, and limitations of ILC. Indeed, the field of ILC is quickly maturing and many ideas to deal with different classes of systems are possible. The major contribution of this phd is to provide a design guideline for the control engineer allowing him/her the oppurtunity to make sound controller designs for practical problems.

In Chapter 5 we provide an experimental implementation of the sliding mode control and ILC approaches of chater 2 and Chapter 4. This is done to show the practical significance of the work done in this thesis. The test bed shown is a simple yet important system that can be encountered in the industry. The sliding mode control laws are shown to achieve superior performance over the conventional PI control for arbitrary tracking tasks. In cases where repetitive following of the the same trajectory is needed the ILC is shown to achieve almost perfect tracking after few iterations and can prove to be useful in serial manufacturing processes.

6.2 Suggestions for Future Work

Past research activities have laid a foundation for the future work. Based on the prior research, the following questions deserve further consideration and investigation.

1. Implementation of equivalent control for state regulation and output tracking ISMC.

2. In [6] the adaptive control law was designed based on the assumption that the known nonlinearity is locally Lipschitz. However, the controller proposed in our work is based on a globally sector bounded nonlinearity. In [42] the sector boundedness condition was relaxed for constant unknown parameters case. Is it possible to achieve the same result for the periodic unknown parameters case?

3. How to deal with non-parametric uncertainties with the periodic adaptive control as well as unknown periodic with unknown periods?

4. The ILC work presented is for LTI systems. It would be more practical to study the properties of ILC for more general nonlinear systems as well as MIMO rather than SISO systems.

5. Can we extend the work of ILC to repetitive learning control (RC)?

6. It would be worthwhile to apply the ILC as well as the other control laws (DISMC and AC) on more complex systems such as mdof manipulators, AC drives, AC-DC and DC-DC converters, etc.

Appendix A

Extension of Discrete-Time SMC to Terminal Sliding Mode for Motion Control

Abstract

Terminal Sliding Mode (TSM) control is known for its high gain property nearby the vicinity of the equilibrium while retaining reasonably low gain elsewhere. This is desirable in digital implementation where the limited sampling frequency may incur chattering if the controller gain is overly high. In this work we integrate a linear switching surface with a terminal switching surface. The switching surface can be designed according to the precision requirement and for the first time, real-time implementation of TSM is carried out. The analysis and experimental investigation show that the TSMC design outperforms the linear SMC.

A.1 Introduction

Recently, a new technique called terminal sliding mode control has been developed in [4] to achieve finite time convergence of the system dynamics in the terminal sliding mode. In [19]-[20], the first-order terminal sliding mode control technique is developed for the control of a simple second-order nonlinear system and an 4^{th}-order nonlinear rigid robotic manipulator system with the result that the output tracking error can converge to zero in finite time.

Most of the terminal sliding mode approaches have been developed from the continuous-time point of view, [4]-[**?**], however less work exists in the design from the discrete-time point of view. In [16] a continuous-time terminal sliding mode controller is first discretized and then applied to a sampled-data system. While it is possible to achieve acceptable result via this approach it makes more sense if the design was tackled entirely from the discrete-time point of view. This would allow us to gain more insight on the performance and stabilty issues and, thereby, achieve the best possible performance. In this paper, a revised terminal sliding mode control law is developed from the discrete-time point of view. It is shown that the new method can achieve better performance than with the linear SM owing to the high gain property of the terminal sliding mode in the vicinity of the origin. To validate the proposed method experiments are conducted on a piezo motor system.

A.2 Discrete-Time Terminal Sliding Mode Control

In this section we will discuss the design of the tracking controller for the system. The controller will be designed based on an appropriate sliding-surface. Further, the stability conditions of the closed-loop system will be analyzed. The relation between TSMC properties and the closed-loop eigenvalue will be explored.

A.2.1 Controller Design and Stability Analysis

Consider the discrete-time sliding-surface below,

$$\sigma_k = \mathbf{s}\mathbf{e}_k + \beta e_{k-1}^p \tag{A.1}$$

where $\mathbf{e}_k = \begin{bmatrix} e_{1,k} & e_{2,k} \end{bmatrix}^T$, $e_{1,k} = r_k - x_{1,k}$ is the position tracking error, $e_{2,k} = \dot{r}_k - x_{2,k}$ is the velocity tracking error, r_k is an arbitrary time-varying reference, σ_k is the sliding function, and $\mathbf{s}, \beta, p$ are positive design constants. The tracking problem is to force $x_{1,k} \to r_k$. The selection of $p < 1$ guarantees a steeper slope of the sliding surface as the states approach the origin which is desirable as seen in Fig.A.1. Also note that p should be selected as a rational number with odd numerator and denominator to gaurantee that the sign of the error remains intact.

Let us first derive the discrete-time TSMC law by using the concept of equivalent control and discuss the TSMC properties associated with stability.

Theorem 13 *The new TSMC law porposed is*

$$u_k = (\mathbf{s}\boldsymbol{\gamma})^{-1} (\mathbf{s}\mathbf{r}_{k+1} - \mathbf{s}\Phi\mathbf{r}_k + \mathbf{s}\Phi\mathbf{e}_k + \beta e_k^p) - (\mathbf{s}\boldsymbol{\gamma})^{-1}\mathbf{s}\hat{\mathbf{d}}_k \tag{A.2}$$

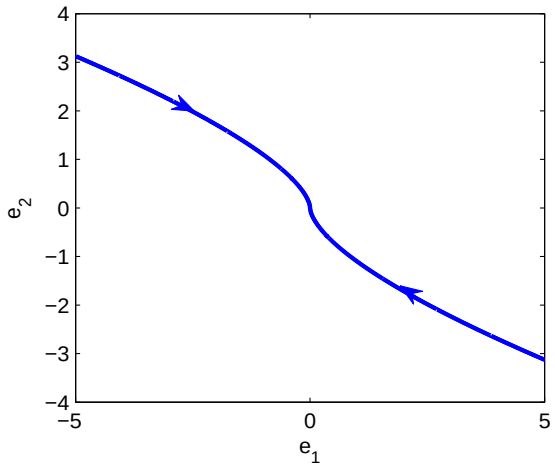

Figure A.1: Phase Portrait of the Sliding Surface

where $\mathbf{r} = \begin{bmatrix} r & \dot{r} \end{bmatrix}^T$ *and* $\hat{\mathbf{d}}$ *is the estimate of the disturbance.*

The controller (A.2) drives the sliding variable to

$$\sigma_{k+1} = \mathbf{s}(\hat{\mathbf{d}}_k - \mathbf{d}_k)$$

and results in the closed-loop error dynamics

$$\mathbf{e}_{k+1} = [\Phi - \boldsymbol{\gamma}(\mathbf{s}\boldsymbol{\gamma})^{-1}\mathbf{s}\Phi]\mathbf{e}_k - \beta(\mathbf{s}\boldsymbol{\gamma})^{-1}e_k^p + \boldsymbol{\delta}_k,$$

where $\boldsymbol{\delta} = \boldsymbol{\gamma}(\mathbf{s}\boldsymbol{\gamma})^{-1}\mathbf{s}\hat{\mathbf{d}}_k - \mathbf{d}_k$ *is due to the disturbance estimation error and is of* $O(T^2)$.

Further, the stable range of closed-loop system is nonlinearly depending on the tracking error e_k.

Proof: The control law (A.2) can be derived using the design method based on equivalent control. To proceed, consider a forward expression of (A.1)

$$\sigma_{k+1} = \mathbf{s}\mathbf{e}_{k+1} + \beta e_k^p. \tag{A.3}$$

The objective of a sliding mode controller is to achieve $\sigma_{k+1} = 0$, therefore, we need to derive an explicit expression in terms of the error dynamics. For this we rewrite the system dynamics (5.6) in terms of the error dynamics. It can be shown that the error dynamics is of the form

$$\mathbf{e}_{k+1} = \Phi \mathbf{e}_k - \boldsymbol{\gamma} u_k - \mathbf{d}_k + \mathbf{r}_{k+1} - \Phi \mathbf{r}_k. \tag{A.4}$$

Substitution of (A.4) into (A.3) and equating the resulting expression of σ_{k+1} to zero we obtain the expression for the equivalent control u_k^{eq},

$$u_k^{eq} = (\mathbf{s}\boldsymbol{\gamma})^{-1} (\mathbf{s}\mathbf{r}_{k+1} - \mathbf{s}\Phi\mathbf{r}_k + \mathbf{s}\Phi\mathbf{e}_k + \beta e_k^p) - (\mathbf{s}\boldsymbol{\gamma})^{-1}\mathbf{s}\mathbf{d}_k. \tag{A.5}$$

Note that the control (A.5) is based the current value of the disturbance $d_{1,k}$ which is unknown and therefore cannot be implemented in this current form. To overcome this, the disturbance will be estimated with the so called delay estimate as follows,

$$\hat{\mathbf{d}}_k = \mathbf{d}_{k-1} = \mathbf{x}_k - \Phi \mathbf{x}_{k-1} - \boldsymbol{\gamma} u_{k-1} \tag{A.6}$$

therefore, the final controller structure is given by

$$u_k = (\mathbf{s}\boldsymbol{\gamma})^{-1} (\mathbf{s}\mathbf{r}_{k+1} - \mathbf{s}\Phi\mathbf{r}_k + \mathbf{s}\Phi\mathbf{e}_k + \beta e_k^p) - (\mathbf{s}\boldsymbol{\gamma})^{-1}\mathbf{s}\hat{\mathbf{d}}_k. \tag{A.7}$$

In order to verify the second part of Theorem 13 with regard to the closed-loop stability, first derive the closed-loop error dynamics. Substitute u_k in (A.2) into (A.4), we obtain

$$\begin{aligned} \mathbf{e}_{k+1} &= \left[\Phi - \boldsymbol{\gamma}(\mathbf{s}\boldsymbol{\gamma})^{-1}\mathbf{s}\Phi\right] \mathbf{e}_k - \beta(\mathbf{s}\boldsymbol{\gamma})^{-1} e_k^p - \mathbf{d}_k \\ &\quad + \boldsymbol{\gamma}(\mathbf{s}\boldsymbol{\gamma})^{-1}\mathbf{s}\hat{\mathbf{d}}_k + (I - \boldsymbol{\gamma}(\mathbf{s}\boldsymbol{\gamma})^{-1}\mathbf{s})(\mathbf{r}_{k+1} - \Phi\mathbf{r}_k). \end{aligned} \tag{A.8}$$

Next, in order to eliminate the term $(I - \boldsymbol{\gamma}(\mathbf{s}\boldsymbol{\gamma})^{-1}\mathbf{s})(\mathbf{r}_{k+1} - \Phi\mathbf{r}_k)$ from the closed-loop dynamics (14), we note that since the objective is to have $\mathbf{x}_k \to \mathbf{r}_k$ then there must exist a control input

$u_{r,k}$ such that $\mathbf{r}_{k+1} = \Phi\mathbf{r}_k + \boldsymbol{\gamma}u_{r,k}$. Thus,

$$(I - \boldsymbol{\gamma}(\mathbf{s}\boldsymbol{\gamma})^{-1}\mathbf{s})(\mathbf{r}_{k+1} - \Phi\mathbf{r}_k) = (I - \boldsymbol{\gamma}(\mathbf{s}\boldsymbol{\gamma})^{-1}\mathbf{s})\boldsymbol{\gamma}u_{r,k} = 0. \tag{A.9}$$

and the final closed-loop error dynamics is

$$\mathbf{e}_{k+1} = [\Phi - \boldsymbol{\gamma}(\mathbf{s}\boldsymbol{\gamma})^{-1}\mathbf{s}\Phi]\mathbf{e}_k - \beta(\mathbf{s}\boldsymbol{\gamma})^{-1}e_k^p + \boldsymbol{\delta}_k \tag{A.10}$$

where $\boldsymbol{\delta}_k = \boldsymbol{\gamma}(\mathbf{s}\boldsymbol{\gamma})^{-1}\mathbf{s}\hat{\mathbf{d}}_k - \mathbf{d}_k$ and is of $O(T^2)$, [**?**]. The sliding surface dynamics is obtained by substituting (A.10) into (A.3) to get

$$\sigma_{k+1} = \mathbf{s}(\hat{\mathbf{d}}_k - \mathbf{d}_k) = \mathbf{s}(\mathbf{d}_{k-1} - \mathbf{d}_k) = O(T^2). \tag{A.11}$$

To evaluate the stable range of (A.10), rewrite (A.10) in the form

$$\mathbf{e}_{k+1} = [\Phi - \boldsymbol{\gamma}(\mathbf{s}\boldsymbol{\gamma})^{-1}\left(\mathbf{s}\Phi + \beta e_k^{p-1}C\right)]\mathbf{e}_k + \boldsymbol{\delta}_k \tag{A.12}$$

where $C = diag(1, 0)$. Denote $\mathbf{l}_k = [l_{1,k}, l_{2,k}] = (\mathbf{s}\boldsymbol{\gamma})^{-1}\left(\mathbf{s}\Phi + \beta e_k^{p-1}C\right)$ the control gain vector, where $l_{1,k}$ is error-dependent. The error dynamics (A.13) can be rewritten as

$$\mathbf{e}_{k+1} = [\Phi - \boldsymbol{\gamma}\mathbf{l}_k]\mathbf{e}_k + \boldsymbol{\delta}_k. \tag{A.13}$$

From (A.13) we see that there must exist certain range for the first element of the gain vector, $l_{1,k}$, such that the closed-loop system is stable. Let $l_{1,min} \leq l_{1,k} \leq l_{1,max}$ where $l_{1,min}$ and $l_{1,max}$ denote the minimum and maximum allowable values for $l_{1,k}$.

From the definition of $\mathbf{l}_k$ we can obtain

$$\beta e_k^{p-1} + s_1\phi_{1,1} + s_2\phi_{2,1} = \mathbf{s}\boldsymbol{\gamma}l_{1,k} \tag{A.14}$$

and

$$s_1\phi_{1,2} + s_2\phi_{2,2} = \mathbf{s}\boldsymbol{\gamma} l_{2,k} \tag{A.15}$$

where $\phi_{i,j}$ are elements of the matrix Φ. From (A.14) we can derive the following inequality

$$\mathbf{s}\boldsymbol{\gamma} l_{1,min} < \beta e_k^{p-1} + s_1\phi_{1,1} + s_2\phi_{2,1} < \mathbf{s}\boldsymbol{\gamma} l_{1,max}, \tag{A.16}$$

from which we can obtain, when $p < 1$,

$$\begin{aligned} |e_k| &> \left(\frac{\beta}{\mathbf{s}\boldsymbol{\gamma} l_{1,max} - s_1\phi_{1,1} - s_2\phi_{2,1}}\right)^{\frac{1}{1-p}} \\ |e_k| &< \left(\frac{\beta}{\mathbf{s}\boldsymbol{\gamma} l_{1,min} - s_1\phi_{1,1} - s_2\phi_{2,1}}\right)^{\frac{1}{1-p}} \end{aligned} \tag{A.17}$$

The first relation gives the minimum-bound of the error and the second relation gives the stable operation range. Note, that by selecting a proper s_1 and s_2 such that the denominator in the second relation is zero for a non-zero β then it is possible to guarantee global stabilty outside of the minimum-error bound. ■

A.2.2 TSMC Tracking Properties

First derive the ultimate tracking error bound of (5.1) when the proposed discrete-time TSMC is applied. Using the discrete-time TSMC law (A.2), in the following we show that the ultimate bound of the tracking error is $O(T^2)$. From the previous subsection we obtained a minimum error bound based on the selection of β which if selected small enough would result in a small error bound.

However, due to the existence of a disturbance term $\boldsymbol{\delta}_k$ the ultimate error bound may be

large. Note that the solution of the closed-loop system (A.13) is

$$\mathbf{e}_k = \left(\Pi_{i=0}^{k}[\Phi - \boldsymbol{\gamma}\mathbf{l}_i]\right)\mathbf{e}_0 + \sum_{i=0}^{k-1}\left(\Pi_{j=0}^{i}[\Phi - \boldsymbol{\gamma}\mathbf{l}_j]\right)\boldsymbol{\delta}_{k-i-1}. \tag{A.18}$$

According to [27] the ultimate error bound would be an order higher than $\boldsymbol{\delta}_k$, which means that the error bound will be $O(T)$. This property holds if the gain $\mathbf{l}_k$ constant and the term $\left(\Pi_{j=0}^{i}[\Phi - \boldsymbol{\gamma}\mathbf{l}_j]\right)\boldsymbol{\delta}_{k-i-1}$ is an infinite series. According to [27], the series will be of the order $O\left(\frac{1}{1-\lambda_{max}}\right)\cdot O\left(\boldsymbol{\delta}\right)$ where λ_{max} is the dominant eigenvalue. Therefore, if the dominant eigenvalue is designed close to the edge of the unit disc, then $O\left(\frac{1}{1-\lambda_{max}}\right) = O(T^{-1})$. This implies a rather bad rejection of the exogenous disturbance. To enhance disturbance rejection, it is desirable to choose the dominant eigenvalue closer to the origin during steady state motion, then $O\left(\frac{1}{1-\lambda_{max}}\right) = O(1)$ and

$$O\left(\frac{1}{1-\lambda_{max}}\right)\cdot O\left(\boldsymbol{\delta}\right) = O\left(\boldsymbol{\delta}\right) = O(T^2). \tag{A.19}$$

However, in practical consideration of sampled-data processes during transient motion, an eigenvalue closer to the origin will result in large initial control effort of the order $O\left(\frac{1}{1-\lambda_{max}}\right) = O(T^{-1})$.

A very useful property that is acquired by using the terminal switching surface is that the system gain $l_{1,k}$ will increase as the error approaches zero because of the nonlinear term e_k^{1-p} in $\mathbf{l}_k$. This means that it is possible to move the dominant eigenvule of the closed-loop system from an initial position nearby the unity disc towards the origin, thus avoid the large initial control effort during the transient period, obtain very stable operation at steady state, and quickly attentuate exogenous disturbances. We will explore more about this property in the

next section.

Finally, we look at what happens to the tracking error when there is a discontinuity in the disturbance. Consider the disturbance term associated with the closed-loop system (A.13). It can be reasonably assumed that the discontinuity occurs rarely, therefore, if we assume that the discontinuity occurs at the kth sampling point, then $\boldsymbol{\delta}_k = O(T)$ rather than $O(T^2)$ as the difference $\mathbf{d}_{k-1} - \mathbf{d}_k$ will no longer be $O(T^2)$ but of the order of $\mathbf{d}_k$ which is $O(T)$. If the discontinuity occurs at a time instance k', then $\boldsymbol{\delta}_k = O(T)$ at $k = k', k'+1, k'+2$, and return to $\boldsymbol{\delta}_k = O(T^2)$ for subsequent sampling instances. Therefore the solution of (A.13) would lead to the worst case error bound

$$|e_k| = O(T) \tag{A.20}$$

for certain time interval but $O(T^2)$ ultimately.

A.2.3 Determination of Controller Parameters

To proceed with the implementation, three control parameters need to be designed: the vector $\mathbf{s}$, the parameter β, and the power p. As was discussed earlier the parameters p and β determine the dynamics of the eigenvalue and this can be seen from Fig.A.2 – Fig.A.5. We can see from these figures, since e_1 leads to high gain feedback, both closed-loop eigenvalues of the discrete-time TSMC will eventually exceed unity and become unstable when e_1 is sufficiently small. This is consistent with the discussion made in previous section that there exists a minimu-bound of tracking error specified by (A.17). From the eigenvalue figures it is clear that the minimum error bound is determined by a critical value of e_1 where at least one

eigenvalue becomes marginal stable. The minimum error bound can be reduced by shifting the curves of eigenvalues leftwards. As shown in Fig.A.2 – Fig.A.5, this can be achieved by either reducing β or increasing p. However, a smaller β implies a smaller range of stability as shown in (A.17). Therefore in TSMC design, a relatively larger p is preferred.

From Fig.A.2 and Fig.A.4, the first eigenvalue, λ_1, is always near unity when the error e_1 is large. Hence this eigenvalue does not generate large inital control efforts, but may generate large steady state error in the presence of disturbance if the eigenvalue does not decrease with respect to error. By incorporating TSM, λ_1 will first drop when e_1 decreases, then rise when e_1 further decreases. A smaller β and a larger p will speed up this variation pattern as e_1 decreases.

The variation pattern of the second eigenvalue, λ_2, is opposite to the first eigenvalue as can be seen from Fig.A.3 and Fig.A.5.

For the system $\mathbf{e}_{k+1} = [\Phi - \boldsymbol{\gamma}\mathbf{l}_k]\mathbf{e}_k$ the solution is $\mathbf{e}_k = V diag(\lambda_1^k, 0)V^{-1}\mathbf{e}_0$ where the matrix V consists of the eigenvectors of $[\Phi - \boldsymbol{\gamma}\mathbf{l}_k]$. This leads us to conclude that the control law (A.7) is proportional to V^{-1} which is a function of λ_1 and will take large values as λ_1 moves towards 0. Thus, it is desirable to have λ_1 closer to the edge of the unit disk so that V^{-1} does not take large values. This is evident from Fig.A.8 and Fig.A.9 where the controller gains, at the initial time step of $k = 1$, $(\mathbf{s}\boldsymbol{\gamma})^{-1}\mathbf{s}\Phi V diag(\lambda_1, 0)V^{-1}$ was plotted w.r.t λ_1. Note, that the nonlinear term βe_k^p has been disregarded as its contribution at the initial time step is neglegible w.r.t the linear term.

Based on the above dicussions the design guideline for discrete TSMC is determined. The

controller gains $\mathbf{l}_k$ can be determined according to the selection of closed-loop eigenvalues. Note that th eigenvalue λ_1 should take a larger value initially and drop when approaching steady state. Thus we can choose λ_1 varying from the initial value 0.995 to the final 0. The other eigenvalue is $\lambda_2 = 0$ when the closed-loop system is in sliding mode. A functions of eigenvalues, the range of the feedback gain vectors can be calculated as $[894,\ 155] \leq \mathbf{l}_k \leq [1.79, \times 10^5\ 240]$.

Next, from relations (17) and (19) we can obtain $\mathbf{s}$, β, and p. The selected $\mathbf{s}$ should ensure that the denominator of the second expression in (19) is close to zero so that the upper limit of e_k is maximized, and at the same time (17) should be satisfied for the given range of l_2. It is not necessary to select $\mathbf{s}$ to make the upper bound on e_1 infinite, as the real system has a maximum displacement limitation of $60 \times 10^{-3} m$. Thus, we select the denominator to take a value of 0.01 and select $l_2 = 200$ from the specified range of l_2. Solving the two simultaneous equations (17) and the denominator of the second expression in (19) being zero for s_1 and s_2 gives $\mathbf{s} = [0.49,\ 0.100]$.

To determine the parameters β and p, firtst look into the relations between these two parameters and the closed-loop eigenvalues. The behavior of the eigenvalues under these parameters are shown in Fig.A.6 and Fig.A.7. It is possible to divide the plots into three regions in which the system has different behaviors. The transient response region is the region in which the error is large enough and the dominant eigenvalue, λ_1, remains close to the edge of the unit disc. As a result, the control effort can be kept at appropriate level despite any large initial error. At this region, disturbance rejection is not a main concern as an $O(T)$

or $O(T^2)$ disturbance would be much smaller than the state errors.

The disturbance rejection region is when the state errors become smaller, reaching $O(T)$ or $O(T^2)$ level. Now, since the eigenvalue also becomes smaller as the controller gain increases, the robustness and disturbance rejection property of the system are enhanced. Finally, the minimum error region is the region in which the eigenvalue goes beyond the unit disc. Therefore, the error will stay around the boundary between the disturbance rejection region and the minimum error region, and the boundary determines the minimum error bound.

Based on the above discussions, from Fig.A.2 and Fig.A.4 it can be see that a larger $\beta = 1$ would lead to a faster response because the dominant eigenvalue, λ_1 , drops quickly in the transient response region. However, it may also lead to a larger steady state error because λ_1 rises quickly and produces a rahter large minimum error region. When smaller $\beta = 0.1$ is used, we can achieve a much smaller minimum error region, but $\lambda_1$drops slowly in the transient response region. In the real-time implemetation, we choose a mid value $\beta = 0.5$ as a tradeoff.

Looking into Fig.A.3 and Fig.A.5, we can obsever that the variation of p will produce the similar trend as β. Namely, when p is close to 0, the transient response region is improved but the minimum error regin is larger. When p is approaching 1, on the other hand, the transient response is slower as the dominant eigenvalue λ_1 drops slowly, but the minimum error regin is getting smaller. In the real-time implemetation, we choose a mid value $p = \frac{5}{9}$ as a tradeoff.

It should also be noted that, in the real-time implementation, the presence of the disturbance will limit the best possible tracking error e_1 to $O(T^2)$ or $O(10^{-6})$ for a smapling perid of 1-ms. Therefore, any selection of larger p and smaller β which result in the minimum tracking

region below $O(T^2)$ would lead to little or no improvements.

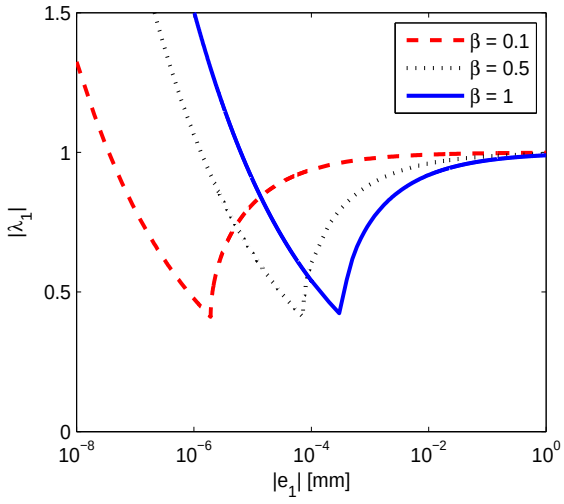

Figure A.2: System eigenvalue λ_1 w.r.t e_1 for different choices of β and $p = \frac{5}{9}$

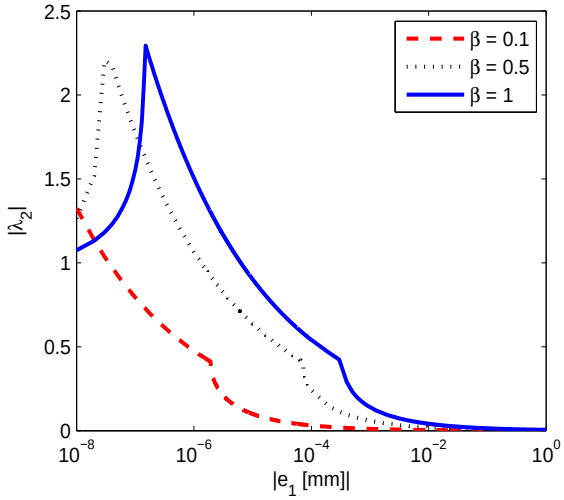

Figure A.3: System eigenvalue λ_2 w.r.t e_1 for different choices of β and $p = \frac{5}{9}$

The reference trajectory designed for the experiment, r_k, is shown in Fig.A.10. For comparison purpose, a PI control is also applied to the piezo motor and PI gains were optimized through intensive tests. The PI gains are at $k_p = 1.5$ and $k_i = 55$. To verify that the PI gains used are optimally tuned, PI gains are made to vary from their optimal values by $\pm 20\%$.

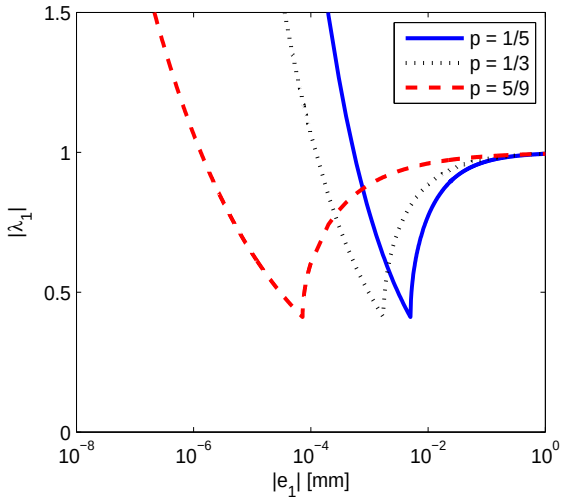

Figure A.4: System eigenvalue λ_1 w.r.t e_1 for different choices of p and $\beta = 0.5$

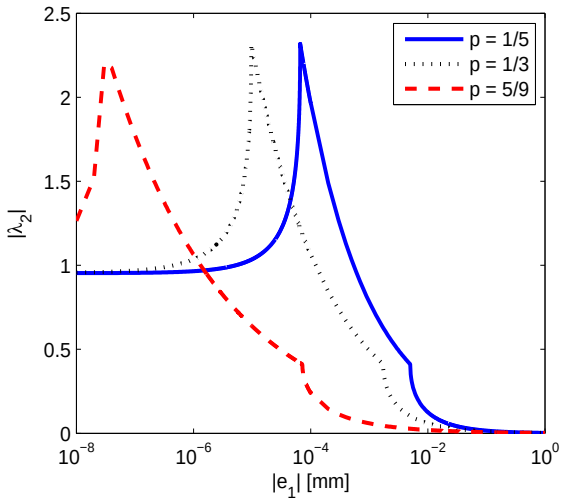

Figure A.5: System eigenvalue λ_2 w.r.t e_1 for different choices of p and $\beta = 0.5$

The optimally tuned PI gains can be determined when other PI values either produce larger tracking errors or lead to oscillatory responses.

A.2.4 Experimental Results and Discussions

In this work, the TSMC is designed in discrete-time, but the real plant is analog in nature. TSMC is applied with the sampling period of $1ms$. The tracking errors of both TSMC and PI

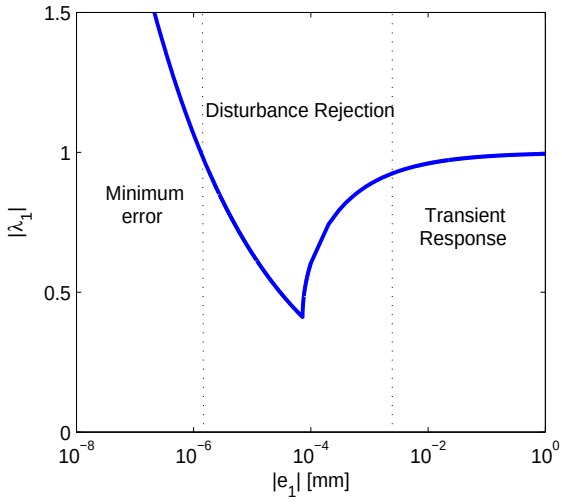

Figure A.6: System eigenvalue λ_1 w.r.t e_1

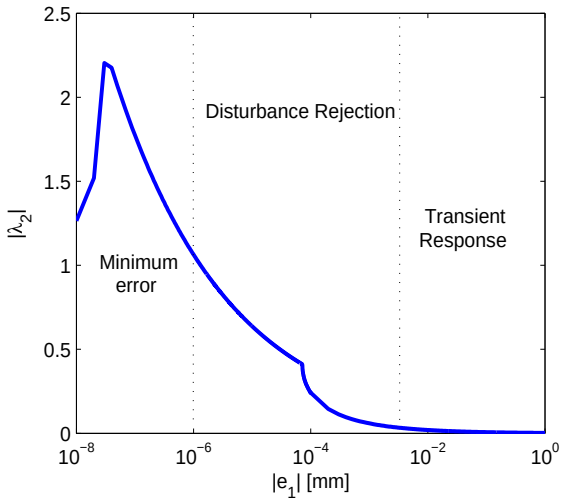

Figure A.7: System eigenvalue λ_2 w.r.t e_1

controllers are shown in Fig.A.11. It can be seen that the tracking performance of the TSMC is far better. Fig.A.12 shows the control signals of TSMC and PI. In Fig.A.13 the reference velocity and the state x_2 are plotted. It is clearly seen that the velocity tracking is very good with minimal chattering. It is well known that sliding mode control requires a fast switching frequency in order to maintain the sliding motion. The proposed TSMC however does not produce much chattering though with the limited sampling frequency.

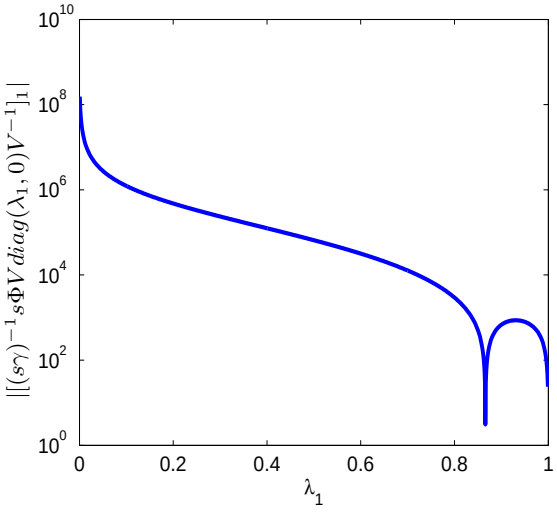

Figure A.8: First element of the system gain $(\mathbf{s}\boldsymbol{\gamma})^{-1}\mathbf{s}\Phi V diag(\lambda_1, 0)V^{-1}$ w.r.t λ_1

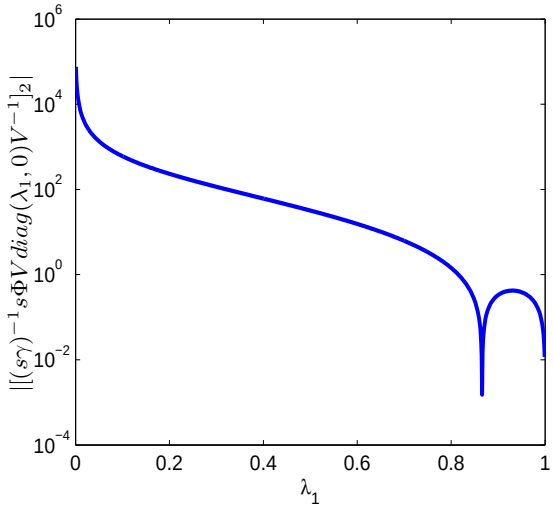

Figure A.9: Second element of the system gain $(\mathbf{s}\boldsymbol{\gamma})^{-1}\mathbf{s}\Phi V diag(\lambda_1, 0)V^{-1}$ w.r.t λ_1

Finally, it is also interesting to check the tracking error bound according to the theoretical analysis and experimental result. Through analysis we have shown the tracking error bound is proportional to the size of the sampling period T. Therefore, we can expect a smooth control response and low tracking error when the sampling period is $1ms$. The magnitude of the tracking error obtained in experiment, as shown in Fig.A.11, is at the scale of 8×10^{-6}, which

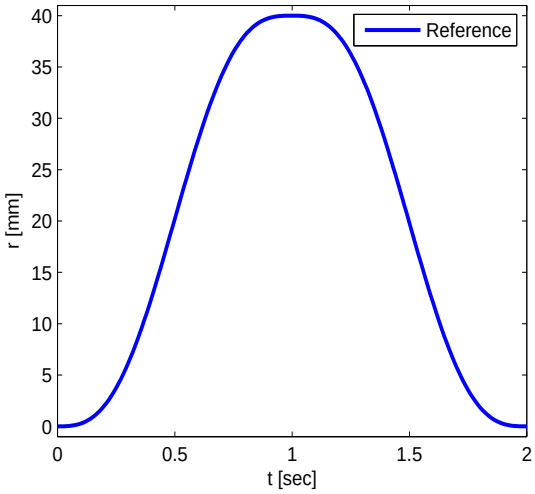

Figure A.10: The reference trajectory

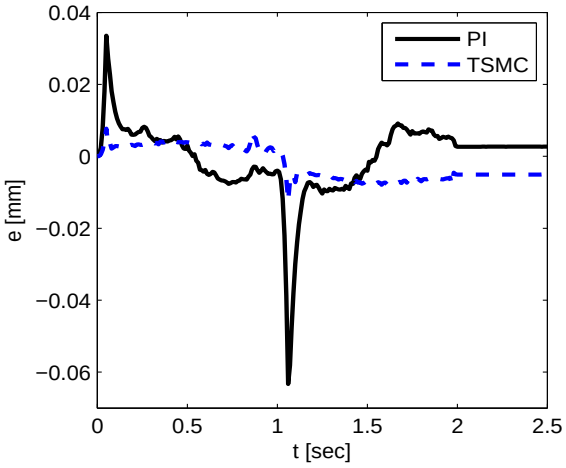

Figure A.11: Tracking error of TSMC and PI control

is consistent with the theoretical error bound of $O(T^2) = O(0.001^2) = O(10^{-6})$.

A.3 Conclusion

This work presents a revised TSM controller based on a linear SM combined with a TSM designed from the discrete-time point of view. Theoretical investigation shows that the revised controller can achieve very good performace. For the first time in this particular area of

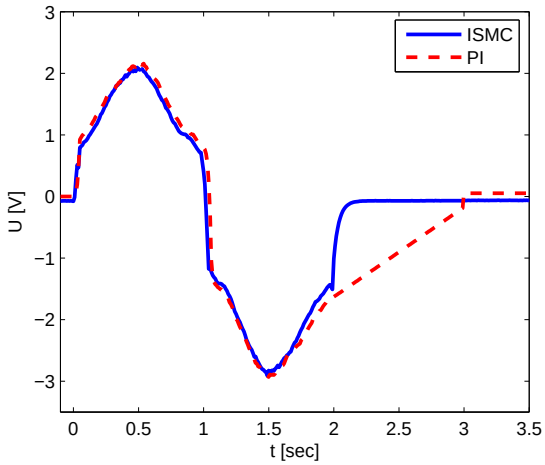

Figure A.12: Comparison of the control inputs of TSMC and PI controllers

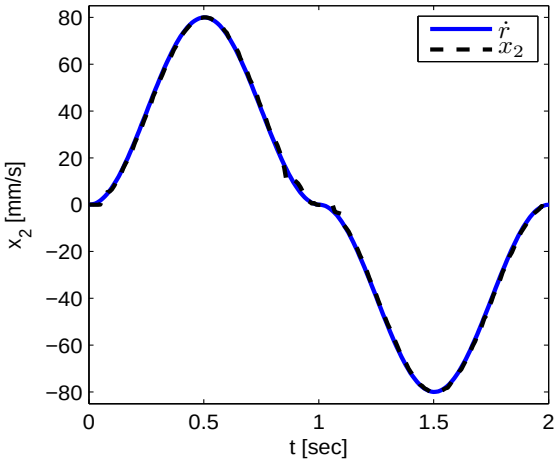

Figure A.13: State x_2 and reference velocity $\dot{r}$

TSMC, a real-time TSMC is implemented. Experimental results on a piezo motor verifies the effectiveness of the proposed control method that achieves a precision level upto micrometers.

Appendix B

Proof of Lemma 1

Consider the Taylor's series expansion of $\mathbf{f}((k+1)T-\tau)$

$$\mathbf{f}(kT+T-\tau)=\mathbf{f}_k+\mathbf{v}_k(T-\tau)+\frac{1}{2!}\mathbf{w}_k(T-\tau)^2+\cdots=\mathbf{f}_k+\mathbf{v}_k(T-\tau)+\boldsymbol{\xi}(T-\tau)^2 \quad \text{(B.1)}$$

where $\mathbf{v}(t)=\frac{d}{dt}\mathbf{f}(t)$, $\mathbf{w}(t)=\frac{d^2}{dt^2}\mathbf{f}(t)$ and $\boldsymbol{\xi}=\frac{1}{2!}\mathbf{w}(\mu)$ and μ is a time value between kT and $(k+1)T$, [29]. Substituting (B.1) into the expression of $\mathbf{d}_k$

$$\mathbf{d}_k=\int_0^T e^{A\tau}\mathbf{B}\mathbf{f}_k d\tau+\int_0^T e^{A\tau}B\mathbf{v}_k(T-\tau)d\tau+\int_0^T e^{A\tau}B\boldsymbol{\xi}(T-\tau)^2 d\tau. \quad \text{(B.2)}$$

For clarity, each integral will be analyzed separately. Since $\mathbf{f}_k$ is independent of τ it can be taken out of the first integral

$$\int_0^T e^{A\tau}B\mathbf{f}_k d\tau=\int_0^T e^{A\tau}Bd\tau\mathbf{f}_k=\Gamma\mathbf{f}_k. \quad \text{(B.3)}$$

In order to solve the second integral term, it is necessary to expand $e^{A\tau}$ into series form. Thus,

$$\int_0^T e^{A\tau}B\mathbf{v}_k(T-\tau)d\tau=\int_0^T\left[e^{A\tau}B-\left(B+AB\tau+\frac{1}{2!}A^2B\tau^2+\cdots\right)\tau\right]d\tau\mathbf{v}_k. \quad \text{(B.4)}$$

Solving the integral leads to

$$\int_0^T e^{A\tau}B\mathbf{v}_k(T-\tau)d\tau=\left[\Gamma-\left(\frac{1}{2!}BT+\frac{1}{3!}ABT^2+\cdots\right)\right]T\mathbf{v}_k. \quad \text{(B.5)}$$

Simplifying the result with the aid of (2.3)

$$\int_0^T e^{A\tau} B\mathbf{v}_k(T-\tau)d\tau = \left[\Gamma - \frac{1}{2}\Gamma + \frac{1}{2}MT^2 - \left(\frac{1}{3!}ABT^2 + \frac{1}{4!}A^2BT^2 + \cdots\right)\right] T\mathbf{v}_k. \quad \text{(B.6)}$$

Simplifying the above expression further

$$\int_0^T e^{A\tau} B\mathbf{v}_k(T-\tau)d\tau = \frac{1}{2}\Gamma\mathbf{v}_k T + \hat{M}\mathbf{v}_k T^3 \quad \text{(B.7)}$$

where $\hat{M}$ is a constant matrix. Finally, note that in (B.2) the third integral is $O(T^3)$, since, the term inside the integral is already $O(T^2)$, therefore

$$\int_0^T e^{A\tau} B\boldsymbol{\xi}(T-\tau)^2 d\tau = O(T^3). \quad \text{(B.8)}$$

Thus, combining (B.3), (B.6) and (B.8) leads to

$$\mathbf{d}_k = \Gamma\mathbf{f}_k + \frac{1}{2}\Gamma\mathbf{v}_k T + \hat{M}T^3\mathbf{v}_k + O(T^3) = \Gamma\mathbf{f}_k + \frac{1}{2}\Gamma\mathbf{v}_k T + O(T^3). \quad \text{(B.9)}$$

Now evaluate

$$\mathbf{d}_k - \mathbf{d}_{k-1} = \Gamma(\mathbf{f}_k - \mathbf{f}_{k-1}) + \frac{1}{2}\Gamma(\mathbf{v}_k - \mathbf{v}_{k-1})T + O(T^3). \quad \text{(B.10)}$$

From (B.1) and letting $\tau = 0$, $\mathbf{f}_k - \mathbf{f}_{k-1} \in O(T)$. From (2.3), $\Gamma \in O(T)$. In the sequel $\mathbf{d}_k - \mathbf{d}_{k-1} \in O(T^2)$, if the assumptions on the boundedness and smoothness of $\mathbf{f}(t)$ hold. Finally, we notice that (B.10) is the difference of the first order approximation, whereas

$$\mathbf{d}_k - 2\mathbf{d}_{k-1} + \mathbf{d}_{k-2} = \Gamma(\mathbf{f}_k - 2\mathbf{f}_{k-1} + \mathbf{f}_{k-2}) + \frac{1}{2}\Gamma(\mathbf{v}_k - 2\mathbf{v}_{k-1} + \mathbf{v}_{k-2}) + O(T^3)$$

is the difference of the second order approximation. Accordingly the magnitude of $\mathbf{d}_k - 2\mathbf{d}_{k-1} + \mathbf{d}_{k-2}$ is $O(T^3)$, [29].

Proof of Lemma 2: If the matrices Φ, Γ and C are partitioned as shown

$$\Phi = \begin{bmatrix} \Phi_{11} & \Phi_{12} \\ \Phi_{21} & \Phi_{22} \end{bmatrix}$$

$$C = \begin{bmatrix} C_1 & C_2 \end{bmatrix}$$

$$\Gamma = \begin{bmatrix} \Gamma_1 \\ \Gamma_2 \end{bmatrix}$$

where $(\Phi_{11}, C_1, \Gamma_1) \in \Re^{m\times m}$, $(\Phi_{12}, C_2) \in \Re^{m\times n-m}$, $(\Phi_{21}, \Gamma_2) \in \Re^{n-m\times m}$ and $\Phi_{22} \in \Re^{n-m\times n-m}$. The eigenvalues of $[\Phi - \Gamma(C\Gamma)^{-1}(C\Phi - \Lambda C)]$ is found from

$$\det\left[\lambda I_n - \Phi + \Gamma(C\Gamma)^{-1}(C\Phi - \Lambda C)\right] = 0 \tag{B.11}$$

$$\det\begin{bmatrix} \lambda I - \Phi_{11} + \Gamma_1(C\Gamma)^{-1}\left(C\begin{bmatrix}\Phi_{11}\\ \Phi_{21}\end{bmatrix} - \Lambda C_1\right) & -\Phi_{12} + \Gamma_1(C\Gamma)^{-1}\left(C\begin{bmatrix}\Phi_{12}\\ \Phi_{22}\end{bmatrix} - \Lambda C_2\right) \\ -\Phi_{21} + \Gamma_2(C\Gamma)^{-1}\left(C\begin{bmatrix}\Phi_{11}\\ \Phi_{21}\end{bmatrix} - \Lambda C_1\right) & \lambda I - \Phi_{22} + \Gamma_2(C\Gamma)^{-1}\left(C\begin{bmatrix}\Phi_{12}\\ \Phi_{22}\end{bmatrix} - \Lambda C_2\right) \end{bmatrix} = 0 \tag{B.12}$$

If the top row is premultiplied with C_1 and the bottom row is premultiplied with C_2 and the the results summed and used as the new top row, using the fact that $C_1\Gamma_1 + C_2\Gamma_2 = C\Gamma$ the following is obtained

$$\det\begin{bmatrix} (\lambda I_m - \Lambda)C_1 & (\lambda I_m - \Lambda)C_2 \\ -\Phi_{21} + \Gamma_2(C\Gamma)^{-1}\left(C\begin{bmatrix}\Phi_{11}\\ \Phi_{21}\end{bmatrix} - \Lambda C_1\right) & \lambda I - \Phi_{22} + \Gamma_2(C\Gamma)^{-1}\left(C\begin{bmatrix}\Phi_{12}\\ \Phi_{22}\end{bmatrix} - \Lambda C_2\right) \end{bmatrix} = 0 \tag{B.13}$$

factoring the term $(\lambda I_m - \Lambda)$ and premultipying the top row with $\Gamma_2(C\Gamma)^{-1}\Lambda$ and adding to

the bottom row leads to

$$\det(\lambda I_m - \Lambda)\det\begin{bmatrix} C_1 & C_2 \\ -\Phi_{21} + \Gamma_2(C\Gamma)^{-1}C\begin{bmatrix}\Phi_{11}\\ \Phi_{21}\end{bmatrix} & \lambda I_{n-m} - \Phi_{22} + \Gamma_2(C\Gamma)^{-1}C\begin{bmatrix}\Phi_{12}\\ \Phi_{22}\end{bmatrix}\end{bmatrix} = 0 \tag{B.14}$$

Thus, we can conclude that m eigenvalues of $[\Phi - \Gamma(C\Gamma)^{-1}(C\Phi - \Lambda C)]$ are the eigenvlaues of Λ. Now, consider

$$\det\begin{bmatrix} C_1 & C_2 \\ -\Phi_{21} + \Gamma_2(C\Gamma)^{-1}C\begin{bmatrix}\Phi_{11}\\ \Phi_{21}\end{bmatrix} & \lambda I_{n-m} - \Phi_{22} + \Gamma_2(C\Gamma)^{-1}C\begin{bmatrix}\Phi_{12}\\ \Phi_{22}\end{bmatrix}\end{bmatrix} = 0 \tag{B.15}$$

Using the following relations

$$C_2\Phi_{21} - C_2\Gamma_2(C\Gamma)^{-1}C\begin{bmatrix}\Phi_{11}\\ \Phi_{21}\end{bmatrix} = -C_1\Phi_{11} + C_1\Gamma_1(C\Gamma)^{-1}C\begin{bmatrix}\Phi_{11}\\ \Phi_{21}\end{bmatrix} \tag{B.16}$$

$$-C_2\Phi_{22} + C_2\Gamma_2(C\Gamma)^{-1}C\begin{bmatrix}\Phi_{12}\\ \Phi_{22}\end{bmatrix} = -C_1\Phi_{12} + C_1\Gamma_1(C\Gamma)^{-1}C\begin{bmatrix}\Phi_{12}\\ \Phi_{22}\end{bmatrix} \tag{B.17}$$

Multiplying (B.15) with $\lambda^{-m}\lambda^m$ we get

$$\lambda^{-m}\det\begin{bmatrix} \lambda C_1 & \lambda C_2 \\ -\Phi_{21} + \Gamma_2(C\Gamma)^{-1}C\begin{bmatrix}\Phi_{11}\\ \Phi_{21}\end{bmatrix} & \lambda I_{n-m} - \Phi_{22} + \Gamma_2(C\Gamma)^{-1}C\begin{bmatrix}\Phi_{12}\\ \Phi_{22}\end{bmatrix}\end{bmatrix} = 0 \tag{B.18}$$

Premultiplying the bottom row with C_2 and subtracting from the top row and using the result as the new top row we get

$$\lambda^{-m}\det\begin{bmatrix} \lambda C_1 + C_2\Phi_{21} - C_2\Gamma_2(C\Gamma)^{-1}C\begin{bmatrix}\Phi_{11}\\ \Phi_{21}\end{bmatrix} & C_2\Phi_{22} - C_2\Gamma_2(C\Gamma)^{-1}C\begin{bmatrix}\Phi_{12}\\ \Phi_{22}\end{bmatrix} \\ -\Phi_{21} + \Gamma_2(C\Gamma)^{-1}C\begin{bmatrix}\Phi_{11}\\ \Phi_{21}\end{bmatrix} & \lambda I_{n-m} - \Phi_{22} + \Gamma_2(C\Gamma)^{-1}C\begin{bmatrix}\Phi_{12}\\ \Phi_{22}\end{bmatrix}\end{bmatrix} = 0 \tag{B.19}$$

using relations (B.16) and (B.17) we finally get

$$\lambda^{-m}\det\begin{bmatrix} \lambda C_1 - C_1\Phi_{11} + C_1\Gamma_1(C\Gamma)^{-1}C\begin{bmatrix}\Phi_{11}\\ \Phi_{21}\end{bmatrix} & -C_1\Phi_{12} + C_1\Gamma_1(C\Gamma)^{-1}C\begin{bmatrix}\Phi_{12}\\ \Phi_{22}\end{bmatrix} \\ -\Phi_{21} + \Gamma_2(C\Gamma)^{-1}C\begin{bmatrix}\Phi_{11}\\ \Phi_{21}\end{bmatrix} & \lambda I_{n-m} - \Phi_{22} + \Gamma_2(C\Gamma)^{-1}C\begin{bmatrix}\Phi_{12}\\ \Phi_{22}\end{bmatrix} \end{bmatrix} = 0 \tag{B.20}$$

We can factor out the matrix C_1 from the top row to get

$$\lambda^{-m}\det(C_1)\det\begin{bmatrix} \lambda I_m - \Phi_{11} + \Gamma_1(C\Gamma)^{-1}C\begin{bmatrix}\Phi_{11}\\ \Phi_{21}\end{bmatrix} & -\Phi_{12} + \Gamma_1(C\Gamma)^{-1}C\begin{bmatrix}\Phi_{12}\\ \Phi_{22}\end{bmatrix} \\ -\Phi_{21} + \Gamma_2(C\Gamma)^{-1}C\begin{bmatrix}\Phi_{11}\\ \Phi_{21}\end{bmatrix} & \lambda I_{n-m} - \Phi_{22} + \Gamma_2(C\Gamma)^{-1}C\begin{bmatrix}\Phi_{12}\\ \Phi_{22}\end{bmatrix} \end{bmatrix} = 0 \tag{B.21}$$

which finally simplifies to

$$\lambda^{-m}\det(C_1)\det\left[\Phi - \Gamma(C\Gamma)C\Phi\right] = 0 \tag{B.22}$$

It is well known that $[\Phi - \Gamma(C\Gamma)C\Phi]$ has atleast m zero eigenvlaues which would be cancelled out by λ^{-m} and, thus, we finally conclude that the eigenvalues of $[\Phi - \Gamma(C\Gamma)^{-1}(C\Phi - \Lambda C)]$ are the eigenvalues of Λ and the non-zero eigenvlaues of $[\Phi - \Gamma(C\Gamma)C\Phi]$.

Details of Papers

Journal Papers

Abidi K., Xu J.-X., and She J.-H., "A Discrete-Time Terminal Sliding Mode Control Approach Applied to a Motion Control Problem," Accepted for publication in IEEE Transactions on Industrial Electronics.

Xu J.-X, Abidi K., "Discrete-Time Output Integral Sliding Mode Control for a Piezo-Motor Driven Linear Motion Stage," Accepted for publication in IEEE Transactions on Industrial Electronics.

Abidi K., Xu J.-X, "A Discrete-Time Periodic Adaptive Control Approach for Time-Varying Parameters with Known Periodicity," IEEE Transactions on Automatic Control, Vol. 53, No. 2, pp. 575-581, March 2008.

Abidi K., Xu J.-X, Yu Xinghuo, "On the Discrete-Time Integral sliding Mode Control," IEEE Transactions on Automatic Control, Vol. 52, No. 4, pp. 709-715, April 2007.

Conference Papers

Kai-Yew Lum, Jian-Xin Xu, Khalid Abidi, and Jing Xu, "Sliding Mode Guidance Law for De-

layed LOS Rate Measurement," Proceedings of the AIAA Guidance, Navigation and Control Conference and Exhibit, 18 - 21 August 2008, Honolulu, Hawaii

Khalid Abidi, Jian-Xin Xu, "A Discrete-Time Periodic Adaptive Control Approach for Time-Varying Parameters with Known Periodicity", *9th IEEE International Workshop on Advanced Motion Control*, March, 2006, Turkey.

Khalid Abidi, Jian-Xin Xu, Yu Xinghuo, "On the Discrete-Time Integral Sliding Mode Control", *International Workshop on Variable Structure Systems - VSS'06*, June, 2006, Italy.

Book Chapter

Xu J.-X, Abidi K., "Output Tracking with Discrete-Time Integral Sliding Mode Control," In Modern Sliding Mode Control Theory, Vol. 375, Springer Berlin/Heidelberg, 2008.

Bibliography

[1] D. S. Naidu, *Optimal control systems.* CRC Press, 2003.

[2] C. Fargeon and C. Castel, *The Digital control of systems: applications to vehicles and robots.* North Oxford Academic, 1989.

[3] I. J. Nagrath, *Control Systems Engineering.* New Age International, 2006.

[4] W. C. Su, S. Drakunov and U. Ozguner, "An $O(T^2)$ boundary layer in sliding mode for sampled-data systems", *IEEE Transactions on Automatic Control*, vol. 45, no. 3, pp. 482-485, 2000.

[5] V. Utkin, "Sliding mode control in discrete-time and difference systems", In Variable Structure and Lyapunov Control, Chapter 5, Editted by A.S.I. Zinober, Springer-Verlag, 193, pp. 87-107, 1994.

[6] J. X. Xu, "A new adaptive control approach for time-varying parameters with known periodicity", *IEEE Transactions on Automatic Control*, vol. 49, no. 4, pp. 579-583, 2004.

[7] R. H. Middleton and G. G. C. Goodwin, "Adaptive control of time-varying linear systems," *IEEE Transactions on Automatic Control*, vol. 33, pp. 150-155, 1988.

[8] A. M. Annaswamy and K. S. Narendra, "Adaptive control of simple time-varying systems," presented at the *IEEE Conference on Decision and Control*, Tampa, FL, Dec. 1989.

[9] F. M. M. Giri, L. Dugard, and J. M. Dion, "Pole placement direct adaptive control for time-varying ill-modeled plants," *IEEE Transactions on Automatic Control*, vol. 35, pp. 723-726, June 1990.

[10] K. S. Tsakalis and P. A. Ioannou, *Linear Time-Varying Systems Control and Adaptation.* Upper Saddle River, NJ: Prentice-Hall, 1993.

[11] R. Marino and P. Tomei, "Adaptive control of linear time-varying systems," *Automatica*, vol. 39, pp. 651-659, 2003.

[12] M. Uchiyama, "Formation of high-speed motion pattern of a mechanical arm by trial," *Transactions of the Society of Instrument and Control Engineers*, vol. 14, no. 6, pp. 706-712, 1978.

[13] M. Garden. "Learning control of actuators in control systems," U.S. Patent 3555252, 1971.

[14] X.-G. Yan, C. Edwards, and S. K. Spurgeon, "Output feedback sliding mode control for non-minimum phase systems with non-linear disturbances," *International Journal of Control*, vol. 77, no. 15, pp. 1353-1361, 2004.

[15] W. Gao, Y. Wang, and A. Homaifa, "Discrete-time Variable Structure Control Systems," *IEEE Transactions on Industrial Electronics*, vol. 42, no. 2, pp.117-122, 1995.

[16] G. Golo and C. Milosavljevic, "Robust Discrete-time Chattering Free Sliding Mode Control," *Systems and Control Letters*, vol. 41, no. 1, pp. 19-28, 2000.

[17] V. Utkin, J. Shi, "Integral sliding mode in systems operating under uncertainty conditions", Proceedings of the *Conference on Decision and Control*, Kobe, Japan, pp. 4591-4596, 1996.

[18] W. J. Cao and J. X. Xu, "Eigenvalue Assignment in Full-Order Sliding Mode Using Integral Type Sliding Surface", *IEEE Transactions on Automatic Control*, Vol.49, no.8, pp. 1355-1360, 2004.

[19] L. Fridman, F. Castanos, N. M'Sirdi N. and Kharfa, "Decomposition and Robustness Properties of Integral Sliding Mode Controllers", Proceedings of the *IEEE VSS* workshop, Spain, 2004.

[20] J. Ackermann, V. Utkin, "Sliding mode control design based on Ackermann's formula", *IEEE Transactions on Automatic Control*, vol. 43, no. 2, pp. 234-237, 1998.

[21] S. H. Zak and S. Hui, "On variable structure output feedback controllers for uncertain dynamical systems," *IEEE Transactions on Automatic Control*, vol. 38, no. 8, 1509-1512, 1993.

[22] R. El-Khazali and R. DeCarlo, "Output feedback variable structure control design," *Automatica*, vol. 31, no. 4, 805-816, 1995.

[23] C. Edwards and S. K. Spurgeon, "Robust output tracking using a sliding-mode controller/observer scheme. *International Journal of Control*, vol. 64, no. 5, 967-983, 1996.

[24] J. J. E. Slotine, J. K. Hedrick and E. A. Misawa, "On sliding observers for nonlinear systems," *Transactions of the ASME: Journal of Dynamic Systems, Measurement and Control*, vol. 109, no. 1, 245-252, 1987.

[25] N. O. Lai, C. Edwards and S. K. Spurgeon, "On discrete time output feedback sliding-mode like control for non-minimum-phase systems. *Proceddings of the 42nd IEEE Conference on Decision and Control*, Hawaii, 1374-1379, 2003.

[26] N. O. Lai, C. Edwards and S. K. Spurgeon, "On discrete time output feedback min-max controller. *International Journal of Control*, vol. 77, no. 2, 554-561, 2004.

[27] K. Abidi and X.J. Xu, "On the discrete-time integral sliding-mode control," *IEEE Transactions on Automatic Control*, vol. 52, no. 4, 709-715, 2007.

[28] cc6) K. J. Åström and B. Wittenmark, *Computer-Controller Systems*, Prentice Hall: Upper Saddle River, NJ, 1997.

[29] S. C. Chapra, R. P. Canale, *Numerical Methods for Engineers*, McGraw Hill, Singapore, 1998.

[30] M. Gafvurt, "Dynamic model based friction compensation on the furuta pendulum," Proceedings of the IEEE International Conference on Control Applications, 1260-1265, 1999.

[31] B. Armstrong-Helouvry, P. Dupont, and C. Canudas De Wit, "A survey of models, analysis tools and compensation methods for the control of machines with friction," *Automatica*, vol. 30, no. 7, 1083-1138, 1994.

[32] K. S. Narendra and A. M. Annaswamy, *Stable Adaptive Systems*. Upper Saddle River, NJ: Prentice-Hall, vol. 3, 1989.

[33] S. S. Sastry and M. Boston, *Adaptive Control: Stability, Convergence and Robustness*. Upper Saddle River, NJ: Prentice-Hall, 1989.

[34] K. P. V. Kokotovic, *Foundations of Adaptive Control*. New York: Springer-Verlag, 1991.

[35] P. A. Ioannou and J. Sun, *Robust Adaptive Control*. Upper Saddle River, NJ: Prentice-Hall, 1969.

[36] G. Feng and R. Lozano, *Adaptive Control Systems*. Oxford, U.K.: Newnes, 1999.

[37] J. X. Xu, S.K. Panda, Y. J. Pan, T. H. Lee and B.H Lam, "A modular control scheme for PMSM speed control with pulsating torque minimization", *IEEE Transactions on Industrial Electronics*, vol. 51, no. 3, pp. 526-536, 2004.

[38] P. R. Pagilla, B. Yu and K. L. Pau, "Adaptive control of time-varying mechanical systems: analysis and experiments", *IEEE/ASME Transactions on Mechatronics*, vol. 5, no. 4, pp. 410-418, 2000.

[39] J. M. Carrasco, E. Galvn, G. E. Valderrama, R. Ortega and A. M. Stankovic, "Analysis and experimentation of nonlinear adaptive controllers for the series resonant converter", *IEEE Transactions on Power Electronics*, vol. 15, no. 3, pp. 536-544, 2000.

[40] K. Kaneko and R. Horowitz, "Repetitive and adaptive control of robot manipulators with velocity estimation", *IEEE Transactions on Robotics and Automation*, vol. 13, no. 2, pp. 204-217, 1997.

[41] Z. Wang, M. M. Polycarpou, J. G. Uber and F. Shang, "Adaptive Control of Water Quality in Water Distribution Networks", *IEEE Transactions on Control Systems Technology*, vol. 14, no. 1, pp. 149-156, 2006.

[42] I. Kanellakopoulos, "A discrete-time adaptive nonlinear system", *IEEE Transactions on Automatic Control*, vol. 39, no. 11, pp. 2362-2365, 1994.

[43] G. C. Goodwin and K. S. Sin, *Adaptive Filtering, Prediction, and Control*. Englewood Cliffs, NJ: Prentice-Hall, 1984.

[44] K.L. Moore, *Iterative Learning Control for Deterministic Systems*, London: Springer-Verlag, 1993.

[45] K.J. Hunt, D. Sbarbaro, R. Zbikowski, and P.J. Gawthrop, "Neural networks for control systemsA survey," *Automatica*, vol. 28, no. 6, pp. 1083-112, 1992.

[46] G. Hillerstrom and K. Walgama, "Repetitive control theory and applications a survey," in the Proceedings of the 13^{th} World Congress Volume D: Control Design II, Optimization, 1997, pp. 1-6.

[47] R.W. Longman, "Iterative learning control and repetitive control for engineering practice," *International Journal of Control*, vol. 73, no. 10, pp. 930-954, 2000.

[48] S. Arimoto, S. Kawamura, and F. Miyazaki, "Bettering operation of robots by learning," *Journal of Robotic Systems*, vol. 1, pp. 123-140, 1984.

[49] D.A. Bristow and A.G. Alleyne, "A manufacturing system for microscale robotic deposition," in the Proceedings of the American Control Conference, 2003, pp. 2620-2625.

[50] H. Elci, R.W. Longman, M. Phan, J.-N. Juang, and R. Ugoletti, "Discrete frequency based learning control for precision motion control," in Proceedings of the IEEE International Conference on Systems, Man, Cybernetics, 1994, pp. 2767-2773.

[51] W. Messner, R. Horowitz, W.-W. Kao, and M. Boals, "A new adaptive learning rule," *IEEE Transactions on Automatic Control*, vol. 36, no. 2, pp. 188-197, 1991.

[52] M. Norrlof, "An adaptive iterative learning control algorithm with experiments on an industrial robot," *IEEE Transactions on Robotics and Automation*, vol. 18, no. 2, pp. 245-251, 2002.

[53] D.-I. Kim and S. Kim,"An iterative learning control method with application for CNC machine tools," *IEEE Transactions Industrial Applications*, vol. 32, no. 1, pp. 66-72, 1996.

[54] D. de Roover and O.H. Bosgra, "Synthesis of robust multivariable iterative learning controllers with application to a wafer stage motion system," *International Journal of Control*, vol. 73, no. 10, pp. 968-979, 2000.

[55] H. Havlicsek and A. Alleyne, "Nonlinear control of an electrohydraulic injection molding machine via iterative adaptive learning," *IEEE/ASME Transactions on Mechatronics*, vol. 4, no. 3, pp. 312-323, 1999.

[56] F. Gao, Y. Yang, and C. Shao, "Robust iterative learning control with applications to injection molding process," *Chemical Engineering Science*, vol. 56, no. 24, pp. 7025-7034, 2001.

[57] 30] J.J. Craig, "Adaptive control of manipulators through repeated trials," in the Proceedings of the American Control Conference, pp. 1566-1573, 1984.

[58] G. Casalino and G. Bartolini, "A learning procedure for the control of movements of robotic manipulators," in the Proceedings of the IASTED Symposium on Robotics and Automation, pp. 108-111, 1984.

[59] S. Kawamura, F. Miyazaki, and S. Arimoto, "Iterative learning control for robotic systems," in the Proceedings of the International Conference on Industrial Electronics, Con-

trol and Instrumentation, pp. 393-398, 1984.

[60] K.L. Moore and J.-X. Xu, "Editorial: Iterative learning control," *International Journal of Control*, vol. 73, no. 10, 2000.

[61] "Iterative learning control" *Asian Journal of Control*, vol. 4, no. 1, 2002.

[62] Z. Bien and J.-X. Xu, *Iterative Learning Control: Analysis, Design, Integration and Applications*. Boston: Kluwer, 1998.

[63] Y. Chen and C. Wen, Iterative Learning Control: Convergence, Robustness, and Applications. London: Springer, 1999.

[64] J.-X. Xu and Y. Tan, *Linear and Nonlinear Iterative Learning Control*. Berlin: Springer, 2003.

[65] K.L. Moore, M. Dahleh, and S.P. Bhattacharyya,"Iterative learning control: A survey and new results," *Journal of Robotic Systems*, vol. 9, no. 5, pp. 563-594, 1992.

[66] R. Horowitz, "Learning control of robot manipulators," *ASME Journal of Dynamic Systems Measurement and Control*, vol. 115, no. 2B, pp. 402-411, 1993.

[67] D.A. Bristow, M. Tharayil, and A.G.Alleyne, "A survey of iterative learning control," *IEEE Control Systems Magazine*, vol. 26, no. 3, pp. 96-114, 2006.

[68] M. Norrlof and S. Gunnarsson, "Time and frequency domain convergence properties in iterative learning control," *International Journal of Control*, vol. 75, no. 14, pp. 1114-1126, 2002.

[69] M. Norrlof and S. Gunnarsson, "Disturbance aspects of iterative learning control," *Engineering Applications of Artificial Intelligence*, vol. 14, no. 1, pp. 87-94, 2001.

[70] J.-X. Xu and K. Abidi, "Discrete-Time Output Integral Sliding-Mode Control for a Piezomotor-Driven Linear Motion Stage," *IEEE Transactions Industrial Applications*, vol. 55, no. 11, pp. 3917-3927, 2008.

[71] E. Holder and V. Sylvester, "An analysis of modern versus classical homing guidance," *IEEE Transactions on Aerospace and Electronic Systems*, vol. 26, no. 4, pp. 599-606, 1990.

[72] K. Becker, "Closed-form solution of pure proportional navigation," *IEEE Transactions on Aerospace and Electronic Systems*, vol. 26, no. 3, pp. 526-533, 1990.

[73] C.-D. Yang and C.-C. Yang, "Analytical solution of 3D true proportional navigation," *IEEE Transactions on Aerospace and Electronic Systems*, vol. 4, no. 1509-1522, 1996.

[74] F. W. Nesline and P. Zarchan, "A new look at classical vs modern homing missile guidance," *Journal of Guidance, Control, and Dynamics*, vol. 4, no. 1, pp. 78-85, 1981.

[75] I.-J. Ha, J.-S. Hur, M.-S. Ko and T.-L. Song, "Performance analysis of PNG laws for randomly maneuvering targets," *IEEE Transactions on Aerospace and Electronic Systems*, vol. 26, no. 5, pp. 713-721, 1990.

[76] P. Zarchan, "Tactical and Strategic Missile Guidance," Vol. 124 of *Progress in Astronautics and Aeronautics*, AIAA, 1990.

[77] J. Ben-Asher, and I. Yaesh, "Advance in Missile Guidance Theory," Vol. 180 of *Progress in Astronautics and Aeronautics*, AIAA, 1998.

[78] P. Zarchan, "Complete statistical analysis of nonlinear missile guidance systems SLAM," *Journal of Guidance and Control*, vol. 2, no. 1, pp. 71-78, 1979.

[79] K.-Y. Lum, "Infinite-dimensional linearization and extended adjoint method for nonlinear homing loop analysis," Proceedings of the *AIAA Guidance, Navigation, and Control Conference and Exhibit* , Austin, TX, pp. 2003-5449, August 2003.

[80] T. Shima, H. Shinar, and H. Weiss, "New interceptor guidance law integrating time-varying and estimation-delay models," *Journal of Guidance, Control, and Dynamics*, vol. 26, no. 2, pp. 295-303, 2003.

[81] H. Hablani, "Endgame guidance and relative navigation of strategic interceptors with delays," *Journal of Guidance, Control, and Dynamics*, vol. 29, no. 1, pp. 82-94, 2006.

[82] J. Xu, K.-Y. Lum and J.-X. Xu, "Analysis of PNG laws with LOS angular rate delay," Proceedings of the *AIAA Guidance, Navigation, and Control Conference and Exhibit* , Hiltonhead Island, SC, USA, AIAA Paper 2007-6788, 2007.

[83] J. Moon, and Y. Kim, "Design of missile guidance law via variable structure control," *Journal of Guidance, Control, and Dynamics*, vol. 24, no. 4, pp. 659-664, 2001.

[84] D. Zhou, C. Mu, Q. Ling and W. Xu, "Optimal sliding-mode guidance of a homing missile," Proceedings of the 38^{th} *Conference on Decision & Control*, pp. 2131-5136, 1999.

[85] T. Shima, M. Idan, and O. M. Golan, "Sliding-mode control for integrated missile autopilot guidance," *Journal of Guidance, Control, and Dynamics*, vol. 29, no. 2, pp. 250-260, 2006.

[86] J.-X. Xu, Y. J. Pan and T. H. Lee, "Sliding mode control with closed-loop filtering architecture for a class of nonlinear systems," *IEEE Transactions on Circuits and Systems II: Express Briefs*, vol. 51, no. 4, pp. 168-173, 2004.

[87] Y. Shtessel and J. Buffington, "Continuous sliding mode control," Proceedings of the 1998 *American Control Conference*, vol. 1, Philadelphia, PA, pp. 562-563, June 1998.

[88] F. B. Hildebrand, Introduction to Numerical Analysis, Dover Publications, New York, 1987.